Journal of Double Star Observations

VOLUME 16 NUMBER 4 SEPTEMBER 1, 2020

Inside this issue:

Inside this issue:

CCD Measurements of the AC Component of WDS 01295+6317

Brenlie Shirts, Ali Talib Saifee, Breckan Shirts, Charmain Brammer, Cameron Pace

1. SUCCESS Academy DSU
2. Southern Utah University

Abstract: Images of WDS 01295+6317AC were gathered with the Great Basin Observatory Telescope. Measurements of separation and position angle of the A and C components of the system were obtained. Our measurements aligned with two prior measurements of the stars, however a speckle observation from 2004 suggests a larger change in separation and position angle than we observed. In an effort to resolve this discrepancy and determine whether the A and C components are physical, we extracted parallax and proper motion data from the Gaia database. However, the stars are so distant (~2,200 pc for Component A and ~3,400 pc for Component C) that we must be careful in interpreting measurements of their proper motion and parallax. We therefore only suggest that the A and C components are not gravitationally bound.

Introduction

In this research paper, we examine WDS 01295+6317 [MLB]. This star system is comprised of three component stars (01295+6317 [MLB 329A], 01295+6317 [MLB 329B], and 01295+6317 [MLB 329C]). Our telescope, the Great Basin Observatory (GBO), does not have the resolution to resolve the A and B components due to their close proximity. Therefore, we only observed the WDS 01295+6317 [MLB 329AC] system. This system was first measured in 1924. Prior to this study, it was last measured in 2004.

This research was conducted using the robotic GBO telescope (Figure 1) located in Great Basin National Park, Nevada. GBO operates under a cooperative that includes Great Basin National Park, Great Basin National Park Foundation, University of Nevada, Reno, Western Nevada College, Concordia University, and Southern Utah University. This telescope has an aperture of 27 inches as well as a focal ratio of f/6.5. Its SBIG STX 16803 camera has a field of view of 27' x 27'. The camera also has a plate scale of 0.4 arcsec per pixel. The GBO telescope is equipped with sixteen filters housed in two nested Finger Lakes filter wheels: LRGB, Ha, OIII, SII, BVRI, griz, and a diffraction grating.

Figure 1: Located in Great Basin National Park, the GBO Planewave CDK700 telescope was used to acquire pictures of the WDS 01295+6317 [MLB 329AC] star system.

WDS 01295+6317 (MLB 329AC) was remotely observed on January 19th, 2019. A sample image is shown in Figure 2, which shows that the A and B components were unresolved. Twenty images were collect-

Received September 19, 2019; revised manuscript received April 3, 2020.

CCD Measurements of the AC Component of WDS 01295+6317

WDS No.	ID	Nights	Date	Observations		θ (°)	ρ (")
01295+6317	MLB 329AC	1	2019.052	20	Mean	152.2	11.30
					Std. Dev.	0.1	0.03
					Std. Error	0.02	0.01

Table 1. Data and observations from our images. Standard deviation, standard error, position angle (θ) and separation (ρ) are shown.

ed of the targeted system with an exposure time of 60 seconds each: this exposure time was used to ensure that neither of the stars were overexposed. The images were taken with the V filter. The images were then calibrated to remove noise. This was done by applying dark, flat, and bias frames using AstroImageJ (Collins et al. 2017). The images were already plate solved by the imaging software. After the process of calibrating and plate solving was complete, the position angle (θ) and separation (ρ) were measured using AstroImageJ. The centroid of the star was utilized to improve the accuracy of the measurements.

Results

Our measurements, together with the standard deviation and error, as well as the number of observations, are shown in Table 1.

Discussion

Table 2 shows that there are 3 measurements of the A and C components of WDS 01295+6317 in the literature, with the latest measurement dating to 2004. (Mason, 2019). Our measurement aligns with the discovery measurement and that taken in 2003, however the 2004 measurement is quite different from the others, as can be seen in Figure 3. The 2003 measurement was taken as part of the fourth US Naval Observatory

Epoch	θ (°)	ρ (")
1924.56	154.7	11.76
2003.7	152.2	11.331
2004.923	119.7	20.1
2019.052	152.2	11.30

Table 2. Historical data for 01295+6317MLB 329AC, as well as our measurements.

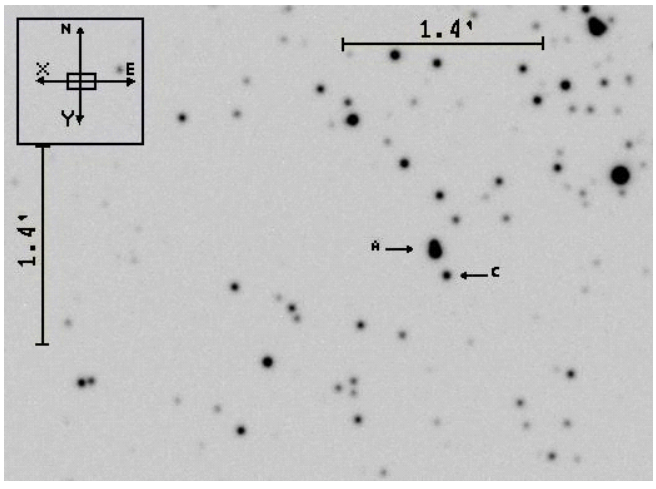

Figure 2: The two stars measured from the WDS 01295+6317 [MLB] system. Shown to the top left is the A central star; the C component star is shown to the bottom right. The B component star is partially behind the A central star, accounting for its elliptical shape.

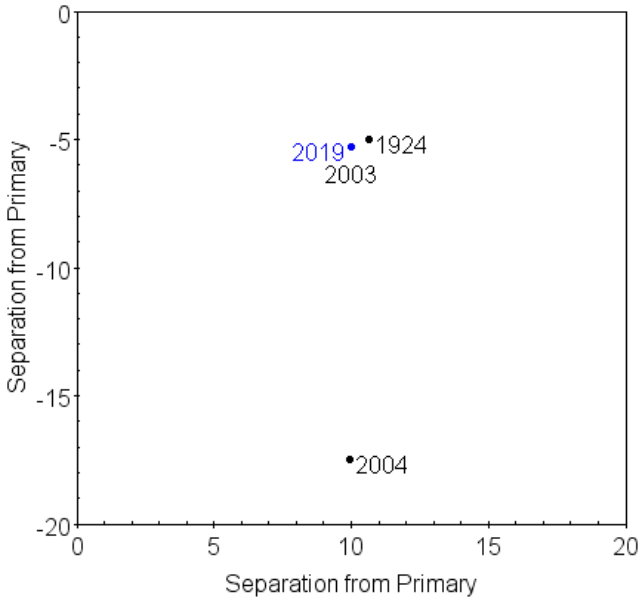

Figure 3: This graph depicts our measurement (blue circle) of the C component, together with historical measurements (black circles). All measurements are in arcseconds, and the primary star is located at the origin. The data point from 2004 is a speckle observation from the USNO .

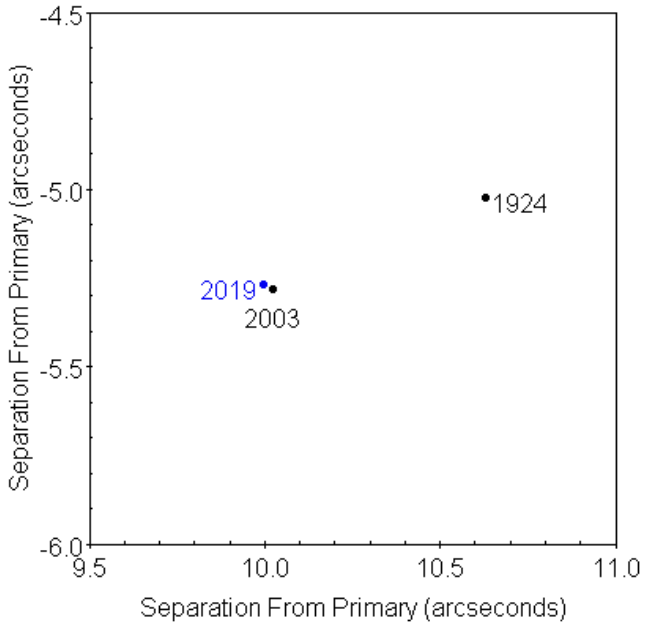

Figure 4. Same as Figure 3, but with the 2004 data point omitted. It can be seen that our measurement is consistent with the measurements made in 2003 and 1924.

CCD Astrograph Catalog (UCAC4; Zacharias et al. 2012), and as such is an astrometric measurement. In contrast, the 2004 measurement is a speckle interferometric observation and was taken as part of the USNO effort to take speckle measurements of double stars (Mason et al. 2006). These authors noted that their observation represented a large change in separation and position angle. Although the 2003 and 2004 observations were both made by observers at the same institution, it must be remembered that they were each made as part of large catalogs that were published at different times, and so it makes sense that the relatively large difference between the two may have gone unnoticed.

There is a possibility the data recorded in 2004 could have been misrecorded and/or miscalculated. As shown in Figure 3, the values for our data and the data from 1924 and 2003 are in agreement. However, the measurement from 2004 is inconsistent with the other measurements. We have shown in Figure 4 the observations of this pair with 2004 data omitted to better show the motion of the star over this time period. The points from 1924, 2003, and 2019 suggest that the C component is moving in a linear fashion, which could indicate that the A and C components are not gravitationally bound.

Proper motion and parallax information for these components was extracted from the Gaia DR 2 (Gaia Collaboration 2016, 2019), and is shown in Table 3. The A component has a parallax of 0.446 mas, while that of the C component is 0.298 mas. Converting these to distances and including the parallax error gives a distance range of 1800-2800 pc for Component A and a range of 3100-3600 for Component C. While there is some possibility of overlap in these distance ranges, these measurements suggest that the components are not physically associated.

If we examine the proper motion of the stars, we see that the RA component of their motion is rather similar, however their DEC proper motions appear to be different. Even so, the extreme distances of these stars make it difficult to draw any conclusions of their physicality, and we merely suggest that this pair may not be physical.

Acknowledgements

This paper is a result of research conducted by undergraduate students at Dixie State University through the Department of Physical Science at Southern Utah University. The research was made possible by a collaboration with the partnership between Southern Utah University and the Great Basin Observatory. First, we would like to thank those who manage and maintain the Great Basin Observatory. We would also like to acknowledge Brian Mason for providing the historical data needed to complete our research. This research made use of AstroImageJ, Astrometry.net, and the Washington Double Star Catalog maintained at the U.S. Naval Observatory. This research also used data from the European Space Agency (ESA) mission Gaia (https:// www.cosmos.esa.int/gaia), processed by the Gaia Data Processing and Analysis Consortium (DPAC, https:// www.cosmos.esa.int/web/gaia/dpac/consortium). DPAC funding is provided by national institutions participating in the Gaia Multilateral Agreement.

Component	Parallax (mas)	Distance (pc)	Proper Motion RA (mas/year)	Proper Motion DE (mas/year)
A	0.446 ± 0.084	1800-2800	-4.253 ± 0.101	0.115 ± 0.108
C	0.298 ± 0.021	3100-3600	-4.228 ± 0.029	0.445 ± 0.028

Table 3: Data obtained from ESA's Gaia astronomy satellite, which describes the movement and location of WDS 01295+6317 [MLB 329AC]. This given data was used to help determine if these are gravitationally bound, specifically the parallax.

References

Mason, B., 2019, The Washington Double Star Catalog, Astronomy Department, U.S. Naval Observatory.

Collins, K. A., Kielkopf, J. F., Stassun, K. G., & Hessman, F. V., 2017, *The Astronomical Journal*, **153** (2), 77.

Gaia Collaboration: T. Prusti, J. H. J. de Bruijne, A. G. A. Brown, A. Vallenari, C. Babusiaux, C. A. L. Bailer-Jones, U. Bastian, M. Biermann, D. W. Evans, et al., 2016b, "The Gaia mission", *A & A*, **595**, pp. A

Gaia Collaboration: A.G.A Brown, A. Vallenari, T. Prusti, J.H.J. de Bruijne, Babusiaux, C.A.L. BailerJones et al., 2018, "Gaia Data Release 2. Summary of the contents and survey properties", *A & A*, Accepted for publication.

"Great Basin Observatory" *Planewave.com*, http://planewave.com/great-basin-observatory/

Mason, B. D., Hartkopf, W. I., Wycoff, G. I., Rafferty, T. J., 2006, "Speckle Interferometry at the US Naval Observatory. XI.," *The Astronomical Journal*, **131**, 2687.

Zacharias, N, Finch, C. T., Girard, T. M., et al., 2012, "The Fourth US Naval Observatory CCD Astrograph Catalog (UCAC4)," *The Astronomical Journal*, **145** (2), 44.

Double Star Observations with a 150mm Refractor from 2017 to 2019

Marc Oliver Maiwald

Witten, Germany
oliver-maiwald@web.de

Abstract: I present 246 measurements of 76 pairs made from 2017 to 2019. For 26 pairs, residuals were calculated.

All observations were made with my 150/3000 folded refractor, filter 11 (yellow – green) and a Alccd QHY 5-II camera. Most observations were made with a 1.4x teleconverter (TK1.4 in Table 1, imaging scale 0.19744 a.s. per pixel), some at direct focus (0.25739 a.s. per pixel, f in Table 1) and only one with a 2x teleconverter (TK2 in Table 1, 0.1385 a.s. per pixel).

For every star and observing run 50 to 100 video files were taken with SharpCap 2.8 and stacked with Registax 5 or Registax 6. The pictures were measured with Reduc 3.88; the number of pictures used for the results is given as "Nr" in Table 1. The residuals were calculated with Binary Star Calculator and are given in Table 2, with "N" meaning the number of nights in which the star was observed.

In Table 3, some measurements and residuals for STF2199 are listed.

Acknowledgements

This paper made use of the Washington Double Star Catalog [1] and the Sixth Catalog of Orbits of Visual Binary Stars [2], both maintained at the U.S. Naval Observatory. Noncommercial software used was: Binary Star Calculator by Brian Workman [3]; Reduc 3.88 by Florent Losse; Registax 5 and Registax 6 by Coer Berrevoets and SharpCap by Robin Glover.

References

1. Mason, Brian et.al. *Washington Double Star Catalog,* http://www.astro.gsu.edu/wds/

2. Hartkopf, William I.; Mason, Brian D., *Sixth Catalog of Orbits of Visual Binary Stars*. http://www.astro.gsu.edu/wds/orb6.html

3. Workman, Brian, Binary Star Calculator, 2013, http://www.saguaroastro.org/content/db/binaries_6th_Excel97.zip

4. Argyle, R.W., "Micrometric Measurements of Double Stars from 1983.0 to 1988.0", *The Webb Society Double Star Section Circular No 4*, pp. 9 – 18, 1989.

5. Argyle, Bob, "Micrometer Measurements from 2003.0 to 2004.0", *The Webb Society Double Star Section Circular, No 12*, pp. 1 – 8, 2004.

6. Alzner, Andreas, "Micrometer Measurements from 1998.02 to 2002.92", *The Webb Society Double Star Section Circular, No 11*, pp. 9 – 31, 2003.

7. Mason, Brian D. et.al., "Speckle Interferometry at the US Naval Observatory. IX", *The Astronomical Journal*, **127**, 539 – 548, 2004.

8. Alzner, Andreas, "Micrometer Measurements from 2006.21 to 2008.12", *The Webb Society Double Star Section Circular, No 16*, pp. 7 – 15, 2008.

9. Maiwald, Marc Oliver, "Double Star Measurements using a Small Refractor", *JDSO*, **9** 189 – 194, 2013.

10. Maiwald, Marc Oliver, "Double Star Observations with a 150mm Refractor in 2013", *JDSO*, **10**, 185 – 192, 2014.

11. Argyle, Bob, "Micrometer Measurements of Double Stars in 2014," *The Webb Society Double Star Section, Circular No 23*, pp. 1 – 5, 2015

12. Schlimmer, Joerg S., "Double Star Measurements using a CMOS Camera, Annual Report of 2018", *JDSO*, **15**, 536 – 543, 2019.

Received February 21, 2020.

Double Star Observations with a 150mm Refractor from 2017 to 2019

Table 1
Double star measurements from 2017 to 2019

Designation	WDS ident	θ	ρ	Date	Nr	Name	Notes
STF 3053 AB	00026+6606	70.45	15.20	2018.804	76		TK1,4
STF 060 AB	00491+5749	325.5	13.41	2017.829	42	η Cas	TK1,4
STF 88 AB	01057+2128	158.8	29.75	2018.88	14	ψ_1 Psc	TK1,4
STF 100 AB	01137+0735	62.9	22.82	2018.88	29	ζ Psc	TK1,4
STF 174	01501+2217	164	2.85	2018.875	31	1 Ari	TK1,4
		164.4	2.85	2018.877	33		TK1,4
STF 180	01535+1918	1	7.39	2018.875	28	γ Ari	TK1,4
		0.8	7.4	2018.877	23		TK1,4
STF 924 AB	06323+1747	211	19.94	2017.122	26	20 Gem	TK1,4
STF 948 AB	06462+5927	66.4	1.88	2017.136	39	12 Lyn	TK1,4
		66.8	1.89	2017.193	32		TK1,4
STF 948 AC	06462+5927	308.9	8.80	2017.136	35	12 Lyn	TK1,4
		308.8	8.84	2017.193	28		TK1,4
STF 1110 AB	07346+3153	54	5.21	2017.095	40	α Gem	TK1,4
		53.7	5.24	2017.120	55		TK1,4
		53.5	5.23	2017.122	44		TK1,4
		53.7	5.22	2017.136	43		TK1,4
		53.2	5.24	2018.135	59		f
		52.5	5.45	2018.146	65		TK1,4
		52.6	5.41	2018.149	87		TK1,4
		53.3	5.41	2018.193	36		TK1,4
		52.4	5.38	2019.124	39		TK1,4
		52.5	5.34	2019.132	50		TK1,4
STF 1196 AB	08122+1739	16.1	1.17	2017.193	81	ζ Cnc	TK1,4
		15.6	1.06	2017.196	69		TK1,4
		16.3	1.08	2017.199	61		TK1,4
		16.5	1.1	2017.204	64		TK1,4
		11.4	1.04	2018.193	31		TK1,4
		10.8	1.14	2018.218	85		TK1,4
		11.8	1.17	2018.229	63		TK1,4
		8.7	1.18	2019.214	60		TK1,4
		8.4	1.21	2019.22	62		TK1,4
STF 1196 AC		61.1	6.32	2017.193	63	ζ Cnc	TK1,4
		61.3	6.29	2017.196	81		TK1,4
		61.4	6.27	2017.199	59		TK1,4
		61.1	6.31	2017.204	40		TK1,4
		61.1	6.21	2018.193	30		TK1,4
		61	6.21	2018.218	68		TK1,4
		61.2	6.23	2018.229	59		TK1,4
		61.2	6.22	2019.214	82		TK1,4
		60.9	6.22	2019.22	67		TK1,4
STF 1333	09184+3522	50.3	1.76	2018.3	36		TK1,4
STF 1334 AB	09188+3648	223.9	2.52	2018.3	26	38 Lyn	TK1,4
		223.4	2.62	2018.302	47		TK1,4
STF 1338 AB	09219+3811	312.8	0.94	2017.196	50		TK1,4
		309.7	1.04	2017.199	50		TK1,4
		310.5	1.08	2017.204	58		TK1,4
		309.4	0.93	2017.207	60		TK1,4
		313.1	1.08	2018.242	48		TK1,4
		313.2	0.99	2018.267	39		TK1,4
		314.5	1.04	2018.292	38		TK1,4
		312.4	1.07	2018.302	41		TK1,4
STT 215	10163+1744	175.5	1.37	2018.267	20		TK1,4
		175.7	1.5	2018.292	35		TK1,4
		176.3	1.66	2019.299	16		TK1,4
		177.2	1.46	2019.302	41		TK1,4
		175.1	1.42	2019.305	27		TK1,4

Table 1 continues on the next page.

Double Star Observations with a 150mm Refractor from 2017 to 2019

Table 1 (continued). Double star measurements from 2017 to 2019

Designation	WDS ident	θ	ρ	Date	Nr	Name	Notes
STF 1424 AB	10200+1950	126.2	4.69	2017.207	36	γ Leo	TK1,4
		126.2	4.68	2017.226	58		TK1,4
		126.6	4.73	2018.242	61		TK1,4
		126.2	4.7	2018.261	53		TK1,4
		126.3	4.73	2018.267	40		TK1,4
		126.3	4.74	2018.294	42		TK1,4
		126.6	4.77	2019.223	37		TK1,4
		126.8	4.81	2019.228	36		TK1,4
S 612	10459+3041	173.6	196.37	2019.277	38	42 LMi	f
STF 1487	10556+2445	112.7	6.62	2017.328	38	54 Leo	TK1,4
STF 1523 AB	11182+3132AB	165	1.88	2017.273	120	ξ Uma	TK1,4
		166.7	1.92	2017.289	56		TK1,4
		164	1.87	2017.298	67		f
		159.2	2.04	2018.292	39		TK1,4
		159.1	2.07	2018.294	34		TK1,4
		155.9	2.11	2019.244	61		TK1,4
		156.1	2.11	2019.247	37		TK1,4
		155.9	2.10	2019.25	64		TK1,4
STFA 19	11279+0251	181.9	88.73	2018.297	36	τ Leo	TK1,4
STF 1622	12161+4040	259.6	11.57	2017.399	26	2 CVn	TK1,4
STF 1670	12417-0127	1.5	2.55	2017.311	45	γ Vir	TK1,4
		1.7	2.66	2017.320	37		TK1,4
		359.9	2.7	2018.305	63		TK1,4
		359.8	2.73	2018.338	50		TK1,4
		359.4	2.67	2018.341	19		TK1,4
		357.5	2.79	2019.303	62		TK1,4
		357.9	2.83	2019.329	63		TK1,4
STT 261	13120+3205	338.2	2.63	2018.349	23		TK1,4
		338.5	2.63	2018.352	24		f
STF 1768 AB	13375+3618AB	92.7	1.58	2017.355	27	25 CVn	TK2
		94.6	1.65	2017.358	70		TK1,4
		95.2	1.65	2017.377	23		TK1,4
		92.5	1.6	2018.344	38		TK1,4
		92.7	1.6	2018.346	41		f
		92.9	1.59	2018.349	37		TK1,4
		93.1	1.67	2018.352	43		f
		92.8	1.66	2019.359	54		TK1,4
		92.8	1.56	2019.362	22		TK1,4
		94.3	1.68	2019.37	25		TK1,4
STF 1821	14135+5147	235.4	13.67	2017.454	22	κ Boo	TK1,4
STFA 26	14162+5122	32.6	39	2017.465	40	ι Boo	TK1,4
STF 1825	14165+2007	152.7	4.37	2018.368	48		f
		152.8	4.38	2018.376	41		f
STF 1835 AB	14234+0824	194.4	6.34	2017.437	28		TK1,4
		194.8	6.3	2017.443	42		TK1,4
STF 1850	14286+2817	261.2	25.5	2017.451	35		TK1,4
STF 1864 AB	14407+1625	111.5	5.52	2017.388	27	π Boo	TK1,4
		111.5	5.51	2017.394	34		TK1,4
		111.5	5.54	2018.376	35		f
		111.6	5.49	2018.382	46		f
STF 1877 AB	14450+2704	343.7	2.99	2017.416	35	ε Boo	TK1,4
		343.8	2.79	2017.418	53		TK1,4
		343.8	2.92	2018.429	35		TK1,4
		344.7	2.93	2018.431	40		TK1,4
STF 1884	14484+2422	55.4	2.19	2018.428	44		f
		55.3	2.19	2018.431	41		f

Table 1 continues on the next page.

Double Star Observations with a 150mm Refractor from 2017 to 2019

Table 1 (continued). Double star measurements from 2017 to 2019

Designation	WDS ident	θ	ρ	Date	Nr	Name	Notes
STF 1888 AB	14514+1906	300.3	5.53	2017.388	38	ξ Boo	TK1,4
		300	5.52	2017.394	43		TK1,4
		299	5.45	2018.357	41		f
		299.1	5.44	2018.368	36		f
		299.7	5.33	2019.365	36		TK1,4
		299.6	5.53	2019.368	29		TK1,4
STT 288	14534+1542	158.1	0.99	2017.416	21		TK1,4
STT 291	15006+4717	155.6	35.58	2018.385	27		f
STFA 28AaBC	15245+3723	170.7	109.13	2017.396	25	μ Boo	TK1,4
		170.7	108.87	2018.385	29		f
STF 1938 BC	15245+3723	3.2	2.26	2017.402	46	μ Boo	TK1,4
		3.5	2.16	2017.405	26		TK1,4
		3	2.26	2018.401	42		f
		2.6	2.28	2018.408	35		f
		2.4	2.25	2019.414	30		TK1,4
		2.1	2.24	2019.431	31		f
STF 1954 AB	15348+1032	172.2	3.97	2018.423	38	δ Ser	f
		171.9	4.05	2018.426	41		f
STF 1965	15394+3638	306	6.37	2018.450	39	ζ CrB	f
STF 2010 AB	16081+1703	13.6	27.01	2018.450	37	κ Her	f
STF 2032 AB	16147+3352	238.5	7.29	2017.432	63	σ CrB	TK1,4
		238.6	7.29	2017.435	29		TK1,4
		238.7	7.28	2018.423	37		f
		238.8	7.28	2018.426	21		f
		238.6	7.31	2019.458	34		TK1,4
		238.8	7.31	2019.461	33		TK1,4
STFA 30 AC	16361+5255	193.1	90.23	2018.489	27	16&17 Dra	f
		193.1	90.22	2018.492	47		f
STF 2078 AB	16361+5255	103.8	3.1	2018.489	80	17 Dra	f
		103.8	3.1	2018.492	35		f
STF 2118 AB	16564+6502	66.5	0.96	2017.479	33	20 Dra	TK1,4
		64.5	0.91	2017.487	36		TK1,4
		66.1	0.94	2017.492	36		TK1,4
STF 2130 AB	17053+5428	1.1	2.58	2017.473	38	μ Dra	TK1,4
		0.7	2.57	2017.478	34		TK1,4
		359.3	2.56	2018.483	24		f
		359.3	2.55	2018.486	36		f
STF 2140	17146+1423	102.9	4.84	2018.533	42	α Her	f
		103	4.83	2018.535	44		TK1,4
		103.2	4.82	2018.538	29		TK1,4
		102.9	4.87	2019.504	35		TK1,4
		103	4.78	2019.510	29		TK1,4
STF 2161Aab	17237+3709	320.9	4.14	2019.504	49	ρ Her	TK1,4
		320.8	4.13	2019.510	39		TK1,4
STFA 35	17322+5511	310.6	62.14	2017.544	24	ν Dra	TK1,4
STFA 34 AB	17346+0935	190.1	41.24	2018.549	33	53 Oph	f
STF 2199	17386+5546	54.4	2.03	2017.544	24		TK1,4
		54.6	2.01	2017.547	10		TK1,4
		54.5	2.06	2018.483	25		f
		53.6	2.03	2018.486	21		f
		54	2.04	2018.492	23		f
STF 2241 AB	17419+7209	12.5	30.1	2017.547	45	ψ Dra	TK1,4
H 6 2 AC	18006+0256	142	54.5	2018.505	26	67 Oph	f
STF 2264	18015+2136	256.4	6.39	2018.519	43	95 Her	f
		256.4	6.37	2018.524	37		f
STF 2308 AB	18002+8000	231	18.72	2017.511	39	40 & 41 Dra	TK1,4
		231.8	18.68	2017.531	35		TK1,4
STF 2308 AC	18002+8000	128.6	225.25	2017.531	32	41 Dra	f

Table 1 continues on the next page.

Double Star Observations with a 150mm Refractor from 2017 to 2019

Table 1 (continued). Double star measurements from 2017 to 2019

Designation	WDS ident	θ	ρ	Date	Nr	Name	Notes
STF 2272 AB	18055+0230	124.1	6.59	2017.471	28	70 Oph	TK1,4
		123.5	6.59	2017.473	46		TK1,4
		122.8	6.65	2018.505	47		f
		122.4	6.63	2018.516	48		f
		121.8	6.68	2019.488	78		TK1,4
		122.2	6.67	2019.491	51		TK1,4
		122	6.72	2019.501	82		TK1,4
STF 2280 AB	18078+2606	182.77	14.323	2018.524	19	100 Her	f
STF 2289	18101+1629	221.1	1.2	2017.656	66		TK1,4
		220.5	1.19	2017.659	44		TK1,4
		221.6	1.29	2018.519	45		TK1,4
		223.1	1.22	2018.535	43		TK1,4
		223.4	1.17	2018.538	39		TK1,4
		222.1	1.24	2018.546	41		TK1,4
STF 2323 AB	18239+5848	348.2	3.76	2017.487	30	39 Dra	Al, TK1,4
		348	3.72	2017.492	36		Al, f
STF 2323 AC	18239+5848	19.5	89.02	2017.487	30	39 Dra	Al, TK1,4
		19.7	88.89	2017.492	37		Al, f
STF 2382 AB	18443+3940	346.2	2.28	2017.468	45	ε Lyr	TK1,4
		345.5	2.26	2017.471	32		TK1,4
		344.7	2.23	2018.494	44		f
		345	2.24	2018.497	44		f
		344.8	2.26	2018.500	38		f
		345.5	2.29	2019.481	18		TK,14
		344.3	2.22	2019.483	42		TK1,4
		345.5	2.27	2019.485	38		TK1,4
		345.6	2.28	2019.499	40		TK1,4
STF 2383CcD	18443+3940	75.3	2.42	2017.468	29	5 Lyr	TK1,4
		75.4	2.46	2017.471	34		TK1,4
		75.1	2.38	2018.497	20		f
		75.3	2.39	2018.500	43		f
		74.5	2.43	2019.481	29		TK1,4
		75.2	2.49	2019.483	31		TK1,4
		74.2	2.36	2019.485	34		TK1,4
		74.9	2.40	2019.499	32		TK1,4
STF 2417	18562+0412	103.7	22.51	2017.656	38	θ Ser	TK1,4
		103.7	22.52	2017.659	36		TK1,4
STF 2579 AB	19450+4508	215.3	2.65	2017.618	29	δ Cyg	TK1,4
		215.2	2.71	2017.64	39		TK1,4
STF 2583 AB	1948+1149	102.3	1.38	2017.618	29	π Aql	TK1,4
		102.7	1.4	2017.64	38		TK1,4
		102.7	1.46	2019.559	27		TK1,4
		102.6	1.3	2019.576	41		TK1,4
		103.8	1.36	2019.581	33		TK1,4
STF 2603	19482+7016	21	3.13	2017.599	31	ε Dra	TK1,4
		20.4	3.15	2017.602	33		TK1,4
STF 2605	19556+5226	174.9	2.75	2017.599	38	Ψ Cyg	TK1,4
		175.1	2.86	2017.602	45		TK1,4
H 5 47 AB	20014+5006	150	41.89	2018.642	49	26 Cyg	f
		150	41.78	2018.645	21		f
STF 2727	20467+1607	265	8.91	2019.713	38	γ Del	TK1,4
STF 2737 AC	20591+0418	66.3	10.55	2019.644	35	ε Equ	TK1,4
		66.5	10.58	2019.663	33		TK1,4
STF 2758 AB	21069+3845	152.7	31.75	2017.662	23	61 Cyg	TK1,4
		152.8	31.75	2017.667	34		TK1,4
		152.8	31.77	2018.732	58		f
		152.8	31.76	2018.735	59		f
		153	31.81	2019.652	42		f
		152.9	31.79	2019.663	38		f

Table 1 concludes on the next page.

Double Star Observations with a 150mm Refractor from 2017 to 2019

Table 1 (conclusion). Double star measurements from 2017 to 2019

Designation	WDS ident	θ	ρ	Date	Nr	Name	Notes
STF 2822 AB	21441+2845	320.7	1.53	2017.667	42	μ Cyg	TK1,4
		320.8	1.56	2018.650	37		TK1,4
		321.1	1.54	2018.658	40		TK1,4
		321.4	1.6	2019.636	34		TK1,4
		321.9	1.54	2019.652	26		TK1,4
STF 2822 AD	21441+2845	197.1	43	2019.639	25	μ Cyg	f
		197	43	2019.652	32		f
STF 2909	22288-0001	161.7	2.34	2017.788	84	ζ Aqr	TK1,4
		162	2.33	2017.832	66		TK1,4
		160.9	2.28	2018.738	66		TK1,4
		160.7	2.3	2018.740	73		TK1,4
		160.5	2.22	2019.811	39		TK1,4
		159.3	2.27	2019.814	35		TK1,4
		160.6	2.4	2019.818	28		TK1,4
STF 3050 AB	23595+3343	341.5	2.47	2018.804	82		TK1,4
		341	2.43	2018.872	36		TK1,4

Table 2. Residuals for Double Stars from 2017 to 2019

Designation	WDS ident	Date	N	θ	ρ	Δθ	Δρ	Ref
STF 948 AB	06462+5927	2017.2	2	66.6	1.88	4.8	0.18	Pop1996b
						0.7	-0.03	WSI2006b
STF 1110 AB	07346+3153	2017.1	4	53.7	5.23	0	0.03	Hei1988a
						0.7	0.09	Doc1985c
		2018.1	4	52.8	5.38	-0.4	0.2	Hei1988a
						0.4	0.26	Doc1985c
		2019.1	2	52.5	5.36	-0.2	0.03	Hei1988a
						0.6	0.11	Doc1985c
STF 1196 AB	08122+1739	2017.2	2	16.1	1.11	4.2	-0.03	Sod1999
						3.3	-0.02	WSI2006b
		2018.2	3	11.3	1.14	2.7	-0.01	Sod1999
						1.8	0	WSI2006b
		2019.2	2	8.5	1.20	3.1	0.06	Sod1999
						2.3	0.07	WSI2006b
STF 1338 AB	09219+3811	2017.2	3	310.5	1	-6.3	0	Sca2002b
		2018.3	2	313.3	1.05	-5.5	0.05	Sca2002b
STT 215	10163+1744	2018.3	2	175.6	1.45	-2.3	-0.12	Zae1984
		2019.3	3	176.4	1.49	-1.3	-0.09	Zae1984
STF 1424 AB	10200+1950	2017.2	2	126.2	4.68	-0.1	0.21	Rab1958
		2018.3	4	126.4	4.72	0	0.24	Rab1958
		2019.2	2	126.7	4.79	0.3	0.31	Rab1958
STF 1523 AB	11182+3132AB	2017.3	3	165.1	1.89	0.7	-0.06	Msn1995
		2018.3	2	159.2	2.05	-0.4	0.01	Msn1995
		2019.2	3	155.9	2.11	0.2	-0.01	Msn1995
STF 1670	12417-0127	2017.3	2	1.6	2.6	0.1	0	Sca2007
		2018.3	2	359.8	2.7	-0.1	-0.01	Sca2007
		2019.3	2	357.7	2.81	-0.7	-0.4	Sca2007
STT 261	13120+3205	2018.4	2	338.4	2.63	0.1	0.03	Kis2012
STF 1768 AB	13375+3618	2017.4	1	94.3	1.63	-0.1	-0.05	Sod1999
		2018.3	4	92.8	1.62	-1.3	-0.05	Sod1999
		2019.4	3	93.2	1.64	-0.6	-0.02	Sod1999

Table 2 continues on the next page.

Double Star Observations with a 150mm Refractor from 2017 to 2019

Table 2 (conclusion). Residuals for Double Stars from 2017 to 2019

Designation	WDS ident	Date	N	θ	ρ	Δθ	Δρ	Ref
		2017.4	2	300.2	5.53	-0.2	0.09	Sod1999
STF 1888 AB	14514+1906	2018.4	2	299	5.45	0.3	0.1	Sod1999
		2019.4	2	297.7	5.34	-0.4	0.08	Sod1999
STT 288	14534+1542	2017.4	1	158.1	0.99	0.8	0.01	Hei1998
		2017.4	2	3.3	2.22	0.3	0.01	Sca2013a
						0.5	-0.01	Sod1999
STF 1938 BC	15245+3723	2018.4	2	2.8	2.27	0.2	0.06	Sca2013a
						0.4	0.04	Sod 1999
		2019.4	2	2.3	2.25	0	-0.05	Sca2013a
						0.2	0.02	Sod 1999
		2017.4	2	238.5	7.29	-0.1	0.07	Rag2009
						-0.1	-0.03	Sca1979
STF 2032 AB	16147+3352	2018.4	2	238.7	7.28	-0.1	0.05	Rag2009
						-0.2	-0.06	Sca1979
		2019.5	2	238.7	7.31	-0.2	0.06	Rag2009
						-0.2	-0.05	Sca1979
STF 2118 AB	16564+6502	2017.5	1	65.7	0.94	-1	-0.2	Sca2002d
STF 2130 AB	17053+5428	2017.5	2	0.9	2.58	0.3	0.03	Pru2012
STF 2199	17386+5546	2017.5	2	54.5	2.02	2.3	0.08	Pop1995d
		2018.5	3	54.1	2.04	2.2	0.1	Pop1995d
		2017.5	2	123.7	6.59	-0.4	0.09	Pbx2000b
STF 2272 AB	18055+0230	2018.5	2	122.6	6.64	-0.6	0.07	Pbx2000b
		2019.5	3	122	6.69	-0.4	0.07	Pbx2000b
STF 2289	18101+1629	2017.6	2	220.9	1.2	5.4	-0.04	Hop1964b
		2018.5	4	222.5	1.23	7.1	-0.01	Hop1964b
		2017.5	2	345.9	2.27	0.3	-0.20	Gzl1956a
						0.7	0.03	Nov2006e
						0.6	-0.06	WSI2004b
		2018.5	3	344.8	2.24	-0.5	-0.22	Glz1956a
STF 2382 AB	18443+3940					-0.1	0.02	Nov2006e
						-0.2	-0.08	WSI2004b
		2019.5	4	345.2	2.26	0.2	-0.2	Glz1956a
						0.7	0.05	Nov2006e
						0.6	-0.05	WSI2004b
		2017.5	2	75.4	2.44	0.3	0.05	Doc1984b
STF 2383CcD	18443+3940	2018.5	2	75.2	2.39	0.5	-0.01	Doc1984b
		2019.5	4	74.7	2.42	0.4	0.02	Doc1984b
STF 2579 AB	19450+4508	2017.6	2	215.2	2.68	-1.1	-0.07	Sca2012c
		2017.7	2	152.8	31.75	0.4	0.04	Pko2006b
						-0.1	-0.02	Kis1997
STF 2758 AB	21069+3845	2018.7	2	152.8	31.76	0.3	0	Pko2006b
						-0.3	-0.06	Kis 1997
		2019.7	3	153	31.8	0.3	-0.01	Pko2006b
						-0.2	-0.06	Kis 1997
		2017.7	1	320.7	1.53	2.2	0.03	Hei1995
STF 2822 AB	21441+2845	2018.7	2	321	1.55	-4	0.07	Hei1995
		2019.6	2	321.6	1.57	-4.6	0.1	Hei1995
		2017.8	1	161.8	2.34	0.2	0.03	Sca2010c
						-1.1	-0.12	Hei1984c
STF 2909	22288-0001	2018.7	2	160.8	2.29	0.3	-0.04	Sca2010c
						-1.2	-0.19	Hei1984c
		2019.8	3	160.1	2.29	0.8	0.07	Sca2010c
						-0.9	-0.23	Hei1984c
STF 3050AB	23595+3343	2018.8	1	341.3	2.46	-0.1	0.02	Hrt2011a
						-1.1	0.34	Sta1977b

Double Star Observations with a 150mm Refractor from 2017 to 2019

Table 3. Residuals for STF 2199

Date	N	θ	ρ	Δθ	Δρ	Obs	Ref	Notes
1924.52	4,3	76.8	1.73	-2.9	-0.01	Phillips	Pop1995d	[4]; a
1986.61	2	63.3	2.15	2.7	0.28	Gellera	Pop1995d	[4]; a
2001.328	4	61.8	2	5.3	0.10	Argyle	Pop1995d	[5]; a
2001.45	2	57.7	1.95	1.3	0.04	Alzner	Pop1995d	[6]
2002.44	1	57.2	1.99	1.0	0.08	Mason et. al.	Pop1995d	[7]
2006.56	2	56.2	1.95	1.2	0.03	Alzner	Pop1995d	[8]
2012.6	2	55.9	2.06	2.5	0.13	Maiwald	Pop1995d	[9]; b
2013.5	2	55.2	2.03	2	0.10	Maiwald	Pop1995d	[10]
2014.286	3	55.8	2.06	2.8	0.13	Argyle	Pop1995d	[11];a
2017.5	2	54.5	2.02	2.3	0.08	Maiwald	Pop1995d	
2018.5	3	54.1	2.04	2.2	0.1	Maiwald	Pop1995d	
2018.540	1	54.7	1.88	2.8	-0.06	Schlimmer	Pop1995d	[12], c
2018.594	1	53.9	1.95	2	0.01	Schlimmer	Pop1995d	[12], c

a) Residuals computed with *Binary Star Calculator* by Maiwald
b) Measurements from [6], residuals calculated for this article.
c) Measurements from [12], residuals calculated for this article.

A New Visual Binary System in Leo

Abdul Ahad
Luton, Bedfordshire, United Kingdom
ahad8307@gmail.com

Abstract: This paper highlights a new double star in Leo previously not listed in the WDS catalog. Upon analysis of astrophysical parameters, proper motions, radial velocities and distances of the component stars, it is concluded that this is a wide gravitationally-bound visual binary system.

Introduction

Using the search method and selection criteria I had outlined in earlier papers, this double star first came to my attention in the autumn of 2015 as an 11th magnitude pair. The system is located approximately 7° west of Regulus along the ecliptic in Leo at J2000 ICRS: 09 38 08.79, +13 20 08.3 (Figure 1). The A and B components are of apparent V-mags 11.06 and 11.50 in the Tycho 2 catalog and are designated TYC 827-706-1 and TYC 827-1383-1, respectively.

Figure 1: The Sickle of Leo imaged by the author with his Canon 300D DSLR camera, indicating position of the new binary.

Observations and Binarity Assessments

At the time of my initial observations in 2015, this was an unknown pair and apart from magnitudes and proper motions listed in various catalogs, there was no other data available in regards to the astrometric properties of the two stars and no hints as to likely order of distance or luminosity class on the H-R diagram. Nevertheless, I became convinced that this was a strong binary star candidate from my own assessments and proceeded to image the pair. A V-band image of 30-sec exposure was obtained on November 17, 2015 at 05:26 UTC using the 0.61-meter Cassegrain telescope of the Sierra Stars Observatory Network (SSON)[1]. I later visually observed this system with my own 4.75-inch f/8.33 refractor at approximately 23:00 UTC on January 15, 2016 utilizing a Super Plössl 10mm eyepiece on the telescope's 1000-mm focal length to produce a field sketch at x100 magnification (Figure 2).

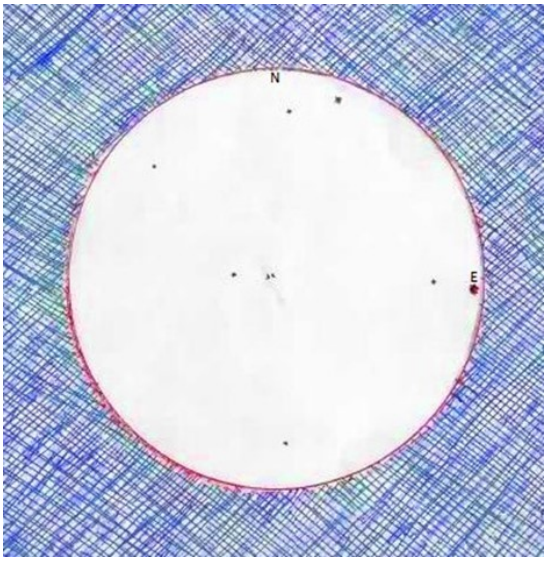

Figure 2: Field drawing made by the author using his 4.75" f/8.33 refractor at a magnification of x100.

From astrometric measurements on the SSON FITS image, I had determined:

- P. A. 64.0°
- Sep. 19.14" (epoch: 2015.880)

Photometric magnitudes of the component stars in various passbands, along with color indices, are shown in Table 1.

Received March 3, 2020.

	Gaia G-mag	B	V	Color Index B-V	J	K	Color Index J-K
A component	11.04	11.59	11.06	+0.53	10.13	9.84	+0.29
B component	11.28	12.01	11.50	+0.51	10.29	10.00	+0.29

Table 1: Magnitudes and Color Indices

	UCAC2 (2004)		Gaia DR2 (2018)	
	μ_α mas yr^{-1}	μ_δ mas yr^{-1}	μ_α mas yr^{-1}	μ_δ mas yr^{-1}
A component	-17.4	-7.9	-19.0	-7.9
B component	-16.0	-8.2	-19.4	-7.5

Table 2: Proper Motion of Components in UCAC2[3] vs Gaia DR2

More recent data releases from the Gaia astrometry mission[2] provide further support to the assertion that this is a physical system. Two sets of historical and current proper motions are compared in Table 2, showing a consistent similarity between components on independent measurements.

Trigonometrical parallaxes from Gaia DR2 are stated as 3.9137 ± 0.0477 and 3.9988 ± 0.0498 mas yr^{-1} for components A and B, indicating distances of 833.3 ± 10.0 and 815.6 ± 10.0 ly, respectively. Notwithstanding the relatively small margins of uncertainty of ±10 ly, which is just 1.2% of the average distance of 824.5 ly, we note that the two stars are thus placed virtually equidistant from Earth. Radial velocities are also found to be broadly similar, though far less reliable, and stated as -0.95 ± 0.71 and -1.33 ± 0.26 km sec-1.

Substituting apparent V-mags of 11.06 and 11.50 and distances deduced from Gaia parallaxes of 833.3 ly and 815.6 ly into the distance modulus, we project absolute magnitudes of +4.0 and +4.5 for the A and B components in this system. These in turn would suggest a pair of main sequence dwarves with surface temperatures, T_{eff} , considerably greater than that of the Sun, and I have determined spectral types of something like F7V and F8V[4]. These classifications are supported by B-V color indices of both stars at around +0.52, and further support comes from 2MASS J-K color indices of +0.29 as I had previously demonstrated in reference [5].

At an average calculated distance of the pair of 824.5 ly, the measured angular separation of 19.14" translates to a linear distance of: Tan (19.14") x 824.5 x 63240 ≈ 4838 AU between components A and B. This distance separation would be comfortably within upper bound of thresholds for gravitational interactions to take place between the component stars, as was previously shown by using the α Librae system as a reference yardstick [6].

Conclusions

Upon consideration of the various astrophysical parameters of this pair discussed in this paper, and the manner in which they all fit together, we conclude that this is a physical system with gravitationally-connected components.

Acknowledgments

This research has made use of the Washington Visual Double Star catalog maintained at the United States Naval Observatory and the SIMBAD and VizieR databases maintained at the Centre de Données astronomiques, Strasbourg, France.

References

[1] Sierra Stars Observatory Network (SSON), http://www.sierrastars.com.

[2] Gaia Data Release 2, Gaia collaboration, 2018.

[3] "The Second US Naval Observatory CCD Astrograph Catalog (UCAC2)", Zacharias, N. et al, 2004.

[4] *Allen's Astrophysical Quantities*, 4th edition, Cox, Arthur N. (editor), Springer, New York, 2000.

[5] Ahad, A. "A New Common Proper Motion Double Star in Cetus", *Journal of Double Star Observations*, **8**, 332-334, 2012.

[6] Ahad, A. "Two New CPM Pairs in Libra", *Journal of Double Star Observations*, **10**, 254-255, 2014.

Investigation of 10 Systems in the Washington Double Star Catalog

Emerson Tiller, Christopher Smithers, Via Niforatos, Ivan Altunin, Kalée Tock
Stanford Online High School

Abstract: We studied 10 double star systems from the Washington Double Star Catalog, fitting trendlines for each in Excel and cross-referencing Gaia Data Release 2 for parallax and proper motion information. LPM 629 and STT 327 lack measurements in Gaia but have complete orbits. STF 42AB and STF 1985 are short arcs that show promise of a physical relationship. GIC 129 is a likely physical system with only 7 observations. HJ 5438, although not currently classified as physical, appears to be so and merits further observations. J 868, D 6, and AG 87 appear to be optical based on Gaia. HDO 182 is inconclusive. We imaged GIC 129 on March 12, 2019 (position angle: 150.47 ± 0.161 degrees, separation: 9.96 ± 0.013"). We also imaged STF 1985 on March 14, 2019 (position angle: 355.52 ± 0.836 degrees, separation: 5.84 ± 0.175").

Introduction

In April 2018, data from the Gaia space telescope were released to the public, allowing for access to measurements of parallax and proper motion (PM) for more than a billion stars. Parallax allows determination of how far stars are from Earth, while proper motion describes how they appear to move on the celestial sphere. These measurements reveal the nature of optical doubles that would otherwise have been unknown from the WDS (Washington Double Star) catalog alone. For example, Gaia data were used by Dugan, et. al. to reclassify J 703 (WDS 07106+1543) to an optical double (Dugan, 2018).

Target Selection

In choosing systems to study, we were looking for stars that were interesting or mysterious. This included a wide range of orbital types from relatively certain (Grade 2) to provisional (Grade 9) or nonexistent. We also looked into doubles for which PM was only listed on one of the system's stars. Some of our systems had a clearly curving historical data plot and some did not. Some of the selected stars had corresponding data in Gaia while other systems did not, as shown in Table 1. We also attempted to find star systems that would be visible by the robotic telescope we were using in Northern Chile during the early part of 2019. However, we found other stars that were interesting and have investigated some of these as well. In total, we found ten systems to study. These are color-coded in Table 1 according to some of their salient features, to be discussed.

Stelledoppie, a search engine for the WDS catalog, was used to find the most recent observation of each star system. Then, the systems were looked up on the US Naval Observatory Ephemerides, which keeps track of the predicted position angle and separation of binary systems with solved orbits.

The values of position angle and separation from the Ephemerides are plotted on a Desmos graph together with the last observed measurements of PA and Sep from Stelledoppie as seen in Figure 1. The last observed measurements of PA and Sep are expected to be similar to those predicted by the Ephemerides for that year. As seen in Figure 1, this is not the case for HDO 182.

Parallax and Radial Separation

Consider the system STF 42AB. From the Gaia measurements in Table 1, the parallaxes of the A and B stars are 18.5581 mas and 19.0305 mas, putting them at 53.88 pc and 52.55 pc from Earth, respectively. There-

(Text continues on page 308)

Received March 4, 2020.

Investigation of 10 Systems in the Washington Double Star Catalog

Discoverer Code and Orbit Grade	Type	WDS Magnitude	Gaia Magnitude	Gaia Parallax (mas*)	Gaia Parallax Error (mas)	Gaia PM RA (mas/yr)	Gaia PM RA error (mas/yr)	Gaia PM Dec (mas/yr)
STT 327 Grade 2	Primary	8.29	7.7	N/A	N/A	N/A	N/A	N/A
	Secondary	8.95	N/A	N/A	N/A	N/A	N/A	N/A
LPM 629 Grade 4	primary	11	N/A	N/A	N/A	N/A	N/A	N/A
	secondary	11.2	N/A	N/A	N/A	N/A	N/A	N/A
STF 42AB Grade 5	Primary	8.39	8.18	18.5581	0.0996	185.505	0.289	-408.101
	Secondary	9.05	9.02	19.0305	0.0719	178.664	0.351	-402.461
STF 1985 Grade 5	primary	7.03	6.856	26.063	0.0508	-91.446	0.081	-61.315
	secondary	8.65	8.4018	26.1413	0.061	-75.227	0.101	-57.666
GIC 129 N/A	primary	14.4	13.1299	27.0904	0.157	-333.125	0.293	-490.43
	secondary	15.4	14.1512	27.0016	0.0556	-314.739	0.11	-499.913
HJ 5438 N/A	primary	10.99	10.75	2.2445	0.0253	11.712	0.033	-17.926
	secondary	14.7	13.799	2.2267	0.0184	11.754	0.025	-18.288
J 868 Grade 5	Secondary	12.62	12.0642	3.5488	0.0441	-28.622	0.067	-12.53
	Primary	12.42	11.453	1.8935	0.0527	14.644	0.079	-2.777
D 6 N/A	primary	9.11	8.9454	3.5251	0.2217	-2.589	0.466	-1.631
	secondary	9.46	9.3203	5.3741	0.3387	-7.62	0.766	-1.879
AG 87 N/A	primary	9.15	8.9649	9.6738	0.1782	49.021	0.333	-66.759
	secondary	10.74	10.475	3.1059	0.0401	11.347	0.079	-19.699
HDO 182 Grade 5	Primary	6.6	6.4654	N/A	N/A	N/A	N/A	N/A
	Secondary	7.01	6.8583	6.3737	0.5868	2.662	1.427	-9.503

* mas = milliarcseconds

Table 1: Ten double star systems: red have complete orbits, orange are physical systems with short arc solutions, green are promising physical systems with sparse observations, blue are optical systems, and purple is inconclusive.

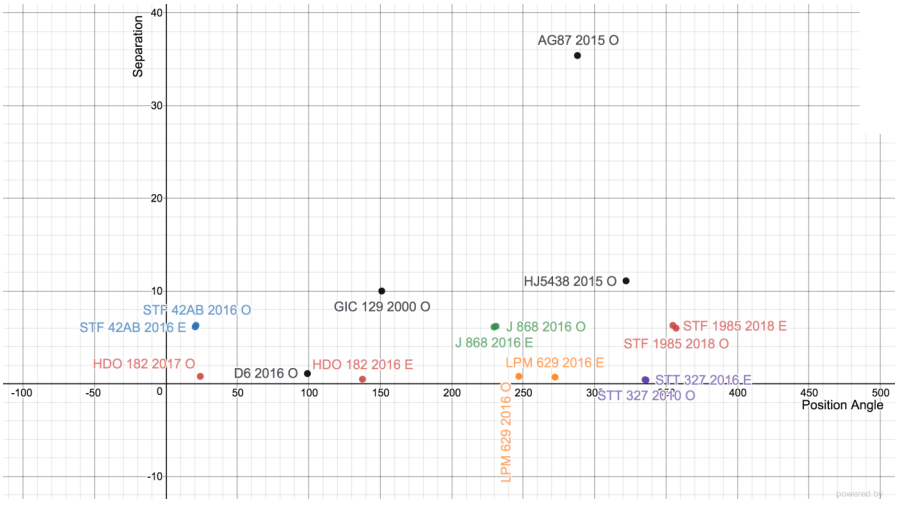

Figure 1: Observed ("O") values and ephemerides ("E") values for our 10 systems with their corresponding years labeled. (https://tinyurl.com/yyucz82u)

Investigation of 10 Systems in the Washington Double Star Catalog

(Continued from page 306)

fore, this system has a radial separation of 53.88 pc - 52.55 pc ≈ 1.3 pc. We estimated the error on radial separation using the tangent line approximation on the function relating the distance from Earth, *D*, to the parallax *P*. Specifically, if *D* = f(*P*), the error on *D* is equal to the error on *P* times the derivative of *D* with respect to *P*. Because,

$$D(P) = \frac{1}{P}, \quad \frac{dD}{dP} = \frac{-1}{P^2}$$

so the error in D is

$$e(D) = \frac{e(P)}{P^2}.$$

Radial separations on all of the systems are shown in Table 2.

As is evident from the table, the large radial separations of the blue systems make them unlikely to be physically connected.

Proper Motion and Difference Vectors

Another value that can inform an assessment of whether the system is likely to be binary or an optical double is the difference in proper motion (PM) of the stars. Proper motion is a vector quantity that shows the direction and rates the stars are moving across the sky in mas/year. If one were to graph the proper motion in RA and Dec of the primary star and compare it to that of the secondary star, the degree to which their movements are similar would be apparent. Stars whose proper motions are very different are less likely to have a physical relationship.

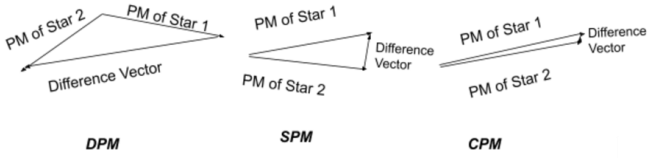

Figure 2: Sample PM Vectors for DPM, SPM and CPM systems.

Relative proper motion (rPM) is an estimate of how the stars in the system move relative to one another. This value is calculated in three steps. First, the magnitude of each star's PM vector is computed as . This results in two different magnitudes for the primary and secondary stars in the system. Then, the difference vector between the primary and secondary PM is calculated. This difference vector magnitude is divided by the larger of the two PM vector magnitudes. The resulting fraction scales the extent to which the stars' PM vectors differ by their magnitude. If the proper motion ratio is less than 0.2, the stars can be classified as having common proper motion, or CPM. Common proper motion is a necessary criterion for inferring a physical connection between the stars. An rPM between 0.2 and 0.6 indicates SPM, or similar proper motion. Finally, any value of rPM that is larger than 0.6 indicates that the stars have DPM, or different proper motion. DPM stars are unlikely to be physical (Harshaw, 2016). Examples of each type of relative motion can be seen in Figure 2, and the rPM is computed for each of our systems in Table 3.

As is evident from Table 3, proper motion suggests

System	Distance to primary with error (pc)	Distance to secondary with error (pc)	Separation with error (pc)
STT 327	N/A	N/A	N/A
LPM 629	N/A	N/A	N/A
STF 42AB	53.8848 ± 0.2892	52.5472 ± 0.1985	1.3376 ± 0.2892
STF 1985	38.3686 ± 0.0748	38.2536 ± 0.0893	0.115 ± 0.0893
GIC 129	36.9134 ± 0.2139	37.0348 ± 0.0763	0.1214 ± 0.2139
HJ 5438	445.5335 ± 5.0221	449.0951 ± 3.711	3.5616 ± 5.0221
J 868	281.7854 ± 3.5017	528.1225 ± 14.6987	246.3371 ± 14.6987
D 6	283.6799 ± 17.8411	186.0777 ± 11.7275	97.6022 ± 17.8411
AG 87	103.372 ± 1.9042	321.9679 ± 4.1569	218.5959 ± 4.1569
HDO 182	N/A	156.8947 ± 14.4446	N/A

Table 2: The radial separations of the components of the systems from Table 1.

System	rPM	Classification
STT 327	N/A	N/A
LPM 629	N/A	N/A
STF 42AB	0.020	CPM
STF 1985	0.151	CPM
GIC 129	0.035	CPM
HJ 5438	0.013	CPM
J 868	1.422	DPM
D 6	0.646	DPM
AG 87	0.728	DPM
HDO 182	N/A	N/A

Table 3. The proper motion ratios of the components of the systems from Table 1.

a physical connection for the orange and green systems, but not the blue systems.

Historical Observations and New Measurements

A plot of historical observations can give further evidence as to whether or not the stars are physical. To construct such a plot, we put ourselves into the reference frame of the primary star by placing it at the origin. Then, we document the position angle and separation of the secondary star in Cartesian coordinates over time. If the secondary star appears to start curving around the primary, then we suspect that it might be in a mutual orbit. To find more evidence as to whether the star is orbiting or not, we can fit both a polynomial (curved) path and also a linear path. The fit with the higher value gives an indication of which type of solution might be more appropriate: an orbital or linear solution. In these fits, it is important to weight the measurements according to their presumed accuracy based on the method of measurement, the aperture of the telescope used, and number of nights of measurement. However, with the short arc binaries covered in this study, the value can be somewhat ambiguous. Due to the small amount of relative movement observed for these systems over time, the secondary star might simply pass the primary on the celestial sphere without orbiting it and still give a high value for the polynomial fit. This is why the other criteria must also be considered. Figure 3 shows an example of what type of fit is most appropriate for given types of historical data.

Instruments Used

The SkyNet (https://skynet.unc.edu) network of robotic telescopes was used for the measurements presented here. There are multiple telescopes and filters to choose from, though we did not use any filters for our images. The two telescopes we used were PROMPT8 and PROMPT3. PROMPT stands for Panchromatic Robotic Optical Monitoring and Polarimetry Telescopes, which were built by the University of North Carolina at Chapel Hill. They are 0.41m Ritchey-Chrétien telescopes, with rapid-readout (< 2 sec) Alta U47+ cameras. PROMPT8 is based in the Cerro Tololo Inter-American Observatory (Coquimbo Region, Chile). It has an aperture of 0.6m, a focal length of

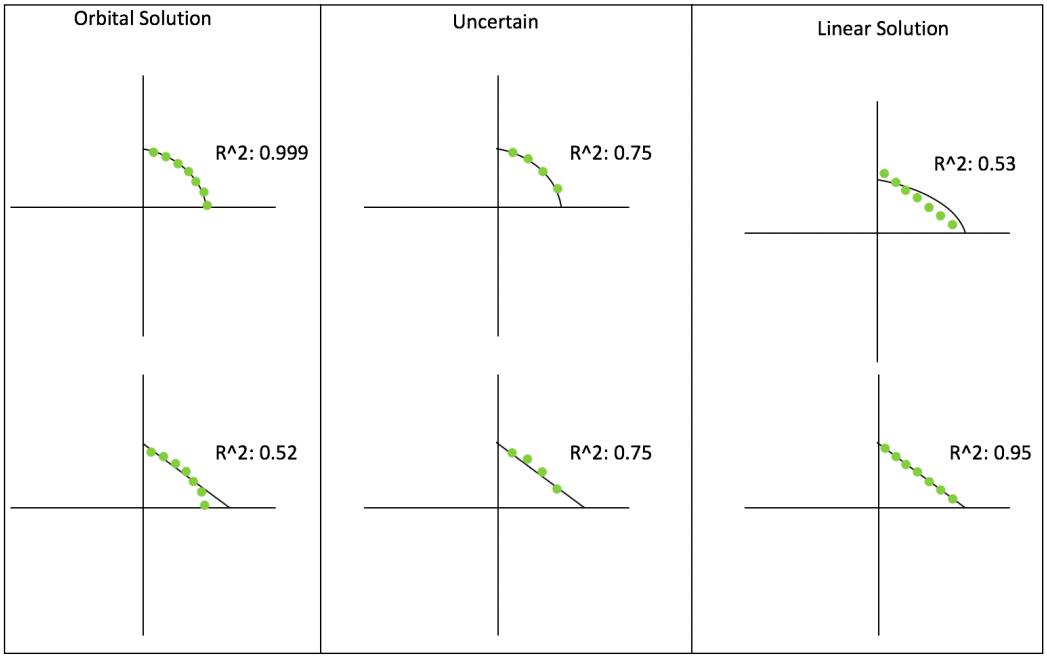

Figure 3: Sample Historical Data Fits with an Orbital Solution, Uncertain, and Linear Solution.

Investigation of 10 Systems in the Washington Double Star Catalog

STF 1985	PA ⁰	Sep "
1	355.79	5.88
2	357.61	5.48
3	356.11	5.82
4	352.49	6.47
5	355.62	5.55
Average	355.52	5.84
Standard Error	0.836	0.175
GIC 129	PA ⁰	Sep "
1	150.34	10.01
2	150.38	9.92
3	150.26	9.9
4	151.18	10.02
5	150.19	9.97
Average	150.47	9.96
Standard Error	0.161	0.013

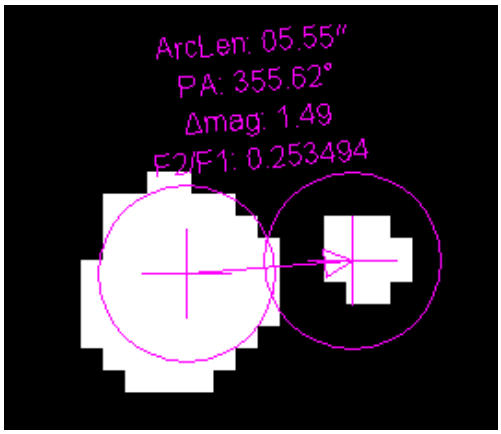

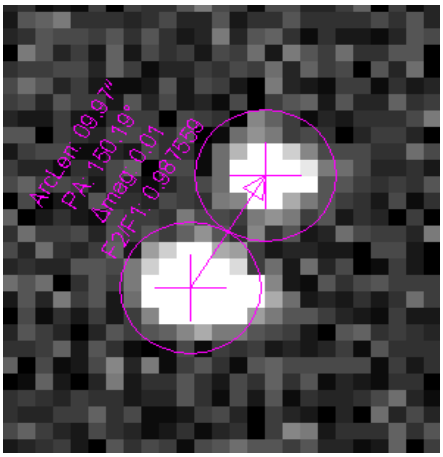

Table 4. Measurements of short arc binary STF 1985 using a 0.5s exposure time on the Prompt 8 Telescope on JD 2458557 (March 14, 2019), and measurements of promising physical system GIC 129 using a 4.17s exposure time on the Prompt 3 Telescope on March 12, 2019.

4200 mm, and a CCD size of 2048 x 2048 pixels. PROMPT3 is in Siding Spring Observatory (Coonabarabran NSW 2357, Australia). It has a 0.4m aperture and a focal length of 2939 mm, with a 1024 x 1024 pixel CCD. While PROMPT's primary use is to follow up gamma ray bursts, it can be used for many other purposes when it is not doing that, such as double star observations.

Measurements Made

Measurements on the systems that were able to be imaged by PROMPT at the time of this study can be seen below in Table 4. The tables are colored according to the scheme of Table 1.

Table 1 Red Systems: Binary Despite Lack of Gaia DR2 Data

Although Gaia DR2 does not have parallax or PM data, the red systems of Table 1 are binary because a sufficient amount of the orbit has been observed, as shown in Figures 4 and 5. It would possible, but highly unlikely, for the stars to move in this way if they were in fact at different distances from Earth. Excel's linear and polynomial fits are not done for the historical data on these systems because performing such fits involves the implicit assumption that the stars' trajectories do not double back on themselves as happens in an orbit. With the exception of an outlying point for STT 327 (which might represent a quadrant flip), their observations fall very close to the predictions of their respective Ephemerides.

Table 1 Orange Systems: Likely Physical with Short-Arc Orbital Solutions

As opposed to binary double star systems, physical doubles are gravitationally related, but not necessarily in an orbit around each other. The term "physical" can

(Text continues on page 312)

Investigation of 10 Systems in the Washington Double Star Catalog

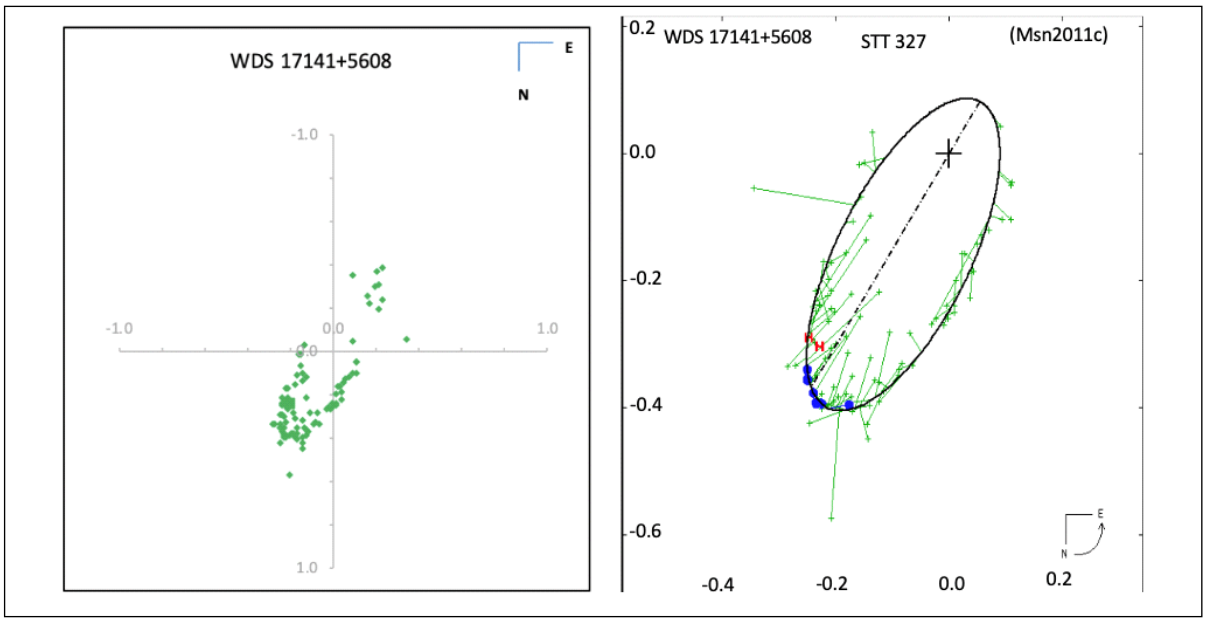

Figure 4: A plot of STT 327's historical data (left) and its proposed orbital solution (right).

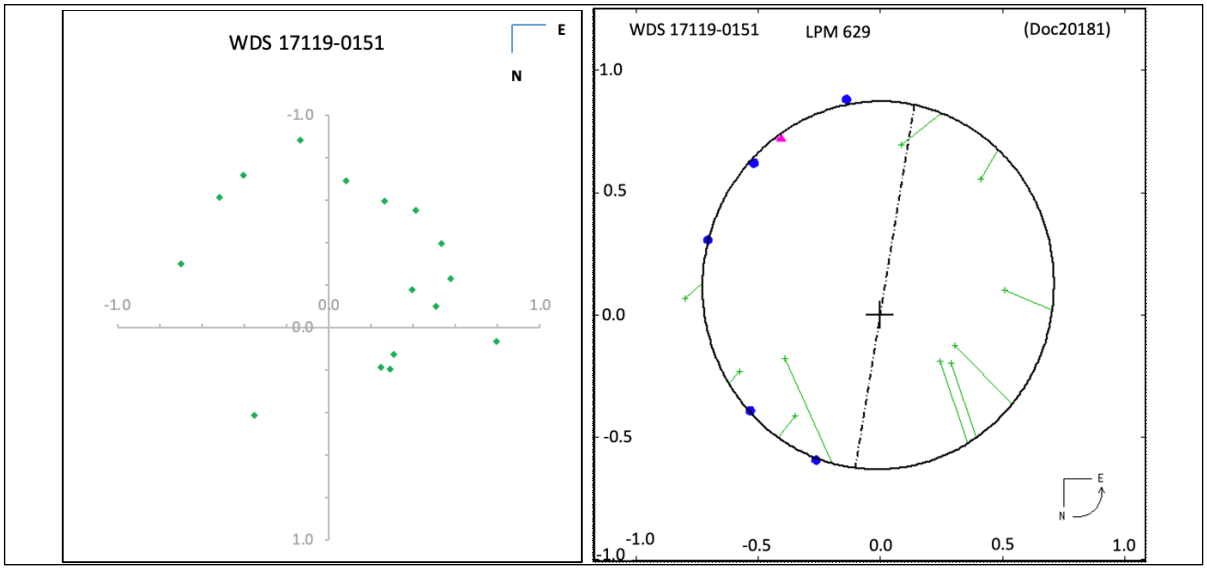

Figure 5: A plot of LPM 629's historical data (left) and its proposed orbital solution (right).

Investigation of 10 Systems in the Washington Double Star Catalog

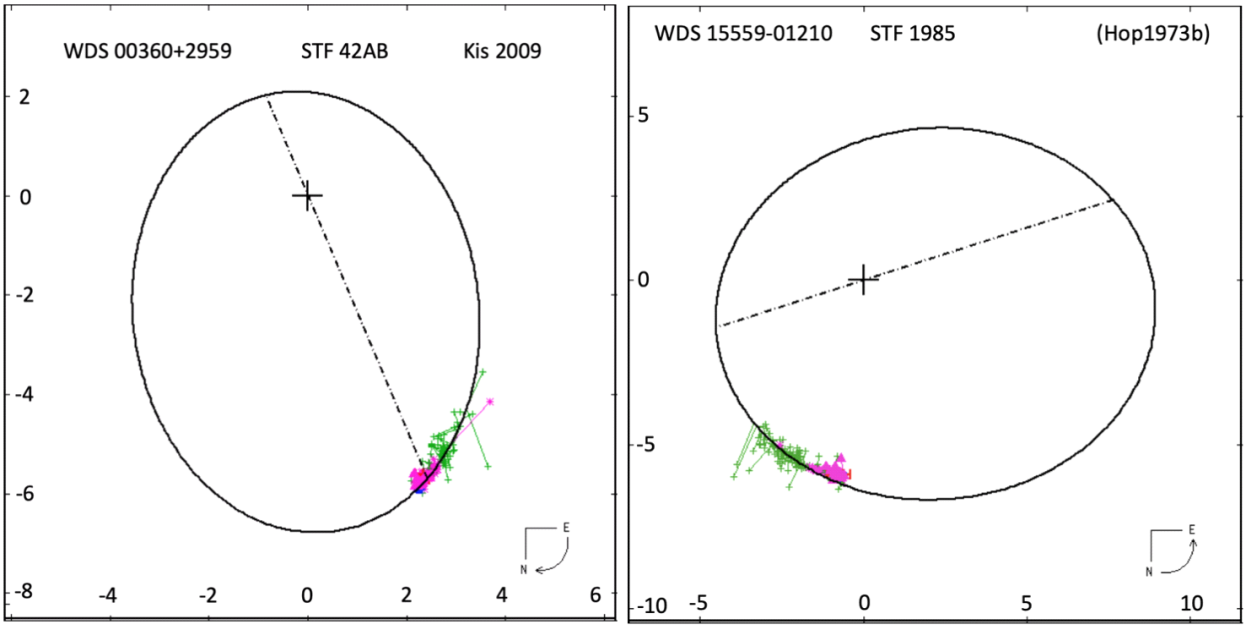

Figure 6: Short-arc binary solutions for physical systems STF 42AB (Kisselev, 2009) and STF 1985.

(Continued from page 310)

either mean that the stars are affecting each other gravitationally, or that they were born in the same gas cloud. The fact that they are in the same region of space and moving in the same direction might be due to their shared history. As is clear from Table 2, the orange and green stars are likely physical, though the amount of arc that the secondary has traversed in the last hundred years is too short to definitely classify them as binary.

For the orange systems, plots of the historical measurements do appear to exhibit curvature. These systems have common proper motion (STF 1985 has rPM 0.151, STF 42AB has rPM 0.020). The components of STF 1985 are less than a parsec apart from each other radially, while the components of STF 42AB are about a parsec apart from each other. However, insufficient time has passed for a large portion of their arcs to have been observed. The current short-arc orbital solutions for these systems are shown in Figure 6.

From examination of the plots, it appears that the more recent data for STF 1985 are deviating from the proposed orbit ephemerides. Some slightly better-fitting parameters were found using Hensley's Desmos tool (Hensley, 2018). They are shown in Figure 7 and at this link, https://www.desmos.com/calculator/csieeekyi1..

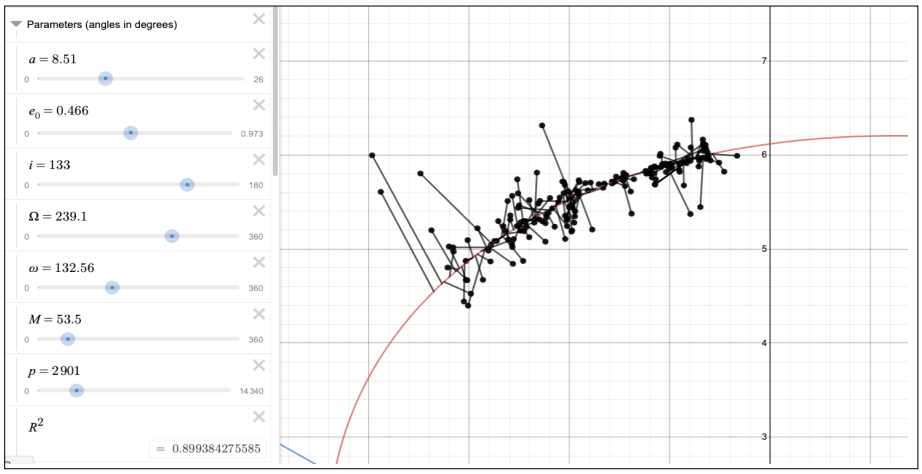

Figure 7: Better-fitting parameters for STF 1985 found using Hensley's Desmos tool (Hensley, 2018). (https://tinyurl.com/y2jkc6es)

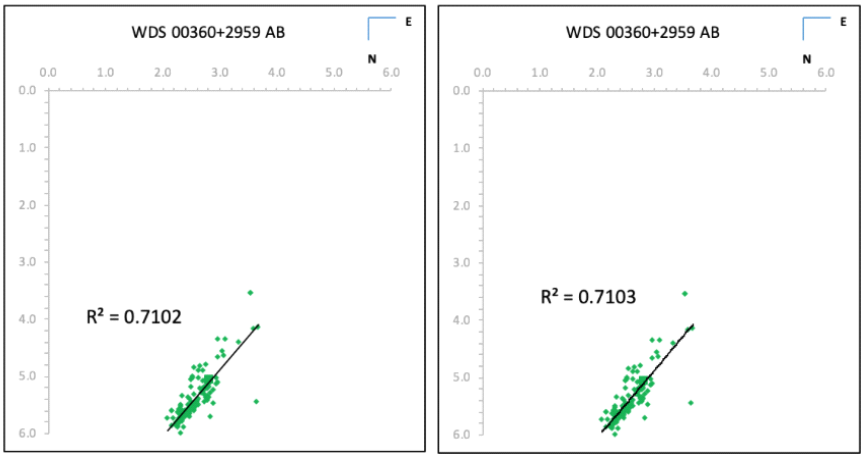

Figure 8: STF 42AB The position of the secondary relative to the primary with a linear line of best fit (left) and with a 2nd order polynomial fit (right).

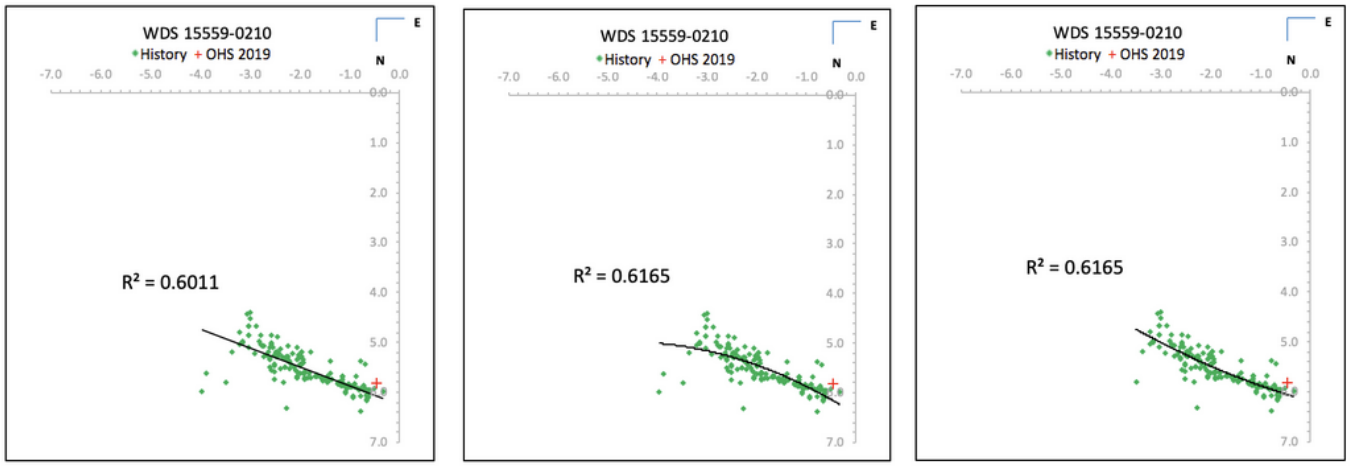

Figure 9: STF 1985 linear (left) and polynomial (right) fits. The polynomial fit at the far right has three outliers removed. The outliers were identified by the fact that they were more than 3 standard deviations from the mean of the other measurements.

However, even with the improved parameters, the data do not definitively show an arc for either of these systems. The early points have a lot of scatter. Linear and polynomial fits for both STF 42AB and STF 1985 are shown in Figures 8 and 9. For STF 1985, the polynomial fit initially appears to curve away from the primary star, which does not bode well for physicality. Removal of the three most egregious outliers (from the years 1823, 1830, and 1872, respectively) causes the polynomial trajectory of the secondary to curve around the primary star as would be expected for a binary system. However, the R^2 values are in all cases so similar that it is not possible to draw a conclusion from the fits. For STF 42AB, the values of both fits are also too close to be discriminant, having a difference of 0.0001. While this system's proposed orbit seems to be following its proposed ephemeris, there is substantial uncertainty because the proposed orbit indicates a period of roughly 1900 years.

Table 1 Green Systems: Candidates for Physicality, In Need of Time and Measurements

The green systems from Table 1 are likely to be physical and possibly even bound based on parallax and proper motion. However, not enough time has passed for an orbital solution to be convincing. Their historical data are too sparse and noisy for the seeming curvature of the fits shown in Figures 11 and 12 to be indicative of their actual trajectories. These systems are shown in Figures 10 and 11.

Harrington et. al. inferred the existence of another, unseen companion for the $0.3M_{\odot}$ dwarf star GIC 129 from its sinusoidally deviating proper motion and paral-

(Text continues on page 314)

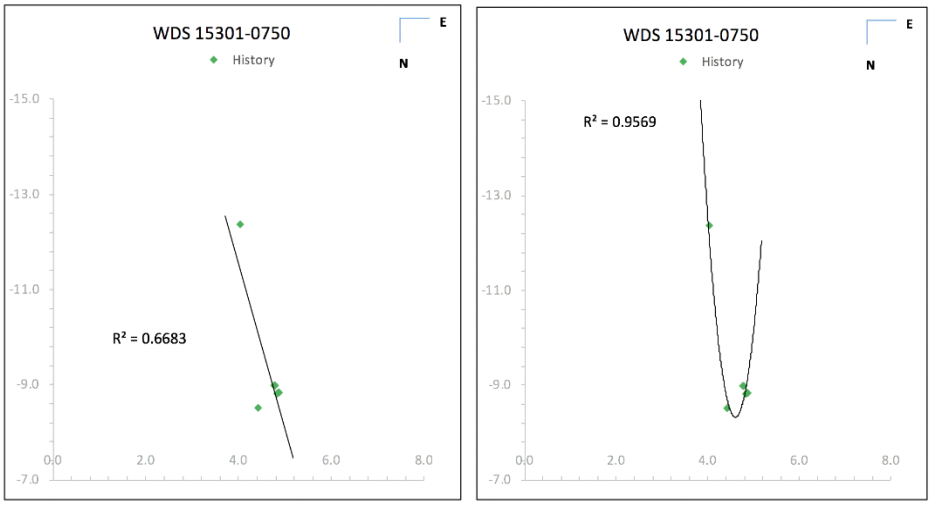

Figure 10. The position of the secondary with respect to the primary star of GIC 129 with a linear line of best fit (left) and a 2nd order polynomial fit (right).

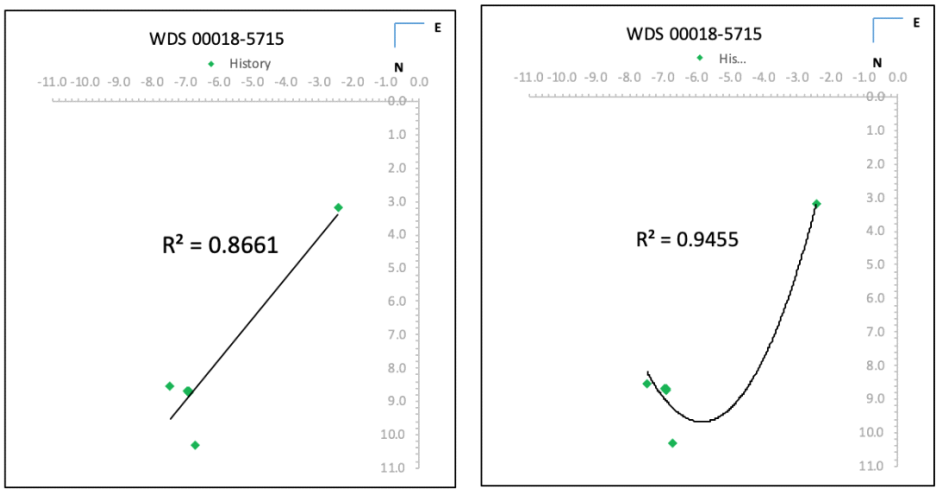

Figure 11. The position of the secondary with respect to the primary star of HJ 5438 with a linear line of best fit (left) and a 2nd order polynomial fit (right).

lax (Harrington et. al., 1988). They plotted the residuals (meaning the error from what would be predicted if the primary star was moving in a straight line and had a constant parallax), and found that those residuals had a sinusoidal variation that was consistent with another mass of approximately $0.1M_{\odot}$ tugging gravitationally on the primary. They were able to solve the orbit, which has a period of 6 years. Follow up observations of GIC 129 could confirm the association of both the WDS secondary and also possibly the unseen companion of this interesting, nearby dwarf star.

Table 1 Blue Systems: Optical Doubles

All three of the blue systems from Table 1 are optical based on the parallax and PM data from Gaia DR2 referenced above. One of these, J 868, has a solved orbit, shown in Figure 12 below, but this system should be reclassified to an optical double.

Purple: Unknown

The purple system, HDO 182, has very strange orbital solution on file, which is shown in Figure 13. When we plot the historical observations, the system appears to be following a different trajectory, as shown in Figure 12 at the right. The two observations at the upper left of the historical data plot were made a long time ago (1901 and 1910, respectively). It is reasona-

(Text continues on page 315)

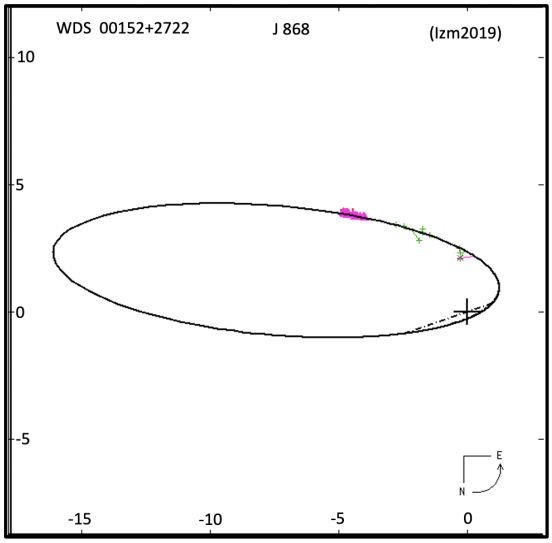

Figure 12: Orbital solution for J868.

ble to assume that with the instruments available at the time, the error of the measurements for such a close double would be large. Therefore, although the fits seem to imply curvature, the curvature should be approached with skepticism, both because of the presumed measurement error and also because of the low R2 values. This system also does not currently have any parallax or PM data, making any further analysis impossible. Thus, we are classifying this system as uncertain.

Conclusion

This project has explored several types of double star systems and we have classified them by color. The red stars (STT 327 and LPM 629) are clearly orbiting, despite lack of parallax or PM data. The orange systems (STF 42AB and STF 1985) are short arc binaries which might be confirmed as they traverse their orbits over time. The green systems (GIC 129 and HJ 5438) are likely physical and possibly gravitationally bound, and are in need of further measurement to confirm their status. The blue systems (J 868, D 6, and AG 87) are optical, and the purple system (HDO 182) is interesting but uncertain. We were able to contribute PA and separation measurements for STF 1985 (a short arc) and GIC 129 as part of this study.

Acknowledgements

This research has made use of the Washington Double Star Catalog maintained at the U.S. Naval Observatory, the SkyNet Robotic Telescope Network, the Stelledoppie catalogue maintained by Gianluca Sordiglioni, and AstroImageJ software written by Karen Collins and John Kielkopf at the University of Louisville, updated for double star astrometry by Karen Collins.

This work has also made use of data from the European Space Agency (ESA) mission Gaia (https://www.cosmos.esa.int/gaia), processed by the Gaia Data Processing and Analysis Consortium (DPAC, https://www.cosmos.esa.int/web/gaia/dpac/consortium). Funding for the DPAC has been provided by national institutions, in particular the institutions participating in the Gaia Multilateral Agreement.

The authors would like to especially thank Dr. Brian Mason for patiently responding to our numerous requests for double star historical data and Richard Harshaw and Rachel Freed for their assistance and ongoing support in guiding us through the analysis.

References

Dugan, Owen, Thomas Robinson, Finnian Carmeci, and Kalée Tock. “CCD Measurements and Reclassification of WDS 07106 +1543 to an Optical Dou-

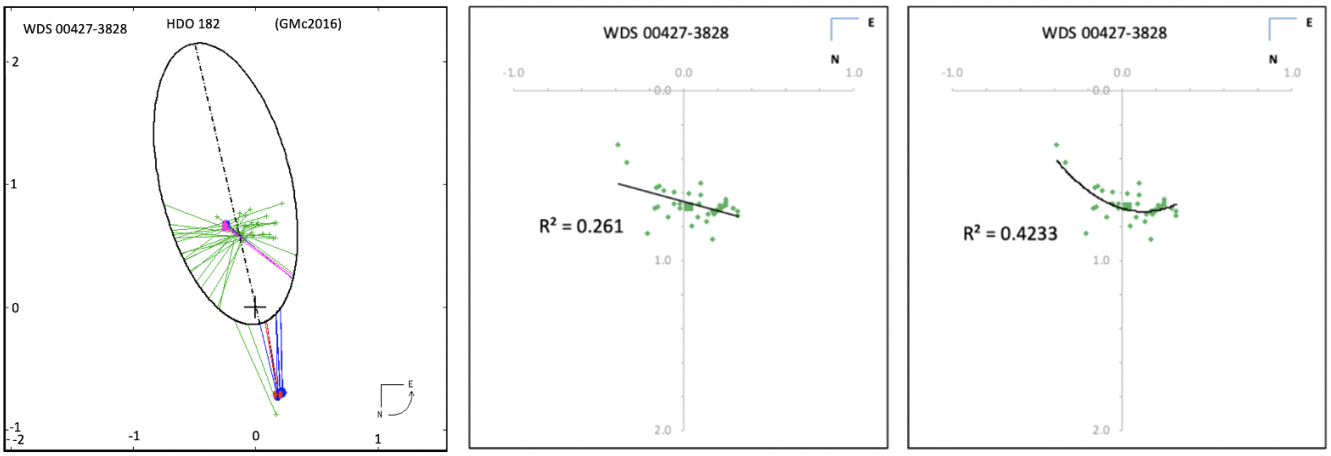

Figure 13. HDO 182’s orbital solution (left) and the historical data with a linear line of best fit (middle) and the 2nd order polynomial fit (right).

(Text continues on page 316)

ble", *Journal of Double Star Observations*, l 15, No. 1, 2018, pp. 119 - 129.

Harrington, Robert S, Dahn, Connard C. "The Unseen Companion of G152-31". The Astronomical Journal: Vol. 96 No. 2, 1988 pp. 718

Harshaw, Richard W. "CCD Measurements of 141 Proper Motion Stars: The Autumn 2015 Observing Program at the Brilliant Sky Observatory, Part 3", Journal of Double Star Observations: Vol. 12 No. 4, 2016 pp. 394 - 396.

Hensley, Hagan. "The Double Star Orbit Initial Value Problem", Journal of Double Star Observations, Vol. 14, No. 2, 2018, pp. 353 - 356.

Kisselev, A.A., L. G. Romanenko, and O. A. Kalinichenko, 2009. "A Dynamical Study of 12 Wide Visual Binaries", Astronomicheskiĭ Zhurnal, 2009, Vol. 86, No. 2, pp. 148–157.

Upgren, A.R. and J.R .Caruso. "Space Motions of Low-Mass Stars", The Astronomical Journal: Vol. 96 No. 2, 1988 pp. 1 - 22.

Wikipedia contributors. (2019, June 27). Position angle. In Wikipedia, The Free Encyclopedia. Retrieved 22 November, 2019.

Additional Stars with Evidence of Orbital Motion

John Greaves
cpmjg@tutanota.com

Abstract: High proper motion pairs with similar parallax and similar but still differential proper motion are examined and presented as candidate orbital motion targets.

Introduction

In Greaves 2020 a list of potentially orbiting pairs lying within 20 parsecs is presented based on candidate selection processes relating to close similarity of parallax and high but significantly differential proper motion within a pair as obtained from Gaia Data Release 2 (eg Brown 2018). The list is also filtered to remove all pairs with published orbits and in some cases measures provided by the Washington Double Star Catalog (henceforth WDS, Mason et al 2001) are utilised as evidence of historic mutual motion for the pair of a form that can be interpreted as indicative of an orbital path.

Here additional candidates are presented to farther distances and with less stringent selection criteria whilst otherwise using the same methodology outlined in Greaves 2020. Basically a greater leniency is adopted with respect to the ratio of parallax for the pairs due to the vagaries of Gaia DR2 parallax measures, extending the parallax ratio threshold from 1:1.01 to 1:1.2. Despite a much larger value this approach is validated by the fact some of the farthest candidates with some of the worst parallax ratios given below lay adjacent in Gaia DR2 parameter space to long known classical pairs with published orbits that also appear in the course of the analysis. As a comparison in Greaves 2004 common proper motion pairs were checked against two astrometric catalogues with mean epochs up to a century or more apart, yet despite this the highest motion objects showed a fixed relationship over that time with both separation and position angle barely altering in the intervening time-- that is, they were either completely unchanged over roughly a century or they showed changes that were of a size that could be readily dismissed as being within the positional uncertainties of the catalogues. The figures presented here show motions in marked contrast to that even over temporal baselines much shorter than a century, although it has to be granted that the proper motions in that study are around an order of magnitude smaller than in the current one.

As with Greaves 2020, the presented objects are at times very challenging observationally. After all, if they were easy their details and orbits would likely already be known, as is the case for many easier pairs, and quite a few difficult ones. Nevertheless all but a few of the objects presented already appear as pairs in the WDS, thus have been observed and indeed measured at some point, at least for the "classical" pairs. Other pairs may well be amenable to the new digital imaging techniques such as drift scanning or so called lucky imaging. Still others may well be beyond even the best equipped amateur using a quality refractor at very high powers due to the pair's faintness and/or large differential magnitude as most pairs able to show significant relative motion over decades are rarely more than a few arcseconds apart, even at greatest separation. Also, as distance increases the number of close-together -on-the-sky relatively nearby pairs found only very recently in modern high resolution surveys, such as Gaia, show a proportionate increase in number. It is not always clear whether these were missed in the past simply because of being too difficult visually as pairs with similar particulars had been discovered in the past and in some instances have even been sufficiently observed over time to have had published orbits. Past classical

Received March 4, 2020.

surveys intended to discover visual double stars with the potential to be orbiters often were undertaken as systematic visual searches down to a relatively bright limiting magnitude, whilst some objects will have been discovered purely serendipitously, whereas surveys like Gaia go deeper, more inclusively and to a high spatial resolution.

Results

These follow several levels.

The results for the most promising objects are presented in Table 1 with the pairs with good measurement history at the WDS having figures illustrating their motion based on data kindly provided by the WDS (Matson & Mason 2020). Some instances of isolated highly disparate measures have been left out of the figures for illustrative purposes, these are usually a small number of outliers not matching other more similar dated measures whilst for others having very long observational history the earliest measure(s) often appear to be approximate and can disagree quite markedly with other measures made only a few years afterwards. The remainder of Table 1 objects not having illustrative figures contain objects with either insufficient measures or measures at times contradictory enough to neither suggest nor deny relative motion analogous to that expected from orbital motion, that is the data are noisy. Individual objects are noted after the table with extra information for each system. For instance, some of these systems are hierarchical, that is there is a candidate orbiting pair which itself forms a common proper motion system with a third star showing relatively fixed motion in comparison to it. The projected separation is giving for some of the pairs as the intrinsically nearer a pair are together the higher the current rate of relative motion is likely to be.

In some instances the pair are logged in the WDS as having a linear solution, however given their similar distances, similar high to very high proper motions (albeit differential ones, yet the motion difference is negligible in comparison to the overall motion) and close projected separation (usually a few arcseconds at most) it would be a remarkable coincidence for them to be merely happenstance associations of two random field stars. Indeed, all WDS linear solution objects with separations of only a few arcseconds could benefit from a cross matching of both components' parallax (to a reliable distance) and their proper motions checked with Gaia DR2 as sufficient agreement listed in the former for objects with high motion in the latter would be indicative of a physical rather than a happenstance association. These objects therefore constitute two levels, those with at least good particulars as well as somewhat confirmatory historical measurements and those that have at least good particulars but few and/or internally contradictory confirmatory historical measurements.

Table 1 carries the WDS Discovery Identifier, the Gaia DR2 Epoch 2015.5 position of the primary, the respective proper motions of the pair, the distance in parsecs of the pair simply derived by inverting their Gaia mean parallax and rounding to the nearest whole number, the Gaia DR2 magnitude for each of the pair and their Gaia DR2 derived position angles and separations rounded to one and two decimals respectively. The table is sorted on increasing distance. The nearer the pair are to the Sun, in combination with the smaller their projected separation is and the greater their differential proper motion, then the 'faster' their orbit is likely to be. However, the projected apparent orbits are not circular, having multiple forms and levels of eccentricity and not strictly elliptical orbits as the primary can be offset from one of the foci, not to mention that as demonstrated by differential proper motion a fixed position primary is an idealised state used for convenience. Accordingly generalising from Kepler's Second Law of planetary motion the apparent motion of the secondary around the primary will not be at a fixed rate and an apparent 'fast' object may in fact be simply near periastron, whilst a slow moving secondary may be near apastron, with eccentric to highly eccentric orbits at times presenting relatively slow monotonic motion well represented by the same linear solution also applicable to optical pairs.

Meanwhile, many of the pairs spat out by the analysis are not "classical" pairs in that they have been first noted and added to the Washington Double Star Catalog since the turn of the millennium and thus have insufficient measures to demonstrate any relative motion at all, even if present. A significant number of these are in fact pairs revealed by datamining (at times better described as data-trawling) of Gaia DR2 so the only measure available for them is predominantly based on the single one derived from the data in that survey. Even some of the "classical" pairs have limited data with measures effectively often consisting of only their discovery epoch positions (of varied quality) and Gaia dr2 epoch positions and little to nothing else. All these other pairs, both "classical" and "new" are listed in Table 2 which is simply presented as a Finding List. These Table 2 objects have little to no confirmatory historical measures and their listing as candidate orbital motion objects is only via inference based on the similarity in their particulars to known orbiting cases and the better evidenced Table 1 cases. Roughly half of these objects have intrinsic projected separations of between 25 and 40 AU but will be difficult visually as the

(Continued on page 321)

Additional Stars with Evidence of Orbital Motion

NAME	RA	Dec	pmra1	pmdec1	pmra2	pmdec2	dist	Gmag1	Gmag2	PA	sep
BEU 6	69.55464	28.21622	396	-92	381	-83	13	11.6	12.1	303.4	1.18
HDO 298	334.56825	-53.62978	441	-630	428	-665	14	5.2	9.2	49.0	1.87
WTR 1	327.29873	-41.55896	279	-229	308	-179	15	10.9	11.3	133.4	2.67
ST 8AB	130.68651	9.55397	224	-632	200	-575	16	8.9	11.9	41.7	1.49
A 53AB	79.80577	-3.07322	700	138	653	99	16	7.5	9.9	305.6	1.55
BU 1246AB	214.75201	-25.81385	-359	365	-366	344	18	5.7	10.6	230.5	3.57
HEI 31	58.61776	16.61533	214	-167	210	-194	20	6.6	10.4	238.8	3.55
WOR 4AB	51.02801	23.78451	215	-120	201	-114	21	9.9	10.8	340.0	2.60
LDS5677	97.66118	-2.09901	-116	-161	-113	-172	21	13.9	15.2	317.6	4.48
LDS 935	184.21326	2.96913	-651	258	-652	284	23	12.1	15.3	177.1	2.13
CPO 138	97.96133	-43.53416	-278	-30	-264	-13	24	10.0	11.6	219.2	3.34
LDS3331	29.80272	3.51934	263	24	266	44	24	10.5	11.1	54.5	4.15
HDO 127BC	152.05216	11.99699	-254	8	-225	9	24	7.9	11.3	94.0	2.05
A 322AB	89.59005	-4.65153	75	-201	79	-237	24	6.8	10.7	34.4	2.22
LDS4802AB	284.41001	53.52067	256	-53	241	-44	25	12.0	12.1	196.3	2.29
LDS1891	281.04350	71.48883	33	151	21	145	25	13.4	13.6	277.7	3.21
GIC 169	325.00791	54.13970	473	340	466	320	29	12.1	14.0	78.2	1.23
KUI 6BC	20.75457	-12.95850	452	-25	481	-34	30	9.8	11.7	327.4	1.37
STF2928AB	339.89525	-12.61580	223	-147	228	-168	37	8.3	8.3	280.8	3.08
HU 1153	222.90500	15.31796	-241	92	-207	102	43	8.2	10.5	296.2	3.02
STF 544AB	66.17416	-8.75398	-111	-171	-130	-153	45	8.3	9.2	352.0	3.34

Table 1. Orbital candidates with evidence of historical relative motion over time. (the Name is the WDS Discovery Code, Right Ascenscion and Declination are in decimal degrees, pmRA are proper motions for Right Ascension in milliarcseconds, pmDec are proper motions for Declination in millarcseconds, dist is the distance in parsecs from taking the mean of the pair's parallax and then simply inverting it, Gmag are the Gaia DR2 magnitudes which are red biased, the PA is the position angle in degrees and separation is in arcseconds).

Table 1 Notes:

BEU 6 This red dwarf pair is had a relatively recent close approach to the primary is but now widening again. Projected separation is around 16 AU, less than the Sun-Uranus distance.

HDO 298 Possibly closing towards periastron as shown in Figure 1. The primary has the spectral type G0 V. The projected separation is 26 AU.

WTR 1 There is a linear solution in the WDS.

ST 8AB The AB pair is widening after a close approach to the primary around the turn of the Millennium. Projected separation is 24 AU (or slightly further than the Sun - Uranus distance). The common motion similar distance LUY 6218 AB C has separation 114.6 arcseconds in position angle 96 degrees (2015.5) and is physically lying at a projected separation of roughly 1800 AU. The CD pair is optical.

A 53AB The historical motion is depicted in Figure 2. A53 AB C is optical. The AB pair have a 2015.5 projected separation of 25 AU.

BU 1246AB The WDS gives the AC pair a linear solution. The AB pair has been very slowly widening for over a century but with some more pronounced movement in position angle.

(Notes continue on the next page)

Additional Stars with Evidence of Orbital Motion

(Table 1 notes continued from page 319)

HEI 31 The WDS measurements are few but it has widened by roughly an arcsecond in 35 years whilst changing about a dozen degrees in position angle. Radial Velocities for the pair are 19 and 18 km/s respectively.

WOR4 AB The pair is slowly widening with motion currently appearing linear as can be seen from Figure 3. There is also a third component giving LDS 884 AB C with C at 99.2 arcseconds separation in a position angle of 118 degrees and of common motion and parallax to AB. The AB projected separation is 54 AU whilst AB C are roughly 2100 AU apart.

LDS 5677 A red dwarf and white dwarf pair.

LDS 935 This red dwarf and white dwarf pair has been slowly closing over the past 80 years.

CPO 138 This pair has closed by one arcsecond over 70 years but with no real change in position angle such that a linear solution would readily represent the historical motion. The common high proper motion and very similar parallax suggest instead that it is in a relative monotonic phase of an eccentric orbit.

LDS 3331 This pair has closed by nearly one arcsecond over 50 years in tandem with over a 20 degrees change in position angle.

HDO 127BC This pair is a well known companion to Regulus, sharing both proper motion and parallax with it and lies 176 arcseconds from said in a position angle of 308 degrees. This equates to a projected separation of around 4250 AU whilst the BC pair have a projected separation of 50 AU at 2015.5. The pair have closed by around 2 arcseconds in 150 years with little change in position angle such that a linear solution would currently represent the motion.

A 322AB The pair has closed by roughly two arcseconds with appreciable change in position angle for just over a century, and gives some hint of an orbital arc, however there is a 70 year plus gap lying between the first and recent observations. A fourth star, denoted LDS 3684 D, lies 89 arcseconds away in 313 degrees position angle and shares the motion and parallax of the AB pair thus it has a projected separation of roughly 2150 AU from the pair in comparison to their own projected separation of 54 AU. The G dwarf primary has a radial velocity of 143 km/s and metallicity less, but not markedly so, than that for the Sun, so could be a Thick Disk object. A 322AB C is optical with a linear solution in the WDS.

LDS 4802AB The fainter star C lies 41.7 arcseconds distant in a position angle of 162 degrees and shares the same motion and parallax as the AB pair lying at a projected separation distance of roughly 1030 AU in comparison to the 57 AU projected separation of the AB pair. C is a white dwarf.

LDS 1891 For over 50 years the pair have widened by more than an arcsecond in tandem with a change in position angle of around a dozen degrees.

GIC 169 The projected searation is 36 AU, which is just a little beyond the Sun - Neptune distance.

KUI 6BC The primary, GAL 307A, shares the same motion and parallax as the BC pair as well as having the same 35 km/s radial velocity as B and lies 40.5 arcseconds from B at a position angle of 313 degrees which equates to a projected separation of around 1220 AU, whilst the projected separation of the BC pair is 41 AU, roughly one and one third the Sun - Neptune distance.

STF 2928AB This pair has a linear solution in WDS whilst Figure 4 suggests an orbital arc with the secondary slowly closing in on the primary in recent decades. Outliers have been retained as there is sufficient density of observations for them not to detract from the overall trend. Much fainter STF 2928 C actually shares the proper motion and parallax of this pair and lies at position angle 48 degrees some 138.6 arcseconds distant which at 2015.5 gives a projected separation of roughly 5100 AU from the 113 AU AB pair's projected separation. D is optical. The BC primary is spectral type G9 V with chromospheric emission lines and is listed as the extremely low amplitude BY Draconis variable of uncertain period NV Aqr, however for close pairs like this duplicity induced pseudo-variability is not unknown and BY Draconis variables are usually mid to late K or M dwarfs, although the differential magnitude between A and B suggests the latter may be a K dwarf which is not too faint to affect the overall brightness at the centimagnitude level. The A, B, C grouping may well present a yellow, orange, red combination visually, if it is possible to split AB whilst retaining C in the field and further C is not too faint for any colour to be discerned.

HU 1153 Noted as with a linear solution in WDS this slowly closing pair is shown in Figure 5. Radial velocities are -11 and -13 km/s respectively.

STF 544AB This pair has widened by just over an arcsecond in around 190 years whilst demonstrating little change in position angle, as shown in Figure 6, such that the motion to date could be well described by a linear solution. WDS notes that the primary is itself a spectroscopic binary. FOX 138C is optical.

Additional Stars with Evidence of Orbital Motion

NAME	dPMRA	dPMDEC	dist	NAME	dPMRA	dPMDEC	dist
NSN 100	9	14	19	HDS 804	13	14	25
DAE 8	28	31	19	A 762	3	18	25
NSN 752	6	11	20	LDS2753	10	20	26
GRV1284	20	26	20	B 620	15	15	26
MCT 12	18	35	21	HDS2687	13	4	26
KPP3116	19	16	21	KPP2995	15	20	26
KPP2786	2	18	21	LDS6202	8	20	27
TSN 118	5	31	21	KPP3113	6	20	27
MCT 10	27	6	21	HDS1691	17	7	27
NSN 596	24	16	21	HDS 484	16	17	27
HDS 544	48	31	21	GRV1285	20	8	28
LDS1261	3	14	22	NSN 616	3	17	28
JNN 61	9	18	22	KPP3199	23	13	29
KPP2790	20	18	22	NSN 760	20	11	30
LAW 19	5	15	22	HDS1060	37	8	30
NSN 374	24	4	22	KUI 6BC	29	9	30
HDS3133	16	3	22	KPP3040	1	22	31
NSN 273	2	16	22	NSN 466	21	14	31
KPP3229	1	29	22	CRC 76	29	15	31
NSN 75	3	19	22	KPP2784	2	27	31
KPP3335	14	17	22	NSN 608	32	5	32
JAO 4	21	10	22	SKF1633	23	4	32
KPP3378	1	19	23	SKF2836	31	28	33
NSN 441	11	17	23	GRV1286	6	30	33
TOK 22	38	7	23	GRV1287	48	8	34
NSN 453	5	13	23	LDS6304	20	12	34
CRC 46	6	21	23	JNN 285	23	1	35
SKF 428	17	19	23	CRC 43	20	58	36
NSN 716	9	15	23	HDS 366	31	14	40
KPP3388	18	10	24	GRV1288	23	10	54
CRC 67	22	15	25	HDS 188	26	11	60
SKF 453AB	13	11	25	GRV1289	23	16	67

Table 2. A Finding List of Candidate Pairs With Orbital Motion Based On Common But Somewhat Different High Proper Motion and Common Distance (The WDS Discovery Code, differential proper motions in both Right Ascension and Declination given in milliarcseconds and their distances in parsecs as the inverted mean of the pairs' parallax are given. Objects denoted GRV1284 through GRV1289 are running numbers used for convenience as there is no matching pair in neither the WDS nor the WDSS at time of writing).

(Continued from page 318)

separations on the sky lie between 0.75 and 2.0 arcseconds.

On a second level Table 2 also includes several objects with the Discovery Code column merely carrying a GRV running number for convenience due to want of a referential handle as they are not currently listed in either the WDS or the WDSS as of March 2020 thus having no identifiers, but are revealed by Gaia DR2 data as a natural consequence in this analysis. To not include them would be negligent as three of the pairs are currently just slightly farther apart than the Sun – Neptune distance and may well be liable to show marked relative motion to observers in the nearer future.

As stated, Table 2 is presented as a finding list for interested observers and/or measurers looking for a project, primarily provided as the data were generated by the analysis and may be of some utility or interest to some as opposed to just being thrown away. Accordingly, and as in the vast majority of cases the last measure in the WDS is either Gaia DR2 derived or the Gaia DR2 measure is given as the pair was discovered via Gaia DR2 data, only minimal information is provided to avoid cluttering things with endless detailed lists. The Discovery Code from the WDS as identifier plus their Gaia DR2 derived differential proper motion in milliarcseconds for each pair in both Right Ascension and Declination are provided plus their inverted mean Gaia DR2 parallax rounded to an integer. The novel pairs have their derived astrometric particulars mentioned after the table.

Table 1 enables better equipped observers to contribute further measurements to be added to those already known in order to enable enough data for orbits to be eventually determined. Table 2 enables all observers, whether well equipped or just the casual observer, to pick target stars to be followed over the years,

(Text continues on page 324)

Additional Stars with Evidence of Orbital Motion

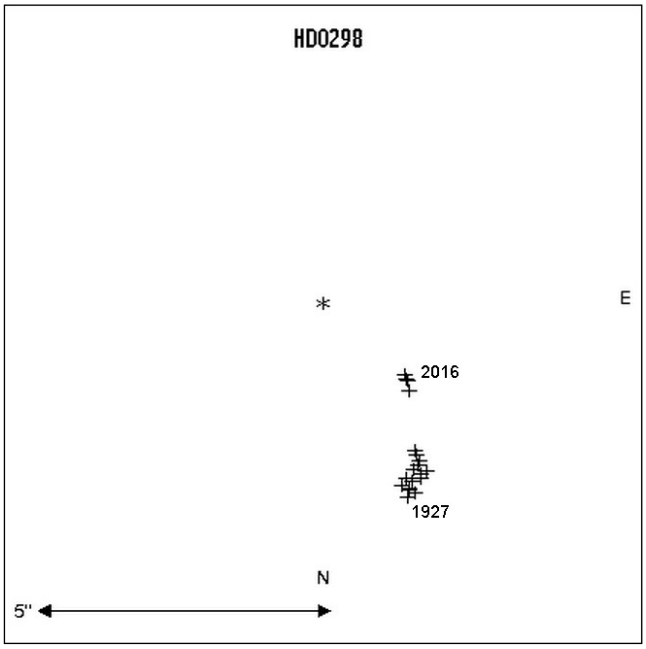

Figure 1 HDO 298

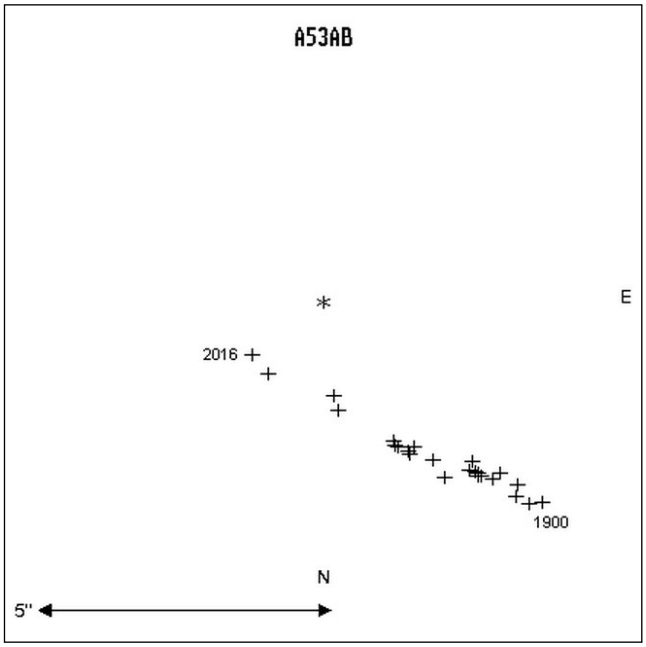

Figure 2 A 53AB

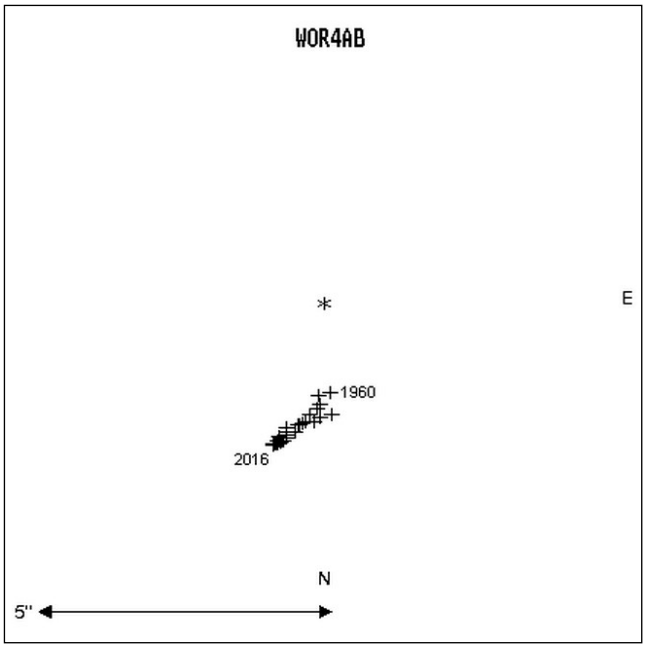

Figure 3 WOR 4AB

Additional Stars with Evidence of Orbital Motion

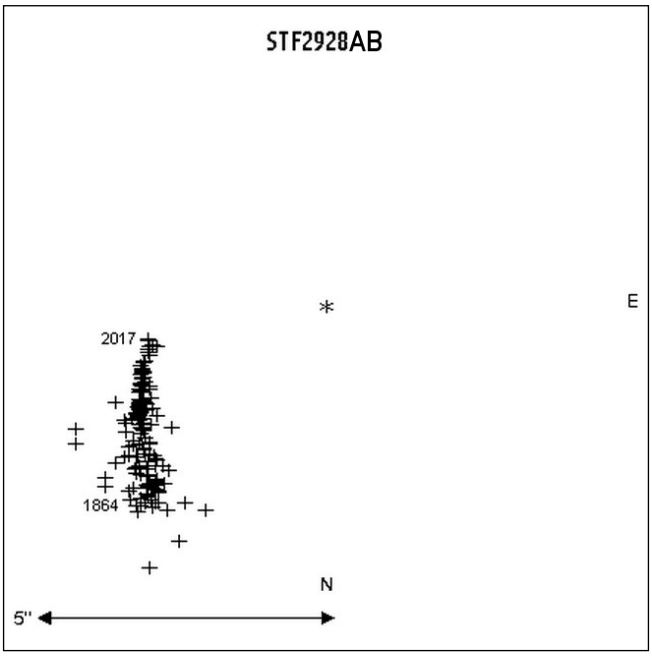

Figure 4 STF 2928AB

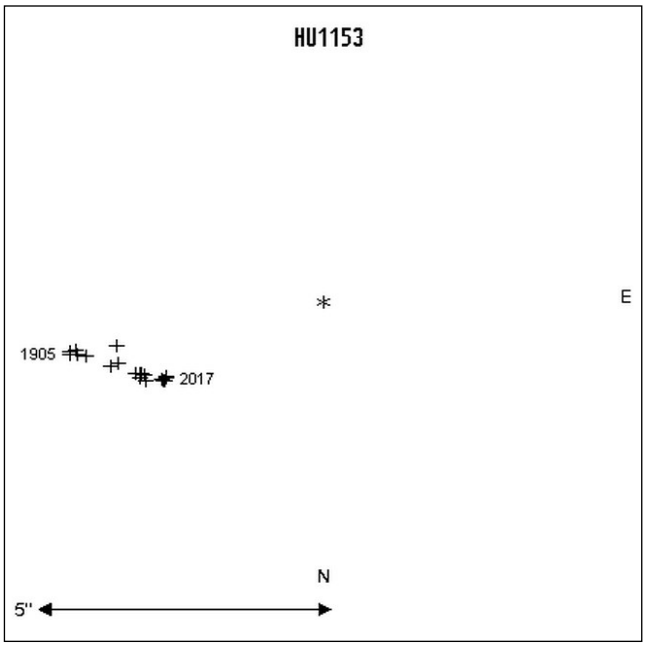

Figure 5 HU 1153

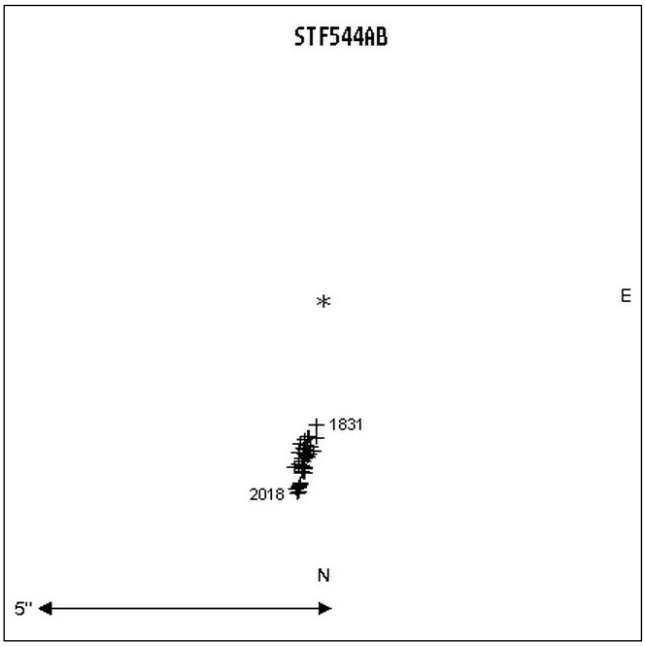

Figure 6 STF 544AB

(Continued from page 321)

whether to make measures for future orbit determinations or simply for the aesthetic pleasure of seeing change in the "fixed heavens". This latter can be rewarding in itself, as it is very engaging to watch either a variable star change it's brightness, see a transient appear in a familiar star field, see the relative motion of very high proper motion star against field stars over years, or see a pair of stairs over years to decades became closer or wider apart and in some rare cases both. These data are therefore also presented to those interested in the changing of the "fixed heavens".

For the new pairs the Gaia DR2 derived positions in decimal degrees, position angles in degrees, separations in arcseconds and magnitudes respectively are GRV1265, 120.01167, -40.04233, 8.2, 1.93, 9.1, 12.7; GRV1266, 319.13574, -47.56831, 162.6, 2.19, 13.1, 13.3; GRV1267, 239.46925, 43.89477, 158.7, 0.93, 12.5, 12.5; GRV1268, 66.75275, 48.88013, 46.8, 1.10, 13.0, 13.1; GRV1269, 358.92394, 25.14404, 45.8, 3.41, 8.7, 14.5; GRV1270, 291.77344, 46.45236, 48.0, 1.67, 8.9, 12.5. GRV 1265, 1267 and 1268 have projected separations of 39, 31 and 37 AU respectively, which are around to just beyond the mean Sun – Neptune distance.

Conclusion

As demonstrated in Greaves 2020 Gaia data release 2 is able to provide high motion pairs of stars with sufficient differential proper motion to suggest orbital motion. Selection of appropriate objects from such a subset of data enables either the measurement over time of the pairs in order to provide extra data potentially enabling an eventual orbital determination, especially for pairs already having a long history of measurement, or for the simple enjoyment of watching (or imaging) the change over time.

References

Brown A.G.A., Vallenari A., Prusti T. et al., 2018, arxiv.org/abs/1804.09365v2

Greaves J., 2004, MNRAS, 355, 585-590

Greaves J., 2020, Webb DSSC 28, in press

Mason B.D., Wycoff G.L., Hartkopf W.I., Douglass G.G., Worley C.E., 2001, AJ, 122, p.3466

Matson R.A., & Mason, B., 2020 (pers. comm.)

Measures of 62 Southern Pairs

Matthew James[1], Rod Letchford[2], Graeme L. White[2], Meg Emery[3] and Stephen Bosi[1]

1. University of New England, Armidale, NSW, Australia
m.b.james27@gmail.com; sbosi@une.edu.au

2. Centre for Astronomy, University of Southern Queensland, Toowoomba, QLD, Australia
Rod.Letchford@usq.edu.au; graemewhiteau@gmail.com

3. Kildare Catholic College, Wagga Wagga, NSW, Australia
megcolemery@gmail.com

Abstract: We report lucky imaging observations of 62 pairs at mid-southern declinations sourced from the WDS with separations larger than 4 arc seconds and magnitude less than 10. The measures comprise separations and PA calibrated against Alpha Centauri AB and drift scans, presented as weighted means of these two calibration methods, with formal internal uncertainties $\delta\rho$ = 80 mas and δPA = 0.056º.

We also compare our measures against 1) extrapolated historic measures, 2) Gaia DR2 data and 3) measures determined from HIPPARCOS and Gaia observations. Our best estimate of our bias against these 3 databases are $\rho \approx 10 \pm 30$ mas and PA $\approx 0.04 \pm 0.08$º. These formal uncertainties are consistent with the internal uncertainties of $\delta\rho$ = 80 mas and δPA = 0.056º.

We also report Rectilinear Elements for 61 pairs, Grade 5 Orbital Elements for 5 pairs and suggest 5 pairs as optical doubles (4 of which are new).

1. Introduction

This companion paper to (James, et al. 2019), reports lucky imaging (Fried, 1977) observations of 62 southern pairs. These data comprise separations, r, and position angles, PA, determined using two different methods of calibration; the video-drift method and calibration against published orbital parameters of Alpha Centauri AB (α Cen AB). Results are compared with extrapolations of historic observations and micro-arcsecond precision positions from the Gaia DR2 (Brown, et al. 2018, Prusti, et al. 2016) and HIPPARCOS databases. A rectilinear analysis is presented and, where possible, orbital parameters estimated.

2. Selection of Pairs

The 62 pairs in this paper were sourced from the Washington Double Star Catolog (WDS, Mason, et al. 2001) with separations limited to those larger than 4 arc seconds and secondary magnitude brighter than 10. These limits were imposed by the instrument's capabilities. All are at mid-southern declinations such that they would be close to the zenith during observation. The location of the pairs on the celestial sphere is shown in Figure 1.

3. Observations

These observations of the 62 pairs follow Paper 1 (James, et al. 2019). In brief, observations were made with the Webster Celestron 14-inch telescope of The University of New England (UNE) Kirby observatory using an ASI120MM-S camera fitted with a Wratten #25 (red) filter. The capture and reduction software used was SharpCaps version 3.1 (see Paper 1) and Reduc version 5.36 (provided by Florent Losse).

Two observing techniques were used. The first was traditional lucky imaging calibrated against ρ and PA of α Cen AB where precise values of ρ and PA were determined from orbital parameters presented by Pourbaix and Boffin (2016).

The second method was the video-drift method of Nugent & Iverson (2011) where the telescope is stationary and where ρ (which is derived from the image scale

Received March 12, 2020.

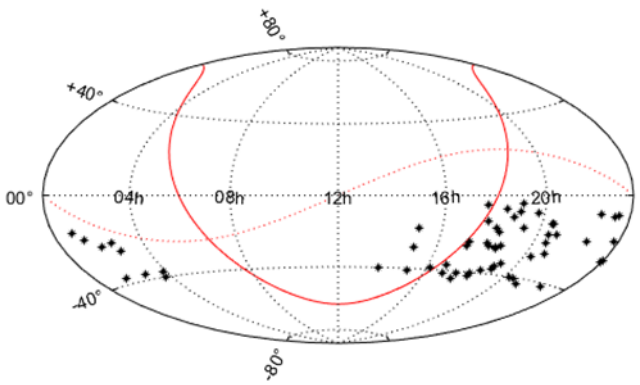

Figure 1. Location of the 62 pairs

of the detector) is determined from the 'angular velocity' of the image movement across the camera detector. The PA is determined by the 'direction' of the movement of the image over the chip.

These two observational techniques were adopted with the intent of finding the best method of calibrating instruments similar in capability to the ones used in this investigation. This is discussed in our follow-up paper (James, et al. 2020b).

4. Astrometric Measures

The measured ρ and PA for the 62 pairs are given in Table 1. Columns 1 and 2 give the WDS designation and discovery code respectively. Column 3 gives the epoch of the new observations reported here.

Columns 3 and 4 give the weighted separation of the two observational techniques in arcsec and the formal uncertainty in ρ, and columns 5 and 6 give the weighted PA in degrees and the formal uncertainty in PA. The average uncertainty of the weighted mean separation is 0.080 arcsec and the average weighted mean uncertainty in PA is 0.056 deg.

5. Historic Data

The historical data for the 62 pairs was requested from Brian Mason of the United States Naval Observatory (UNSO).

It is worth reminding the reader that, if not diligent, false conclusions can be drawn from otherwise seemingly clear trends in data. Figure 2 shows an instance of what at first might seem to be evidence for orbital motion. However, such a conclusion would be spurious. For the pair WDS 23238-0828, the left plots are of ρ and PA with Epoch. Both plots show strong curvature which might be taken (uncritically) as evidence that the secondary is in orbit around the primary. The true sky motion of the pair is revealed in the right-side rectilinear plot which shows the true straight-line motion of the secondary with respect to the primary.

6. Rectilinear Motion for 62 Pairs

The rectilinear motion of the 62 pairs is presented in Table A5 and Figure A5 (in the Appendix). The Rectilinear Elements x_0, x_a, y_0, y_a, t_0, θ_0 and ρ_0 are defined in Letchford, White and Ernest, 2018a. In this paper the value of t_0 differs in that it is set equal to the mean of observational epochs (2018.6 ± 0.15 - over a period of 56 days). The broad straight line is the proper motion trajectory of the secondary, relative to the primary, based on the HIPPARCOS and Gaia positions only.

Additionally, no available HIPPARCOS or ASCC data were available on component B of the pair WDS 15103-4100 (COO 178) exists; thus, it is not included in the rectilinear plots (Figure 5) or rectilinear element table (Table 5).

Quick scrutiny of the rectilinear plots of Figure 5 shows:

- The obvious erroneous observation among the historic data set. These have been rejected from the computation of the extrapolated historic data.

(text continues on page 329)

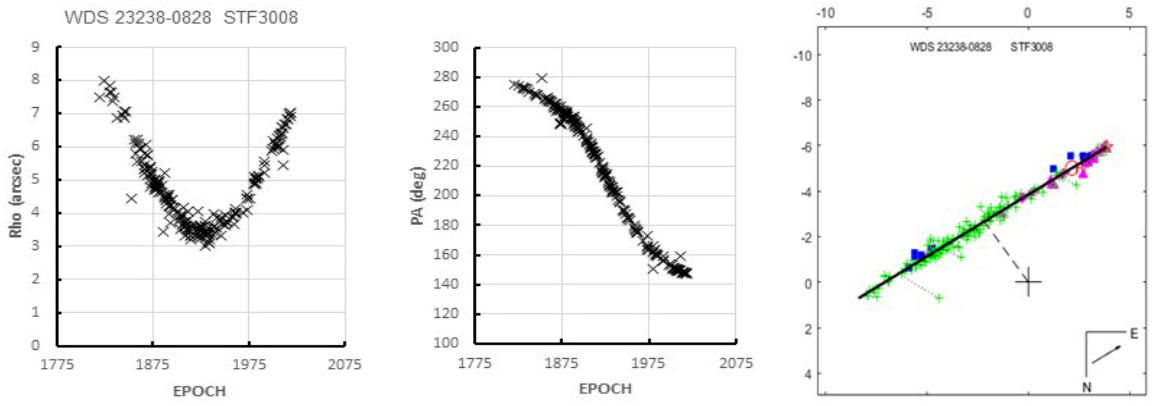

Figure 2. (Left to right) ρ with Epoch, PA with Epoch and Rectilinear Plot for pair WDS 23238-0828.

Measures of 62 Southern Pairs

WDS	DISC	Epoch	Sep (arcsec)	SEM Sep (arcsec)	PA (deg)	SEM PA (deg)
00582-1541	S 390	2018.696	6.452	0.015	216.290	0.059
01225-1905	HJ 2043	2018.712	5.115	0.020	72.134	0.309
01397-3728	HJ 3452	2018.712	19.610	0.082	277.769	0.024
01590-2255	H 2 58AB	2018.696	8.711	0.022	302.246	0.074
02360-2124	HJ 3511	2018.712	14.702	0.042	98.232	0.058
02442-2530	BSO 1AB	2018.712	12.529	0.042	192.518	0.062
02486-3724	HJ 3532	2018.712	5.320	0.019	144.265	0.054
03398-4022	DUN 15	2018.712	7.681	0.026	328.043	0.048
03486-3737	DUN 16	2018.712	8.409	0.042	217.178	0.044
13493-4031	DUN 146	2018.562	68.511	0.306	86.642	0.019
15036-2751	HJ 4727AB	2018.658	7.346	0.020	221.429	0.107
15045-1754	S 665	2018.658	25.073	0.078	90.534	0.019
15103-4100	COO 178	2018.658	4.872	0.030	74.720	0.216
16086-3906	DUN 199AC	2018.658	44.441	0.107	183.572	0.019
16482-3653	DUN 209AB	2018.562	24.011	0.061	138.274	0.039
16540-4148	JC 23AF	2018.562	56.702	0.496	19.114	0.017
17153-2636	SHJ 243AB	2018.696	5.140	0.011	139.764	0.087
17180-2417	H 3 25	2018.696	9.988	0.027	353.349	0.095
17290-4358	DUN 217	2018.696	13.427	0.030	168.274	0.048
17317-4102	ARY 114AC	2018.562	64.868	0.169	250.599	0.009
17398-0458	STF2191AB	2018.696	26.350	0.063	266.705	0.030
17464-1318	STF2204	2018.696	14.509	0.051	24.027	0.053
18026-2415	ARG 31AC	2018.614	35.600	0.089	26.296	0.013
18064-4145	HJ 5011	2018.614	28.143	0.075	344.074	0.030
18089-2528	WNO 21	2018.614	13.484	0.048	64.327	0.069
18106-1645	S 700AB	2018.696	18.812	0.101	291.235	0.151
18106-1645	S 700AC	2018.696	28.618	0.088	352.874	0.032
18108-4026	HJ 5023	2018.696	8.654	0.029	275.919	0.050
18187-1837	SHJ 264AB,C	2018.696	17.230	0.050	51.048	0.039
18247-0636	STF2313	2018.614	5.762	0.019	195.693	0.072
18281-2645	ARY 126AC	2018.600	54.054	0.125	135.204	0.051

Table 1. Weighted Average Measures of Drift and Lucky Imaging (Tracking) Observations for the 62 Pairs.

Table 1 concludes on the next page.

Measures of 62 Southern Pairs

WDS	DISC	Epoch	Sep (arcsec)	SEM Sep (arcsec)	PA (deg)	SEM PA (deg)
18290-2635	WNO 6	2018.600	41.804	0.099	182.311	0.049
18334-3844	DUN 222	2018.562	20.470	0.053	358.654	0.023
18399-2531	ARG 32AB	2018.616	7.032	0.019	219.503	0.064
18399-2531	ARG 32AC	2018.616	53.217	0.126	284.941	0.009
18459-1030	STF2373	2018.616	4.117	0.012	337.020	0.034
19006-0807	STF2425	2018.616	29.534	0.086	177.100	0.027
19011-3704	BSO 14AB	2018.559	12.825	0.037	280.033	0.051
19027-3606	HJ 5080	2018.616	5.484	0.011	245.883	0.066
19050-0402	SHJ 286	2018.616	39.705	0.157	209.937	0.028
19127-3351	HJ 5094AB	2018.600	31.571	0.104	181.613	0.048
19177-1558	S 715	2018.600	8.380	0.022	16.967	0.054
19181-1557	S 716	2018.600	4.969	0.012	196.095	0.078
19431-0818	STF 45AB	2018.636	96.268	0.460	145.488	0.015
20178-4011	DUN 230	2018.562	9.675	0.036	117.438	0.065
20205-2912	HJ 5188AC	2018.712	27.266	0.084	320.898	0.025
20284-1309	STF2683	2018.712	22.795	0.100	66.820	0.067
20299-1835	SHJ 324	2018.636	21.947	0.083	238.443	0.052
20322-2209	HJ 2973AB	2018.712	39.386	0.119	128.953	0.018
20338-4033	JC 18AB	2018.562	4.413	0.014	223.593	0.090
20484-1812	S 763AB	2018.636	15.605	0.051	293.786	0.024
20501-2722	HJ 5226	2018.712	18.658	0.065	67.357	0.038
21022-4300	DUN 236	2018.562	57.422	0.265	73.193	0.018
22246-4127	JC 19AB	2018.562	14.790	0.045	58.811	0.038
22258-2014	S 808AB	2018.658	6.869	0.020	152.910	0.091
22305-0807	STF2913	2018.658	8.067	0.025	327.936	0.054
23141-0855	STF2993AB	2018.658	25.068	0.061	175.134	0.040
23141-0855	S 826AC	2018.658	79.127	0.336	131.875	0.020
23238-0828	STF3008	2018.636	7.053	0.028	146.790	0.079
23460-1841	H 2	2018.614	6.950	0.021	135.798	0.090
23544-2703	LAL 192	2018.614	6.455	0.022	272.184	0.066
23595-2631	LAL 193	2018.614	10.373	0.031	169.436	0.039

Table 1 (conclusion). Weighted Average Measures of Drift and Lucky Imaging (Tracking) Observations for the 62 Pairs.

(Continued from page 326)

- For some observations where the two stars are of very similar magnitude, an obvious misidentification of the primary has occurred, and the recorded PA is in error by 180 degrees. They are (magnitudes from SIMBAD):
  - WDS 00582-1514 (HD 5659) where the V magnitudes of the components are 7.712 and 7.804.
  - WDS 17153-2636 (36 Oph) where V = 5.03 and 5.08.
  - WDS 19177-1558 (HD 180562) where V = 7.038 and 7.87.
  - WDS 19181-1557 (HD 180695) where V = 7.712 and 7.804.

Irrespective of these data misadventures, the rectilinear plots are of three types. The first type is a curved path of a companion in a short period orbit. In Figure 5 (Appendix) WDS 17153-2636 (36 Oph) shows such a curved path and an orbit of period 507 ± 18 years is determined by us in Table 6 and Figure 6 (Appendix).

6.1. Five Optical Doubles

A clear straight-line trajectory of the secondary relative to a stationary primary is expected when a pair is an optical double and large differences in parallax are an indication of non-gravitational systems. Examples of linear trajectory rectilinear plots in Figure 5 are (parallaxes are from Gaia DR2, units are milliarcseconds (mas));

- WDS 19127-3351, Parallax of the primary is 1.97 ± 0.11 and the parallax of the secondary is 13.88 ± 0.13.
- WDS 22246-4127, Parallax of the primary is 15.53 ± 0.05, parallax of the secondary is 7.29 ± 0.07.
- WDS 23141-0855, Parallax of the primary is 24.55 ± 0.05, parallax of the secondary is 11.38 ± 0.05.
- WDS 23460-1841, Parallax of the primary is 16.2 ± 0.2, the parallax of the secondary is 20.4 ± 0.4.
- WDS 23238-0828, Parallax of the primary is 5.45 ± 0.04 and the parallax of the secondary is 9.43 ± 0.04. This is a confirmed optical pair (Peirce, 1882; MacEvoy, 2010).

On the basis of the Rectilinear plots of Figure 5, and the very different parallaxes, we confidently categorize 4 of these pairs as optical doubles and confirm the fifth (WDS 23238-0828) as an optical double.

7. Orbits for 5 Pairs

Following the technique presented in Letchford, White and Ernest, 2018b, Table A6 presents Grade 5 Orbital Elements for five pairs. All pairs reported here display very short arcs. Column headings in Table A6 are described in Letchford, White and Ernest, 2018b. For this analysis, all historic data is considered and unweighted. Figure 6 (Appendix) shows these best fit and iterative orbits. WDS 17153-2636 (36 Oph) has an orbit of period 507 ± 18 years. The WDS Sixth Orbit Catalog reports a 470.9-year period from Irwin, Yang and Walker (1996), which is based on the period of 548.7 years derived by Brosche (1960). Our value of 507 ± 18 years in consistent with these prior computations.

A literature search for the binary status of 5 pairs found 3 as 'known binaries' (referenced in ADS and SIMBAD).

- WDS 01590-2255 is a known binary
- WDS 02360-2124 is a known binary, however, has only been suggested to be a bound system recently by Andrews, Chaname & Agueros, 2017.
- WDS 17153-2636 is a known binary
- WDS 18247-0636 is a known binary
- WDS 23595-2636 is an unknown binary

Regarding the unknown pair WDS 23590-2636, a grade 5 orbital is presented in Table 6 and Figure 6. Within the confidence of our results we nominate WDS 23590-2636 as a binary system.

8. Precision, Bias and Comparison with Other Data Sets.

8.1 Comparison with History Data.

Following Paper 1, linear extrapolations of the historic data were derived and the parameters A, B, C, and D were determined. These define the best linear fit to the trends in the data.

The parameters A-D were used to determine the predicted ρ and PA at the epoch of our observation and these values are given in Table 3 (Appendix).

There is good agreement between the weighted measures reported here and the measures obtained from extrapolation. The mean bias in ρ is -0.009 ± 0.027 arcseconds, and the mean bias in PA is -0.098 ± 0.078 degree; the bias is defined as the difference, this work (TW) minus historic data.

Figure 3 shows the difference in r and PA for 57 of the 62 pairs measures of this work with those determined from linear fits of the historic data. Pairs with a poor historic linear fit were not appropriate for comparison and were treated as outliers, the criterion being that ρ or PA differs by 2 standard deviations or more, from

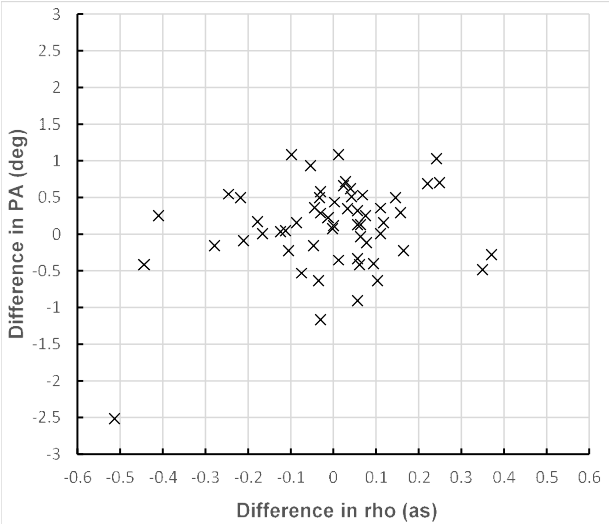

Figure 3. The comparison of measures (extrapolation of historic data – This paper (TW)). The mean bias in ρ is -0.009 ± 0.027 arcseconds, and the mean bias in PA is 0.098 ± 0.078 degree.

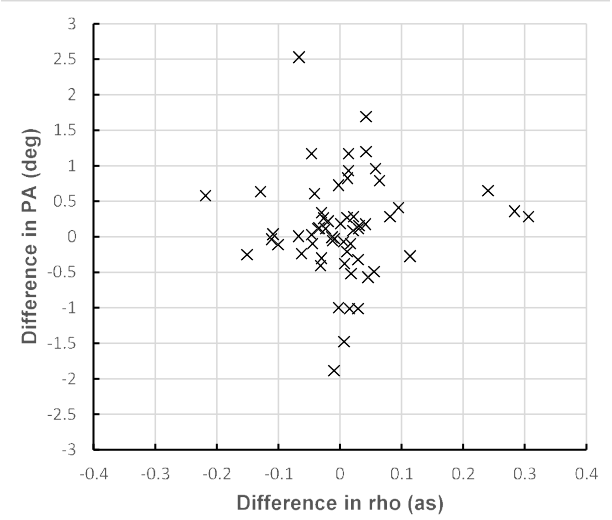

Figure 4. The comparison of measures (Gaia DR2 ρ and PA – TW). The mean bias in ρ is 0.005 ± 0.021 arcseconds, and the mean bias in PA is 0.129 ± 0.094 degree.

the mean of the differences. The following pairs 18334-3844 (DUN 222), 19127-3351 (HJ 5094AB), 22246-4127(JC 19AB), 23141-0855 (S 826AC), 23238-0828 (STF3008) were treated as outliers here.

8.2 Comparison with Gaia DR2 Data

Once more following Paper 1, Table A3 (Appendix) also gives the comparison of the measures in Table 1 (this work) with precision values from Gaia DR2. All measures are compared at the epoch of observation (~2018.6).

Again, there is good agreement between the weighted measures reported here and the measures obtained from Gaia DR2. The mean bias in ρ is 0.005 ± 0.021 arcseconds, and the mean bias in PA is 0.129 ± 0.094 degree. Again, here bias is defined as the difference, TW minus Gaia DR2 data.

Figure 4 shows the difference (for 58 of the 62 pairs measures) between this work and those determined from Gaia DR2. Pairs outside 2 standard deviations of the mean difference were considered outliers and omitted from the plot. We suspect that our work may have isolated discrepancies in the DR2. The following pairs 18334-3844 (DUN 222), 22246-4127 (JC 19AB), 23141-0855 (S 826AC), 23238-0828 (STF3008) were treated as outliers.

8.3 Comparison with Space-Based Positions

The projected movement of the secondary relative to the primary shown in the rectilinear plots of Figure A5 as a dark line is the linear extrapolation of the Hipparcos and Gaia position at epoch 1991.25 and 2015.5 respectively. All positions shown in this figure are for equinox J2000.

Armed with this space-based differential proper motion, a comparison is made between our measures in Table 1 and the separations and PAs at the epoch of the observations (~2018.6).

This comparison gives a mean bias in separation of -0.032 ± 0.042 arcsec and a mean bias in PAs of -0.112 ± 0.081 degree. These biases again, are defined as TW minus space-based data.

8.4 Table of Comparisons

Table 2 gives a summary of the bias as found by the three methods described above in Section 8. Our best estimate of bias in separations is ~10 mas, and ~40 millidegrees in PA.

Assuming that the uncertainties in the Hipparcos and Gaia data are negligible compared with our measures, we assert that our separations have a formal uncertainty of ~30 mas and the formal uncertainty in the PAs is ~80 millidegrees.

9. Conclusion

We report lucky imaging measures of ρ and PA of 62 southern pairs calibrated against both Alpha Centauri AB and drift scans and present them as final weighted measures. The formal uncertainties for the weighted measures are 0.080 arcsec in ρ and 0.056 deg in PA.

We also report a comparison of our measures against extrapolated historic measures, Gaia DR2 and HIPPARCOSS/Gaia space-based measures. Our best estimate of bias within these three approaches are ~10 mas in r and ~0.04 degrees in PA, and the formal uncertainty is ~30 mas and ~80 millidegrees in r and PA respectively.

BIAS COMPARISON	Sep (arcsec)	SEM Sep	PA (DEG)	SEM PA
Extrapolated Historic Data	-0.009	0.03	0.1	0.08
Gaia DR2	0.005	0.02	0.13	0.09
HIPPARCOS/Gaia Motion	-0.03	0.04	-0.11	0.08
Overall Estimate	-0.012	0.03	0.04	0.08

Table 2: Comparison of Bias and Uncertainty.

We present also Rectilinear Elements for the 61, Grade 5 Orbital Elements for 5 pairs and suggest 5 pairs as optical doubles.

Acknowledgements

The Washington Double Star Catolog maintained by the USNO. (WDS), https://ad.usno.navy.mil/wds

SIMBAD Astronomical Database, operated at CDS, Strasbourg, France, http://simbad.u-strasbg.fr/simbad/

The Aladin sky atlas developed at CDS, Strasbourg Observatory, France, https://aladin.u-strasbg.fr/

The Gaia Catalogue (Gaia DR2, Gaia Collaboration, 2018), from VizieR (Gaia DR2), http://vizier.u-strasbg.fr/viz-bin/VizieR-3?-source=I/345/gaia2

The University of New England for the use of the Kirby Observatory.

Thanks to Florent Losse for use of the Reduc software.

Thanks to Jenny Stephens of Kildare Catholic College, Wagga Wagga.

References

Andrews, J. J., Chanamé, J & Agüeros, M. A., 2017, "Wide Binaries in Tycho-Gaia: search method and the distribution of orbital separations", Royal Astronomical Society, 472, 675-699

Brosche, P., 1960, "Eine Bemerkung zur Massenbestimmung langperiodischer Doppelsternsysteme und Anwendung auf ads 10417", Astronomische Nachrichten, 285(5), 261-264.

Brown, A.G.A., et al., 2018, "Gaia Data Release 2 - Summary of the contents and survey properties", Astronomy and Astrophysics, 616, A1.

Fried, D. L., 1977, "Probability of getting a lucky short-exposure image through turbulence", Journal of the Optical Society of America, 68(12), 1651-1658.

Irwin, A. W., Yang, S. L. S., & Walker, G. A. H., 1996, "36 Ophiuchi AB: Incompatibility of the orbit and precise Radial Velocities" Astronomical Society of the Pacific, 108, 580-590.

James, M., Emery, M., White. G.L., Letchford, R.R. & Bosi, S.G., 2019a, "Measures of Ten Sco Doubles and the Determination of Two Orbits." Journal of Double Star Observations, 15(3), 489-503.

James, M., 2019., BSc Honours Thesis, University of New England, Australia.

Letchford, R.R., White, G.L., & Ernest, A.D., 2018a, "The Southern Double Stars of Carl Rümker II: Their Relative Rectilinear Motion" Journal of Double Star Observations, 14(2), 208–222.

Letchford, R.R., White, G.L., & Ernest, A.D., 2018b, "The Southern Double Stars of Carl Rümker III: Quantified Probability of Boundedness and Preliminary Grade 5 Orbits for Some Very Long Period Doubles." Journal of Double Star Observations, 14 (4), 761–770.

Mason, B.D., Wycoff, G.L., Hartkopf, W.I., Douglass, G.G., & Worley, C.E., 2001, "The 2001 US Naval Observatory double star CD-ROM. I. The Washington double star catalog." Astron J, 122, 3466-3471.

MacEvoy, B., 2010, Private communication, http://www.handprint.com/ASTRO/index.html.

Nugent, R.L., & Iverson, E.W., 2011, "A New Video Method to Measure Double Stars", Journal of Double Star Observations, 7(3),185-194.

Peirce, C. S., 1882, Harvard Ann, 13, 17.

Pourbaix, D., & Boffin, H.M.J., 2016, Astronomy and Astrophysics, 586, A90.

Prusti, T., et al., (Gaia Collaboration)., 2016, The Gaia mission, Astronomy & Astrophysics, 595, A1.

United States Naval Observatory., n.d., The Washington Double Star Catalog. Retrieved from http://ad.usno.navy.mil/wds/

White, G.L., Letchford, R.R. & Ernest, A.E., 2018, "Uncertainties in Separation and Position Angle of Historic Measures – Alpha Centarui AB Case Study", *Journal of Double Star Observations*, **14** (3), 432-442.

Measures of 62 Southern Pairs

Appendix

WDS	DISC	Rho				PA			
		This Work	History	GAIA	RE	This Work	History	GAIA	RE
00582-1541	S 390	6.452	6.406	6.464	6.419	216.290	216.139	216.077	215.523
01225-1905	HJ 2043	5.115	5.127	5.179	5.187	72.134	73.224	72.926	73.641
01397-3728	HJ 3452	19.610	19.713	19.655	20.059	277.769	277.133	277.203	276.283
01590-2255	H 2 58AB	8.711	8.607	8.682	8.295	302.246	302.021	302.589	304.213
02360-2124	HJ 3511	14.702	14.577	14.720	14.786	98.232	98.264	97.714	97.863
02442-2530	BSO 1AB	12.529	12.569	12.493	12.102	192.518	193.143	192.634	189.987
02486-3724	HJ 3532	5.320	5.246	5.341	5.429	144.265	143.734	144.353	145.758
03398-4022	DUN 15	7.681	7.745	7.649	7.779	328.043	328.010	327.631	328.032
03486-3737	DUN 16	8.409	8.411	8.400	7.634	217.178	217.291	215.291	210.494
13493-4031	DUN 146	68.511	68.398	68.411	62.385	86.642	86.693	86.524	86.088
15036-2751	HJ 4727AB	7.346	7.343	7.362	7.534	221.429	221.506	220.420	218.209
15045-1754	S 665	25.073	24.894	25.060	25.092	90.534	90.709	90.530	90.459
15103-4100	COO 178	4.872	4.818	4.885	4.786	74.720	75.656	75.654	260.621
16086-3906	DUN 199AC	44.441	44.195	44.223	44.082	183.572	184.118	184.146	184.095
16482-3653	DUN 209AB	24.011	23.567	23.882	23.259	138.274	137.858	138.912	141.072
16540-4148	JC 23AF	56.702	56.603	56.656	56.659	19.114	20.204	20.280	20.305
17153-2636	SHJ 243AB	5.140	4.628	5.106	4.489	139.764	137.250	139.886	172.426
17180-2417	H 3 25	9.988	10.230	10.001	10.431	353.349	354.375	354.174	354.157
17290-4358	DUN 217	13.427	13.397	13.433	13.414	168.274	168.852	168.200	168.280
17317-4102	ARY 114AC	64.868	64.656	65.174	64.407	250.599	250.509	250.885	250.397
17398-0458	STF2191AB	26.350	26.392	26.238	26.514	266.705	267.220	266.674	266.895
17464-1318	STF2204	14.509	14.511	14.463	14.269	24.027	24.465	24.056	24.643
18026-2415	ARG 31AC	35.600	35.189	35.532	35.414	26.296	26.550	26.308	26.731
18064-4145	HJ 5011	28.143	28.217	28.185	29.022	344.074	344.325	345.267	347.112
18089-2528	WNO 21	13.484	13.441	13.495	13.411	64.327	64.694	64.593	64.649
18106-1645	S 700AB	18.812	18.836	18.842	18.809	291.235	291.901	291.349	292.756
18106-1645	S 700AC	28.618	28.736	28.509	28.589	352.874	353.026	352.911	353.044
18108-4026	HJ 5023	8.654	8.717	8.613	8.760	275.919	276.042	276.525	275.003
18187-1837	SHJ 264AB,C	17.230	17.388	17.244	17.261	51.048	51.342	52.216	50.442
18247-0636	STF2313	5.762	6.011	5.857	6.047	195.693	196.396	196.105	196.959
18281-2645	ARY 126AC	54.054	54.067	54.095	54.284	135.204	134.849	135.383	135.476

Table A3: Measures at date of observation for this work (weighted α Cen AB orbital parameter and Video-drift measures), historics, GAIA DR2, and derived from Rectilinears (RE).

Table A3 concludes on the next page.

Measures of 62 Southern Pairs

WDS	DISC	Rho				PA			
		This Work	History	GAIA	RE	This Work	History	GAIA	RE
18290-2635	WNO 6	41.804	41.860	41.917	41.959	182.311	181.977	182.037	181.992
18334-3844	DUN 222	20.470	21.322	21.344	21.376	358.654	359.032	358.418	357.954
18399-2531	ARG 32AB	7.032	7.382	7.049	7.135	219.503	219.013	219.409	217.689
18399-2531	ARG 32AC	53.217	53.363	53.299	53.296	284.941	285.436	285.222	285.108
18459-1030	STF2373	4.117	4.151	4.125	4.164	337.020	337.369	336.642	336.416
19006-0807	STF2425	29.534	29.562	29.592	30.640	177.100	177.819	178.055	179.455
19011-3704	BSO 14AB	12.825	12.936	12.822	12.736	280.033	280.386	280.763	280.977
19027-3606	HJ 5080	5.484	5.541	5.472	5.526	245.883	246.013	245.822	245.306
19050-0402	SHJ 286	39.705	39.620	39.555	38.331	209.937	210.092	209.679	208.888
19127-3351	HJ 5094AB	31.571	29.774	31.505	22.335	181.613	178.655	184.141	192.272
19177-1558	S 715	8.380	8.442	8.387	8.423	16.967	16.555	15.491	14.437
19181-1557	S 716	4.969	5.063	4.961	4.948	196.095	195.695	196.069	195.594
19431-0818	STF 45AB	96.268	96.489	96.551	97.083	145.488	146.183	145.847	146.015
20178-4011	DUN 230	9.675	9.753	9.645	9.825	117.438	117.325	117.138	116.131
20205-2912	HJ 5188AC	27.266	27.099	27.246	27.303	320.898	320.902	321.117	321.212
20284-1309	STF2683	22.795	22.763	22.750	23.000	66.820	67.105	66.724	66.975
20299-1835	SHJ 324	21.947	21.934	21.923	21.882	238.443	238.666	238.557	238.450
20322-2209	HJ 2973AB	39.386	39.107	39.417	39.385	128.953	128.795	129.115	129.105
20338-4033	JC 18AB	4.413	4.522	4.413	4.424	223.593	223.604	223.782	224.421
20484-1812	S 763AB	15.605	15.771	15.543	15.583	293.786	293.560	293.551	294.044
20501-2722	HJ 5226	18.658	18.626	18.680	18.626	67.357	67.855	67.641	67.609
21022-4300	DUN 236	57.422	57.386	57.451	57.433	73.193	72.564	72.865	72.747
22246-4127	JC 19AB	14.790	14.327	15.035	25.084	58.811	64.538	65.164	74.041
22258-2014	S 808AB	6.869	7.240	6.898	6.855	152.910	152.627	151.897	150.871
22305-0807	STF2913	8.067	8.125	8.040	8.090	327.936	328.252	328.200	328.625
23141-0855	STF2993AB	25.068	25.137	25.110	25.308	175.134	175.668	176.826	175.974
23141-0855	S 826AC	79.127	77.289	78.566	105.377	131.875	130.493	127.883	119.657
23238-0828	STF3008	7.053	4.384	7.064	3.425	146.790	140.137	153.042	218.276
23460-1841	H 2	6.950	7.008	7.005	6.424	135.798	134.898	135.305	136.728
23544-2703	LAL 192	6.455	6.424	6.452	6.647	272.184	271.023	271.190	269.913
23595-2631	LAL 193	10.373	10.155	10.613	10.565	169.436	169.937	170.084	170.184

Table A3 (conclusion). Measures at date of observation for this work (weighted α Cen AB orbital parameter and Video-drift measures), historics, GAIA DR2, and derived from Rectilinears (RE).

Measures of 62 Southern Pairs

WDS	DISC	Diff PA	Diff Rho	Diff PA	Diff Rho	Diff PA	Diff Rho
		GAIA-TW		HIST-TW		HIST-GAIA	
00582-1541	S 390	-0.213	0.012	-0.151	-0.046	0.062	-0.058
01225-1905	HJ 2043	0.792	0.064	1.090	0.012	0.298	-0.052
01397-3728	HJ 3452	-0.567	0.045	-0.636	0.103	-0.069	0.058
01590-2255	H 2 58AB	0.343	-0.030	-0.225	-0.105	-0.568	-0.075
02360-2124	HJ 3511	-0.519	0.018	0.032	-0.124	0.550	-0.142
02442-2530	BSO 1AB	0.116	-0.036	0.625	0.040	0.509	0.076
02486-3724	HJ 3532	0.088	0.021	-0.531	-0.074	-0.619	-0.095
03398-4022	DUN 15	-0.412	-0.031	-0.033	0.064	0.379	0.096
03486-3737	DUN 16	-1.887	-0.010	0.113	0.001	2.000	0.011
13493-4031	DUN 146	-0.118	-0.101	0.051	-0.113	0.168	-0.012
15036-2751	HJ 4727AB	-1.009	0.016	0.077	-0.003	1.087	-0.019
15045-1754	S 665	-0.004	-0.013	0.175	-0.178	0.178	-0.166
15103-4100	COO 178	0.934	0.014	0.936	-0.054	0.002	-0.067
16086-3906	DUN 199AC	0.574	-0.218	0.546	-0.245	-0.028	-0.027
16482-3653	DUN 209AB	0.638	-0.129	-0.417	-0.444	-1.055	-0.315
16540-4148	JC 23AF	1.166	-0.046	1.090	-0.099	-0.076	-0.053
17153-2636	SHJ 243AB	0.121	-0.034	-2.514	-0.512	-2.636	-0.478
17180-2417	H 3 25	0.825	0.013	1.026	0.242	0.201	0.229
17290-4358	DUN 217	-0.074	0.006	0.578	-0.030	0.652	-0.036
17317-4102	ARY 114AC	0.286	0.306	-0.090	-0.212	-0.376	-0.518
17398-0458	STF2191AB	-0.031	-0.111	0.515	0.042	0.546	0.154
17464-1318	STF2204	0.029	-0.046	0.438	0.002	0.409	0.048
18026-2415	ARG 31AC	0.012	-0.067	0.254	-0.411	0.242	-0.343
18064-4145	HJ 5011	1.193	0.042	0.251	0.074	-0.942	0.032
18089-2528	WNO 21	0.265	0.012	0.366	-0.043	0.101	-0.055
18106-1645	S 700AB	0.114	0.030	0.666	0.024	0.552	-0.006
18106-1645	S 700AC	0.038	-0.108	0.153	0.119	0.115	0.227
18108-4026	HJ 5023	0.606	-0.041	0.123	0.063	-0.483	0.104
18187-1837	SHJ 264AB,C	1.168	0.014	0.295	0.158	-0.873	0.144
18247-0636	STF2313	0.412	0.095	0.704	0.249	0.291	0.154
18281-2645	ARY 126AC	0.179	0.042	-0.355	0.013	-0.534	-0.029
18290-2635	WNO 6	-0.274	0.114	-0.334	0.056	-0.060	-0.057
18334-3844	DUN 222	-0.235	0.874	0.379	0.853	0.614	-0.022
18399-2531	ARG 32AB	-0.094	0.017	-0.489	0.349	-0.395	0.333
18399-2531	ARG 32AC	0.281	0.082	0.496	0.146	0.215	0.064
18459-1030	STF2373	-0.378	0.007	0.349	0.034	0.726	0.026
19006-0807	STF2425	0.955	0.058	0.719	0.028	-0.236	-0.031
19011-3704	BSO 14AB	0.730	-0.003	0.353	0.111	-0.377	0.114
19027-3606	HJ 5080	-0.061	-0.012	0.131	0.056	0.191	0.068
19050-0402	SHJ 286	-0.257	-0.151	0.155	-0.086	0.413	0.065
19127-3351	HJ 5094AB	2.528	-0.066	-2.958	-1.797	-5.486	-1.730
19177-1558	S 715	-1.476	0.007	-0.412	0.062	1.064	0.055
19181-1557	S 716	-0.026	-0.009	-0.400	0.094	-0.374	0.102
19431-0818	STF 45AB	0.359	0.283	0.695	0.221	0.336	-0.062
20178-4011	DUN 230	-0.300	-0.030	-0.113	0.079	0.187	0.109
20205-2912	HJ 5188AC	0.219	-0.020	0.004	-0.166	-0.215	-0.147
20284-1309	STF2683	-0.096	-0.045	0.285	-0.031	0.381	0.013
20299-1835	SHJ 324	0.114	-0.024	0.223	-0.012	0.109	0.011
20322-2209	HJ 2973AB	0.162	0.031	-0.157	-0.279	-0.320	-0.310
20338-4033	JC 18AB	0.189	0.000	0.012	0.109	-0.178	0.109
20484-1812	S 763AB	-0.235	-0.062	-0.226	0.165	0.009	0.227
20501-2722	HJ 5226	0.285	0.022	0.498	-0.032	0.214	-0.054
21022-4300	DUN 236	-0.327	0.029	-0.629	-0.036	-0.302	-0.065
22246-4127	JC 19AB	6.353	0.246	5.727	-0.462	-0.626	-0.708
22258-2014	S 808AB	-1.013	0.029	-0.283	0.371	0.730	0.342
22305-0807	STF2913	0.264	-0.027	0.316	0.058	0.052	0.085
23141-0855	STF2993AB	1.693	0.042	0.534	0.069	-1.159	0.027
23141-0855	S 826AC	-3.991	-0.561	-1.382	-1.837	2.610	-1.277
23238-0828	STF3008	6.252	0.011	-6.653	-2.668	-12.905	-2.679
23460-1841	H 2	-0.493	0.055	-0.901	0.057	-0.407	0.002
23544-2703	LAL 192	-0.994	-0.003	-1.161	-0.031	-0.167	-0.028
23595-2631	LAL 193	0.647	0.240	0.501	-0.218	-0.146	-0.458

Table A4: Difference in the measures determined for this work (TW), hisorical data (HIST), and Gaia DR2 (GAIA).

Measures of 62 Southern Pairs

WDS	DISC	x0	xa	y0	ya	t0
		±	±	±	±	±
00582-1541	S 390	-5.2244	0.0001	-3.7296	-0.0011	1940.7543
		0.0118	0.0002	0.0130	0.0002	850.5143
01225-1905	HJ 2043	1.4610	0.0012	4.9771	-0.0005	1953.5703
		0.0058	0.0001	0.0134	0.0002	920.5884
01397-3728	HJ 3452	2.1952	0.0055	-19.9383	0.0065	1948.9966
		0.0052	0.0001	0.0298	0.0004	361.3999
01590-2255	H 2 58AB	4.6639	-0.0005	-6.8594	-0.0056	1930.2237
		0.0116	0.0001	0.0138	0.0002	80.1596
02360-2124	HJ 3511	-2.0226	-0.0002	14.6465	-0.0011	1953.6573
		0.0067	0.0001	0.0342	0.0006	15506.0950
02442-2530	BSO 1AB	-11.9185	-0.0037	-2.0988	-0.0083	1942.0339
		0.0144	0.0002	0.0492	0.0007	241.2325
02486-3724	HJ 3532	-4.4882	0.0024	3.0550	0.0013	1945.9391
		0.0050	0.0001	0.0056	0.0001	186.6285
03398-4022	DUN 15	6.5994	-0.0010	-4.1186	0.0008	1941.1690
		0.0046	0.0001	0.0056	0.0001	958.2834
03486-3737	DUN 16	-6.5784	-0.0017	-3.8740	-0.0137	1934.2705
		0.0045	0.0001	0.0051	0.0001	18.6075
13493-4031	DUN 146	4.2560	-0.0040	62.2394	0.0893	1950.0286
		0.0162	0.0002	0.0110	0.0002	6.5108
15036-2751	HJ 4727AB	-5.9199	0.0054	-4.6600	-0.0027	1947.6650
		0.0096	0.0001	0.0099	0.0001	140.8817
15045-1754	S 665	-0.2009	-0.0003	25.0914	-0.0005	1948.2751
		0.0010	0.0000	0.0796	0.0012	186907.5167
16086-3906	DUN 199AC	-43.9699	-0.0020	-3.1482	-0.0011	1952.7770
		0.0004	0.0000	0.0017	0.0000	201.3896
16482-3653	DUN 209AB	-18.0940	0.0038	14.6144	0.0191	1949.5819
		0.0304	0.0005	0.0302	0.0005	90.9595
16540-4148	JC 23AF	53.1379	0.0004	19.6613	-0.0012	1952.6081
		0.0123	0.0002	0.0098	0.0002	7042.2868
17153-2636	SHJ 243AB	-4.4500	0.0066	0.5917	0.0334	1937.6418
		0.0050	0.0001	0.0063	0.0001	11.3784
17180-2417	H 3 25	10.3771	-0.0045	-1.0620	0.0006	1924.7128
		0.0039	0.0000	0.0269	0.0003	119.0806
17290-4358	DUN 217	-13.1344	-0.0003	2.7248	0.0004	1949.9603
		0.0059	0.0001	0.0199	0.0003	17131.8812
17317-4102	ARY 114AC	-21.6092	0.0094	-60.6742	-0.0379	1991.7989
		0.0091	0.0004	0.0075	0.0003	22.0390
17398-0458	STF2191AB	-1.4360	0.0004	-26.4753	0.0027	1923.9121
		0.0023	0.0000	0.0293	0.0003	3006.9364
17464-1318	STF2204	12.9694	0.0024	5.9496	0.0000	1922.9025
		0.0356	0.0004	0.0303	0.0003	1265.1774
18026-2415	ARG 31AC	31.6294	0.0035	15.9291	-0.0021	1959.9759
		0.2942	0.0053	0.2845	0.0051	12043.6334
18064-4145	HJ 5011	28.2907	-0.0186	-6.4731	-0.0181	1957.0944
		0.0254	0.0004	0.0167	0.0003	89.8055
18089-2528	WNO 21	5.7420	0.0012	12.1192	0.0015	1971.4747
		0.0199	0.0005	0.0304	0.0007	3392.0721
18106-1645	S 700AB	7.2755	-0.0076	-17.3448	-0.0037	1960.9327
		0.0564	0.0010	0.0494	0.0009	605.7845
18106-1645	S 700AC	28.3787	-0.0014	-3.4624	-0.0008	1952.3457
		0.0321	0.0005	0.0222	0.0004	11568.8688
18108-4026	HJ 5023	0.7641	0.0022	-8.7271	0.0020	1941.7357
		0.0376	0.0005	0.0267	0.0004	1301.2426
18187-1837	SHJ 264AB,C	10.9929	-0.0037	13.3077	0.0028	1948.4464
		0.0211	0.0003	0.0208	0.0003	435.1843
18247-0636	STF2313	-5.7836	0.0018	-1.7637	0.0019	1934.6681
		0.0081	0.0001	0.0197	0.0002	622.6877
18281-2645	ARY 126AC	-38.7020	0.0202	38.0648	0.0079	1996.4457
		0.0109	0.0006	0.0109	0.0006	195.0099
18290-2635	WNO 6	-41.9332	0.0011	-1.4584	-0.0006	1970.5975
		0.0005	0.0000	0.0024	0.0001	1426.1575

Table A5: Rectilinear Elements of the Secondary Component of the 62 Pairs (In-depth details in Letchford, White and Ernest, 2018a)

Table A5 concludes on the next page.

Measures of 62 Southern Pairs

WDS	DISC	x0	xa	y0	ya	t0
		±	±	±	±	±
18334-3844	DUN 222	21.3622	-0.0003	-0.7631	0.0029	1943.0966
		0.0025	0.0000	0.0599	0.0008	1875.3057
18399-2531	ARG 32AB	-5.6460	0.0030	-4.3619	-0.0022	1941.4198
		0.0115	0.0002	0.0119	0.0002	259.4075
18399-2531	ARG 32AC	13.8905	0.0028	-51.4535	0.0007	1954.3728
		0.0022	0.0000	0.0057	0.0001	584.6560
18459-1030	STF2373	3.8166	-0.0003	-1.6662	0.0008	1932.5191
		0.0114	0.0001	0.0191	0.0002	3084.2071
19006-0807	STF2425	-30.6390	0.0119	0.2915	0.0104	1928.8816
		0.0609	0.0007	0.0433	0.0005	317.8516
19011-3704	BSO 14AB	2.4252	-0.0016	-12.5029	-0.0014	1945.2068
		0.0099	0.0001	0.0376	0.0005	1231.8330
19027-3606	HJ 5080	-2.3085	0.0009	-5.0204	0.0004	1941.6415
		0.0108	0.0001	0.0173	0.0002	2520.2942
19050-0402	SHJ 286	-33.5615	-0.0115	-18.5175	-0.0209	1958.6131
		0.0015	0.0000	0.0019	0.0000	3.4228
19127-3351	HJ 5094AB	-21.8246	-0.1405	-4.7473	0.0530	1949.8259
		0.0007	0.0000	0.0038	0.0001	0.7064
19177-1558	S 715	8.1573	-0.0019	2.1000	0.0040	1929.4843
		0.0066	0.0001	0.0160	0.0002	205.9884
19181-1557	S 716	-4.7663	0.0000	-1.3302	-0.0006	1932.3242
		0.0090	0.0001	0.0222	0.0003	1837.5219
19431-0818	STF45AB	-80.4996	0.0074	54.2667	0.0007	1929.1407
		0.0114	0.0001	0.0130	0.0002	510.0643
20178-4011	DUN 230	-4.3272	-0.0017	8.8208	-0.0036	1944.2837
		0.0074	0.0001	0.0106	0.0001	302.2190
20205-2912	HJ 5188AC	21.2820	-0.0016	-17.1036	-0.0004	1959.5577
		0.0084	0.0002	0.0084	0.0001	2610.3672
20284-1309	STF2683	8.9960	-0.0008	21.1674	-0.0028	1929.7784
		0.0553	0.0006	0.0488	0.0006	4406.0174
20299-1835	SHJ 324	-11.4500	0.0002	-18.6478	-0.0008	1950.9119
		0.0395	0.0006	0.0487	0.0008	34918.1703
20322-2209	HJ 2973AB	-24.8421	-0.0003	30.5625	0.0003	1951.7920
		0.0025	0.0000	0.0026	0.0000	15621.2016
20338-4033	JC 18AB	-3.1598	-0.0004	-3.0966	0.0007	1936.9804
		0.0084	0.0001	0.0084	0.0001	1194.4817
20484-1812	S 763AB	6.3492	-0.0014	-14.2311	-0.0001	1954.1102
		0.0287	0.0005	0.0467	0.0008	7468.7603
20501-2722	HJ 5226	7.0953	0.0000	17.2218	0.0010	1954.6303
		0.0416	0.0007	0.0727	0.0012	36919.9427
21022-4300	DUN 236	17.0342	0.0004	54.8487	-0.0001	1950.8127
		0.0013	0.0000	0.0026	0.0000	11913.1212
22246-4127	JC 19AB	6.8967	0.0100	24.1172	-0.1643	1950.0529
		0.0198	0.0003	0.0164	0.0003	7.7483
22258-2014	S 808AB	-5.9882	-0.0019	3.3369	-0.0023	1946.3114
		0.0081	0.0001	0.0111	0.0002	227.9759
22305-0807	STF2913	6.9074	-0.0010	-4.2123	-0.0005	1931.2844
		0.0146	0.0002	0.0179	0.0002	2283.0812
23141-0855	STF2993AB	-25.2456	0.0039	1.7769	0.0029	1940.1590
		0.0035	0.0000	0.0306	0.0004	621.2004
23141-0855	S 826AC	-52.1406	-0.0048	91.5732	-0.4773	1949.2814
		0.0413	0.0006	0.0414	0.0006	6.7973
23238-0828	STF3008	-2.6887	-0.0335	-2.1216	0.0617	1921.9226
		0.0080	0.0001	0.0133	0.0001	8.9509
23460-1841	H 2	-4.6773	-0.0040	4.4033	0.0072	1945.1662
		0.0079	0.0001	0.0079	0.0001	46.1036
23544-2703	LAL 192	-0.0101	0.0029	-6.6467	0.0028	1948.3459
		0.0005	0.0000	0.0122	0.0002	240.0132
23595-2631	LAL 193	-10.4105	-0.0003	1.8012	0.0023	1958.9360
		0.0046	0.0001	0.0177	0.0003	394.4704

Table A5 (conclusion). Rectilinear Elements of the Secondary Component of the 62 Pairs (In-depth details in Letchford, White and Ernest, 2018a)

Measures of 62 Southern Pairs

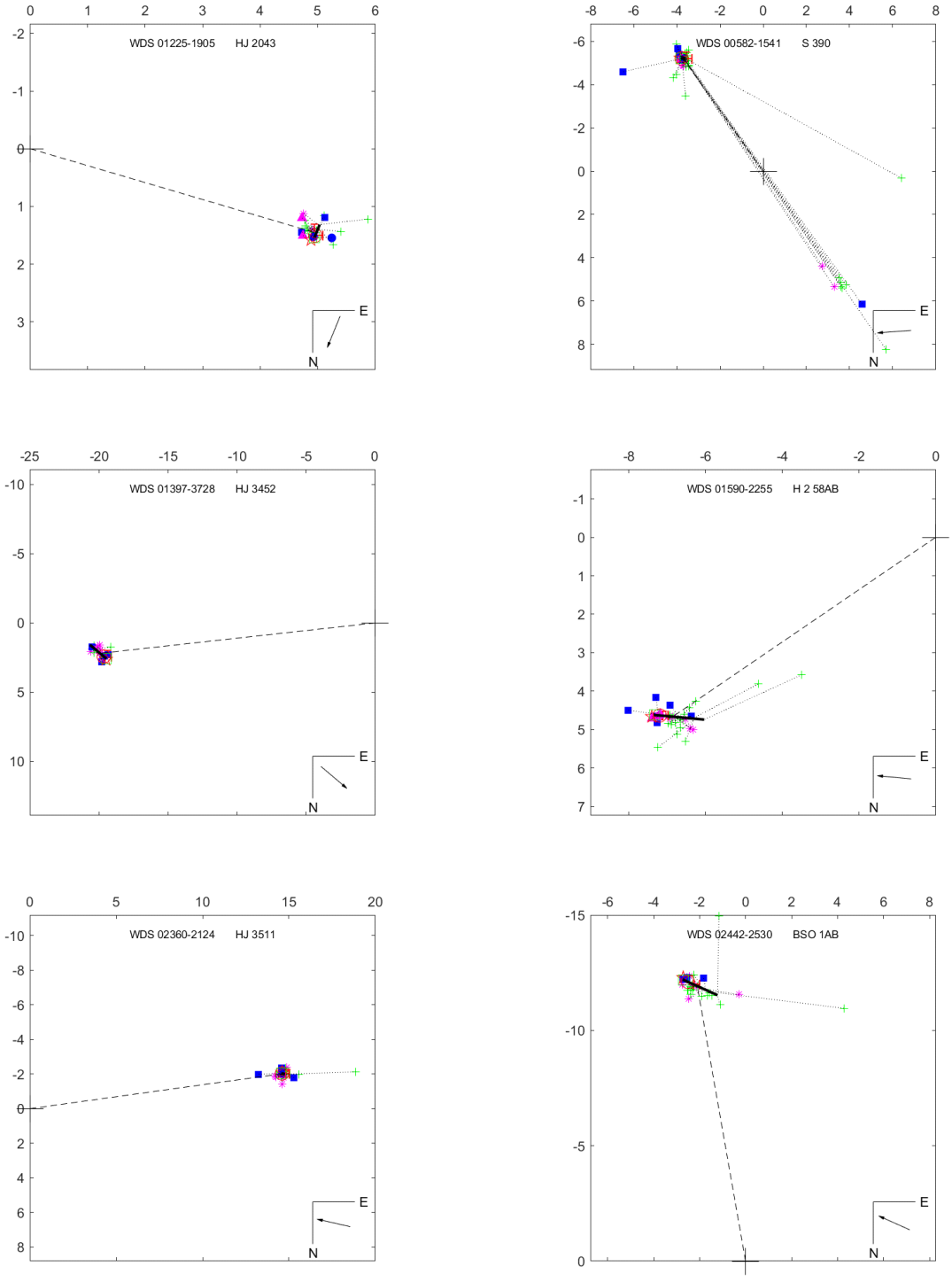

Figure A5. Rectilinear Motion of 61 Pairs. 15103-4100 (COO 178) removed (Section 7). (Details of computational technique is given in Letchford, White and Ernest, 2018a.)

Continues on the next page.

Measures of 62 Southern Pairs

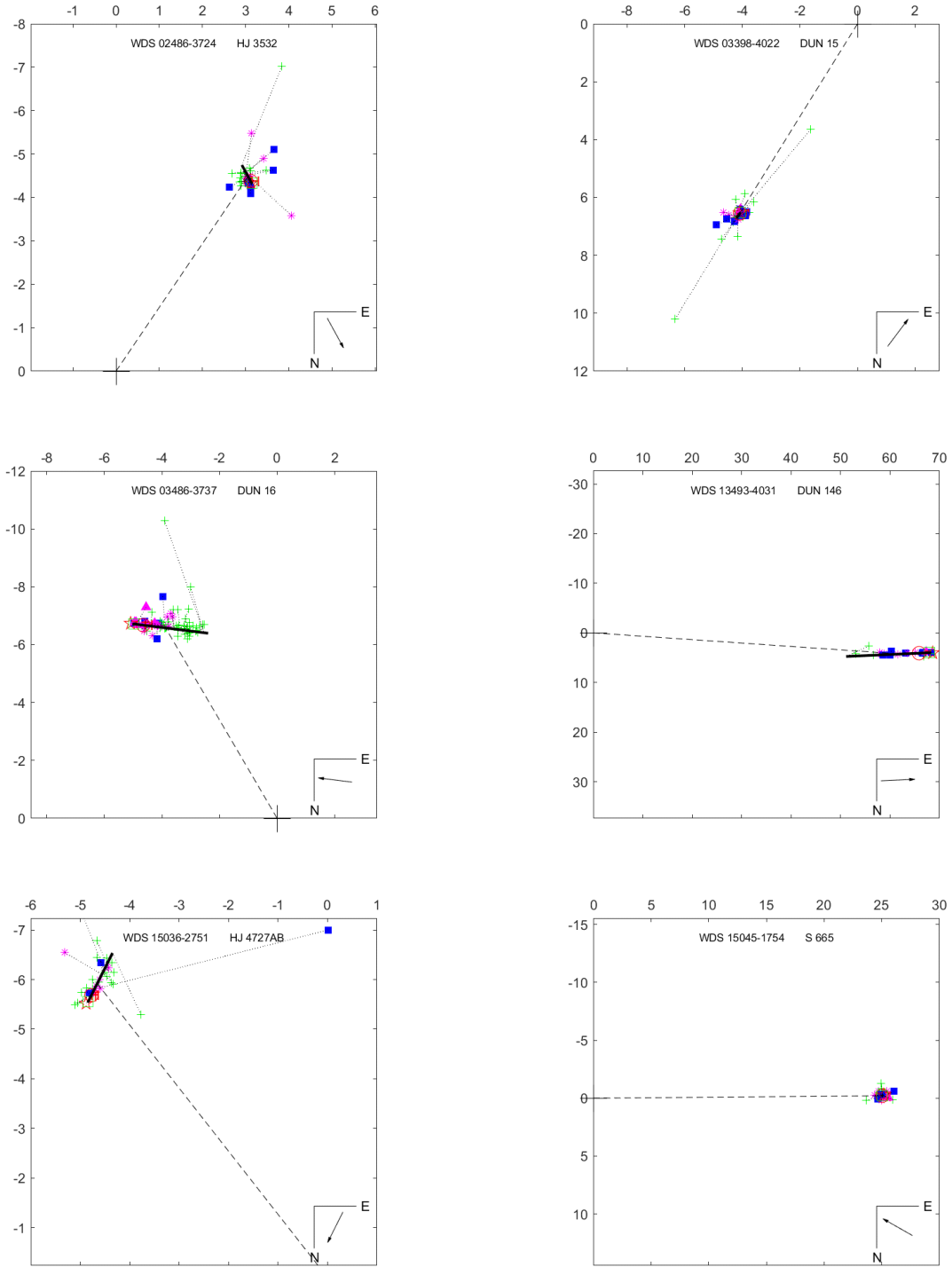

Figure A5. Rectilinear Motion of 61 Pairs. 15103-4100 (COO 178) removed (Section 7). (Details of computational technique is given in Letchford, White and Ernest, 2018a.)

Continues on the next page.

Measures of 62 Southern Pairs

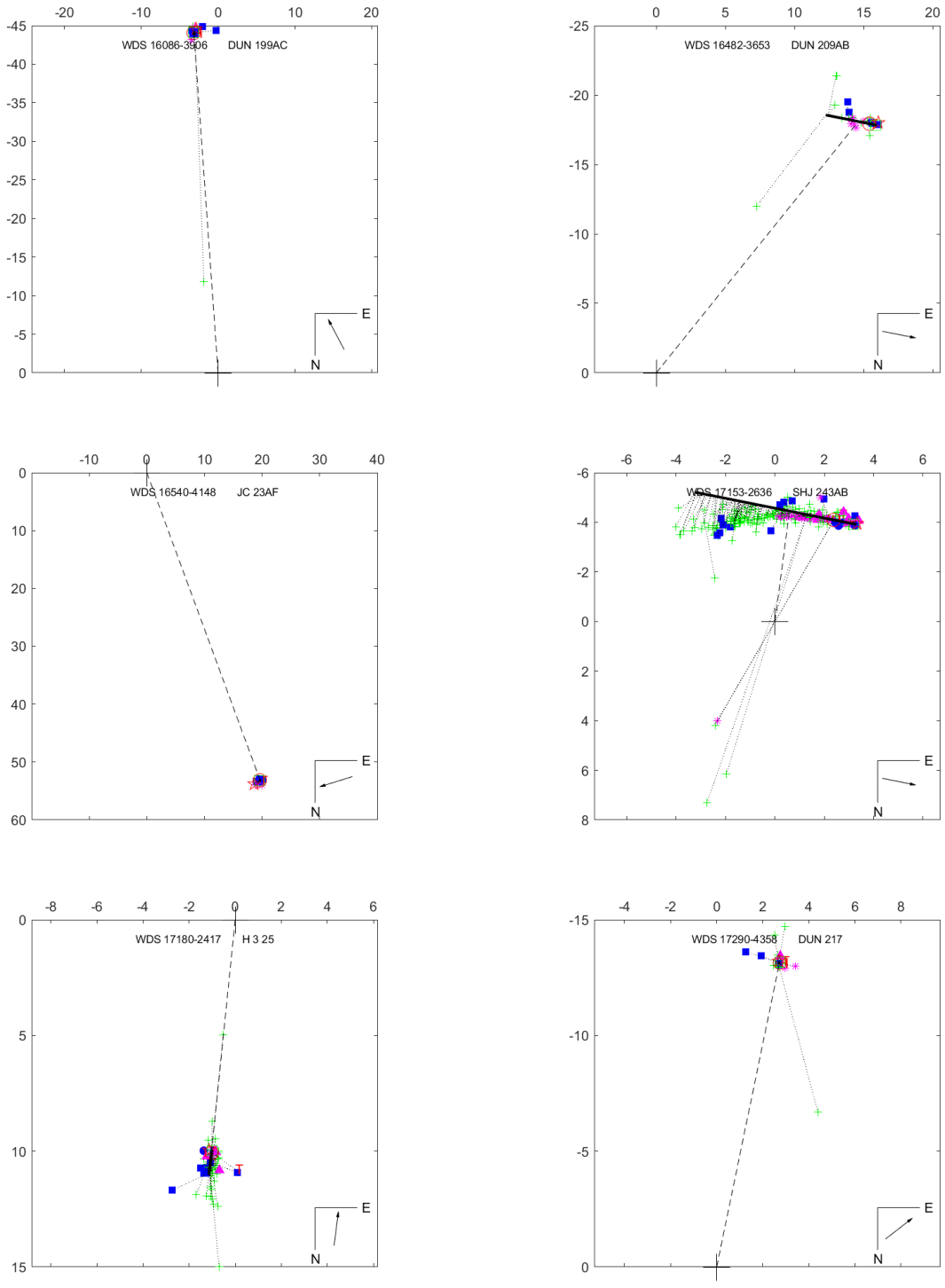

Figure A5. Rectilinear Motion of 61 Pairs. 15103-4100 (COO 178) removed (Section 7). (Details of computational technique is given in Letchford, White and Ernest, 2018a.)

Continues on the next page.

Measures of 62 Southern Pairs

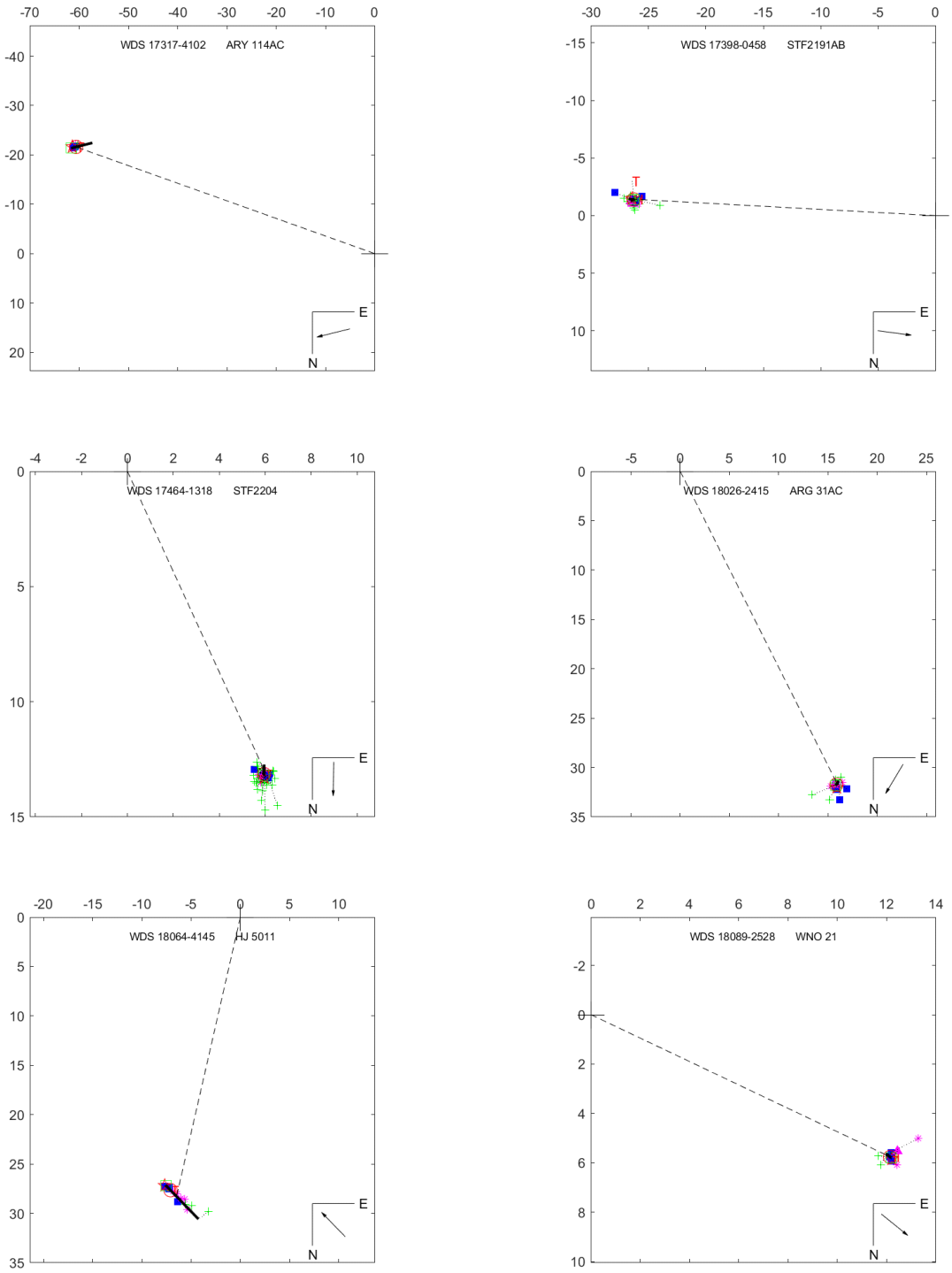

Figure A5. Rectilinear Motion of 61 Pairs. 15103-4100 (COO 178) removed (Section 7). (Details of computational technique is given in Letchford, White and Ernest, 2018a.)

Continues on the next page.

Measures of 62 Southern Pairs

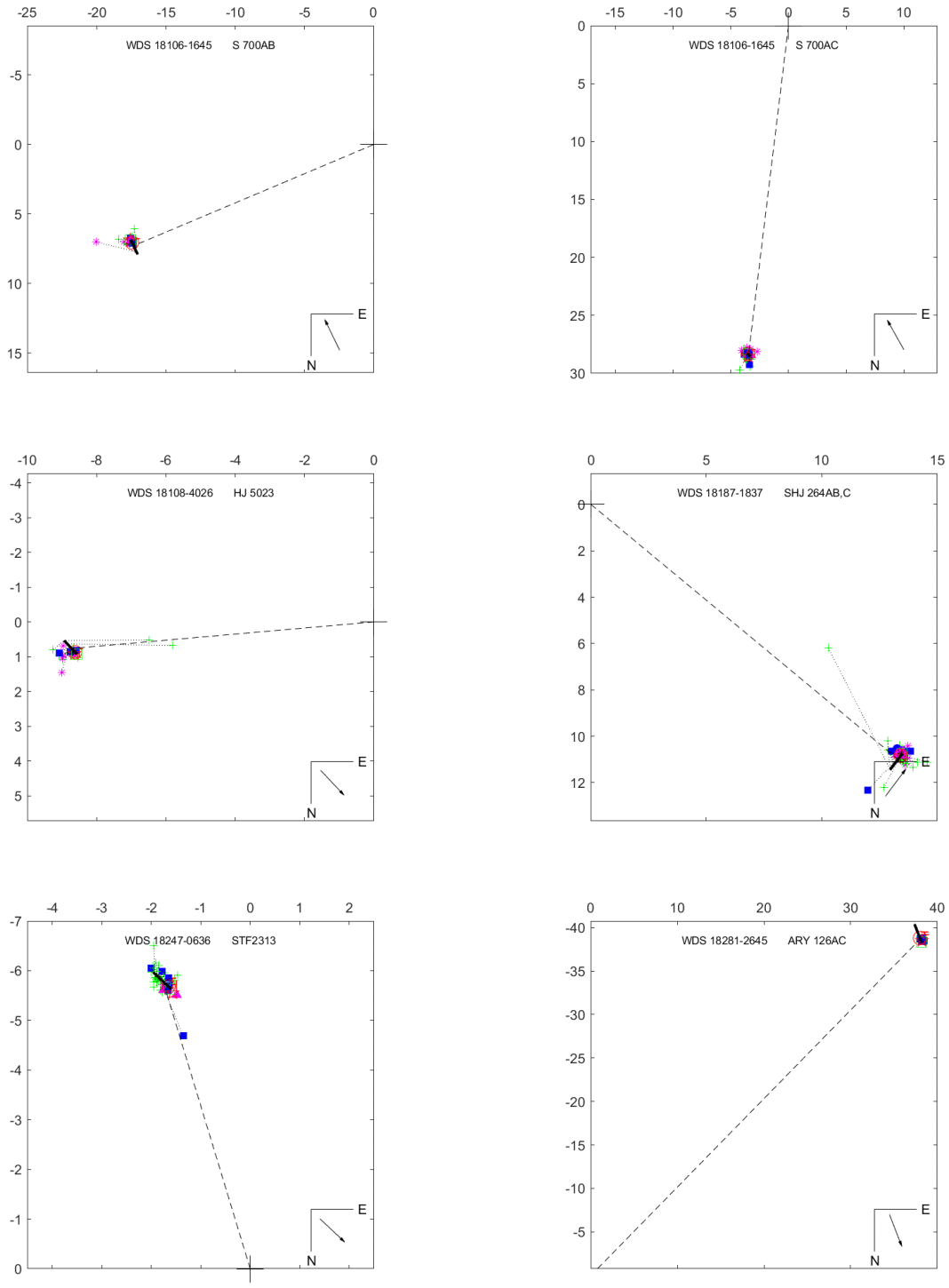

Figure A5. Rectilinear Motion of 61 Pairs. 15103-4100 (COO 178) removed (Section 7). (Details of computational technique is given in Letchford, White and Ernest, 2018a.)

Continues on the next page.

Measures of 62 Southern Pairs

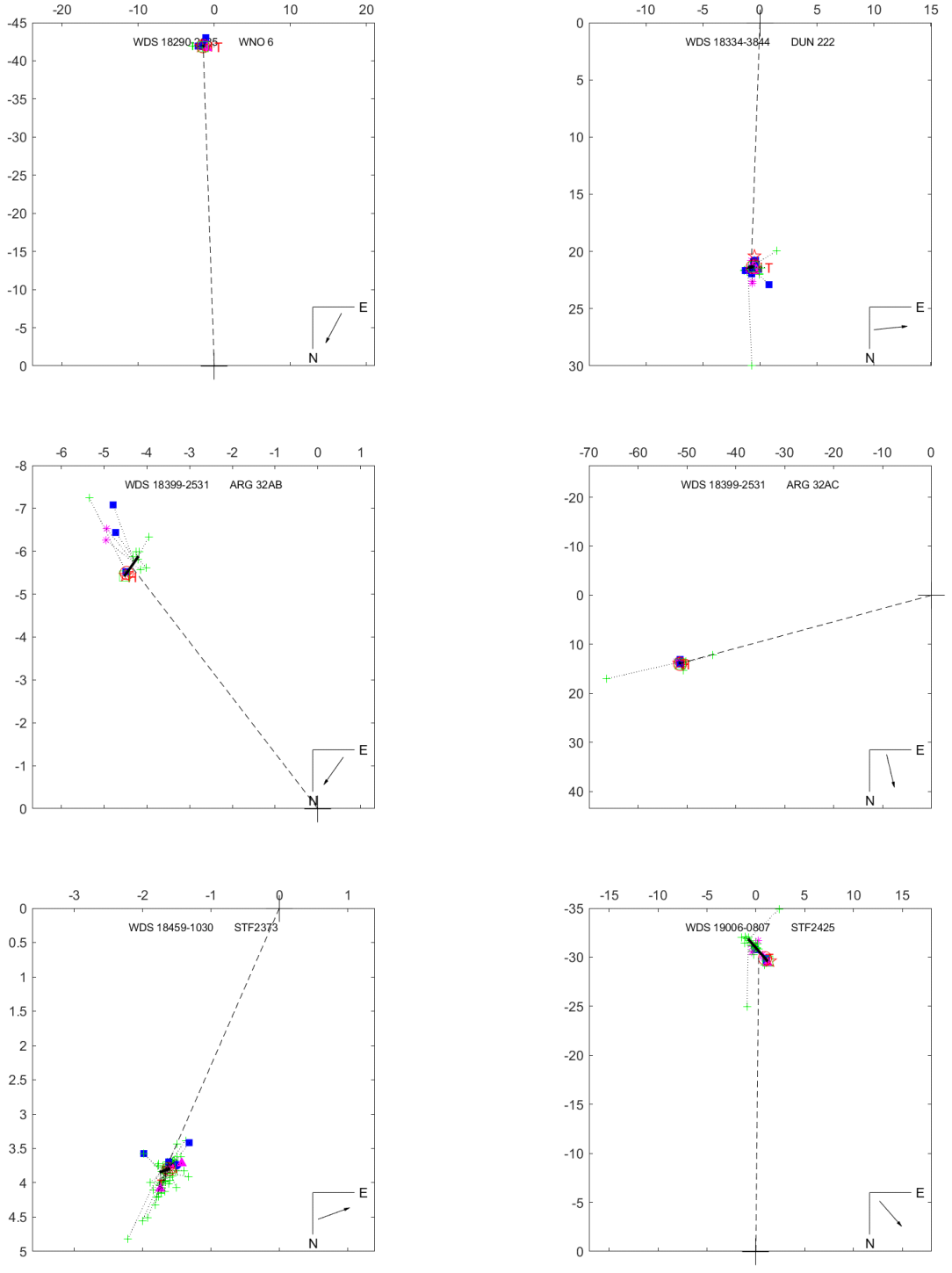

Figure A5. Rectilinear Motion of 61 Pairs. 15103-4100 (COO 178) removed (Section 7). (Details of computational technique is given in Letchford, White and Ernest, 2018a.)

Continues on the next page.

Measures of 62 Southern Pairs

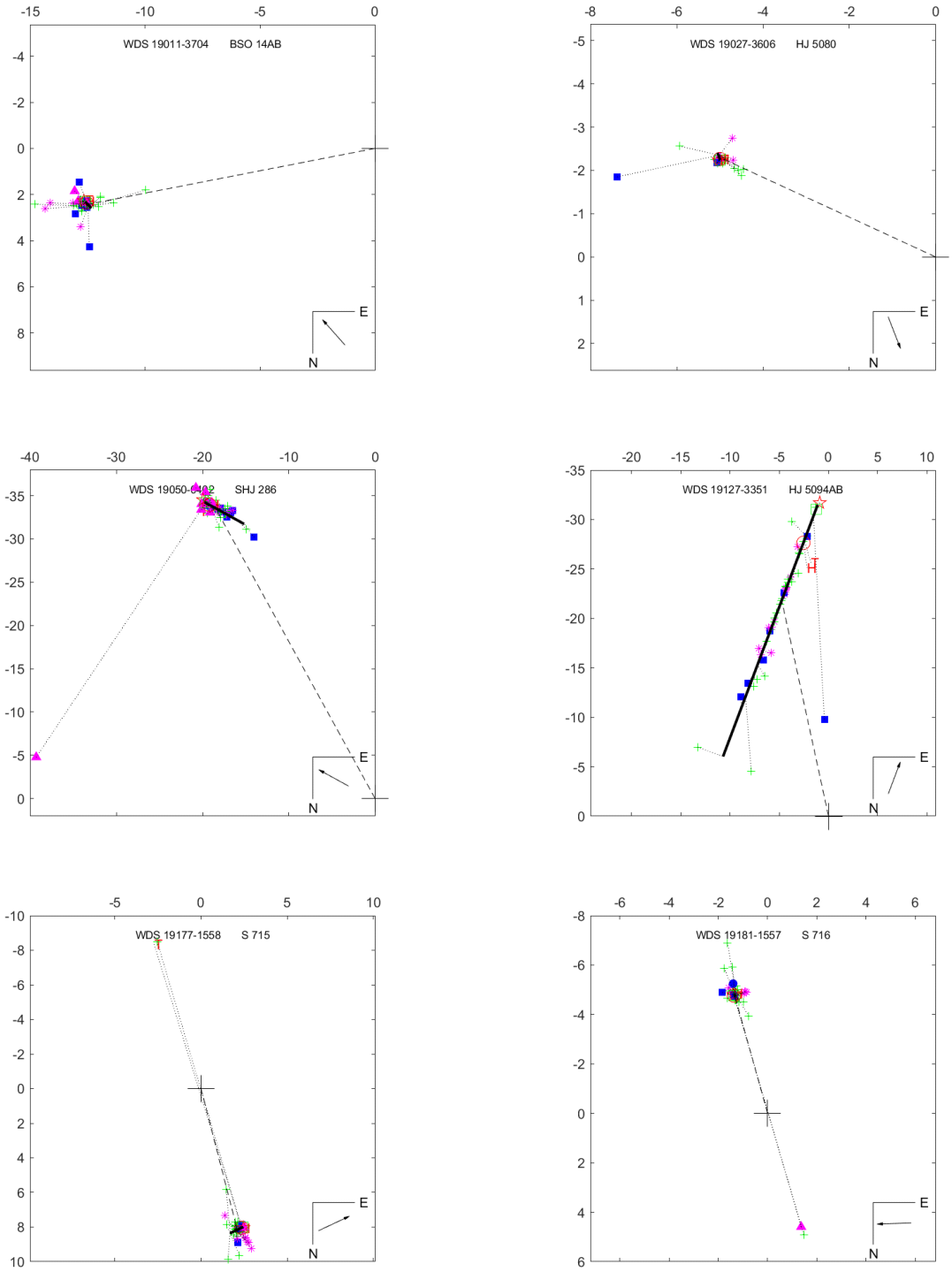

Figure A5. Rectilinear Motion of 61 Pairs. 15103-4100 (COO 178) removed (Section 7). (Details of computational technique is given in Letchford, White and Ernest, 2018a.)

Continues on the next page.

Measures of 62 Southern Pairs

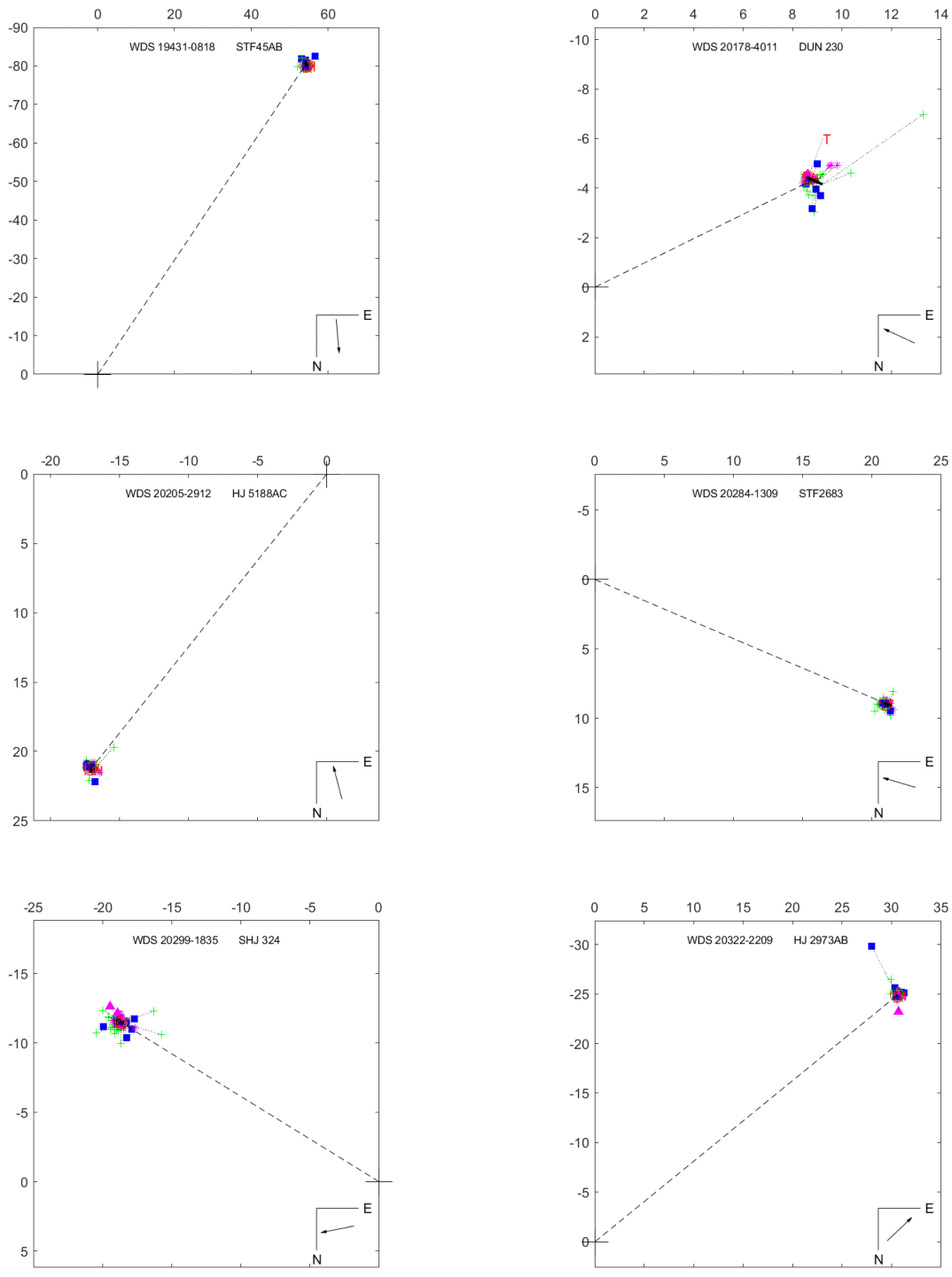

Figure A5. Rectilinear Motion of 61 Pairs. 15103-4100 (COO 178) removed (Section 7). (Details of computational technique is given in Letchford, White and Ernest, 2018a.)

Continues on the next page.

Measures of 62 Southern Pairs

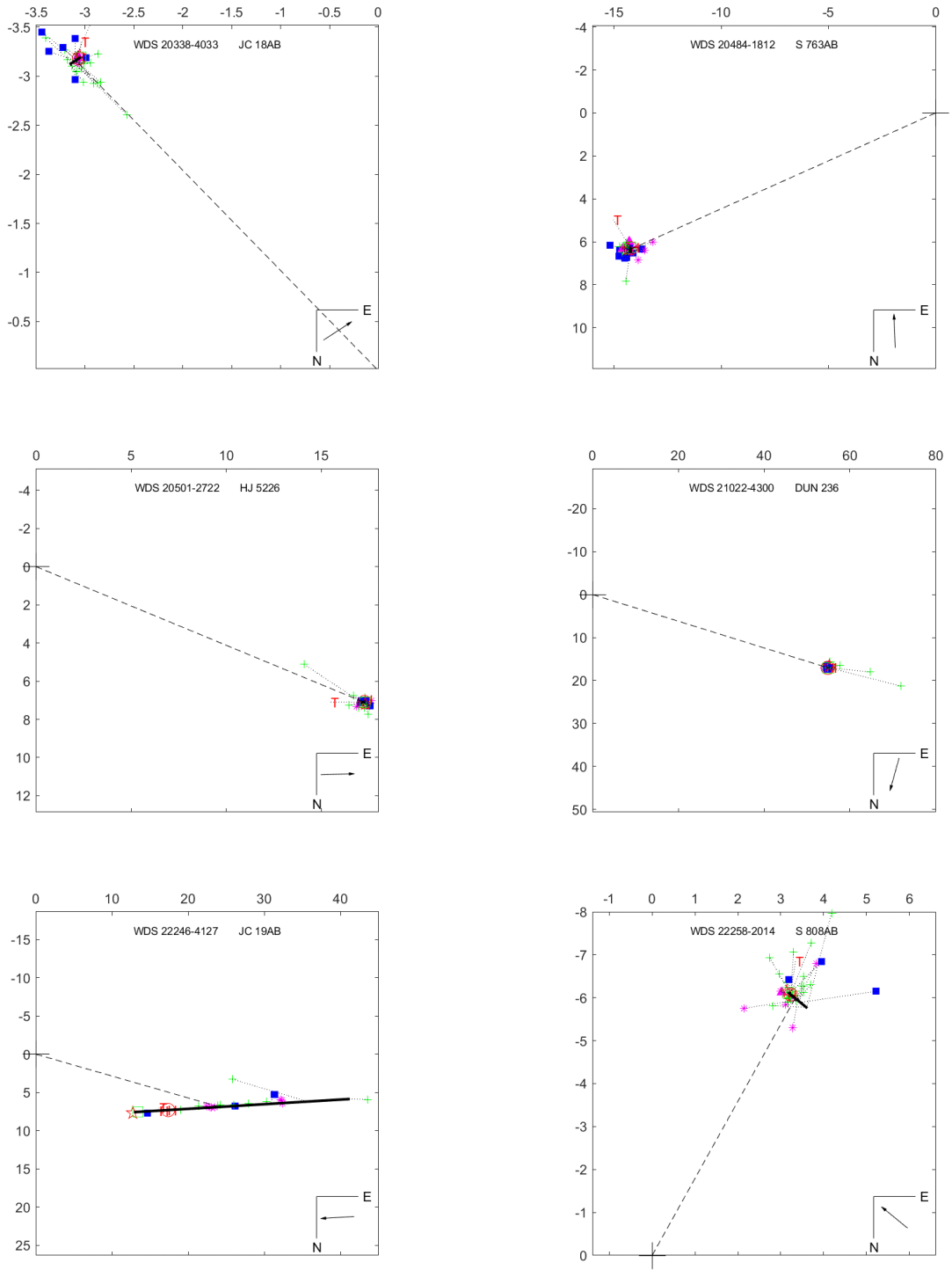

Figure A5. Rectilinear Motion of 61 Pairs. 15103-4100 (COO 178) removed (Section 7). (Details of computational technique is given in Letchford, White and Ernest, 2018a.)

Concludess on the next page.

Measures of 62 Southern Pairs

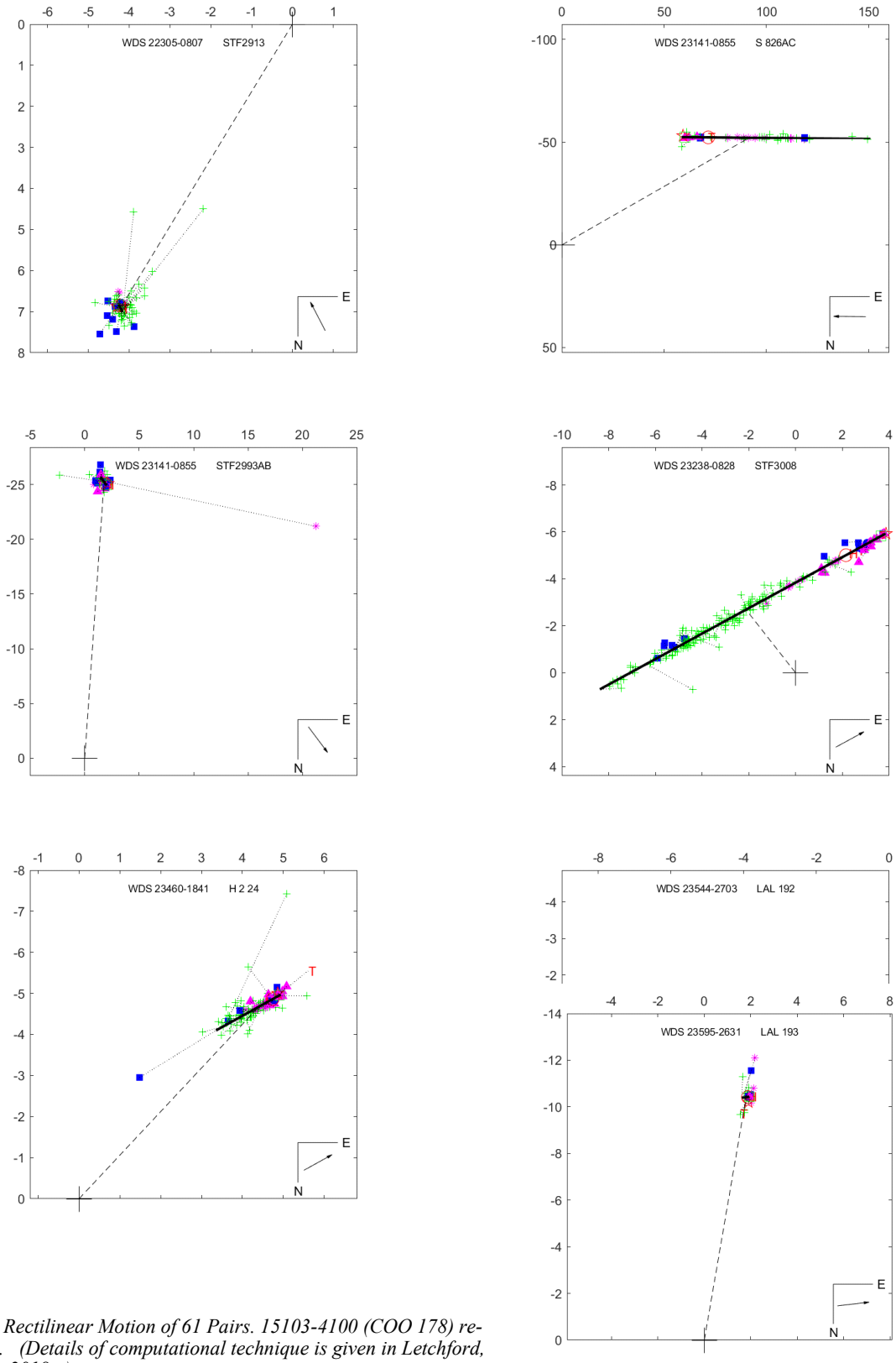

Figure A5. Rectilinear Motion of 61 Pairs. 15103-4100 (COO 178) removed (Section 7). (Details of computational technique is given in Letchford, White and Ernest, 2018a.)

Measures of 62 Southern Pairs

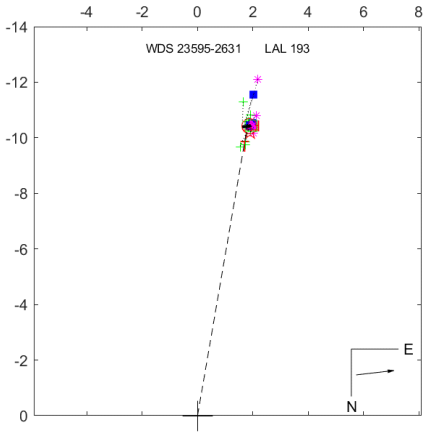

Figure A5 (conclusion). Rectilinear Motion of 61 Pairs. 15103-4100 (COO 178) removed (Section 7). (Details of computational technique is given in Letchford, White and Ernest, 2018a.)

WDS	Disc	P yrs	a"	i°	Ω°	T yr	e	ω°
		±	±	±	±	±	±	±
01590-2255	H 2 58AB	19551.176	12.760	169.176	179.714	700.866	0.820	108.335
		3179.441	1.072	1.989	3.583	4.794	0.005	2.159
02360-2124	HJ 3511	218347.189	30.564	64.094	66.945	16144.608	0.866	192.003
		15408.740	1.497	1.202	2.473	1256.611	0.029	5.971
17153-2636	SHJ 243AB	507.062	12.490	100.386	87.635	2205.223	0.899	91.981
		18.044	0.273	0.150	1.893	9.874	0.002	0.976
18247-0636	STF2313	6685.981	6.473	104.775	38.582	5262.567	0.604	56.992
		3551.475	1.515	1.617	14.506	915.520	0.046	22.403
23595-2631	LAL 193	364086.947	71.700	119.721	163.699	2009.785	0.850	348.262
		51528.580	5.789	1.196	5.522	4.595	0.012	6.091

Table A6. Grade 5 Orbital Elements for 5 Pairs.
(Details of computational technique is given in Letchford, White and Ernest, 2018b)

Measures of 62 Southern Pairs

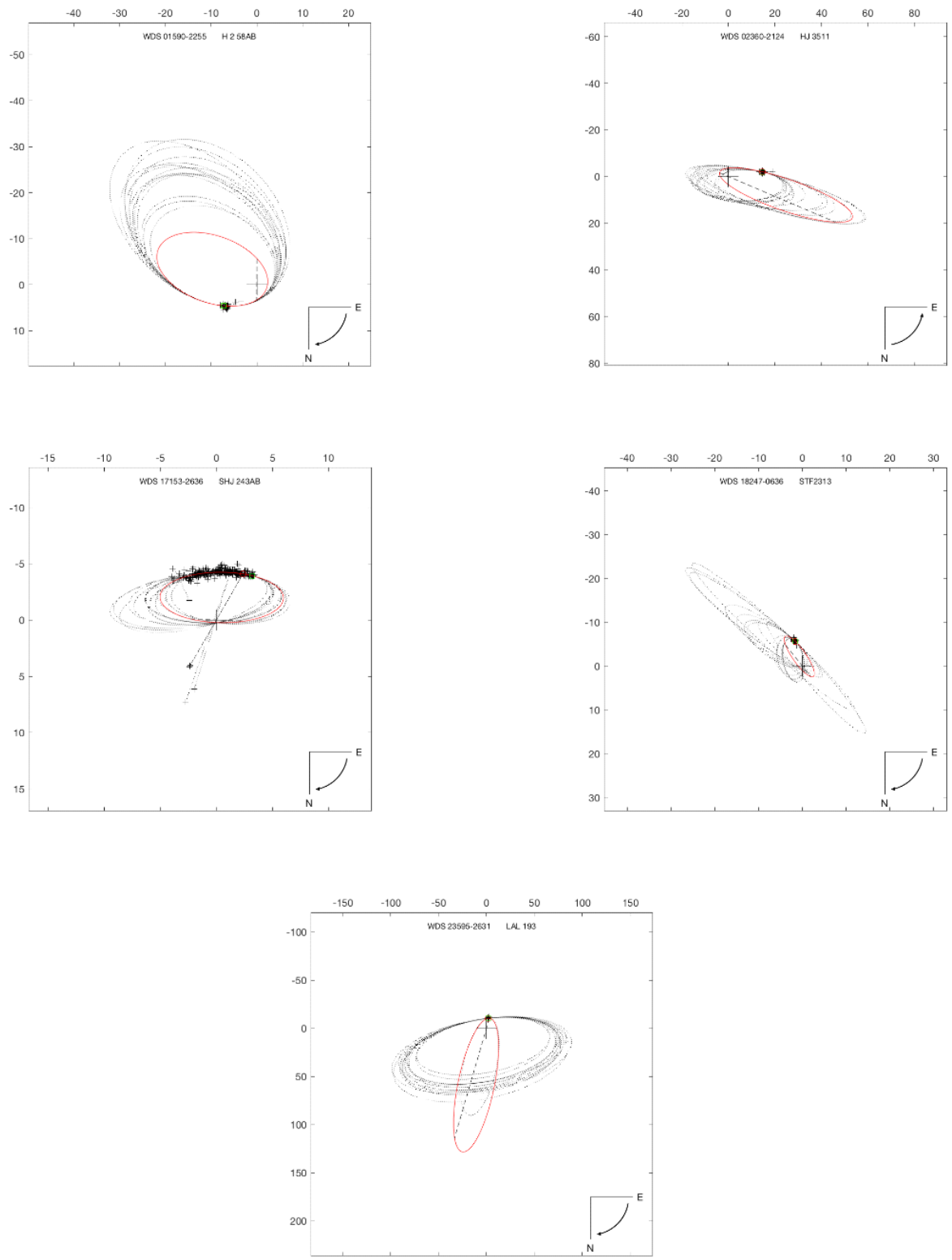

***Figure A6**: Family of Orbits for the 5 Pairs. (Details of computational technique is given in Letchford, White and Ernest, 2018b)*

Astrometric Measurement of WDS 13433-2458 AB

Roswell Roberts[1], Derek Chow[1], Kevin Lu[1], Marie Yokers[2], Pat Boyce[3], and Grady Boyce[3]

1. Westview High School, San Diego California
2. San Diego Mesa College, San Diego, California
3. Boyce Research Initiatives and Education Foundation, San Diego California

Abstract: By utilizing Las Cumbres Observatory (LCO) telescopes equipped with CCD imaging, measurements of theta and rho of the double star system WDS 13433-2458 AB (HJ 2671) were made. When compared to the 18 previous measurements of the system, the data does not point to signs of orbital motion and suggest that WDS 13433-2458 AB may not be physical.

Introduction

By determining the true nature of double and multiple star systems—whether or not they are gravitationally bound—astronomers can determine the masses of the system (and of each star if the distance is known and a good orbit derived); and other stellar characteristics such as radius, density, and the mass-luminosity relationship (MLR), can be estimated. As part of the Boyce Research Initiatives and Education Foundation (BRIEF), this research project aims to assist in the verification of whether a system is a gravitationally associated double or an optical double.

WDS 13433-2458 AB (HJ 2671AB) was selected after meeting the following criteria: right ascension (RA) of 12 to 16 hours for reduced air mass during imaging, delta magnitude of 3 or less, and separation of 5 to 15 arcseconds for image clarity.

Materials and Methods

Historical data for HJ 2671 AB was provided by the United States Naval Observatory, from which we derived a historical chart of theta and rho over time, Figure 1. The first measurement of HJ 2671 was in 1831 and it has been measured a total of 18 times (with the most recent observation being in 2016). Several sources,-- the Washington Double Star Catalog (WDS), GAIA, and Aladin 10-- were consulted for stellar data such as radial velocity, proper motion vectors, and parallax data. Key data points from GAIA are shown in Table 1.

The Las Cumbres Observatory (LCO) 0.4m telescopes were used to observe HJ 2671AB. Requests for these images were processed through the LCO Observing Portal with exposure times calculated using the LCO Exposure Time Calculator. SBIG CCD cameras with 2048 X 3072 pixels had a resolution of 0.57" per pixel and a field of view of 19′ X 29′. An SDSS-g filter was used to photograph HJ 2671 on Julian Date 2458580 at for a total of 12 images at 3 seconds exposure time each. With this telescope setting we deter-

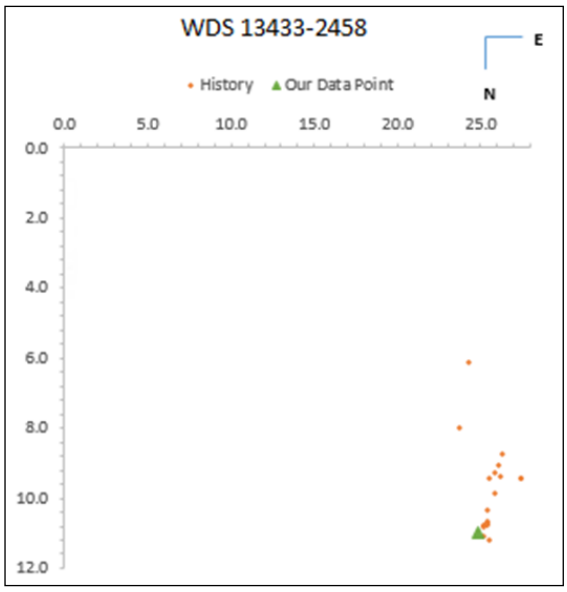

Figure 1. Historical Graph

Received March 3, 2020.

Astrometric Measurement of WDS 13433-2458 AB

	Primary Star	Secondary Star
	HJ 2671 A	HJ 2671 B
Proper Motion RA	-33.407	-38.895
Proper Motion RA Error	0.109	0.089
Proper Motion Dec	-14.294	0.8
Proper Motion Dec Error	0.108	0.081
Parallax	7.9587	1.8924
Parallax Error	0.0588	0.047
Radial Velocity	-13.12	-79.31
Radial Velocity Error	0.69	0.35

Table 1. Table of Gaia data

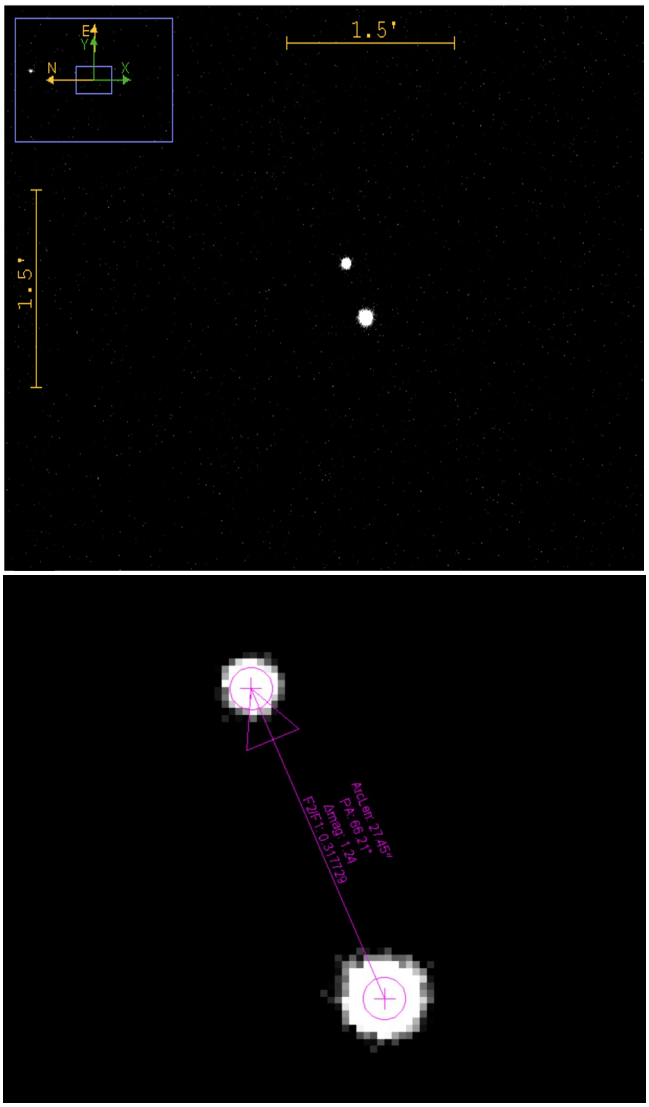

Figure 2. Images of HJ 2671 AB being measured in AstroimageJ

mined that on 2458580, HJ 2671 AB had a theta value of 66.099 degrees and a rho value of 27.507 arcseconds.

Each image was processed through the Our Solar Siblings (OSS) Pipeline to remove image imperfections and insert World Coordinate System (WCS) coordinates into the image files (Fitzgerald 2018). AstroImageJ (AIJ) was used to provide measurements of theta and rho, Figure 2, in order to compare them to the measurements found in the historical data. Once measured, the mean and standard deviations of the measurements were calculated, Table 2.

Results

Table 1 outlines the data obtained from the GAIA database. Table 2 shows the Mean, Standard Deviation, and Standard Error of the Mean for the position angle (θ) and separation (ρ) measured for HJ 2671AB.

Discussion

A graph of the historical data of the star, Figure 1, shows a roughly linear pattern in the movement of the B star relative to A. The trend indicates that the B star is moving in a northwesterly direction with a proper motion value of <-38.895, 0.800>. However, considering the individual motions of A and B against the celestial sphere, the A star is not moving in the same direction as the B star, but instead is moving in a southwesterly direction with a proper motion value of <-33.407, -14.294>, illustrated in Figure 3 where the proper motion vectors of the A and B star have been superimposed onto the image in Aladin10. Additionally, data from the GAIA satellite indicate the radial velocities of

Epoch 2019.264	Mean	Standard Deviation	Standard Error of Mean
Theta (degrees)	66.099°	0.065°	0.021°
Rho (seconds)	27.505"	0.028"	0.009"

Table 2: The mean, standard deviation, and standard error of the mean of the data collected

the A and B star respectively are -13.12 and -79.31. Since both of these values are negative, the two stars are moving away from Earth but because there is a 66.19 difference in radial velocities, we do not believe that they are moving away from Earth together.

Analysis of this data suggests that the stars are not

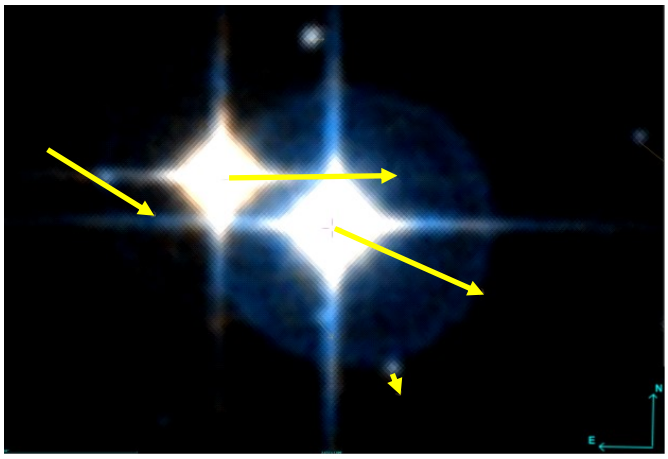

Figure 3: An image of HJ 2671 AB with proper motion vectors

moving together and instead are pursuing different paths through space. This is further supported by parallax data acquired from the GAIA satellite. The A star has a parallax of 7.9587 and an error of 0.0588, which puts the A star at a distance of 406.61 to 412.66 light years away from Earth. The B star's parallax is 1.8924 with a parallax error of 0.0471, placing the B star at a distance of 1681.19 to 1767.03 light years away, making the two stars separated by at least 1268.53 light years. The distance by which these two stars are separated is considerable and considering the inverse square relationship between the force of gravity and distance, we do not believe that HJ 2671 A is gravitationally bound to HJ 2671 B over a distance of 1268.53 light years.

Conclusion

The large distance between the A and B stars, the lack of a trend indicative of an orbit on the historical graph that included our current measurements, and the difference in proper motion vectors suggest that the star system is not a physical double.

Acknowledgments

We thank Brian Mason and the United States Naval Observatory for providing historical measurement data. We also thank Worldwide telescope systems for use of the LCO and the Boyce Research Initiatives and Education Foundation (BRIEF) for their generous support throughout the study that allowed us to access the remote telescope system and the necessary software. Additionally, we thank Michael Fitzgerald at the OSS Pipeline for processing images and removing imperfections made by the camera. This work has made use of data from the European Space Agency (ESA) mission Gaia (https://www.cosmos.esa.int/gaia), processed by the Gaia Data Processing and Analysis Consortium (DPAC, https://www.cosmos.esa.int/web/gaia/dpac/consortium). Funding for the DPAC has been provided by national institutions, in particular the institutions participating in the Gaia Multilateral Agreement.

References

Collins, K. A., Kielkopf, J. F., Stassun, K. G., and Hessman, F. V., 2018, "AstroImageJ: image processing and photometric extraction for ultra-precise astronomical light curves", *The Astronomical Journal*, **153**(2):77.

Fitzgerald, M.T., (2018, accepted), "The Our Solar Siblings Pipeline: Tackling the data issues of the scaling problem for robotic telescope-based astronomy education projects.", Robotic Telescopes, Student Research and Education Proceedings

Mason, B. and Hartkopf, W., 2015, The Washington Double Star Catalog. Astrometry Department, U.S. Naval Observatory.

Double Star Photometry - June 2019

Wilfried R.A. Knapp
Vienna, Austria
wilfried.knapp@gmail.com

Abstract: The WDS catalog currently (March 2020) contains about 150,800 objects. About 50,000 of these come with a magnitude for the primary with single digit precision indicating an estimation rather than a precise measurement and over 16,000 objects are listed with magnitudes in the blue or red band (WDS note codes B/K/R/I) and thus in need of a measurement in the V band. After eliminating all objects not suited for resolution with the tools currently available to me (angular separation too small, too faint, too bright), about 26,000 objects remained as targets of interest for this project. The selection criterion for the objects for a specific report is then at a given point of time simply the currently highest given altitude to eliminate atmospheric effects as far as possible – so this is then a more or less random selection out of the mentioned 26,000 objects. This report covers about 70 such objects (including some KPP objects also in need of photometry) with images taken June 2019 with V-filter to allow for visual magnitude measurement by differential photometry. This paper lists also a few WDSS objects as several newly detected likely physical pairs reported in Knapp 2019 were meanwhile included in the WDSS catalog. All objects were additionally checked for potential gravitational relationship using GAIA DR2 data for a Monte Carlo simulation of the spatial distance between the components of a pair and StarHorse median mass values for calculating tidal radii for these components.

1. Introduction

One single image was taken for all selected objects with iTelescope iT24 with V-filter and 20 seconds exposure time and the imaging conditions were overall quite favourable.

The images were plate solved with Astrometrica using the URAT1 catalog with reference stars in the Vmag range of 8.5 to 16.5 giving not only RA/Dec coordinates but also photometry results for all reference stars used including an average Vmag error. The objects were then located in the center of the image and astrometry/photometry was then done by the rather comfortable Astrometrica procedure with point and click at the components delivering RA/Dec coordinates and Vmag measurements based on all reference stars used for plate solving.

2. Results of Image Processing

The measurement results are given in Table 1 with the following structure:

- WDS/WDSS = WDS/WDSS ID
- Disc = WDS discoverer designation (blank for WDSS objects)
- C = Components (AB if blank)
- RA/Dec = Positions for primary and secondary in HH:MM:SS.sss/DD.MM.SS.ss format
- dRA/dDec = Plate solving errors for RA and Dec in arcseconds
- Sep = Calculated separation in arcseconds
- e_Sep = Separation error
- PA = Calculated position angle in degrees
- e_PA = Position angle error
- Mag = Vmags for both components measured by differential photometry
- e_Mag = Magnitude errors
- SNR = Signal to noise ratio for both components
- dVmag = Plate solving error in Vmag
- Date = Julian observation epoch
- Notes = Additional comments listed below Table 1

(Text continues on page 357)

Received March 23, 2020.

Double Star Photometry - June 2019

WDS/WDSS	Disc	C	RA	Dec	dRA	dDec	Sep	Err Sep	PA	Err PA	Mag	Err Mag	SNR	dVmag	Date	Notes
14516+3453	ALI 131		14 51 38.779	34 52 34.39	0.15	0.13	8.74786	0.19849	112.659	1.300	9.817	0.140	100.67	0.14	2019.41891	1)
			14 51 39.435	34 52 31.02							12.156	0.143	36.04			
15157+3642	ALI 601		15 15 43.604	36 41 59.46	0.06	0.09	4.41002	0.10817	292.815	1.405	10.885	0.040	172.57	0.04	2019.41892	1)
			15 15 43.266	36 42 01.17							12.628	0.045	50.56			
15096+2930	BRT 28	A	15 09 23.049	29 31 00.83	0.05	0.06	6.13670	0.07810	209.710	0.729	12.330	0.041	118.32	0.04	2019.41894	1)
		B	15 09 22.816	29 30 55.50							12.270	0.041	117.19			
15096+2930	BRT 28	B	15 09 22.816	29 30 55.50	0.05	0.06	6.37134	0.07810	181.174	0.702	12.270	0.009	117.19	0.04	2019.41894	1)
		C	15 09 22.806	29 30 49.13							12.654	0.041	103.41			
15096+2930	BRT 28	A	15 09 23.049	29 31 00.83	0.05	0.06	12.12235	0.07810	195.169	0.369	12.330	0.041	118.32	0.04	2019.41894	1)
		C	15 09 22.806	29 30 49.13							12.654	0.041	103.41			
15155+3049	BRT 251		15 15 34.100	30 48 20.36	0.08	0.09	5.23061	0.12042	10.072	1.319	12.157	0.041	106.45	0.04	2019.41896	1)
			15 15 34.171	30 48 25.51							13.228	0.043	64.87			
14270+3517	BU 9028	B	14 27 01.968	35 16 27.23	0.09	0.06	13.09059	0.10817	219.713	0.473	11.540	0.041	164.46	0.04	2019.41903	1)
		C	14 27 01.285	35 16 17.16							14.103	0.045	50.11			
15302+4235	BVD 241		15 30 13.174	42 34 23.01	0.07	0.08	18.03097	0.10630	251.068	0.338	15.815	0.045	31.40	0.03	2019.41897	2)
			15 30 11.630	42 34 17.16							15.776	0.047	29.00			
14280+3546	COU1266	A	14 27 58.309	35 47 38.06	0.08	0.10	15.76307	0.12806	274.257	0.465	11.661	0.070	135.98	0.07	2019.41898	1)
		C	14 27 57.017	35 47 39.23							12.776	0.071	90.31			
15080+4355	CVR 778		15 08 02.570	43 54 30.18	0.06	0.07	12.85196	0.09220	316.873	0.411	15.519	0.048	39.46	0.04	2019.41898	1)
			15 08 01.757	43 54 39.56							16.329	0.061	23.30			
15028+3551	DAM 83	B	15 02 42.152	35 51 53.51	0.06	0.06	13.04841	0.08485	284.967	0.373	12.760	0.041	101.00	0.04	2019.41902	1) 5)
		C	15 02 41.115	35 51 56.88							16.253	0.103	10.98			
15028+3551	DAM 83	C	15 02 41.115	35 51 56.88	0.06	0.06	15.23443	0.08485	289.958	0.319	16.253	0.103	10.98	0.04	2019.41902	1) 6)
		D	15 02 39.937	35 52 02.08							16.986	0.138	7.73			
15053+2914	DAM 368		15 05 17.878	29 13 43.76	0.07	0.07	26.43643	0.09899	14.100	0.215	11.025	0.060	185.69	0.06	2019.41899	1)
			15 05 18.370	29 14 09.40							14.284	0.064	48.28			
14557+4355	FYM 235		14 55 44.207	43 55 20.79	0.07	0.08	11.46298	0.10630	351.599	0.531	10.190	0.040	174.80	0.04	2019.41900	1)
			14 55 44.052	43 55 32.13							13.462	0.043	67.31			
14496+4344	FYM 236		14 49 35.986	43 44 21.30	0.10	0.06	17.66585	0.11662	123.772	0.378	11.437	0.041	132.91	0.04	2019.41900	1)
			14 49 37.341	43 44 11.48							12.966	0.042	82.64			
14496+4344	FYM 236	B	14 49 37.341	43 44 11.48	0.10	0.06	30.36377	0.11662	175.496	0.220	12.966	0.042	82.64	0.04	2019.41900	1)
		C	14 49 37.561	43 43 41.21							15.178	0.057	26.02			
14500+4319	FYM 651		14 49 58.785	43 19 06.45	0.06	0.06	8.59804	0.08485	141.727	0.565	13.904	0.035	60.49	0.03	2019.41901	1)
			14 49 59.273	43 18 59.70							14.525	0.039	43.30			
14260+3422	GIC 118		14 25 59.507	34 22 11.96	0.05	0.06	559.73740	0.07810	357.759	0.008	10.243	0.040	220.48	0.04	2019.41901	1)
			14 25 57.739	34 31 31.27							13.540	0.043	65.98			
14554+4354	HDS2106		14 55 25.664	43 54 06.62	0.05	0.04	5.38150	0.06403	39.542	0.682	11.104	0.031	181.96	0.03	2019.41902	1)
			14 55 25.981	43 54 10.77							13.407	0.036	56.02			
15028+3551	HJ 245		15 02 43.374	35 52 01.03	0.06	0.06	16.64948	0.08485	243.149	0.292	12.598	0.041	112.05	0.04	2019.41902	1)
			15 02 42.152	35 51 53.51							12.760	0.041	101.00			

Table 1. Results for measured WDS/WDSS objects

Table 1 continues on the next page.

Double Star Photometry - June 2019

WDS/WDSS	Disc	C	RA	Dec	dRA	dDec	Sep	Err Sep	PA	Err PA	Mag	Err Mag	SNR	dVmag	Date	Notes
14185+3837	HJ 545		14 18 31.573	38 37 53.39	0.11	0.08	9.15664	0.13601	243.119	0.851	12.737	0.042	89.33	0.04	2019.41903	1)
			14 18 30.876	38 37 49.25							13.238	0.043	75.04			
14270+3517	HJ 550		14 26 59.543	35 16 37.85	0.09	0.06	31.38455	0.10817	109.759	0.197	11.105	0.040	179.84	0.04	2019.41903	1)
			14 27 01.955	35 16 27.24							11.541	0.041	166.44			
14270+3517	BU 9028	B	14 27 01.955	35 16 27.24	0.09	0.06	12.97396	0.10817	219.158	0.478	11.541	0.041	166.44	0.04	2019.41903	1)
		C	14 27 01.286	35 16 17.18							14.104	0.045	51.16			
14453+3649	HJ 557		14 45 18.648	36 48 27.76	0.06	0.05	17.89427	0.07810	48.445	0.250	10.793	0.030	218.33	0.03	2019.41904	1)
			14 45 19.763	36 48 39.63							13.335	0.033	78.78			
15129+3145	HJ 569		15 12 52.948	31 44 11.13	0.07	0.08	13.53711	0.10630	67.731	0.450	13.129	0.052	86.37	0.05	2019.41904	1)
			15 12 53.930	31 44 16.26							14.400	0.020	54.66			
15181+3452	HJ 571		15 18 09.734	34 52 31.83	0.07	0.07	10.07076	0.09899	220.917	0.563	11.535	0.060	159.79	0.06	2019.41905	1)
			15 18 09.198	34 52 24.22							12.351	0.010	112.94			
14454+2911	HJ 2745		14 45 23.167	29 10 53.74	0.08	0.08	12.46251	0.11314	127.694	0.520	9.687	0.050	239.40	0.05	2019.41906	1)
			14 45 23.920	29 10 46.12							12.890	0.051	92.06			
15099+3208	HJ 2769		15 09 58.995	32 09 27.40	0.09	0.11	15.70319	0.14213	22.288	0.519	11.576	0.051	138.05	0.05	2019.41906	1)
			15 09 59.464	32 09 41.93							13.635	0.053	60.08			
14292+4009	KPP 737		14 29 11.217	40 08 58.25	0.06	0.08	6.46079	0.10000	11.984	0.887	11.525	0.008	133.42	0.05	2019.41907	1)
			14 29 11.334	40 09 04.57							12.454	0.051	93.65			
15124+3650	KPP 762		15 12 23.616	36 49 38.62	0.03	0.04	6.62771	0.05000	270.173	0.432	11.226	0.050	194.64	0.05	2019.41623	1)
			15 12 23.064	36 49 38.64							14.334	0.056	42.71			
14512+4518	KPP 865		14 51 14.162	45 17 52.23	0.06	0.06	7.32581	0.08485	218.162	0.664	13.016	0.042	96.40	0.04	2019.42165	1)
			14 51 13.733	45 17 46.47							13.591	0.042	76.61			
15101+4208	KPP1194		15 10 03.732	42 07 29.38	0.05	0.06	9.29519	0.07810	147.737	0.481	12.042	0.060	168.03	0.06	2019.42166	1)
			15 10 04.178	42 07 21.52							12.706	0.061	120.51			
16006-3112	KPP1232		16 00 34.558	-31 12 04.76	0.11	0.11	9.31302	0.15556	200.905	0.957	10.329	0.150	187.41	0.15	2019.42517	3)
			16 00 34.299	-31 12 13.46							16.277	0.157	22.82			
14231+4106	KPP1278		14 23 03.226	41 05 30.19	0.06	0.07	9.69335	0.09220	55.072	0.545	11.379	0.070	210.88	0.07	2019.42167	1)
			14 23 03.929	41 05 35.74							13.409	0.071	83.66			
15170+4109	KPP1471		15 17 00.619	41 09 21.87	0.10	0.09	11.10507	0.13454	145.848	0.694	14.800	0.120	22.68	0.11	2019.41622	1)
			15 17 01.171	41 09 12.68							14.630	0.118	25.31			
16074-3127	KPP2285		16 07 26.366	-31 27 23.41	0.11	0.12	19.28244	0.16279	304.494	0.484	12.146	0.090	146.86	0.09	2019.42518	3)
			16 07 25.124	-31 27 12.49							14.264	0.091	68.11			
15281+4257	KPP2315		15 28 03.340	42 57 04.80	0.06	0.06	19.50863	0.08485	211.295	0.249	13.197	0.051	93.95	0.05	2019.42169	1)
			15 28 02.417	42 56 48.13							13.746	0.052	72.07			
14446+3606	KPP2387		14 44 35.205	36 06 28.54	0.04	0.03	20.58977	0.05000	21.402	0.139	13.378	0.023	98.40	0.02	2019.41624	2)
			14 44 35.825	36 06 47.71							14.339	0.027	61.55			
14523+3344	KPP2427		14 52 17.481	33 44 24.52	0.10	0.12	21.48360	0.15620	282.883	0.417	12.819	0.099	26.00	0.09	2019.41618	1) 7)
			14 52 15.802	33 44 29.31							13.276	0.111	16.43			
14354+3349	KPP3283		14 35 21.861	33 48 56.90	0.07	0.08	11.25538	0.10630	156.992	0.541	10.069	0.060	281.93	0.06	2019.41630	2) 7)
			14 35 22.214	33 48 46.54							16.907	0.116	10.48			

Table 1 (continued). Results for measured WDS/WDSS objects

Table 1 continues on the next page.

Double Star Photometry - June 2019

WDS/WDSS	Disc	C	RA	Dec	dRA	dDec	Sep	Err Sep	PA	Err PA	Mag	Err Mag	SNR	dVmag	Date	Notes
1434569+323125			14 34 56.935	32 31 25.65	0.08	0.08	16.45251	0.11314	354.619	0.394	11.579	0.050	172.17	0.05	2019.41626	1)
			14 34 56.813	32 31 42.03							15.718	0.067	24.24			
1451558+422143			14 51 55.741	42 21 42.27	0.08	0.12	6.04587	0.14422	103.682	1.367	16.888	0.199	5.14	0.05	2019.41629	2) 8)
			14 51 56.271	42 21 40.84							16.497	0.172	6.11			
1457587+342221			14 57 58.739	34 22 21.01	0.07	0.05	22.49998	0.08602	51.032	0.219	10.834	0.040	214.77	0.04	2019.41624	2)
			14 58 00.152	34 22 35.16							14.717	0.047	43.14			
1459511+321436			14 59 51.165	32 14 34.37	0.15	0.13	31.18997	0.19849	6.962	0.365	13.000	0.113	20.41	0.10	2019.41619	1) 7)
			14 59 51.463	32 15 05.33							13.784	0.138	10.89			
1504122+365201			15 04 12.193	36 52 01.66	0.08	0.08	13.69580	0.11314	31.481	0.473	10.939	0.070	199.01	0.07	2019.41625	2)
			15 04 12.789	36 52 13.34							15.297	0.077	33.21			
1507269+304714			15 07 26.912	30 47 15.03	0.08	0.07	8.80014	0.10630	283.873	0.692	9.738	0.040	251.30	0.04	2019.41625	2)
			15 07 26.249	30 47 17.14							14.908	0.050	36.16			
1517078+334051			15 17 07.747	33 40 52.54	0.09	0.09	9.52596	0.12728	357.973	0.766	10.395	0.050	246.73	0.05	2019.41627	2)
			15 17 07.720	33 41 02.06							15.652	0.066	24.57			
1518536+375547			15 18 53.632	37 55 47.88	0.10	0.09	58.34342	0.13454	346.920	0.132	10.169	0.060	266.56	0.06	2019.41628	1)
			15 18 52.516	37 56 44.71							16.164	0.076	22.70			
1529277+375636			15 29 27.739	37 56 38.52	0.07	0.09	12.04792	0.11402	109.845	0.542	9.403	0.060	315.43	0.06	2019.41628	2) 7)
			15 29 28.697	37 56 34.43							16.246	0.085	17.39			
1530278+364816			15 30 27.653	36 48 17.05	0.08	0.09	32.66008	0.12042	180.126	0.211	7.923	0.061	85.75	0.06	2019.41629	2) 9)
			15 30 27.647	36 47 44.39							15.808	0.079	20.80			
14592+3956	KPP4338	A	14 59 12.370	39 56 15.24	0.07	0.08	6.69689	0.10630	17.697	0.909	15.836	0.065	26.06	0.05	2019.41627	2) 7)
		B	14 59 12.547	39 56 21.62							16.525	0.085	15.22			
14592+3956	KPP4338	A	14 59 12.370	39 56 15.24	0.07	0.08	56.72695	0.10630	309.665	0.107	15.836	0.069	26.06	0.06	2019.41627	2)
		C	14 59 08.573	39 56 51.45							15.955	0.071	24.37			
16029-3210	PRO 128	A	16 02 56.977	-32 09 43.00	0.11	0.12	6.29022	0.16279	130.798	1.482	8.830	0.120	127.48	0.12	2019.41621	3)
		B	16 02 57.352	-32 09 47.11							11.851	0.124	34.18			
16029-3210	KPP4386	A	16 02 56.977	-32 09 43.00	0.11	0.12	44.05602	0.16279	345.801	0.212	8.830	0.120	127.48	0.12	2019.41621	3)
		C	16 02 56.126	-32 09 00.29							15.357	0.123	41.91			
15211+3102	KZA 81		15 21 07.728	31 01 53.07	0.07	0.07	7.99082	0.09899	173.535	0.710	13.605	0.052	75.37	0.05	2019.42170	1) 10)
			15 21 07.798	31 01 45.13							15.297	0.061	31.02			
15216+3059	KZA 83		15 21 37.000	30 59 39.92	0.05	0.06	12.31196	0.07810	43.573	0.363	13.521	0.041	99.09	0.04	2019.42171	4)
			15 21 37.660	30 59 48.84							14.582	0.044	59.20			
15219+3052	KZA 84	A	15 21 59.837	30 52 17.33	0.06	0.08	65.28545	0.10000	354.103	0.088	12.743	0.061	113.02	0.06	2019.42171	1)
		B	15 21 59.316	30 53 22.27							13.215	0.061	87.28			
15219+3052	KZA 84	A	15 21 59.837	30 52 17.33	0.06	0.08	99.12207	0.10000	9.118	0.058	12.743	0.061	113.02	0.06	2019.42171	1)
		C	15 22 01.057	30 53 55.20							13.730	0.062	67.89			
15274+3102	KZA 90		15 27 25.450	31 01 41.16	0.03	0.04	19.88001	0.05000	298.284	0.144	13.924	0.043	63.09	0.04	2019.42172	1)
			15 27 24.088	31 01 50.58							14.745	0.048	40.42			
15309+4145	KZA 92	A	15 30 49.357	41 44 58.54	0.04	0.04	15.17901	0.05657	279.442	0.214	13.725	0.043	71.09	0.04	2019.42172	1)
		B	15 30 48.019	41 45 01.03							14.291	0.045	52.45			
		A	15 30 49.357	41 44 58.54							13.725	0.043	71.09			
		C	15 30 48.295	41 45 21.78							14.576	0.047	42.93			

Table 1 (continued) Results for measured WDS/WDSS objects

Table 1 concludes on the next page.

Double Star Photometry - June 2019

WDS/WDSS	Disc	C	RA	Dec	dRA	dDec	Sep	Err Sep	PA	Err PA	Mag	Err Mag	SNR	dVmag	Date	Notes
15323+4003	KZA 100	A	15 32 20.616	40 02 51.81	0.04	0.05	19.70541	0.06403	45.833	0.186	12.204	0.051	140.03	0.05	2019.42173	1)
		B	15 32 21.847	40 03 05.54							14.609	0.056	43.85			
15323+4003	TOB 133	A	15 32 20.616	40 02 51.81	0.04	0.05	16.64330	0.06403	287.808	0.220	12.204	0.051	140.03	0.05	2019.42173	1) 7)
		C	15 32 19.236	40 02 56.90							15.878	0.075	18.86			
15340+4110	KZA 101		15 33 57.869	41 09 39.94	0.07	0.07	9.31491	0.09899	205.031	0.609	13.752	0.072	67.73	0.07	2019.42173	1)
			15 33 57.520	41 09 31.50							14.075	0.073	56.78			
14243+3917	LDS 958		14 24 08.626	39 17 27.03	0.08	0.07	11.40932	0.10630	151.430	0.534	11.957	0.060	143.55	0.06	2019.42174	1)
			14 24 09.096	39 17 17.01							12.831	0.061	97.55			
15103+3044	LDS 972		15 10 15.810	30 44 08.56	0.05	0.07	10.85139	0.08602	349.803	0.454	12.283	0.071	117.41	0.07	2019.42174	1)
			15 10 15.661	30 44 19.24							12.745	0.071	97.62			
14415+2957	LDS6298		14 41 27.559	29 57 01.36	0.05	0.07	5.99134	0.08602	102.532	0.823	12.593	0.051	97.21	0.05	2019.42175	1)
			14 41 28.009	29 57 00.06							13.838	0.055	49.49			
14390+3002	MMA 7		14 39 00.419	30 02 03.98	0.06	0.07	17.55449	0.09220	155.946	0.301	11.255	0.050	173.28	0.05	2019.42175	1) 11)
			14 39 00.970	30 01 47.95							14.044	0.055	48.73			
15106+3923	NI 34		15 10 36.373	39 23 14.61	0.06	0.06	7.03732	0.08485	101.891	0.691	13.417	0.082	63.98	0.08	2019.42176	1)
			15 10 36.967	39 23 13.16							14.126	0.083	46.99			
14260+3422	PWS 7	A	14 25 59.500	34 22 11.98	0.08	0.08	26.96191	0.11314	295.412	0.240	10.291	0.070	231.16	0.07	2019.42177	1)
		C	14 25 57.533	34 22 23.55							14.487	0.077	32.44			
14260+3422	PWS 7	A	14 25 59.500	34 22 11.98	0.08	0.08	63.74214	0.11314	215.903	0.102	10.291	0.070	231.16	0.07	2019.42177	1) 12)
		D	14 25 56.481	34 21 20.35							15.936	0.147	7.88			
14260+3422	GIC 118	A	14 25 59.500	34 22 11.98	0.08	0.08	559.70839	0.11314	357.756	0.012	10.291	0.070	231.16	0.07	2019.42177	1) 14)
		B	14 25 57.730	34 31 31.26							13.544	0.072	58.36			
14260+3422	PWS 7	B	14 25 57.730	34 31 31.26	0.08	0.08	88.00245	0.11314	13.588	0.074	13.544	0.072	58.36	0.07	2019.42177	1) 13)
		E	14 25 59.403	34 32 56.80							16.118	0.121	10.46			
14287+3304	TVB 16		14 28 43.437	33 03 53.75	0.04	0.04	49.54408	0.05657	317.178	0.065	10.496	0.040	232.92	0.04	2019.42177	1)
			14 28 40.758	33 04 30.09							11.383	0.041	160.38			
14413+3337	UC 2821		14 41 20.244	33 36 44.92	0.04	0.05	20.14114	0.06403	28.083	0.182	14.804	0.051	34.50	0.04	2019.42178	1) 7)
			14 41 21.003	33 37 02.69							16.383	0.098	11.69			
15129+3430	UC 2960		15 12 56.497	34 30 13.55	0.05	0.05	46.33488	0.07071	268.454	0.087	11.122	0.050	192.92	0.05	2019.42178	1)
			15 12 52.750	34 30 12.30							14.351	0.057	39.14			
15258+3117	UC 3001		15 25 50.284	31 16 48.89	0.06	0.06	5.80962	0.08485	48.231	0.837	13.243	0.072	66.04	0.07	2019.42179	1)
			15 25 50.622	31 16 52.76							13.900	0.074	44.77			
15301+3232	UC 3016		15 30 03.002	32 32 11.89	0.07	0.06	22.63660	0.09220	243.359	0.233	12.032	0.080	129.08	0.08	2019.42179	1)
			15 30 01.402	32 32 01.74							13.887	0.082	53.45			
14488+3232	UR 14		14 48 45.330	32 32 23.36	0.06	0.06	10.73893	0.08485	41.524	0.453	11.755	0.061	139.25	0.06	2019.42180	1)
			14 48 45.893	32 32 31.40							13.465	0.062	62.69			

Table 1 (conclusion) Results for measured WDS/WDSS objects

Notes:

1) iT24 1x20s
2) iT24 1x40s
3) iT32 1x60s
4) iT24 1x30s
5) SNR C <20
6) SNR C <20 and SNR D <10
7) SNR B <20
8) SNR A and B <10
9) Primary saturated and secondary in spike of primary
10) Faint companion close to B
11) SKF1030 BC not resolved
12) SNR D <10
13) SNR E <20
14) GIC 118 listed again due to overlap with PWS 7

Double Star Photometry - June 2019

(Continued from page 352)

3. Cross-Match with Gaia DR2

All listed objects were cross-matched with Gaia DR2 to check for potential gravitational relationship by using the DR2 data for a Monte Carlo simulation to determine the spatial distance between the components. Additionally the median StarHorse masses were used to calculate the tidal radii of the components and the minimum period of a potential circular orbit (see Appendix for details). The results are given below in Table 2 with the following structure:

- Object = WDS discoverer designation or WDSS ID
- C = Components (AB if blank)
- pmRA1 = Proper motion primary RA in mas
- pmDE1 = Proper motion primary DE in mas
- pmRA2 = Proper motion secondary RA in mas
- pmDE2 = Proper motion secondary DE in mas
- CPMS = Estimated likelihood for common proper motion
- Plx1 = Parallax primary in mas
- e_Plx1 = Error parallax primary
- Plx2 = Parallax secondary in mas
- e_Plx2 = Error parallax secondary
- Min_D_AU = Minimum spatial distance in AU between components
- LPGR= Likelihood of potential gravitational relationship
- M1_50 = DR2 StarHorse median mass value primary (red type if other source or estimation based for example on luminosity)
- M2_50 = DR2 StarHorse median mass value secondary (red type if other source or estimation based for example on luminosity)
- Min_P_M50= Minimum orbit period with DR2 StarHorse median mass values (blank for LPGR <0.5)
- TR1_AU = Tidal radius primary in AU
- TR2 AU = Tidal radius secondary in AU

Most objects in Table 2 were already cross-matched with Gaia data in other reports, so no 2015.5 values for separation and position angle are given. For the objects with LPGR>50 WDS code "T" is suggested for likely physical by common parallaxes but in most cases the potential orbit period is far too long to detect any changes in separation and position angle by visual observation over a reasonable time frame. For the objects with LPGR <10 WDS code "U" for likely optical is suggested.

4. Objects of Specific Interest

Comments on several of the listed objects:

- GIC 118 (WDS 14260+3422): The components of this pair are listed as high proper motion stars GJ 178-25/26 with very similar proper motion data. Resolved in DR2 with a separation of 559.60962 arcseconds and position angle of 357,754 (per 2015.5, measurement currently not included in the WDS catalog) but with missing parallax and proper motion data for B – so potential gravitational relationship assessment is currently not possible. If the parallax value for B is very similar to A then the likelihood for gravitational relationship is despite the huge angular separation very high
- KPP4338 (WDS 14592+3956): Triple star system with less than 50% likelihood for gravitational relationship despite common proper motion. StarHorse median star masses for the close components A ~0.50 and B ~0.45 added up for assessing gravitational relationship with component C
- BRT 28 (WDS 15096+2930): Most likely optical triple. DR2 parallax for C negative and no StarHorse data available. So no assessment for potential gravitational relationship is possible, but assessment would be optical even with identical parallax values for all components
- COU1266 (WDS 14280+3546): Most likely optical triple. The StarHorse median star masses for the close components A and B of~0.97 /0.84 have been added up for assessing the potential gravitational relationship with component C
- LDS 958 (WDS 14243+3917): Likely physical pair, but the observation history for this object is in relation to the assumed huge minimum orbit period far too short to allow for the calculation of reliable orbital elements
- UC 2960/ KPP4383 (WDS 15129+3430): Most likely physical triple. The StarHorse median star masses for the close components A and C of~0.75 /0.28 have been added up for assessing the potential gravitational relationship with component B. The observation history for this object is in relation to the assumed huge minimum orbit period far too short to allow for the calculation of reliable orbital elements
- PRO 128/ KPP4386 (WDS 16029-3210): Most likely physical triple star system with the StarHorse median star masses for the close components A ~0.95 and B ~0.70 added up for assessing gravitational relationship with component

(Text continues on page 360)

Object	Comp	pmRA1	pmDE1	pmRA2	pmDE2	CPMS	Plx1	e_Plx1	Plx2	e_Plx2	Min_D_AU	LPGR	M1_50	M2_50	P_M50_min	TR1_AU	TR2_AU
ALI 131		-12.278	-7.189	-15.108	-5.618	0	3.5423	0.0253	3.4851	0.0257	2504	8.61	1.57840824	0.92411393	79665	125635	96131
ALI 601		-4.454	15.886	-4.906	15.467	62	2.1753	0.0807	2.2889	0.0225	1985	1.99	1.12201691	0.99257237	61151	105925	99628
BRT 28	AB	-1.506	8.932	-1.470	8.701	39	1.3630	0.0237	1.3143	0.0239	4502	1.57	1.11459005	1.16240954	201323	105574	107815
BRT 251		2.558	11.416	2.461	11.227	78	2.2348	0.0244	2.2012	0.0368	2346	6.51	1.10971236	0.92608744	80065	105343	96233
BU 9028	BC	9.356	-24.879	3.183	-17.712	0	2.8509	0.0259	0.9352	0.0206	128177873	0.00	1.12660313	0.96644312		106142	98308
BVD 241		8.703	-47.694	11.150	-46.377	1	5.2866	0.0272	5.2148	0.0251	3432	7.45	0.54968297	0.54928178	192859	74141	74114
COU1266	AC	-1.607	-25.666	-0.917	-26.292	31	3.6092	0.1246	3.5264	0.0295	4448	7.12	1.8183257	0.89001006	181261	134845	94340
CVR 778		14.595	-46.848	15.558	-47.341	78	6.0677	0.0235	5.8868	0.0420	6420	0.06	0.586797	0.55000627		76603	74162
DAM 83	BC	-14.465	-15.719	-4.085	-2.577	0	2.6981	0.0246	0.0858	0.0518	534446046	0.00	0.93826455	0.88105631		96864	93865
DAM 83	CD	-4.085	-2.577	-4.632	-15.786	0	0.0858	0.0518	0.5546	0.0682	191584944	0.00	0.88105631	0.76419747		93865	87418
DAM 368		28.942	-34.686	1.979	-1.590	0	2.2876	0.0310	0.8864	0.0225	116918269	0.00	1.10054755	0.87599903		104907	93595
FYM 235		-35.794	16.565	14.644	5.285	0	6.0202	0.0251	5.3530	0.0151	3499469	0.00	1.11616802	0.7499485		105649	86600
FYM 236	AB	-1.944	-5.076	1.015	5.126	0	0.7428	0.0248	1.4186	0.0213	96045821	0.00	1.81717348	1.15403044		134803	107426
FYM 236	BC	1.015	5.126	-9.331	-3.288	0	1.4186	0.0213	0.7465	0.0230	93293676	0.00	1.15403044	0.94784707		107426	97357
FYM 651		7.470	-13.471	7.479	-13.348	97	1.4729	0.0164	1.4852	0.0185	5749	5.74	0.97782969	0.87846684	321690	98885	93727
GIC 118		-288.047	-163.587				18.7204	0.0308					0.71640342			84641	
HDS2106		-98.366	21.858	3.288	1.388	0	4.1587	0.0223	1.5667	0.0150	76959053	0.00	1.01935387	0.97562587		100963	98774
HJ 245		-9.574	16.828	-14.465	-15.719	0	2.4935	0.0245	2.6981	0.0246	1755169	0.00	0.9589572	0.93826455		97926	96864
HJ 545		-14.868	-17.906	-14.830	-17.738	97	1.8230	0.0222	1.8373	0.0136	4931	8.74	1.05228388	0.98682624	243827	102581	99339
HJ 550	AB	9.193	-24.855	9.356	-24.879	95	2.8025	0.0282	2.8509	0.0259	11012	8.03	1.12660313	1.25388205	753114	111977	106142
BU 9028	BC	9.356	-24.879	3.183	-17.712	0	2.8509	0.0259	0.9352	0.0206	129561191	0.00	1.29596531	1.07931876		113840	103890
HJ 557		-1.384	4.183	-9.479	-4.904	0	3.2072	0.1139	5.6043	0.4826	2996670	0.00	1.24328959	0.67420071		111503	82110
HJ 569		-12.142	0.367	2.596	-5.647	0	1.1942	0.0216	0.7538	0.0243	62013270	0.00	1.08479381	0.96430647		104153	98199
HJ 571		-20.798	16.964	-20.947	17.017	97	2.1498	0.0266	2.1319	0.0242	4593	9.23	1.21927595	1.04703474	207944	110421	102325
HJ 2745		7.183	-3.464	-36.012	3.049	0	4.1887	0.0672	0.4369	0.0330	297768808	0.00	1.43110442	0.98123032		119629	99057
HJ 2769		-4.754	-0.454	-4.625	5.531	0	0.7510	0.0264	1.1123	0.0164	52023440	0.00	1.09173465	1.0804162		104486	103943
KPP 737		-36.477	5.541	-37.731	5.172	5	4.5887	0.0262	4.6092	0.0246	1402	35.52	0.96836668	0.84652919	39176	98406	92007
KPP 762		13.369	-53.017	13.730	-53.028	97	3.3623	0.0263	3.3942	0.0173	1949	16.17	1.13363004	0.75215507	62995	106472	86727
KPP 865		-46.152	-10.884	-45.252	-8.177	0	3.1314	0.0403	3.2120	0.0139	2297	2.85	0.90190834	0.75055546	86114	94969	86635
KPP1194		27.708	-44.576	27.308	-47.307	4	2.8671	0.0238	2.8540	0.0268	3207	15.99	1.00410509	0.90971845	132008	100205	95379
KPP1232		-27.497	32.446	-24.457	32.394	0	5.9557	0.0531	6.5700	0.0543	1453796	0.00	1.09536171	0.45056438		104660	67124
KPP1278		-6.371	-34.302	-6.214	-34.442	97	1.9368	0.0222	2.1057	0.0146	2713587	0.00	1.31306148	0.92768383		114589	96316
KPP1471		-52.090	22.180	-51.973	22.391	97	2.1987	0.0181	2.1941	0.0178	4950	13.05	0.80948603	0.80622399	275511	89971	89790
KPP2285		-27.085	-19.102	-27.118	-19.089	97	1.9473	0.0466	1.9867	0.0363	9519	4.02	1.14598346	0.86212909	659028	107051	92851
KPP2315		-25.980	38.159	-26.071	38.465	97	2.9276	0.0162	2.9782	0.0156	6594	2.39	0.88597614	0.80264676	414361	94126	89591
KPP2387		-23.856	32.029	-23.833	32.082	97	2.5167	0.0187	2.5578	0.0209	8037	5.68	0.89961785	0.78544545	558098	94848	88625
KPP2427		-38.577	7.476	-38.966	7.394	97	5.3122	0.0276	5.2654	0.0281	3976	24.60	0.79451609	0.78641623	200467	89136	88680
KPP3283		-91.017	122.293	-92.558	123.685	80	12.3304	0.0254	12.2626	0.0418	940	81.11	0.88923627	0.33327028	26218	94299	57730

Table 2: Results for WDS/WDSS objects cross-matched with DR2

Table 2 concludes on the next page.

Double Star Photometry - June 2019

Object	Comp	pmRA1	pmDE1	pmRA2	pmDE2	CPMS	Plx1	e_Plx1	Plx2	e_Plx2	Min_D_AU	LPGR	M1_50	M2_50	P_M50_min	TR1_AU	TR2_AU
1434569+323125		8.562	7.552	7.406	7.239	1	8.4002	0.0241	8.4402	0.0291	1935	63.28	0.78226888	0.44955844	77089	88446	67049
1451558+422143		-69.815	-61.366	-70.747	-58.148	64	16.3315	0.0514	16.5229	0.0429	389	12.18	0.30112374	0.10000000	12174	54875	31623
1457587+342221		-24.970	-14.738	-24.700	-14.997	97	7.4963	0.0228	7.5481	0.0174	2988	42.54	0.89589983	0.54922241	136648	94652	74110
1459511+321436		-5.434	-74.094	-6.786	-73.893	78	8.9666	0.0286	9.0100	0.0405	3457	65.38	0.70420969	0.67513931	174019	83917	82167
1504122+365201		0.113	11.741	0.937	10.866	0	6.4677	0.0283	6.4616	0.0229	2097	64.35	0.89962214	0.54833275	80253	94848	74049
1507269+304714		-39.641	11.551	-40.531	11.694	39	5.9464	0.0273	5.9782	0.0185	1472	49.21	1.24609315	0.64326817	41313	111629	80204
1517078+334051		-48.264	49.056	-46.581	49.533	62	7.1523	0.0246	7.1204	0.0301	1324	56.67	0.94547701	0.49805927	40332	97236	70573
1518536+375547		-32.561	35.824	-33.170	35.961	76	12.3257	0.0255	12.2505	0.0381	4737	79.13	0.88934904	0.35087180	294342	94305	59234
1529277+375636		-1.059	78.495	-2.194	78.403	97	14.0384	0.0216	14.1258	0.0348	854	92.17	0.91987765	0.30053675	22705	95910	54821
1530278+364816		-70.350	35.696	-68.772	33.882	39	10.1120	0.0245	10.1378	0.0442	3229	89.32	1.36173046	0.44899613	137119	116693	67007
KPP4338	AB	31.380	-100.074	31.318	-100.109	100	7.0719	0.0288	7.0309	0.0341	955	38.07	0.49981353	0.45078489	30443	70697	67141
KPP4338	AC	31.380	-100.074	31.543	-99.432	97	7.0719	0.0288	7.1140	0.0308	7943	46.52	0.95059842	0.50052989	590898	97499	70748
PRO 128	AB	14.986	-8.083	20.564	-10.649	5	17.8766	0.0449	17.9747	0.0599	336	99.30	0.94995517	0.69776762	4820	97466	83532
KPP4386	AC	14.986	-8.083	16.887	-9.911	1	17.8766	0.0449	17.8270	0.0538	2467	99.98	1.64772279	0.40063110	86091	128364	63295
KZA 81		4.130	-5.913	-8.233	-4.594	0	1.1712	0.0158	0.8350	0.0264	39860540	0.00	1.02551091	0.90299577		101268	95026
KZA 83		3.241	-4.234	-3.336	11.967	0	0.8851	0.0152	1.2072	0.0188	41537293	0.00	1.08076024	0.95913965		103960	97936
KZA 84	AB	-33.191	3.311	-3.736	14.395	0	1.1817	0.0220	1.8785	0.0187	49482767	0.00	1.06632674	0.95057410		103263	97497
KZA 84	AC	-33.191	3.311	-30.130	10.845	0	1.1817	0.0220	1.0760	0.0155	96162	0.00	1.06632674	0.87924296		103263	93768
KZA 90		2.617	-31.248	0.004	-5.392	0	1.2724	0.0170	0.5916	0.0217	129670276	0.00	0.9935267	0.94216430		99676	97065
KZA 92	AB	-0.890	-35.792	-25.510	-6.779	0	0.9158	0.0142	0.8092	0.0175	2741666	0.00	0.95292526	0.94978899		97618	97457
KZA 92	AC	-0.890	-35.792	-5.868	8.292	0	0.9158	0.0142	0.7535	0.0187	18170122	0.00	0.95292526	1.01162338		97618	100579
KZA 100	AB	-6.796	-4.484	2.316	-7.776	1	0.4880	0.0196	1.1223	0.0808	143826991	0.00	1.12984598	0.83040154		106294	91126
TOB 133	AC	-6.796	-4.484	-6.430	-3.161	0	0.4880	0.0196	0.4554	0.0319	32976	0.30	1.12984598	0.95606363	41691165	106294	97779
KZA 101		-15.870	-12.682	-14.783	-8.599	0	3.1484	0.0126	2.8285	0.0699	243101	0.00	0.94165927	0.84872156		97039	92126
LDS 958		-61.616	60.642	-62.315	60.997	97	6.6934	0.0249	6.7104	0.0237	1700	69.19	0.84804177	0.79038435	55080	92089	88904
LDS 972		-60.720	65.408	-61.182	65.546	97	3.0781	0.0267	3.0668	0.0273	3486	17.22	0.92553163	0.88164902	153980	96205	93896
LDS6298		242.333	-74.204	241.697	-74.255	100	4.7377	0.0338	4.7288	0.0223	1263	35.18	0.79709589	0.69806242	36916	89280	83550
MMA 7	AB	5.859	-2.868	5.994	-3.288	1	3.0388	0.0377	2.8315	0.0408	6021	0.01	1.13633692	0.81318367		106599	90177
NI 34		136.934	93.448	129.989	-236.220	0	9.3607	0.0253	8.6784	0.0224	1355839	0.00	0.649854	0.59933537		80614	77417
PWS 7	AC	288.047	-163.587	5.192	-18.058	0	18.7204	0.0308	1.6057	0.0236	110173773	0.00	0.71640342	0.8455283		84641	91953
PWS 7	AD	288.047	-163.587	0.611	-0.220	0	18.7204	0.0308	0.3369	0.0466	376535544	0.00	0.71640342	1.06376851		84641	103139
PWS 7	BE			-24.065	-2.463				0.5669	0.1604				0.78494287		0	88597
TVB 16		-4.993	-14.357	-7.605	-17.594	0	0.5360	0.0340	0.8980	0.0337	59056718	0.00	1.13549817	1.1719209		106560	108255
UC 2821		-64.428	13.379	-64.731	13.537	97	2.2771	0.0234	2.2924	0.0461	8671	6.14	0.75319648	0.65033954	685367	86787	80644
UC 2960		-84.807	-25.850	-84.821	-23.985	78	15.5270	0.0240	15.5562	0.0257	2973	100.00	1.035218	0.46499601	133062	101746	68191
UC 3001		-56.999	37.489	-57.245	37.199	100	2.1410	0.0179	2.1131	0.0175	2722	7.14	0.92255819	0.8551262	107100	96050	92473
UC 3016		-60.079	16.365	-60.160	16.706	97	2.8814	0.0492	2.9104	0.0142	7710	10.14	0.96888816	0.7833004	514293	98432	88504
UR 14		-55.782	22.447	-55.141	21.923	78	5.2791	0.0263	5.2218	0.0218	2018	15.90	0.89858049	0.7468487	71083	94793	86420

Table 2 (conclusion). Results for WDS/WDSS objects cross-matched with DR2

Double Star Photometry - June 2019

(Continued from page 357)

C. The observation history for this object is in relation to the assumed huge minimum orbit periods far too short to allow for the calculation of reliable orbital elements. Rather different proper motion values might suggest a random encounter

- KPP3283 (WDS 14354+3349): Likely physical pair. The observation history for this object is in relation to the assumed huge minimum orbit period far too short to allow for the calculation of reliable orbital elements.

5. Summary

Many of the measured objects show the expected magnitude difference larger than 0.5 compared with the WDS catalog data especially for the secondary but for many objects the given WDS magnitudes were simply confirmed within the given error range.

12 objects have parallaxes and angular separations allowing for a higher than 50% likelihood for overlapping tidal radii suggesting potential gravitational relationship. If these objects are indeed physical systems then in all cases potential orbits would be in the range of many thousand years, so no human time span is sufficient to sample enough measurements to calculate reliable orbital elements. Additionally all these objects have so far a very "slim" observation history anyway not really suited for the calculation of reliable orbital elements even for much shorter periods. Only 7 of these objects have also proper motion values suggesting common proper motion which might indicate that 5 of these objects are rather random encounters than star systems with gravitational relationship strong enough for an orbit.

29 objects are with a likelihood of 100% opticals and 19 objects have less than 10% likelihood for gravitational relationship. 13 of these objects have DR2 proper motion data suggesting common proper motion – this makes clear once more that common proper motion alone is no good criteria for assessing a double star as likely physical system. Additional 14 objects show less than 50% likelihood for overlapping tidal radii with 11 of these with proper motion data suggesting common proper motion offering room for ambiguity.

6. Acknowledgements:

- The following tools and resources have been used for this research:
- Washington Double Star Catalog
- Gaia DR2 catalog
- DSS2 images
- Aladin Sky Atlas v10.0
- iTelescope
- iT24: 610mm CDK with 3962mm focal length. Resolution 0.625 arcsec/pixel. V-filter. No transformation coefficients available. Located in Auberry, California. Elevation 1405m
- AAVSO VPhot
- Astrometrica v4.10.0.427
- URAT1 catalog
- AstroPlanner v2.2
- MaxIm DL6 v6.08
- Gaia DR2 StarHorse catalog available through the Gaia@AIP services hosted by the Leibniz-Institute for Astrophysics Potsdam using the ADQL query interface at gaia.aip.de

6. References:

F. Anders, A. Khalatyan, et al., 2019, "Photo-astrometric distances, extinctions, and astrophysical parameters for Gaia DR2 stars brighter than G = 18", *Astronomy & Astrophysics,* DOI 10.1051/0004-6361/201935765.

Knapp, Wilfried R. A., 2018, "A New Concept for Counter-Checking of Assumed Binaries", *Journal of Double Star Observations*, **14**, No. 3, 487-491.

Knapp, Wilfried R. A., 2019, "Physical Pairs Found in Gaia DR2", *DSSC27*, pp. 55-72.

Double Star Photometry - June 2019

Appendix

Description of the PGR assessment procedure (according to Knapp 2018, extended):

- Gaia DR2 data for RA/Dec and Plx are used for a Monte Carlo simulation assuming a normal distribution for these parameters with the given error range as standard deviation. The distance between the components is calculated from the inverted simulated parallax data and the simulated angular separation using the law of cosine:

$$\sqrt{a^2 - 2ab\cos(\gamma) + b^2}$$

with *a* and *b* = distance vectors for the stars A and B in lightyears calculated as (1000/Plx)*3.261631 and γ = angular separation in degrees calculated as

$$\gamma = \arccos\left[\sin(DE1)\sin(DE2) + \cos(DE1)\cos(DE2)\cos(|RA1 - RA2|)\right]$$

- The tidal radius of the Sun TR($M_\odot$) is considered to correspond with the outer rim of the assumed Oort cloud at a distance of ~100,000 AU as the radius at which the Sun's gravitational force is equivalent to the gravitational force of the stellar neighborhood. For objects with significantly different mass from the Sun this tidal radius TR has to be recalculated for a corresponding gravitational acceleration of 5.87329×10^{-13} m/s^2. Potential gravitational relationship PGR is assumed to be given with overlapping tidal radii of two stellar objects, which does not necessarily mean that an orbit exists but that at least the movement of both stars through space should be noticeable influenced mutually by gravitational forces

- The likelihood for potential gravitational relationship (LPGR) is the percentage of simulation distance results smaller than the sum of the tidal radii TR1+TR2 out of the simulation sample with a size of 120,000 corresponding with the likelihood that the real distance is smaller than TR1+TR2 with an margin of error of 0.37% at 99% confidence

- The minimum, median and maximum distance is the smallest, median and largest result of the simulation sample

- Ignoring the likely effects of eccentricity the smallest/median/largest distance is used as estimation for the value for the semi-major axis of a potential circular orbit. This allows for the calculation of a minimum/median/maximum orbit period assuming zero inclination using either median mass data from StarHorse (Anders et al. 2019) or if not available mass data from other sources (for example estimation from luminosity$^{\wedge(1/4)}$ for assumed masses between 0.43 and 2 Sun masses)

Using the Six Astrometric Parameters from Gaia DR2 III: Revealing Optical Pairs in the Washington Double Star Catalog

John Greaves

Northants, U.K.
cpmjg@tutanota.co

Abstract: The release of Gaia DR2 has led to the availability of up to seven million objects with six astrometric parameters from an homogeneous source with which an assumed common proper motion pair can be assessed for validity. Here an example is given by way of demonstrating 48 presumed common proper motion GRV objects listed in the Washington Double Star Catalog are in fact optical doubles.

Introduction

In Greaves (2019), Paper I, Gaia DR2 (Gaia Team, 2018) data were utilised to affirm common proper motion pairs of the GRV discovery code, this small subset of the Washington Double Star Catalog (henceforth WDS, Mason et al 2001) being chosen preferentially as the author was familiar with the nature of these pairs and the methodologies used to discover them due to being the original declarer of them. In this paper those same six astrometric parameters , namely the positions, parallax, proper motions, and radial velocities of the objects, are used to assess the full GRV subset within the WDS for optical pairs for the cases where all six parameters are available in Gaia DR2. As well as highlighting the mistakes made in the derivation of the original objects it will also demonstrate how the use of the full six parameters can distinguish between pairs that are reasonably safely assumed of common motion when only the basic four parameters of position and proper motions are used, and in some cases even when parallax is included as a fifth parameter, and pairs that appear to be equally safely assumed of common motion according to the same four or five parameters but which may not in fact be moving together.

Methodology

Using the CDS VizieR catalogue service the GRV discovery codes are bled from the WDS table (https://vizier.u-strasbg.fr/viz-bin/VizieR-3?-source=B/wds/wds) and then crossed with the Gaia DR2 Catalogue utilising the CDS X-Match service (http://cdsxmatch.u-strasbg.fr/). The search radius is left at a rather high 75 arcseconds as many of the early published GRV objects had separations of up to 70+ arcseconds. Thus for each input position taken from the WDS any object within the radius distance contained in Gaia DR2 will also be returned. As the common motion pair may have a larger separation than other field stars, especially given the limiting magnitude of Gaia DR2 relative to the limiting magnitude of the vast majority of the GRV objects, this also leads to some false positive matches.

However, as all full six parameters are needed many are removed simply by removing all the objects with blank and negative parallax, followed by the remaining handful that didn't have proper motions for both pairs and finally by the rather sizeable number of pairs that do not have radial velocity data for both objects. Then there is the issue of to how small a value for the parallax can be taken with confidence as a valid figure and here a parallax of 1 millarcsecond was taken as the lower limit, ostensibly 1 kiloparsec, below which parallax values are here deemed too noisy to aid in matching pairs, which leads to the further removal of

Received April 25, 2020.

objects. Stars of high to very high common proper motion are usually related but stars at such great distances of around a kiloparsec or more will not have proper motions of such sizes.

From within the outlook of this paper the results also unfortunately include many false positives in the form of pairs that are actually valid common motion pairs, although this is of course fortunate in terms of the GRV objects taken as a whole given that they are supposed to be common motion objects. Further, there still exist a number of cases where field stars also have a radial velocity available but these are usually plain enough to see as the CDS X-Match service returns an angular distance between the input position and the output position and this in tandem with the most recent separation quoted in the WDS can be used to assist filtering out irrelevant objects. This could be done automatically but in this instance it is done by hand.

Thus after the removal of all valid seeming objects and false objects a subset remains of pairs of objects, or rarely trios of objects, which are then double checked by hand as stated because it is still possible for a nearby field star having a radial velocity available by coincidence given the separations involved. In the case when the primary, the secondary and one or more field stars all have radial velocities available this is usually evident enough by each "pair" having had three or more objects returned during the crossmatch and the X-Match position and separation difference aid identification of the valid secondary. However checking by hand as opposed to automated checking also covered the remote possibility of either the primary or the secondary alone having radial velocity data available for them whilst a field star of coincident size of separation also had an available radial velocity, leading to an apparent pair of stars each with the full six parameters but with one of them not actually being part of the pair. This was in fact the case for a few GRV pairs due mostly to their separations being so high.

Then all six astrometric parameters were assessed and in terms of the proper motions and radial velocities any parameter value for an object within ten of the other object in the pair is deemed acceptable, giving a limit likely to be generously above the error value in nearly all cases. For radial velocities this will also be comfortably above any differential radial motion due to orbital motion, especially in the case of such large separation pairs at distances of hundreds of parsecs (thus of large projected actual separation) which would predominantly if not completely have a radial velocity difference of less than 1 kms-1 if valid pairs. Less leniency is given in terms of difference in parallax, nevertheless for parallax values of less than 5 millarcseconds a value within plus or minus 1 has been permitted even though that could lead to one of the pair appearing to have up to half/twice the parallax of the companion, 5 millarcseconds is 200 parsecs. A better system would use errors as a percentage of value to allow for such scaling issues arising from the use of small to large parameter values but in this instance the purpose is not to find common motion pairs but to debunk them by showing pairs blatantly not connected.

Results

This results in 48 GRV pairs being shown to be optical alignments, as listed in Table 1 where the identifier for the pair, the position angle and separation from the WDS (representing their positions), the parallax of each star, the proper motions of each star and the radial velocities are listed. Positions aren't given as the position in the derived form of the separation in tandem with position angle are inherent in the definition of the pair as being a "double star". Only the most evident cases are included in this instance. Roughly a quarter to a third as many again could not be firmly defined as optical and thus are not included in the list. Albeit somewhat contradictorily.

As noted, this approach is somewhat contradictory because in this paper the point is to show with some level of surety the pairs that are optical, despite earlier surveys having suggested they could be considered common motion objects and/or earlier methodologies permitting them to be considered as such. However, the proper approach is only to include two stars as a common proper motion pair with some level of surety such that given their ambiguity (in light of the new data, and possibly even originally) they should have never been included in the original GRV objects lists in the first place! That is, in the usual approach of adding data with confidence they may not have been included as GRV objects due to their ambiguity in the first place had the current Gaia DR2 data been available at that time, yet here in the current approach the somewhat opposite practice of objects only being removed from the list (that is, classed as optical) if there is confidence in doing so is taken.

This may sound somewhat artificial but the Gaia DR2 radial velocities are derived from what are relatively low resolution spectroscopy and often there is no independent confirmation for many of them. This can lead to the case such that there can be a not too wide a pair having parallax and proper motions that are comfortably similar yet the radial velocities differ markedly. Without any independent data it is not possible to say whether the other five astrometric parameters are in the wrong or whether the radial velocities are in the wrong, especially if the now available parallax values are also in good agreement.

Disc	PA	Sep	plx1	plx2	pmra1	pmra2	pmdec1	pmdec2	RV1	RV2
GRV 24	232	65.5	3.0	1.8	-8.1	-8.1	-10.3	-11.6	-8.0	-41.1
GRV 68AB	36	44.7	4.7	3.4	54.2	38.6	15.5	18.8	7.2	-1.4
GRV 69	332	63.1	1.0	2.7	8.5	12.2	-11.4	-13.6	22.7	-7.8
GRV 75	153	45.8	2.7	3.1	30.2	27.8	-25.0	-17.3	3.8	28.0
GRV 80	199	70.2	2.4	1.3	19.7	5.2	-11.4	-6.4	17.6	6.8
GRV 93	249	31.2	2.1	1.8	27.5	27.5	-8.9	-16.3	9.2	39.5
GRV 95	141	73.9	6.1	2.6	22.6	14.5	-16.0	-11.5	-35.2	-12.0
GRV 128	207	36.3	2.2	3.5	14.2	23.2	-11.1	-9.6	20.7	-23.1
GRV 134	165	30.9	4.0	3.7	48.5	38.2	-11.4	-17.6	16.9	44.5
GRV 282	194	69.5	1.4	2.9	-10.0	-4.8	-19.8	-11.9	18.0	-20.0
GRV 288	61	24.3	1.2	1.0	-10.2	-5.0	-15.9	-8.2	-54.7	-23.4
GRV 308	213	38.1	2.5	1.3	16.1	11.9	7.8	9.9	-61.5	-15.7
GRV 327	143	43.8	1.1	3.2	-12.9	-10.8	-13.0	-22.8	63.2	30.0
GRV 346	11	66.6	4.8	1.7	-11.0	4.4	-41.1	-7.9	23.7	-38.5
GRV 357	275	22.5	3.2	1.4	-9.8	-18.2	-22.8	-22.4	1.1	-14.1
GRV 381	340	35.8	1.4	3.4	-9.0	-10.3	-11.1	-12.6	-0.2	30.6
GRV 395	211	59.7	1.0	3.0	-11.1	-13.2	-10.2	-12.8	7.2	-14.5
GRV 407	221	59.2	2.5	1.6	-6.8	-12.8	-11.7	-8.8	8.0	-16.0
GRV 435	206	61.8	1.7	1.4	-8.6	-5.5	-9.1	-8.9	14.8	-63.9
GRV 463	32	35.2	1.9	3.0	-23.8	-30.8	-22.5	-17.8	0.9	-31.0
GRV 470	317	54.1	6.1	1.5	17.5	14.7	-17.6	-11.0	-16.0	-41.0
GRV 479	117	52.1	1.2	1.2	-19.5	-10.9	-14.8	-13.2	-71.0	-13.6
GRV 490	328	31.7	4.2	5.5	-15.2	-15.7	-22.0	-27.0	5.2	17.4
GRV 491	21	31.4	3.2	1.4	-15.1	-19.7	-16.5	-17.4	-30.8	3.3
GRV 492	171	58.7	2.2	3.0	15.4	15.0	-9.8	-7.3	-38.3	-24.3
GRV 501	154	24.5	5.7	1.2	-30.1	-20.9	-23.7	-17.6	13.6	-70.0
GRV 506BC	162	72.4	2.3	1.4	-16.5	-18.9	-24.0	-17.0	-45.9	-7.3
GRV 507AB	317	92.7	1.9	2.3	-13.0	-16.5	-11.7	-24.0	9.9	-45.9
GRV 521	306	45.5	2.0	1.0	-10.0	-14.2	-10.1	-10.1	8.1	-10.7
GRV 522	256	45.4	9.9	6.9	28.6	21.6	45.7	52.9	7.4	21.2
GRV 573	286	29.5	2.2	2.3	-21.1	-29.8	-15.0	-14.1	-32.7	12.1
GRV 575	113	59.4	7.5	2.1	38.0	23.0	16.4	21.2	-33.1	4.8
GRV 600	324	67.9	1.0	2.1	-14.1	-14.9	-14.2	-7.3	-11.2	-25.3
GRV 604	251	22.4	1.4	1.6	-27.7	-18.6	-22.9	-19.7	-46.7	-1.9
GRV 611	60	19.5	3.6	4.2	41.5	49.2	22.9	14.3	-16.3	-58.9
GRV 629	7	18.7	2.7	1.5	-37.4	-20.4	-29.5	-21.4	-36.0	8.9
GRV 665	174	64.7	4.8	2.2	12.9	12.2	-11.5	-9.2	-23.2	-1.9
GRV 676	320	32.8	1.3	1.4	-17.5	-12.3	-11.1	-15.7	-8.1	-25.2
GRV 681	340	44.6	1.7	2.5	20.0	27.9	15.1	17.3	9.6	-71.2
GRV 696	244	64.1	6.7	2.8	-13.8	-16.6	-20.0	-28.3	10.6	-20.2
GRV 698	252	49.9	1.2	9.6	17.0	10.0	-15.8	-9.6	-38.4	-15.5
GRV 710	59	61.6	1.9	3.8	-13.9	-17.4	-9.8	-19.1	-17.2	-4.4
GRV 727	180	31.9	3.7	2.2	-13.8	-13.2	-8.9	-6.7	-5.1	48.4
GRV 742	106	64.6	2.0	3.0	-10.7	-12.2	-13.3	-11.5	-22.5	47.5
GRV 754	24	22.9	1.3	3.0	-13.6	-9.7	-17.4	-17.5	60.4	31.4
GRV 790	212	26.0	5.3	1.5	-10.0	-7.8	-29.4	-22.2	-0.5	-34.5
GRV 954	261	58.1	1.0	1.4	-10.4	-7.9	-16.4	-11.2	-0.3	15.3
GRV 969	156	43.1	3.6	2.2	13.7	14.9	-10.2	-16.5	-30.6	8.3

Table 1. Astrometric Details For The Optical GRV Common Proper Motion Pairs. The GRV identifier, position angle in degrees and separation in arcseconds from the WDS, parallax in milliarcseconds, proper motion in milliarcseconds per year and radial velocity in kilometres per second for each star in each of the pairs taken from GAIA DR2, are given.

Table 1 consists of 48 optical GRV pairs, or more properly 46 optical GRV pairs and 1 GRV optical triple where not one of the three objects match any of the others. The total of 46 doubles and 1 triple is 47, not 48, the mismatch is because the triple seems to be listed in the WDS as GRV 507AB and GRV 507AC whilst the B and C comites are also there as GRV 506BC, such that GRV 506C = 507C and is nearer to GRV 507A than GRV506B = GRV507B is, which is a little confusing and probably stems back to an oversight in the original paper. Even more confusing is that Gaia DR2 now reveals that GRV507B is very roughly 30 arcseconds from a 16th magnitude star also having similar proper motion which could have been included in the system using the Greaves 2004 methodologies if known about at that time. Meanwhile GRV 507A has a 15th magnitude star lying only 4.3 arcseconds away with much closer, albeit relatively small valued, proper motion and parallax to GRV 507A which would have been unresolved in astrometric surveys prior to GAIA and yet would make a valid common motion comes to GRV507A than either GRV 507B or C! These other two stars have no available radial velocity data with which to assess them more deeply, however. This triplet (quintuplet) of stars lies in the constellation Pegasus which as noted in the Discussion has a handful of apparent similar motion pairs each of similar scale motions not confirmed when radial velocity is included.

Likely reasons for GRV pair stars formerly being wrongly assumed of common proper motion are given in the following Discussion section.

Discussion

Examination of Table 1 on an object by object basis revealed one certainty. The selection criteria for proper motions for the objects from the original Greaves 2004 paper were insufficiently stringent. Basically, the error ranges on the proper motions were taken too much at face value instead of using a larger multiple of that value. The method predominantly worked, but it was inadequate for pairs with motions only a little to twice the size of the error limit that also had motion differences of only just under the same error limit, and more especially so the wider the pair were. A caveat here is to note that the original search was targeted at proper motion pairs directly such that any pairs having differential proper motion due to significant orbital motion would also be rejected. Apparent orbital motion, however, is a function of distance from us and apparent separation and although this latter can be quite sizeable for stars quite close to the Sun differential motion can be shown empirically to shrink to negligible levels quite quickly for quite nearby stars, eg Greaves (2020). Similarly the further away a binary is the smaller the apparent separation can possibly appear such that this value falls below the angular resolution of the original paper's data.

Even then the main problem appears to have occurred as a consequence of "Galactography", or the nature of the distribution of stars in the Milky Way. Examination of the objects in Table 1 revealed that most of the demonstrably optical objects of this sort were in the constellation of Cygnus, with a handful more in the adjacent regions of Aquila and Vulpecula. Basically they were in the direction of the Local Spiral Arm. A large amount of the Local Arm lies within a kiloparsec radially for this particular direction and although it has a spread of about a kiloparsec or so in radial depth many stars within it will lie within the distance limits used in this analysis for the GRV objects, as now revealed by Gaia DR2. Thus in that direction there is not necessarily a random distribution of relatively adjacent field stars. Yet it is possible that the proximity of the Local Arm in Cygnus is enough for stars within it to have above error value level proper motions for pre-Gaia surveys. One noteworthy thing about these optical objects is that they mostly scale at roughly 20 masy-1 proper motion and often have similar Right Ascension and Declination motions overall, that is quite a few of the separate pairs have similar scale proper motions as any other pair in that group.

This gives the possibility of apparent motion due to their location within the relatively proximate Local Arm with any attendant general organised internal motion relative to the Sun that it may possess. This part of the sky is unique in providing a significant subset of the optical pairs of similar details only differentiated with the addition of radial velocity data. There also exists a handful of objects in a relatively not too large region of Pegasus that also seem to be similar in motion between themselves yet are shown not to be true pairs by their radial velocity difference, but these are much fewer in number as well as having no readily discernible reason for being of some level of commonality with other pairs.

Alternatively the Gaia DR2 radial velocity data towards these directions could simply be compromised. That is taken as unlikely however as such a systematic trend would have been noticed for although the proper motions for these optical pairs are relatively small they are not significantly so relative to the Gaia DR2 presumed errors.

As the current analysis utilises only data having all six astrometric parameters there are likely more GRV objects in the direction of Cygnus that are optical but due to null or negative parallax values and/or lack of radial velocity measure for both stars in the pair it is not easy to be certain for any particular pair. Certainly

GRV 268, the 17th most colour contrasted pair listed in Table 4 of Greaves 2004 appears to be the only valid pair in the list of colour contrast objects up to that point in said Table, with the previous 16 being readily assumed to be optical. Unfortunately none of them are common to this work so there is likely no joint radial velocity for them to be assessed as suggested in this paper.

Later published GRV objects had less of this problem because by then the author had understood that too much confidence had been given to the proper motion error values and besides the surveys used for later papers were of less accuracy anyway so the author tended to raise the threshold to around 50 masy^{-1} or even 100 mas^{-1} in the case of some data sources (although part of that reason was an attempt to provide objects about which something could be said about either the stars and/or the utility of the data source for double star work rather than just providing large endless lists). Thus Table 1 carries few of the highest numbered GRV objects, although another reason for this will be that these tended to be fainter objects and therefore less likely to have all six astrometic parameters available in Gaia DR2 anyway.

For the rest of the objects from elsewhere on the sky the radial velocities show that the original identification of the pair as of common proper motion was simply wrong. There can be three reasons for this, one simply being that the proper motion values had too low a cutoff level both in absolute terms and also relative to their errors in tandem with too large an upper limit on separation distance. The table suggests that the wider the pair and the lower the proper motion the more likely a false common motion will be attributed to the pair, which also sounds somewhat intuitive when stated. A second reason may simply be that Gaia DR2 proper motion data are superior to the data used in the original analysis, again this could have been avoided somewhat by having not used such a low cutoff threshold for the proper motions thus avoiding potentially pushing the original source data beyond its capabilities.

Based on the author's experience over the years it becomes increasingly clear that the wider the separation between a pair the higher a proper motion value ought to be used. There aren't likely to be any orbiting pairs (which often have differential proper motions sufficient to emulate a mismatch) missed because just about all the nearby orbiting wide pairs are going to be known whilst the more distant and wide the pair the greater the chance of coincidental values, especially for large separations and low motion. There have been many attempts to define a double star over the centuries, with a famous name in the field per epoch usually putting forward their own method or variations upon older methods, but these are often geared towards gravitational interaction and thus orbital motion which is not a concern for the type of doubles that are co-moving objects. The situation is still not clearly defined after all these years even in the professional literature, with the Washington Double Star Supplement (http://ad.usno.navy.mil/wds/Supplement/wdss.html) containing many very wide pairs (arcminutes in some instances) from professional papers using various professional surveys and declaring pairs not always having particularly large proper motions and even if valid most certainly beyond the point of potential gravitational interaction. Meanwhile nearby young Moving Groups (eg TW Hya or b Pictoris Groups) are defined from objects which although having parameters more accurately and precisely defined by large professional instruments still have negligible proper motions and radial velocities in absolute terms not necessarily that markedly different from field adjacent field stars as well as being near enough to us for negligible radial distance (measured as parallax) differences to be ignored, as after all the Groups have depth as well as height and width.

It is still not clear, therefore, what limiting criteria to use safely for wider pairs, although proper motions over 50 masy^{-1} are generally safe 100 masy^{-1} is safer still, especially for some data sources, whilst restricting angular separation to 30 arcseconds or less reduces the chance of false alarm coincidence even further. This at least will result in lists having more quality over quantity but will also throw away a great number of valid wide pairs. The more distant the pair the more problematic especially for wide pairs with relatively low proper motions and the further the pair the smaller the proper motion is going to be. The possibility of adding, hopefully safe, radial velocity data thanks to Gaia DR2 can permit a double check when all the other parameters are in adequate agreement, including for wider, distant, low motion pairs, especially as radial velocity values are independent of distance. However the radial velocity values have also to be large enough and sufficiently different relative to the likely accuracy regime of their source.

If none of the above scenarios apply there only remains the third reason, hopefully in the minority, which is the simplest of all. The author just plain got it wrong! The GRV objects involved were manually double checked during publication on more than one occasion before both their submission and after, including at galley stage, yet clearly false candidates were still missed, and the error of selection was due to the author, not the data nor the methodology. It cannot get any simpler than that.

Conclusion

The six astrometric parameters from Gaia DR2 are used to find optical pairs in an ostensibly common motion subset of WDS doubles, with emphasis on radial velocity use although keeping the other parameters in play. A total of 48 GRV common proper motion pairs, more properly 46 pairs and 1 triplet, are found to be most likely optical. Some have a regional bias on the sky and may be due to a quirk of Galactic structure and commonality of kinematics in that direction, others may be a consequence of the difference in accuracy between the original source data and the Gaia DR2 data for proper motion but more likely reflect the use of too low threshold points in the original analysis rather than inherent failings in the original source data. Other pairs appear valid enough under the original four parameters and remain so when parallax is added as a fifth parameter until radial velocity is also taken into consideration. Finally it is clear that no matter how careful an analysis is conducted and checked and re-checked some results will still be just plain wrong due to author error.

Acknowledgements

This analysis utilized the VizieR and CDS X-Match services of the Centre de Données astronomiques de Strasbourg and the United States Naval Observatory Washington Double Star Catalog and its Supplement.

References

Greaves, J., *MNRAS*, **355** , 585, 2004.

Greaves, J., *JDSO*, **15**, 59, 2019.

Greaves, J., *JDSO*, **15**, 317, 2020.

Mason B.D., et al., *Astron. J.*, **122**, 3466, 2001.

Observations of Double Star WDS 09545-8025

Ryan Bangeter, Nonnie Woodruff, Sariah Phipps, and Lesilie Greer

Brigham Young University - Idaho
Rexburg, Idaho

Abstract: CCD images were gathered from the South African Astronomical Observatory, part of the Las Cumbres Observatory (LCO) network, using a 0.4 meter telescope. The resulting images were then processed using AstroImageJ to determine the position angle and separation of the star. The data was analyzed and compared with existing Gaia and historical information. Results from historical data, Gaia data, and recent observations suggest that the system is a binary system. The data collected shows the two stars have an average seperation angle of 9.311 ± 0.007 arcseconds and position angle of 285.70 ± 0.17º strongly suggests that the Double Star WDS 09545-8025 is a gravitationally bound binary system, but could require a few thousand more years of data.

I. Introduction

The search for binary stars compares two stars in close proximity. Two types of double star classications are optical pair and gravitationally bound system. An optical pair is a set of stars that appear to be orbiting one another, but have do not orbit around a common center of mass (CM). A gravitationally bound system is a set of stars that orbit one another around a common CM. There are several means used to verify whether a system is an optical double or a physical binary. Two stars whose parallax and proper motion is similar suggests the stars to share a CM which moves relative to Earth. One can calculate the star system's mass, and predict the stars' individual masses, separation distance from one another, as well as the gravitational force the objects exert on one another. Making these predictions can help to consider the star system a optical pair or gravitationally bound system.

WDS 09545-8025 was first observed in 1836 by John Hershel [1] and most recently in 2015 making a total of 15 observations since it was first discovered. The objective of this research was to measure the position angle (θ) and separation (ρ) of WDS 09545-8025 and compare resulting measurements with previous data.

II. Methods and Materials

The selection of the star was made using Dave Rowe's Gaia Double Star Selection Tool (GDS) [2]. Criteria used for selecting this double star was that the magnitude of the primary star should be between 7 and 12 with delta magnitude less than 1, and separation to be limited between 5 and 10 arcseconds. These specific conditions fit the criteria to be imaged from a 0.4 meter telescope provided by the Las Cumbres Observatory (LCO) network [3]. Declination was restricted to be between -80 and -90 with the most recent observation being at least five years ago. Five possible systems resulted with only two being recorded as physical doubles. WDS 09545-8025 had more recorded observations compared to the other four, and so it was chosen.

An observation request was sent to LCO which used the South African Astronomical Observatory 0.4 meter telescope. The binary star system was imaged using a clear filter on a SBIG STX6303 camera [4]. Initially two sets of ten images were requested with differing exposure times of one second and two seconds. This was to help determine the Signal to Noise (S/N) ratio required to collect the highest quality images of the stars. Despite the two different exposure times, both sets of data did not provide an adequate S/N ratio. New sets of ten images with three and four second exposure times were requested, and both sets provided equally low quality images. Eventually, data was requested for ten second exposures and fifteen second exposures. The ten second exposures provided the best

Received April 3, 2020.

Observations of Double Star WDS 09545-8025

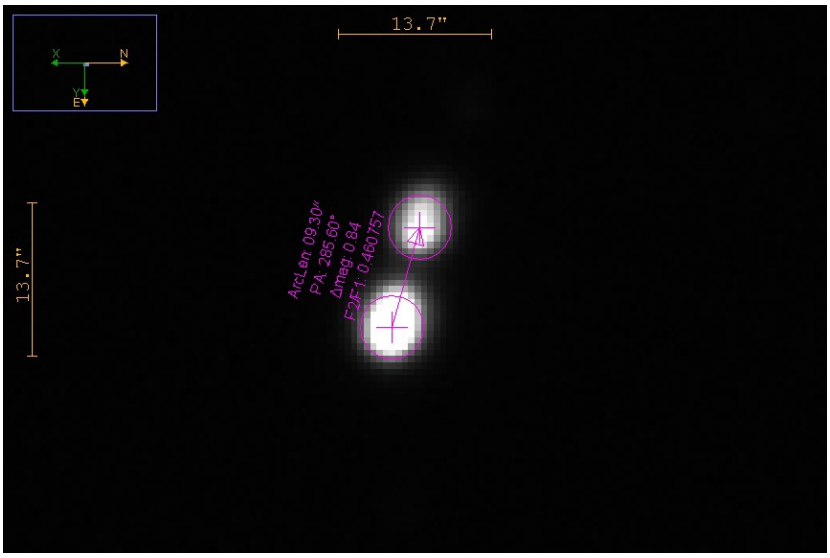

Figure 1. Image from AstroImageJ of WDS 09545-8025. Top star: Secondary. Bottom star: Primary

S/N ratio, which were then oficially requested to the LCO telescope, resulting in seven quality images like the image provided in Figure 1.

AstroImageJ is an interactive software program that was used to determine the separation and position angle of the star. The application uses color images and pixel saturation to easily align the images of the stars. With the stars aligned, state of the art software calculates the separation and position angle instantaneously [5].The gathered data was entered into a spreadsheet and compared to historical data.

The WDS number for the double stars studied was plugged into VizieR in order to find the Gaia data. The data consisted of information such as parallax, proper motion, radial velocity, and temperature [6]. Gaia Data was compiled into Table 1 for quick reference.

Gaia Data		
Star	**Primary**	**Secondary**
Parallax (mas)	2.73 ± 0.02	2.75 ± 0.02
Proper Motion RA (mas/yr)	-17.43 ± 0.04	-17.58 ± 0.04
Proper Motion DEC (mas/yr)	15.74 ± 0.04	15.86 V 0.03
Radial Velocity (km/s)	1.72 ± 1.35	0.57 ± 1.5
Temperature (K)	6400	6500
Luminosity ($L_\odot$)	11.65	5.28

Table 1. Results from the second Gaia Data release.

III. Results

The seven observations from the LCO are arranged in Table 2, which were used to calculate the average separation distance and position angle. The average separation is 9.311 arcseconds with a standard deviation of 0.007, and the average position angle is 285.70 with a standard deviation of 0.17. These results are similar to those found in the historical data of the stars' previous observations.

Brian Mason, a US Naval Observatory Astronomer, shared the historical data on the WDS 09545-8025 stars. Microsoft Excel was used to separate the data out

10 Second Exposures		
Image	**Separation (as)**	**Position Angle (deg)**
1	9.313	285.65
2	9.312	285.92
3	9.300	285.91
4	9.308	285.72
5	9.323	285.44
6	9.323	285.73
7	9.307	285.58
Average	9.311	285.70
Std. Dev.	0.007	0.17
Std. Dev. of Mean	0.003	0.064

Table 2. Data collected from LCO and measured with AstroImageJ.

Observations of Double Star WDS 09545-8025

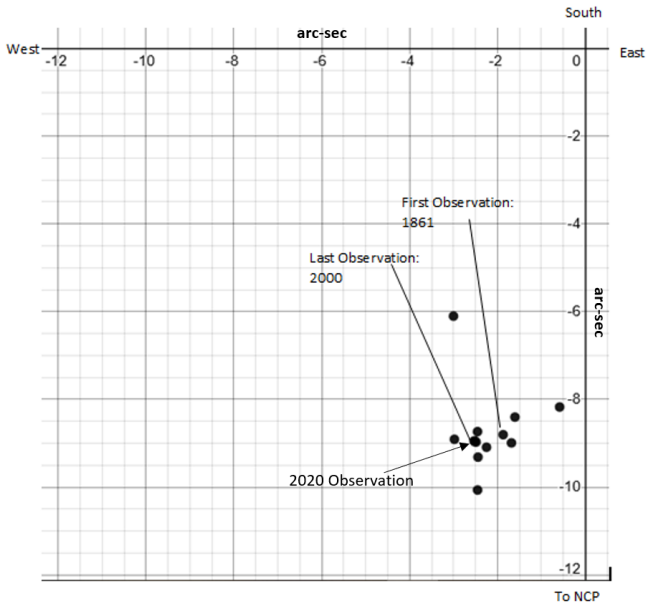

Figure 2. 1836-2000 Historical Data; includes 2020 observation

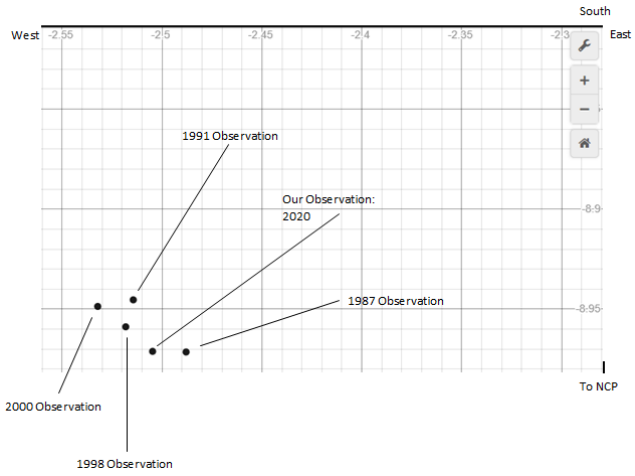

Figure 3. Five most recent observations.

into lists of observation times, position angle, and separation. Using basic trigonometry, the separation and position angle were used to create Figure 2 and Figure 3. The first and final average observations were added to the historical data and marked in the figures to show the most recent observation compared to past observations.

IV. Discussion

After comparing results of the observations with historical data and Gaia data, the likelihood of the pair being gravitationally bound becomes apparent. All historical data on the star shows that the secondary star 3 has stayed in relatively the same position to the primary star and Gaia data shows that both share very similar parallax and proper motion as seen in Table 2.

As discussed earlier, an optical double consists of two stars that appear close to one another, but are not gravitationally bound, whereas a physical binary is made of two stars that orbit a common center of mass. One way to determine if the system truly is a gravitationally bound binary is to look at the parallax and proper motion. Referring back to Table 1, the parallax of the primary star is 2.73 mas and the secondary star is 2.75 mas. The closeness in parallax values suggests the stars are gravitationally bound. The similar proper motion between the Primary and Secondary star reiterates the same ideal, the difference between proper motion being only 0.13 mas. However, parallax values under 5 mas are to be taken with some skepticism as the star system is well into the range where the Gaia instruments will have some error, especially with such small values.

Both stars studied in the Gaia data were classified in the dataset to be Main Sequence stars. Copying the model of an HR diagram, the two stars were positioned along the diagram with respect to their temperatures and luminosity in Figure 4 [7]. Main Sequence stars follow a trend, though with some amount of uncertainty due to each star's unique nature. Main Sequence stars that have a solLum between ($M > 0.7M_{\odot}$) fit the mass-luminosity relationship as follows:

$$\frac{L}{L_{\odot}} = 1.02\left(\frac{M}{M_{\odot}}\right)^{3.92} \qquad [8]$$

This equation helped calculate the approximate mass of the Primary star to be $1.85M_{\odot}$ and the Secondary star to be roughly $1.52M_{\odot}$. The spectral type for these stars would be massive F-type stars, falling in the temperature range with slightly more mass than the average Main Sequence F-type range.

AstroImageJ approximates the separation between the two starts is about 920 AU using the right ascension and declination of the two stars' position and their distance from Earth. Kepler's 3rd Law helped to calculate a minimum orbital period of the binary system was calculated to be at least 15000 years. Using Newton's gravitational equation, the predicted mass of both stars, and the approximated separation, we calculate the gravitational force of these stars is roughly 3.96×10^{22} N. With the proper motion of the stars gathered from Gaia Data, it is highly likely that these stars are gravitationally bound.

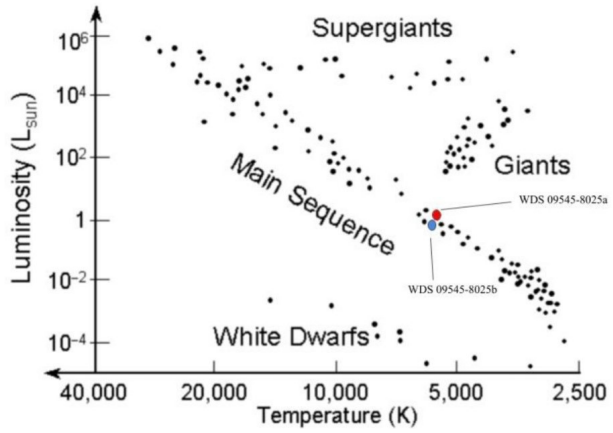

Figure 4. HR Diagram with studied stars relative placement marked. Red - Primary star. Blue - Secondary star.

V. Conclusion

Given the minimum orbital period of 15,000 years and the imperceptible motion of the Secondary Star it will take thousands of years worth of observations to prove this system to be a gravitationally bound binary. But, despite the immense time frame needed, the provided evidence strongly suggests that WDS 09545-8025 is gravitationally bound binary. The most recent observations show that the average separation of the stars is about 9.3 arcseconds with an average position angle of 285.70 degrees. The approximate mass of the Primary and Secondary stars were calculated to be 1.85 $M_\odot$ and 1.52 $M_\odot$. From this, the respective gravitational pull on both stars from each other is roughly 3.96 x 10^{22} N. This along with Gaia data showing both stars to have similar parallax and proper motion strongly suggests the possibility that the stars are gravitationally bound.

VI. Acknowledgements

We would like to thank the BYUI Physics Department for presenting us with the opportunity to participate in this project as well as Rachel Freed for providing us with much needed guidance at the beginning of the project. This research has made use of the VizieR-catalogue access tool, CDS, Strasbourg, France (DOI: 10.26093/cds/vizier). The original description of the VizieR service was published in 2000, A&AS 143, 23.

This research has made use of the Washington Double Star Catalog maintained at the U.S. Naval Observatory.

VII. References

[1] J. Herschel, *Cape of Good Hope Astronomical observations 1834-1838*, Cape Results, 1847.

[2] E. S. Agency, “Gaia overview”, 2016.

[3] S. Phipps. https://lco.global/observatory/0.4m, 2020.

[4] “Las cumbres observatory: 0.4-meter," 2020.

[5] kielkopf, “*Astroimagej imagej for astronomy*”, https://www.astro.louisville.edu/software/astroimagej/, 2019.

[6] O. F. et al, “The vizier database of astronomical catalogues”, https://vizier.u-strasbg.fr/viz-bin/VizieR-5?-ref=VIZ5e46f7c1b720\&-out.add=.\&-source=I/345/gaia2\&-c=148.61907667555\%20-80.42132805992,eq=ICRS,rs=2\&-out.orig=o",doi = 10.26093/cds/vizier,.

[7] R. W. Pogge, “Lecture 10: Synthesis: The hertzsprung-russell diagram”, http://www.astronomy.ohio-state.edu/~pogge/Ast162/Unit1/hrdiag.html, 2008.

[8] B. Ryden and B. M. Peterson, *Foundations of Astrophysics*, Pearson, 2010.

A Comparison of Photometric Techniques for Astrometry of Close Double Stars

Ryan Caputo, Caroline Wiese, and Kalée Tock

Stanford Online High School
Stanford, California, United States

Abstract: We study the accuracy of various photometry packages and AstroImageJ for measuring the separation and position angle of close double stars using a traditional imaging method. In particular, we focus on twelve systems with separations at and above the stars' full width at half maximum (FWHM) - separations ranging from two to seven arcseconds. Gaia DR2 serves as our reference to judge accuracy. Our images have a FWHM of 2.0", and AstroImageJ's residuals were roughly -0.1" down to just over twice the FWHM. The photometric algorithms presented mixed results. DOPPhot had the lowest residuals of the photometries, yet still presented a comparatively large random error of ±0.2". However, it outperformed AstroImageJ at closer separations, maintaining this ±0.2" error down to 1.5x the FWHM, 3.0". These results are surprisingly accurate given the modest imaging equipment used - a 100mm telescope operating at 714mm focal length.

Introduction

The desire to measure close double stars drives us to attempt increasingly difficult pairs. In a previous study of a close double star system, STF 619 (4.0" separation), measurements of position angle and separation made by AstroImageJ deviated slightly from the expected values (Wiese et al., 2020). Specifically, the star centroids were roughly 0.3" closer together than predicted based on previous measurements. This may be partially because the light from one star bled into its companion, 4.0" away. When the images were reduced with DAOPhot photometry, however, the measurements were more accurate, as shown in Figure 1.

This prompted us to study when a given photometry is best suited to accurately measure the position angle and separation of close double stars. The algorithms we compare are AstroImageJ (AIJ), DAOPhot (DAO), DOPPhot (DOP), Source EXtractor (SEX), Source Extractor Kron (SEK), and PSFEx-Extractor (PSFEx). DAOPhot and DOPPhot are photometric reduction algorithms that were specifically developed to distinguish stars in crowded starfields, such as those of globular clusters (Stetson, 1987; Schechter, 1993). Similar imaging difficulties apply to close double stars because the light of one star bleeds into the other due to atmospheric scintillation. The SEX, SEK, and PSFEx algorithms

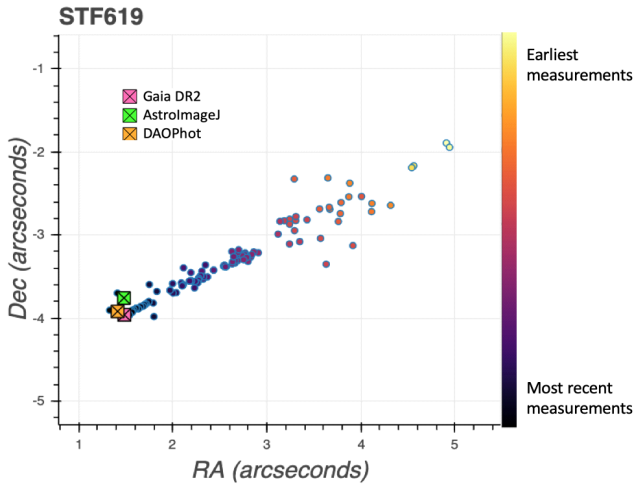

Figure 1. Plot of STF619's historical data, with the measurements of AstroImageJ, DAOPhot, and Gaia Data Release 2 overlaid. The historical measurements are plotted chronologically, with the earliest measurements lightest in color.

Received May 13, 2020.

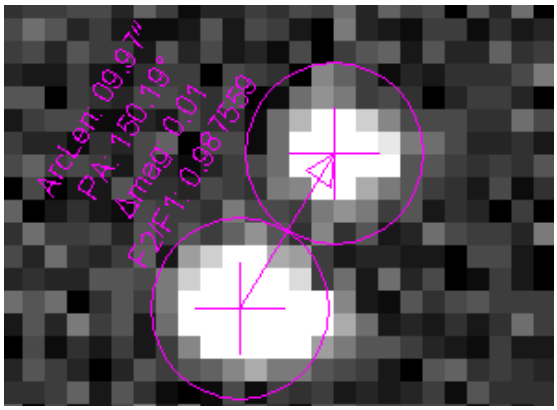

Figure 2. Double star data reduction in AstroImageJ software.

were developed by Bertin and Arnouts (Bertin and Arnouts, 2018). To assess their accuracy, we compared our measurements to the values reported in Gaia Data Release 2 (DR2) because it is the most accurate and recent astrometric data available (Lindegren, et al. 2018; Marakov, 2007).

The AIJ software is popular for double star data reduction because it has features designed for double star astrometry, as shown in Figure 2. In AIJ, a weighted average aperture photometry algorithm is used to calculate star centroids (Howell, 2006).

Target Selection

To choose double star systems to image, the Washington Double Star (WDS) catalog was searched using Stelle Doppie. The search was restricted to systems with a delta magnitude of less than 0.5, more than 50 historical observations, and systems in which the last observation was made in the last year. From the systems that met these criteria, we selected 12 doubles with separations ranging from two to seven arcseconds. Since we expected our measurements would begin to significantly deviate from Gaia DR2 at around four arcseconds, we centered the target systems at four arcseconds of separation. The targets with small separations of around three arcseconds were selected knowing that accurate measurements may not be possible. Our goal was to identify the separation at which our measurements began to substantially deviate from those reported in Gaia DR2.

Imaging Equipment

As described in Caputo, 2019, a four-inch refractor telescope was used to image each of the selected systems. The telescope has a focal length of 714 mm, and no Barlow or other image magnifier was used. The camera is a ZWO ASI-1600mm, with a pixel size of 3.8 µm, yielding a pixel scale of 1.12 arcseconds per pixel. Figure 3 shows two doubles with different separations imaged using this system.

By visual inspection of Figure 3, STF 2655 is well separated. However, STF 559 is not sufficiently resolved for confident astrometry, as will be shown below. Charles Bracken, in The Deep Sky Imaging Primer, explains the various limiting factors for resolving two point sources, including the atmosphere, optics, and sensor undersampling (Bracken, 2017). In this case, we believe that the atmosphere is the dominant limiting factor because the starlight is overlapping due to scintillation. In addition, our images appear to be slightly undersampled, further limiting our resolving power. To better quantify this, Steve Howell writes in his Handbook of CCD Astronomy that effective sampling can be modeled by the following equation:

$$r = \frac{FWHM}{p}$$

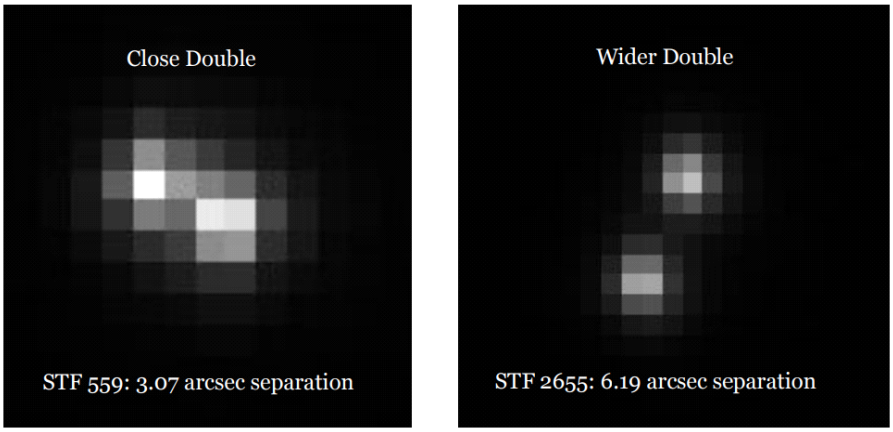

Figure 3: *A close double (STF 559) and a wide double (STF 2655) imaged for this study.*

In this equation, p is the pixel scale and the FWHM is the full width at half maximum of the stars in equivalent units. An r value less than 1.5 indicates undersampling (Howell, 2006). The software PixInsight was used to measure the FWHM of the images, and the average was 2.0". This gives an r value of 1.8, close to Howell's criterion of $r < 1.5$, which is similar to the Nyquist theorem stating that twice the spatial frequency of a given oscillation is required to perfectly reconstruct the original signal (Lévesque, 2014). Here, the "oscillation" is the FWHM, and the spatial frequency is the pixel scale of 1.12 arcseconds per pixel. By Howell's criterion, the images are close to being undersampled. This might affect the ability of the telescope to resolve down to the atmosphere-seeing limit, such as in the case of STF 559. A smaller sampling might allow more accurate measurements to be made in the same seeing conditions until the seeing limit is reached.

Note that the error on the centroid position introduced by undersampling is independent of the separation of the stars. However, when the separation is low, the error on centroid position causes a larger percent error on separation. Averaging many measurements increases the accuracy because the centroid position error is random, not systematic. However, highly accurate results cannot be obtained from poor measurements.

Centroiding in AstroImageJ

AstroImageJ uses the Howell centroid algorithm to compute the centroid of a star (Howell, 2006). It is a weighted average, otherwise known as an intensity centroid algorithm. It produces an astrometric, not photometric, measurement. The algorithm gives highly repeatable results such that it is relatively independent of the starting location, as long as the user clicks somewhat near the centroid (Collins, 2017). From our rough testing, deviations of a pixel (which are visually clearly off center) yielded the same centroid results for most stars. To better measure the centroid, AstroImageJ employs a sigma-clipping algorithm to reject background pixels with a flux greater than two standard deviations from the mean flux of the background region. Figure 4 shows the rejected pixels, labeled with white dots. Pink circles have been placed around the white dots for clarity. Many of these "background" pixels actually contain the secondary star, and the algorithm correctly rejects them to get a better measure of the true background. However, because the rejection algorithm does not operate within the innermost aperture, if the innermost measuring aperture contains starlight from the other star, the centroid will be computed incorrectly. Setting the size of the innermost aperture is therefore very important because too large a size will erroneously draw the centroids closer, while too small a size will not sample the entire point spread function of the star. Some of the inner apertures used in this study needed to have a radius between one and two pixels because the two stars were so close. While this might degrade the accuracy of our measurements, a larger size would have included the secondary star. As Buchheim notes, when the secondary star is so close to the primary that there is not a well-defined "valley" between them, making aperture photometry inaccurate (Buchheim, 2008). For this reason, our smaller separation measurements are excluded from the measurements we will report below.

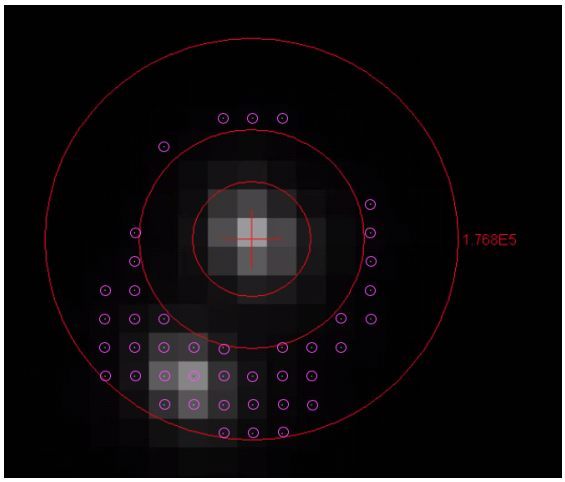

Figure 4: Sigma-clipping rejection for STF 2655.

Historical Observations and Our Measurements

The plots in Figure 5 (below) are color-mapped; darker points are most recent. All of the historical data points have been corrected to account for Earth's axial precession since the time of their measurement, and outliers more than three standard deviations from the mean have been removed. For each plot, our measurement using AstroImageJ is green, Gaia DR2 is pink, and DOPPhot is orange. Note that there is no green measurement for STT 437AB since we were not able to resolve it sufficiently to measure it in AstroImageJ. Also, DOPPhot was not able to measure STF 2947AB, so there is no orange measurement for that system. The other photometric algorithms each only measured the larger half of the separations, and including their points would make these plots more difficult to read. Therefore, their output is not shown on the historical data plots, though their residuals are studied in Figure 6.

There are several cases for which the data shows a clear trend. These include STT 437AB and STF

(Text continues on page 377)

A Comparison of Photometric Techniques for Astrometry of Close Double Stars

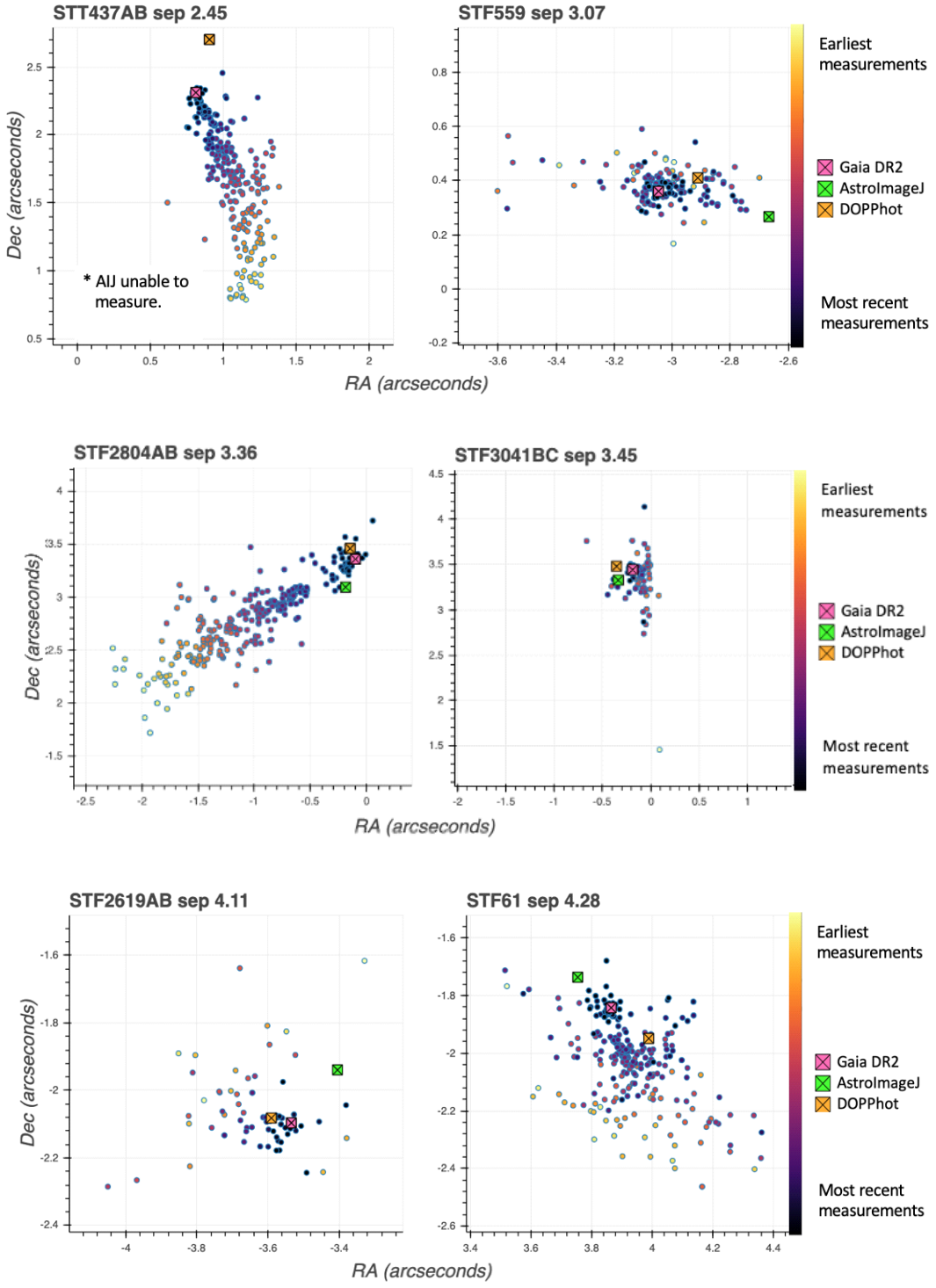

Figure 5. Plots of historical measurements and our results (continued on next page).

A Comparison of Photometric Techniques for Astrometry of Close Double Stars

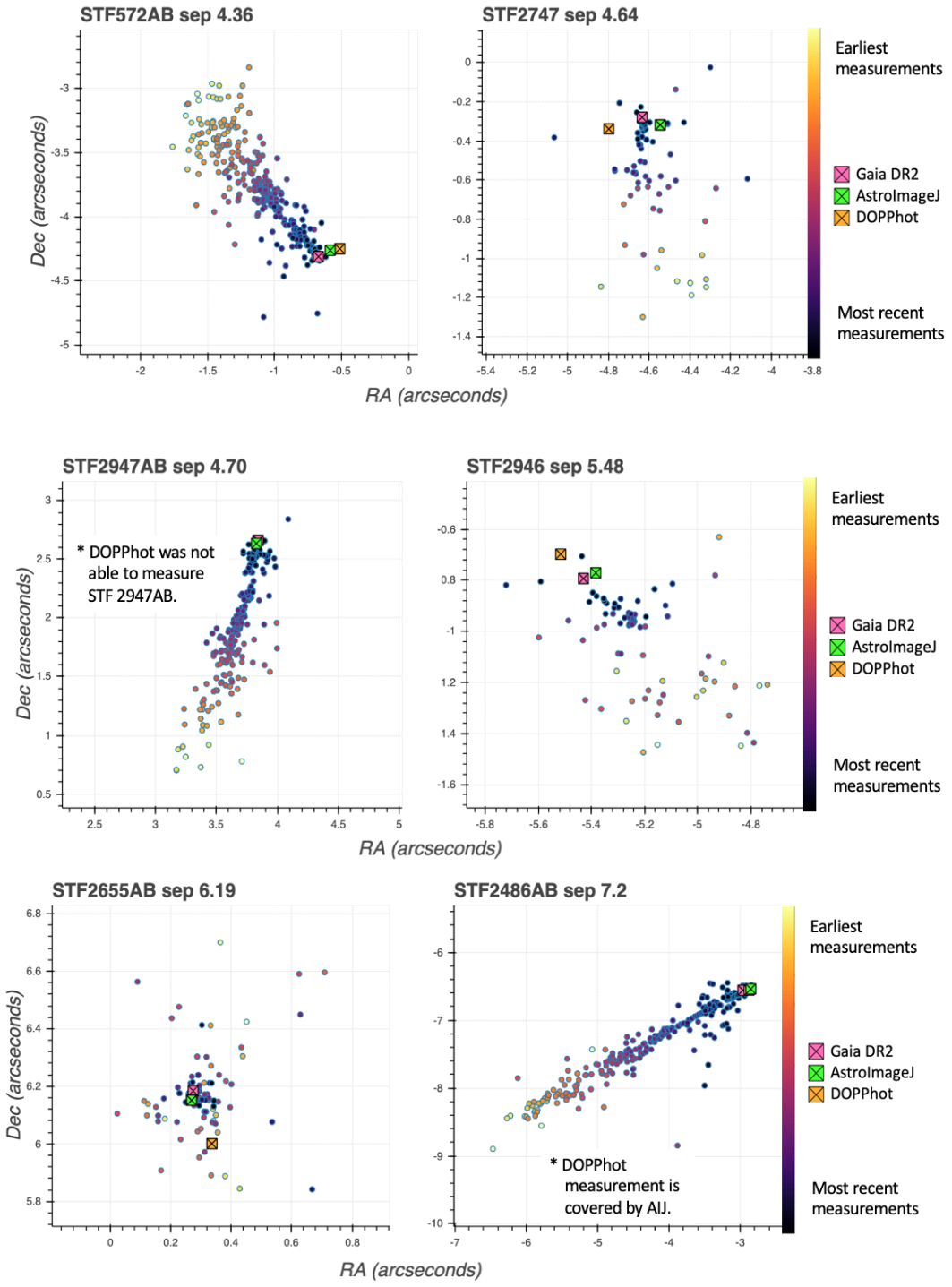

Figure 5. Plots of historical measurements and our results .

A Comparison of Photometric Techniques for Astrometry of Close Double Stars

(Continued from page 374)

2486AB, which are short-arc binaries with orbital solutions. STF 2804, STF 572AB, and STF 2947AB have linear solutions. In these cases, the Gaia DR2 point follows the trend more closely than the measurements from AstroImageJ or DOPPhot, solidifying our selection of it as our standard.

Some of these stars have more scatter than others, such as STF 3041BC. This is most likely because the stars are moving in the sky slowly relative to each other, so past and current measurements do not show much trend.

Analysis

Photometry may substantially affect the accuracy of astrometric measurements of close double stars, especially those with separations approaching the FWHM. Figure 6 below shows the residuals for all the photometric methods and AIJ. AIJ's intensity centroid algorithm contains a systematic error that pulls close centroids closer together. DOPPhot, which uses a Gaussian model, does not have this systematic error. For the images studied here, measurements in AIJ above 4.5" separation contain a systematic error of -0.1". Below 4.5", the magnitude of AIJ's systematic error increases rapidly and is no longer accurate enough for confident measurements. We are not confident enough to suggest adding 0.1" to measurements in AIJ because this study is only confined to a single telescope operating during a single night.

We expect all the algorithms to converge to an accurate measurement with increasing separation, as a larger separation is intuitively easier to measure. However, to our surprise, not all the algorithms converged, though our limited data set makes any generalization tentative. We initially looked at those that did converge, and they are AIJ, SEX, and possibly PSFEx. AIJ shows the most clear convergence trend, underestimating the separation and converging to a systematic error of -0.1" at separations above 4.5". SEX converges slightly more slowly, but from above rather than from below. Of these two, AIJ has a narrow lead on accuracy. PSFEx behaves strangely near 4" - the residuals are very large and erratic. Looking past these few outliers, there are only a few data points on which to base our judgement. There appears to be convergence from below, but the four data points present are not enough to form solid conclusions. Of the algorithms which converge, AIJ appears to be the most accurate. We do not know why these algorithms have a systematic error even at larger separations of 7", for these stars were clearly resolved in the images, but the trend appears regardless.

DOPPhot is the only algorithm which has residuals scattered around zero, with a range of approximately ±0.2". As a comparison, DAOPhot's residuals range from 0" to +0.4" - giving it the same scatter as DOPPhot but around a systematically overestimated separation. This means that DOPPhot appears to be more accurate than DAOPhot. Furthermore, DOPPhot is the only photometry of the six studied here to have a low error of ±0.2" for separations between 3" and 4". However, it is important to note that only DOPPhot and AIJ were able to measure separations in this range.

Our images have an average FWHM of 2.0", measured with the software PixInsight. A 2.0" FWHM should allow separations of approximately twice the FWHM (4") to be accurately measured with standard weighted-average astrometry; for the photometric algorithms, separations equal to the FWHM should be measurable (Buchheim, 2008). We established AIJ as performing accurately within ±0.1" above 4.5" separation - consistent with Buchheim's criterion. However, for DOPPhot, we do not see this expected accuracy in the 2" - 3" range, and we believe this to be limited by pixel scale, as shown in Figure 3 above. The stars are not undersampled as defined by the seeing limit. However, because DOPPhot is able to resolve within the seeing limit (1.5x the FWHM instead of 2x), the pixel sampling needs to be correspondingly finer to maintain proper resolution. This could perhaps improve the accuracy of DOPPhot, pushing its capabilities to 1x the FWHM or reducing the error below ±0.2", whereas AIJ will likely see little improvement.

Despite the sampling issues identified above, it is important to note that DOPPhot did still measure most of the closest-separation stars within ±0.2", which is impressive. Increasing sampling can be done by simply adding a Barlow or other image magnifier. Thus, DOPPhot holds the potential to be very accurate down to separations equal to the FWHM.

Measurements to Report

Five double stars - above 4.5" - have low enough systematic errors that we are confident in our measurements. They are reported below in Table 2.

Conclusion

We measured 12 systems from the Washington Double Star catalog and studied the effect of photometry on astrometry. We report measurements for five systems above 4.5" in separation. For these images, whose stars have FWHM of 2.0", measurements of separations above 4.5" have the lowest residuals with AIJ's aperture photometry. In general, for separations more than twice the FWHM, AIJ is a good choice, even if the

(Text continues on page 379)

A Comparison of Photometric Techniques for Astrometry of Close Double Stars

System	Date	Number of Images	Position Angle (°)	Std. error on Position Angle (°)	Separation (″)	Std. Error on Separation (″)
STF2747	2019.85	32	266.0	0.15	4.56	0.008
STF2947AB	2019.85	40	55.5	0.08	4.65	0.011
STF2946	2019.85	31	261.9	0.08	5.44	0.015
STF2655AB	2019.85	30	2.5	0.08	6.16	0.014
STF2486	2019.85	40	203.6	0.09	7.14	0.012

Table 2. Five double stars measured in October, 2019.

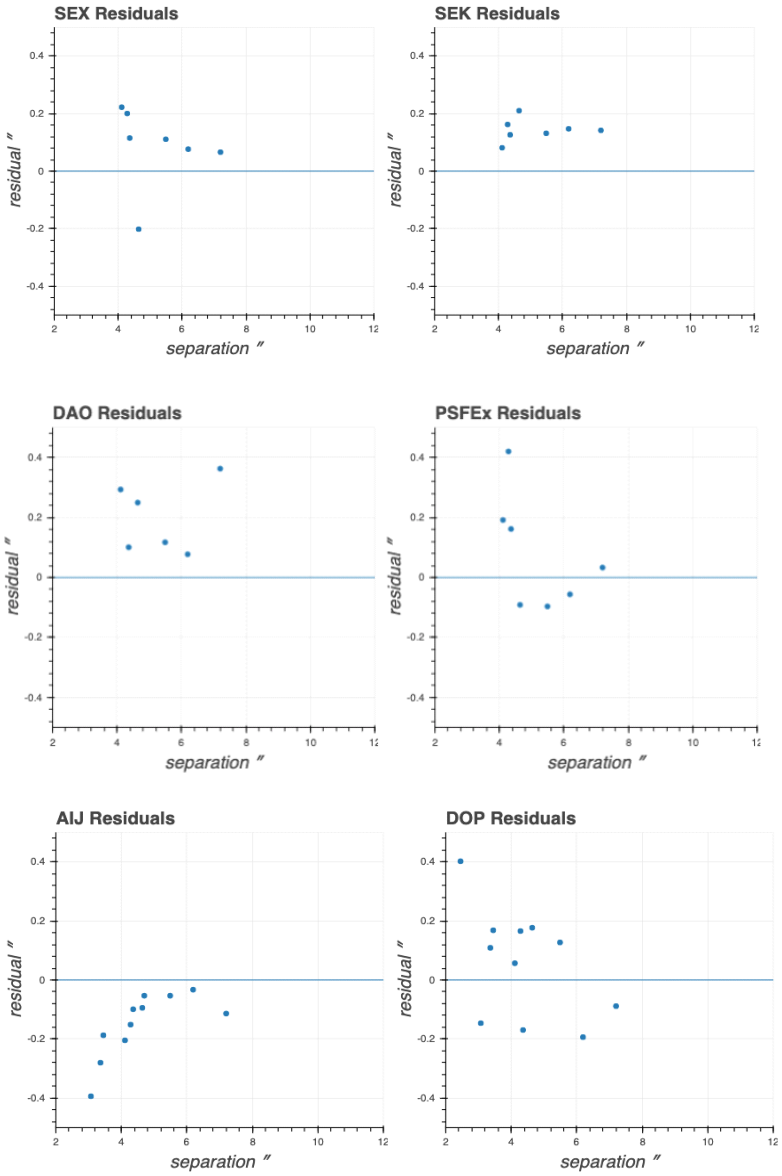

Figure 6: Residuals for the various photometries as a function of separation..

(Continued from page 377)

pixel scale large such that the stars are separated by only a few pixels. For stars separated by less than twice their FWHM, a point-spread method such as DOPPhot might give more accurate measurements. We believe a smaller pixel scale is more important to properly sample stars for DOPPhot because it is able to measure within the seeing limit, albeit to a limited extent. The specific telescope, camera, and seeing conditions are huge variables which affect the closest measurable separation. The results here might not directly translate to different observers. However, our analysis suggests that measurements of close double stars are possible at a relatively large pixel scale using a small 100mm telescope, assuming the seeing conditions are good.

Acknowledgments

We would like to thank Karen Collins and John Kielkopf for writing AstroImageJ; it is such an excellent and intuitive program for double star reduction, among its many other purposes. Its functionality has exceeded expectations when put to the test.

This research was made possible by the Washington Double Star catalog maintained by the U.S. Naval Observatory, the Stelledoppie catalog maintained by Gianluca Sordiglioni, Astrometry.net, AstroImageJ software, and Stellarium software by Fabien Chéreau.

This research also made heavy use the European Space Agency's Gaia Data Release 2 (https://www.cosmos.esa.int/gaia), processed by the Gaia Data Processing and Analysis Consortium (DPAC, https://www.cosmos.esa.int/web/gaia/dpac/consortium). Funding for the DPAC has been provided by national institutions, in particular, those participating in the Gaia Multilateral Agreement.

Special thanks to Bob Buchheim and Richard Harshaw for reviewing our paper. Thanks also to Bob Buchheim and Michael Fitzgerald for assisting us with photometric analysis.

References

Bertin, E., & Arnouts, S. 2018. Sextractor: Software for source extraction. Astronomy and Astrophysics Supplement Series, 117 (2), 393–404.

Bracken, Charles, 2017, The Deep Sky Imaging Primer, 2nd Edition, Deep Sky Publishing. ISBN 978-0999470909.

Buchheim, Robert, 2008, CCD Measurements of Visual Double Stars. Proceedings of the 27th Annual Conference of the Society for Astronomical Sciences, pp. 13 - 23.

Caputo, Ryan, 2019. The Human Element: Why Robotic Telescope Networks are not always Better, and Performing Backyard Research. Journal of Double Star Observations, Vol. 15, No. 3, pp. 408 - 415.

Collins, Karen A., et al., 2017. AstroImageJ: Image processing and photometric extraction for ultra-precise astronomical light curves. The Astronomical Journal, Vol. 153, No. 2.

Howell, Steve B. 2006. Handbook of CCD Astronomy, 2nd Edition. Cambridge University Press.

Lévesque, Luc, 2014. Nyquist sampling theorem: understanding the illusion of a spinning wheel captured with a video camera. Physics Education, Vol 14, No. 6.

Lindegren, Lennart et. al. 2018. Gaia Data Release 2: The Astrometric Solution. Astronomy and Astrophysics, 616, A2.

Mason, Brian, 2020, "Catalog Access and New Lists of Neglected Doubles", Journal of Double Star Observations, 16 (1), 3 - 4.

Marakov, Valerie, Claus Fabricius, and Julien Frouard, 2007. "Double Stars and Astrometric Uncertainties in Gaia DR1". The Astrophysical Journal Letters, 840:L1 (6pp), 2017 May 1.

Schechter, P., & Mateo, M. (1993). DOPhot, a CCD photometry program: Description and tests. Publications of the Astronomical Society of the Pacific,105, 1342–1353.

Stetson, P., 1987. Daophot: A computer program for crowded-field stellar photometry. Publications of the Astronomical Society of the Pacific, 99, pp. 191 –222.

Wiese, Caroline and Alexander Jacobson, Alessandra Richardson-Beatty, Fay-Ling Laures, Ryan Caputo, 2020. Reevaluating Double Star STF 619, Journal of Double Star Observations, 16 (2), 105 - 112.

Astronomical Association of Queensland 2019 Programme: Blue Star Observatory Measurement of Twelve Neglected Southern Multiple Stars

Peter N. Culshaw, Diane Hughes, John Hughes, Des Janke, Graeme Jenkinson

Astronomical Association of Queensland, Australia.
bluestars@iprimus.com.au

Abstract: This paper presents the final results of a 2019 programme of photographic measurements of twelve southern multiple stars

Introduction

These latest results are part of an ongoing programme commenced in 2008 by the Double Star Section of the Astronomical Association of Queensland. The target stars were selected from the Washington Double Star Catalog (WDSC) and were observed in Queensland, Australia from a latitude of approximately 27° S.

Method

Nightly sets of one hundred images were obtained with an Atik 460EX mono CCD camera used in conjunction with an equatorially mounted 400mm F4.5 Newtonian reflector, after which the images were stacked using Atik DAWN software and then analysed using the astrometric double star program REDUC (Losse, 2008). Approximately ten stacked images of each target were taken per night for seven nights and the results averaged to obtain measures of separation and position angle with sufficient confidence.

The mean 95% confidence intervals for the new measures were ±1.228º in PA and ±0.181" in separation. The results are given in Table 1.

Full details of the method are given in Napier-Munn and Jenkinson (2009). Subsequent work on the errors inherent in the method is described in Napier-Munn and Jenkinson (2014). As proficiency has grown in the use of this equipment with the 400mm reflector, close doubles with considerable magnitude difference between the components have been successfully measured.

Fellow AAQ members Culshaw, Hughes and Hughes provided invaluable assistance with image processing using Losse's REDUC software, and Janke with processing the original FITS image files into JPEG photographs.

Results

For all of the systems shown below, the WDSC information is first reproduced, showing the epoch 2000 position, magnitudes, separation, PA, and the last recorded measurement. The new measurements are then given in tabular form, including the mean and standard deviation and 95% confidence limits. Any uncertainties between the images and the last recorded measurements are discussed. Finally a conclusion is given as to whether any movement of the component stars has occurred in PA or separation, based on the P-value for the t-test comparing the new mean values with the catalogued value ($P < 0.05$ is considered as evidence of change).

As detailed in the tabulated results (Table 1), B2305 shows a large difference in PA between the 1938 measure and our 2019 result. A possible incorrect North-South alignment in the original measure may explain the difference.

RSS529 shows a very large change in PA over 43 years. Unlike B2305 this would not seem to be explained by incorrect North-South alignments.

Received May 2, 2020.

System	Last listed measure			New measure			Comment
	PA °	Sep. "	Epoch	PA °	Sep. "	Epoch*	
JSP 14	215	3.1	1944	213.78	3.28	2019.836	Slight change consistent with previous measures.
B 2305	341	1.5	1938	164.20	5.25	2019.288	Possible incorrect 1938 measure.
RST5373	118	2.8	1987	109.91	2.92	2019.335	PA decreasing.
RST2829	332	3.5	1987	331.45	3.66	2019.354	Little change evident.
B 241	59	3.3	1942	56.23	3.26	2019.272	Definite decrease in PA.
DON 586	298	5.0	1941	296.16	4.01	2019.354	Modest decrease in both.
B 438	104	4.4	1927	119.41	5.28	2019.565	Increases in both axes.
RSS 529	244	11.2	1976	168.72	12.62	2019.565	Large change in PA.
SEE 385AB	5	4.8	1943	11.05	5.84	2019.567	Increases in both axes.
RST3233	304	2.2	1945	300.41	10.36	2019.565	Clear change in both axes.
RST3237	178	3.2	1941	170.62	3.20	2019.696	Clear change in PA only.
A 373	11	3.0	1927	9.99	2.82	2019.696	Little change evident.

** Epochs of new measures given in Besselian years as the average of the observations making up the measure.*

Table 1. Measurements results of 10 Negelected Southern Multiple Stars

Please note that all attached images are aligned with North to the bottom and East to the right.

Acknowledgements

This research has made use of the Washington Double Star Catalog maintained at the U.S. Naval Observatory.

The Edward Corbould Research Fund administered by the Astronomical Association of Queensland for granting of funds to upgrade imaging camera and observatory computer to suit.

References

Losse, F. Reduc software, V4.5.1. http://www.astrosurf.com/hfosaf/uk/tdownload.htm

Napier-Munn, T.J. and Jenkinson, G., 2009, "Measurement of some neglected southern multiple stars in Pavo", *Webb Society Double Star Section Circular,* **17**, 6-12.

Napier-Munn, T.J and Jenkinson G., 2014, "Analysis of Errors in the Measurement of Double Stars Using Imaging and the Reduc Software", *Journal of Double Star Observations*, **10** No.3.

Argyle, R.W., 2012. Observing and Measuring Visual Double Stars 2nd edition. Springer.

... Blue Star Observatory Measurement of Twelve Neglected Southern Multiple Stars

JSP14	RA. 00 52.5	DEC. -31 38	Last Measure 1944
Sculptor	MAG. 9.89 & 13.5	PA. 215°	SEP. 3.1"
Date	**No. images**	**PA°**	**Sep"**
23 October 2019	10	215.22	3.342
27 October2019	10	213.08	3.288
1 November 2019	10	214.7	3.113
4 November 2019	10	215.65	3.222
10 November 2019	10	212.88	3.307
12 November 2019	10	211.14	3.428
Mean		**213.778**	**3.283**
Standard deviation		1.714	0.107
95% CI +/-		1.799	0.113
P(t) movement		0.141	0.009

COMMENTS: Slight decrease in PA is consistent with the two previous measures in 1928 & 1944. Very small if any change in separation. Six nights imaging only due to extended poor weather.

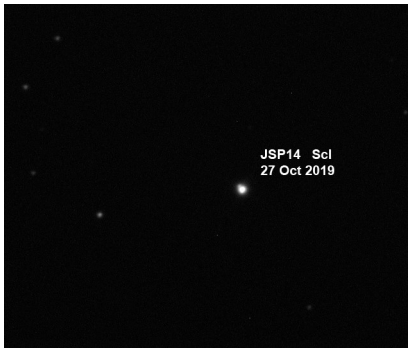

B2305	RA. 12 54.5	DEC. -46 08	Last Measure 1938
Centaurus	MAG. 9.77 & 13.00	PA. 341°	SEP. 1.5"
Date	**No. images**	**PA°**	**Sep"**
05 April 2019	10	164.85	5.413
06 April 2019	10	163.66	5.187
07 April 2019	10	163.49	5.394
08 April 2019	10	162.99	5.345
12 April 2019	10	166.11	5.116
26 April 2019	10	163.65	5.165
27 April 2019	10	164.68	5.112
Mean		**164.204**	**5.247**
Standard deviation		1.070	0.132
95% CI +/-		0.989	0.122
P(t) movement		0.000	0.000

COMMENTS: Large difference in PA may be due to incorrect N-S alignment of 1938 measures.

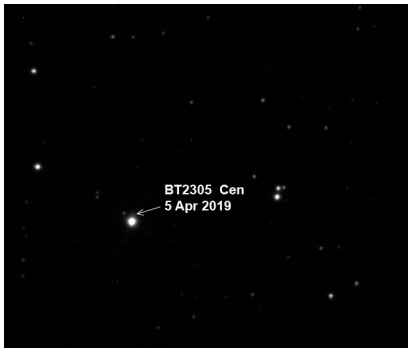

RST5373	RA. 12 59.9	DEC. -00 14	Last Measure 1987
Virgo	MAG. 8.3 & 13.0	PA. 118°	SEP. 2.8"
Date	**No. images**	**PA°**	**Sep"**
29 April 2019	10	111.05	2.934
05 May 2019	10	108.66	2.700
06 May 2019	10	109.68	3.132
07 May 2019	10	110.26	2.915
Mean		**109.913**	**2.920**
Standard deviation		1.006	0.177
95% CI +/-		1.601	0.281
P(t) movement		0.000	0.000

COMMENTS: PA appears to be decreasing after an increase from 112° between 1946 & 1987. Little change in separation since initial 1946 measure. Four nights imaging only due to extended poor weather.

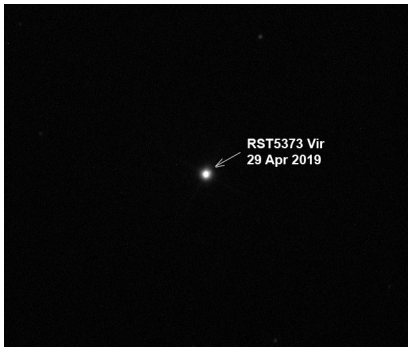

... Blue Star Observatory Measurement of Twelve Neglected Southern Multiple Stars

RST2829 Centaurus	RA. 13 02.6	DEC. -31 47	Last Measure 1987
	MAG. 8.72 & 13.8	PA. 332°	SEP. 3.5"
Date	No. images	PA°	Sep"
27 April 2019	10	330.95	3.752
29 April 2019	10	332.59	3.317
05 May 2019	10	333.52	3.976
06 May 2019	10		
07 May 2019	10	329.94	3.626
12 May 2019	10	330.35	3.833
22 May 2019	10	331.36	3.467
Mean		**331.452**	**3.662**
Standard deviation		1.366	0.243
95% CI +/-		1.434	0.255
P(t) movement		331.452	3.662

COMMENTS: Little evident movement over the last 32 years. Poor quality images from 06 May not included.

B241 Centaurus	RA. 13 09.4	DEC. -30 37	Last Measure 1942
	MAG. 9.36 & 13.3	PA. 59°	SEP. 3.3"
Date	No. images	PA°	Sep"
03 April 2019	10	56.31	3.142
05 April 2019	10	57.69	3.281
06 April 2019	10	56.34	3.384
07 April 2019	10	50.84	3.047
12 April 2019	10	55.21	3.222
15 April 2019	10	54.53	3.324
17 April 2019	10	57.3	3.181
Mean		**56.230**	**3.256**
Standard deviation		1.202	0.091
95% CI +/-		1.262	0.096
P(t) movement		0.00	0.00

COMMENTS: Definite decrease in PA. Poor quality images of 07 April were not included.

B438 Sagittarius	RA. 19 32.4	DEC. -33 45	Last Measure 1927
	MAG. 9.0 & 14.5	PA. 104°	SEP. 4.4"
Date	No. images	PA°	Sep"
29 June 2019	10	118.14	5.290
30 June 2019	0	0.00	0.000
3 July 2019	10	121.84	5.322
9 July 2019	10	120.77	5.175
10 July 2019	0	0.00	0.000
20 August 2019	10	118.34	5.313
21 August 2019	10	117.97	5.319
Mean		**119.412**	**5.284**
Standard deviation		1.774	0.062
95% CI +/-		2.202	0.077
P(t) movement		0.000	0.000

COMMENTS: Increases in both axes since the only previous measure in 1927. Two nights of images not used due to poor seeing/image quality.

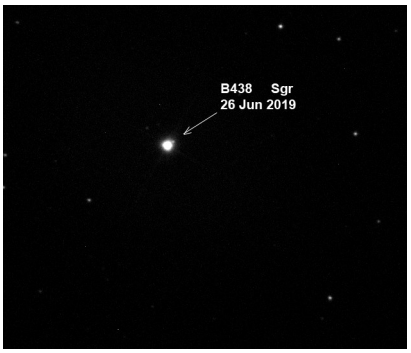

DON586 Centaurus	RA. 13 11.3	DEC. -46 36	Last Measure 1941
	MAG. 8.56 & 14.0	PA. 298°	SEP. 5.0"
Date	No. images	PA°	Sep"
27 April 2019	10	299.26	3.801
29 April 2019	10	297.44	3.813
05 May 2019	10	293.94	4.283
06 May 2019	10	293.52	4.294
07 May 2019	10	294.39	4.079
12 May 2019	10	296.92	3.922
22 May 2019	10	297.66	3.894
Mean		**296.161**	**4.012**
Standard deviation		2.203	0.210
95% CI +/-		2.037	0.194
P(t) movement		0.069	0.000

COMMENTS: The previous 1929 & 1941 measures showed no movement in either axis, but there now appears to be a modest decrease in both.

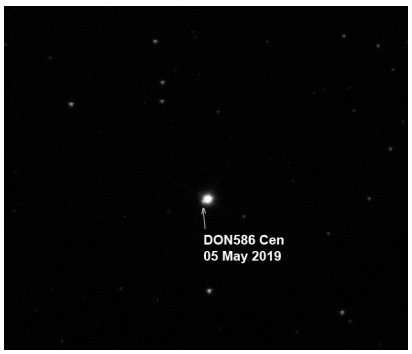

SEE385AB Sagittarius	RA. 19 37.1	DEC. -21 38	Last Measure 1943
	MAG.8.4 & 14.1	PA. 5°	SEP. 4.8"
Date	No. images	PA°	Sep"
29 June 2019	10	10.52	5.793
30 June 2019	10	11.81	5.922
09 July 2019	10	11.25	5.883
20 August 2019	10	14.89	5.714
21 August 2019	10	10.71	5.767
23 August 2019	10	14.59	6.156
24 August 2019	10	10.97	5.816
Mean		**11.052**	**5.836**
Standard deviation		0.505	0.064
95% CI +/-		0.627	0.080
P(t) movement		0.000	0.000

COMMENTS: Increase in both axes since previous measurement. As highlighted, results from 20 & 23 August were not used due to poor image quality.

RSS529 Sagittarius	RA. 19 32.5	DEC. -35 27	Last Measure 1976
	MAG. 8.7 & n/a	PA. 244°	SEP. 11.2"
Date	No. images	PA°	Sep"
29 June 2019	10	169.51	12.591
30 June 2019	10	168.64	12.547
03 July 2019	10	168.48	12.789
09 July 2019	10	168.34	12.417
10 July 2019	10	168.54	12.751
20 August 2019	10	168.60	12.834
21 August 2019	10	168.94	12.441
Mean		**168.721**	**12.624**
Standard deviation		0.393	0.169
95% CI +/-		0.364	0.156
P(t) movement		0.000	0.000

COMMENTS: Considerable change in PA since the only previous measurement in 1976.

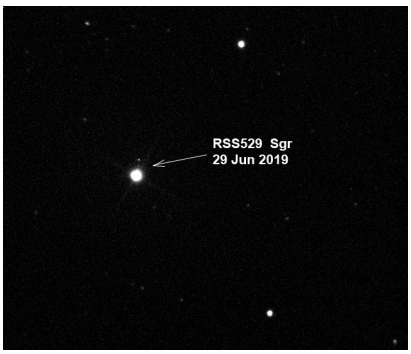

RST3237	RA. 19 44.8	DEC. -18 32	Last Measured 1941
Sagittarius	MAG. 9.23 & 13.70	PA 178°	Sep 3.2"
Date	**No. images**	**PA°**	**Sep"**
23 August 2019	10	171.9	2.688
24 August 2019	10	169.75	3.051
01 September 2019	10	170.11	3.343
02 September 2019	10	169.96	3.51
03 September 2019	10	171.37	3.388
Mean		**170.618**	**3.196**
Standard deviation		0.956	0.330
95% CI +/-		1.187	0.410
P(t) movement		0.000	0.980
COMMENTS: Clear movement in PA only. Five nights imaging only due to extended poor weather.			

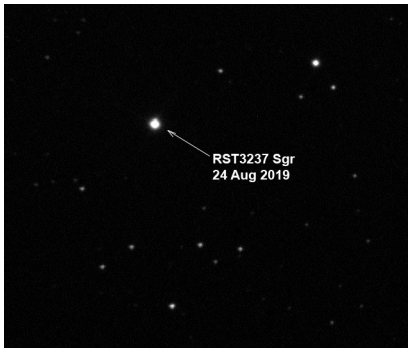

RST3233 Sagittarius	RA. 19 38.6	DEC. -33 55	Last Measure 1945
	MAG. 10.4 & 12.1	PA. 304°	SEP. 2.2"
Date	**No. images**	**PA°**	**Sep"**
29 June 2019	10	299.85	10.781
30 June 2019	10	300.81	10.404
03 July 2019	10	300.38	10.19
09 July 2019	10	300.68	10.281
10 July 2019	10	300.35	10.103
20 August 2019	10	299.98	10.338
21 August 2019	10	300.83	10.458
Mean		**300.411**	**10.365**
Standard deviation		0.390	0.220
95% CI +/-		0.361	0.203
P(t) movement		0.000	0.000
COMMENTS: Clear movement in both axes evident 74 years after last measurement.			

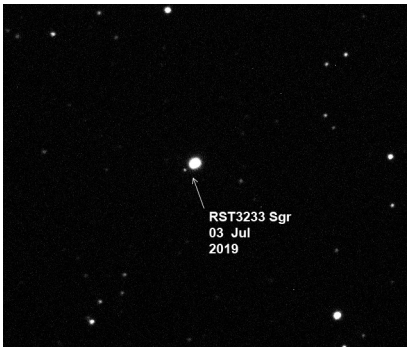

A373	RA. 19 45.2	DEC. +05 00	Last Measured 1927
Aquila	MAG. 9.47 & 14.20	PA. 11.0°	Sep. 3.0"
Date	**No. images**	**PA°**	**Sep"**
23 August 2019	10	9.03	2.964
24 August 2019	10	9.59	2.783
31 August 2019	10	10.82	2.529
01 September 2019	10	9.39	2.782
02 September 2019	10	9.96	2.828
03 September 2019	10	11.15	3.013
Mean		**9.990**	**2.817**
Standard deviation		0.834	0.171
95% CI +/-		0.875	0.179
P(t) movement		0.031	0.046
COMMENTS: Poor quality images of 30 August not used. Very little movement evident.			

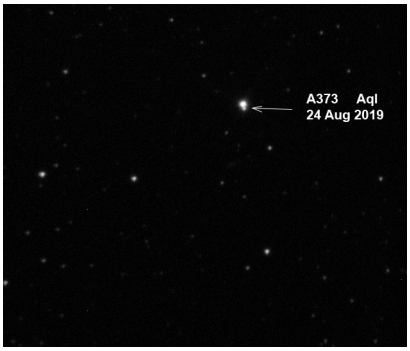

Using Plot Tool 3.19 to Generate Graphical Representations of the Historical Measurement Data

Richard Harshaw

Phoenix, AZ
rharshaw51@cox.net

Abstract: The Plot Tool (Version 3.19) is an Excel utility that generates Cartesian plots of the measurement history of any double star using the Datarequest text file supplied by the WDS at the U. S. Naval Observatory. This powerful tool allows a double star researcher to better detect short arc binaries and linear cases much better than standard data mining methods or trusting that a star one has selected for research is starting to show a trend in the data.

1. Introduction

As an editor for this journal, I review dozens of manuscripts every year. Most of their authors present their data in graphical formats, which is (to my visual way of seeing the world) the clearest way to show patterns and relationships in data (even though that can sometimes be misleading, owing to the brain's tendency to see patterns where none actually exist, a phenomenon known as "pareidolia").

I usually see graphs where the author is trying to show a trend or pattern in the observational data, and often a graph like this is presented:

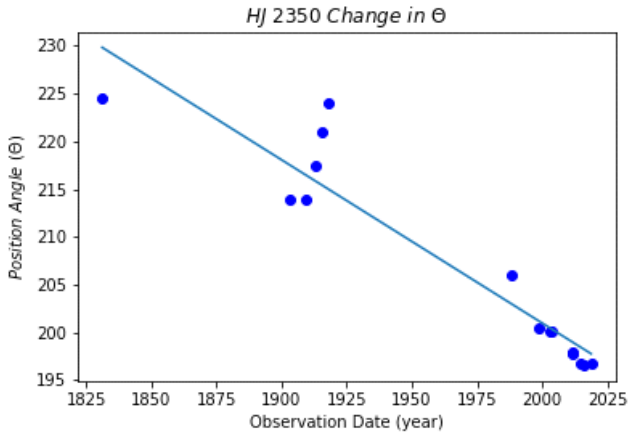

Figure 1: Typical "Change over time" plot

Just exactly what does a plot like this tell us? Not as much as some people think. We can see that over time, theta is decreasing. But so what? Over time, every double star will show a change in theta (although it may take centuries to show up). The slope of the line is not very helpful in telling us anything useful about this pair either.

A better plot would be to show the measurements as recorded in a "Datarequest.txt" file that one can obtain from the WDS. This shows how the stars appear to move relative to each other over time and this can let true trends begin to surface—a short arc in the case of a gravitationally-bound pair in a mutual orbit, or a straight line in the case of two unrelated stars that happen to lie close to each other along our line of sight but are in fact not binary at all.

So how to generate such a plot?

2. A Tool Five Years in the Making

Five years ago, I decided to generate plots of the measurements of double stars and requested (eventually) some 8,000 sets of data from Dr. Brian Mason at the U. S. Naval Observatory (the curators of the Washington Double Star catalog, or WDS for short). The first attempt at generating plots was somewhat crude but helpful in detecting "short arc binaries" (or SABs), stars of immense interest to astronomers as they are probably in an orbit about their barycenter, but for which no solution has yet been proposed. Such pairs should rise to the top of any observing agen-

Received April 9, 2020.

da if one wants to collect useful data on a system.

Similarly, when the plot showed the data lying along a straight line (more or less), we have what is called a linear (or LIN) case. Such cases can be one of two types: (1) the stars are not related at all and are just passing by each other along the plane of the sky and hence are of no interest to us as tools to determine orbits, or (2) the stars are in a very large orbit that is nearly edge-on and thus the points may be interpreted as a LIN case where in fact we may have an orbital case with such a slight amount of arcing that we cannot detect any arc yet. Hypothetically, it should be possible in such cases to determine the rate of change in position over a set time interval (such as a decade, or 50 years, or a century) and see if the points fall along a regular time cadence. If they do, the pair is more than likely LIN in nature. But if the points start bunching up (or spreading out) over time, we may be seeing orbital velocity changes projected onto the plane of the sky. I say "hypothetically" because I have not yet been able to make this checking tool work. But in theory, it should. And there is always the dead giveaway when a "LIN" case suddenly reverses direction and starts to move 180° from its recent motion. Now we know we are dealing with a SAB but without the arc.

Like most Excel spreadsheet programmers, I am notoriously bad on documenting what I do, often embedding notes in some of the cells that contain important steps while keeping the screen as clean as possible. (Excel Notes are indicated by a tiny red triangle in the upper right corner of a cell that has notes attached to it.) As a computer professor once told me, "Real programmers don't document!" He was kidding (I think), but there is a hefty dose of truth in that statement!

3. Structure and Functions in the Plot Tool 3.19 spreadsheet

You may a copy of the Plot Tool 3.19.xlsx by clicking this link: http://www.jdso.org. This action will take you to the JDSO server where a copy of Plot Tool 3.19.xlsx awaits your download underneath this article.

General Structure

There are three pages (or "sheets") in the workbook. I will not take the time here to explain complex Excel functions and processes. If you are not very adept at Excel, you can still use Plot Tool 3.19, but don't expect me to tutor you on the intricacies of Excel. It is a powerful and complex program and it has taken me 15 years to master it—or at least become proficient with it.

The first sheet is called "Instructions." I highly suggest you read that sheet as it will tell you how to use the Plot Tool (as will this paper).

The second sheet is called "Data Plot." This is the page where Excel graphs all the data in the Datarequest.txt file you request from Brian Mason at the U. S. Naval Observatory.

To obtain data on any double star in the WDS, send an email to Brian Mason (brian.d.mason@navy.mil). In the message header, put "Datarequest". In the body of the email, type the WDS number of the star. For example, the WDS number of HJ 2010 is 01027+4742. So you would type that number in the body of your email. I suggest you also add your name and some tag line about your research program (for example, I used "Richard Harshaw / Cave Creek, Arizona / Brilliant Sky Observatory"). Dr. Mason and I know each other well now so when he gets an email from me, he knows who I am, but he may not know you until you have contributed several measurements to the WDS.

Dr. Mason is very good at getting a reply to you quickly—usually within 24 hours, but don't panic if it takes longer than that as he is also an observer and from time to time travels to major observatories for observing runs and is not readily available.

If you want data on more than one star, list the WDS numbers in your email, one WDS number per line. There is no limit to how many files you may request but bear in mind that the reply may run into several megabytes. For large requests, Dr. Mason may compress the data into a "TAR ball" (a compression utility popular with UNIX systems) and send it to you. TAR extraction utilities are available for free on the internet. A 1 MB TAR ball may expand to 15 or 20 MB or more.

The third page of the workbook is called "Datarequest.txt" and this is the sheet where you will dump the data text file Dr. Mason sends you.

Handling the Datarequest.txt File

Datarequest.txt files can be very small or very huge, depending on the double star and how much it has been observed. Whatever the size, you will want to look it over before importing it into The Plot Tool.

Most people try to use the Windows Notepad program. I don't advise that. Notepad makes a mess of line breaks and page formatting, and it is easy to get confused with it. The same can be said of Notepad++, a third-party improvement on Notepad.

The folks at the WDS use a UNIX program called Gedit. You can download it for free at this web site (https://gedit.en.softonic.com/). (Be sure to use this website. There are many clones and knockoffs of Gedit out there and I cannot vouch for them. I can vouch for Gedit.) Gedit runs just fine in any Windows environment. I suggest after you download and install it that you play with it a little to get used to how it works.

When I receive datarequests from Dr. Mason, I

Using Plot Tool 3.19 to Generate Graphical Representations of the Historical Measurement Data

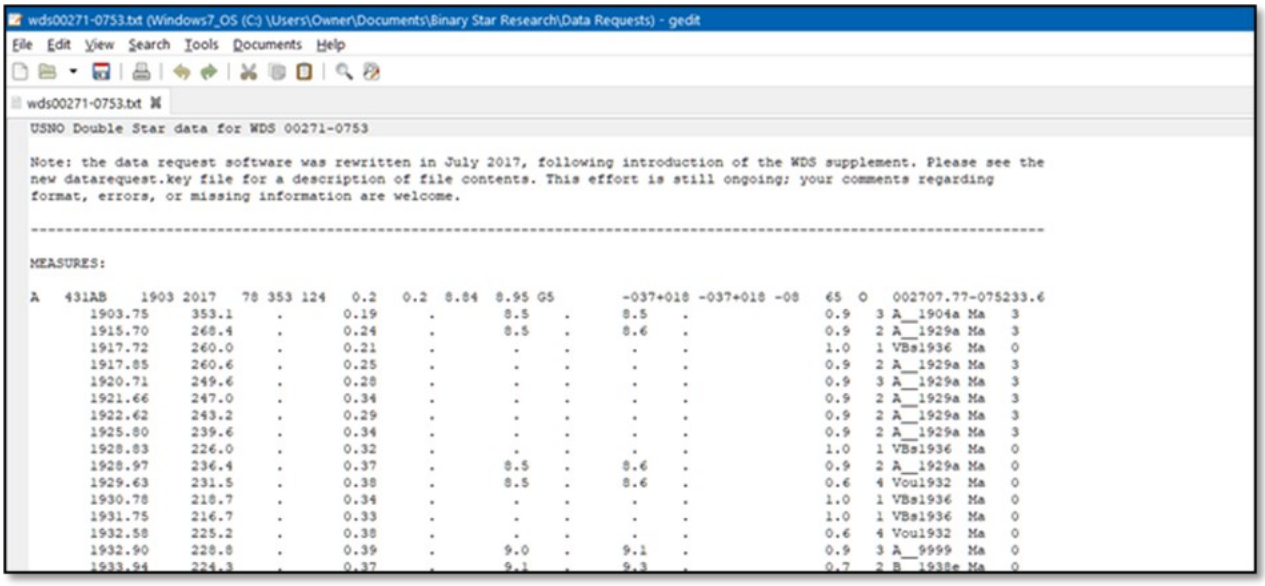

Figure 2: A Datarequest.txt file displayed in Gedit.

have my Outlook program save them into a special file folder under my Binary Stars file folder. I named this folder, surprisingly, Datarequests.

I then open Gedit and navigate to the Datarequests file folder and find the file(s) I want to work with. (You can open multiple files at once with Gedit.)

Figure 2 is a typical Datarequest.txt file as opened in Gedit.

This shows the top portion only of the file (this one is large). Note the WDS number at the very top of the file and the Discoverer Code (A 431 AB) just below the entry "Measures". I will leave it to the reader to figure out the format of the datarequest.txt file from the key that Dr. Mason always sends with every datarequest. Get to know how to read this file. It can make your life as a double star astronomer so much more productive.

Before we can dump this text file into the Plot Tool, we need to edit it. You will want to scan through the file and look for any lines with either a missing value for θ, a mission value for ρ, or both. There are none of these in Figure 2, but Figure 3 is one from another datarequest file.

Here we see that there are missing values for θ and/or ρ in 1974.699, 1974.86, 1975.83 and 1976.80. If we import these null value records into Plot Tool, it will not display the data correctly. So you must DELETE any record with a null value in either q or r.

Finally, be sure to remove any record flagged by the WDS as not reliable. These records will have a capital X at the right end, between the method (here, Ma, Sc, etc.) and the number (2, etc.), which is the number of nights the pair was observed. Any record with an X between the method and nights should also be DELETED.

Once all the null records and X flags have been deleted, select the entire file (in Windows, use CTRL+A) and then go to the Plot Tool "Datarequest.txt" page and paste it there (Windows, CTRL+V).

You may then close the text file (and I suggest you save it when you do).

For the examples in this paper, I will be using WDS 02157+2503 (aka COU 79).

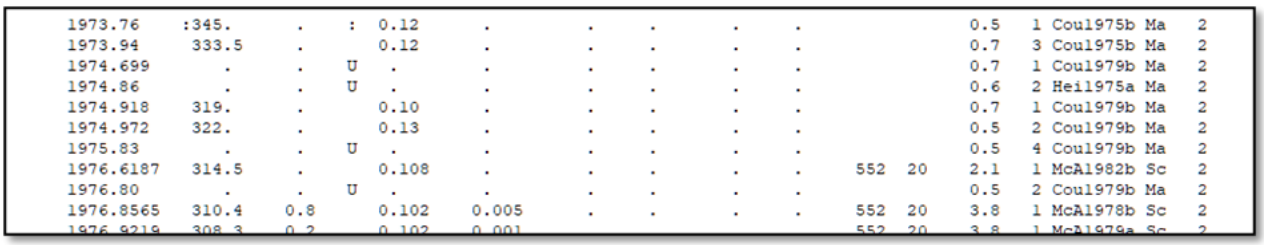

Figure 3: Datarequest showing Null Values in Theta and/or Rho

Using Plot Tool 3.19 to Generate Graphical Representations of the Historical Measurement Data

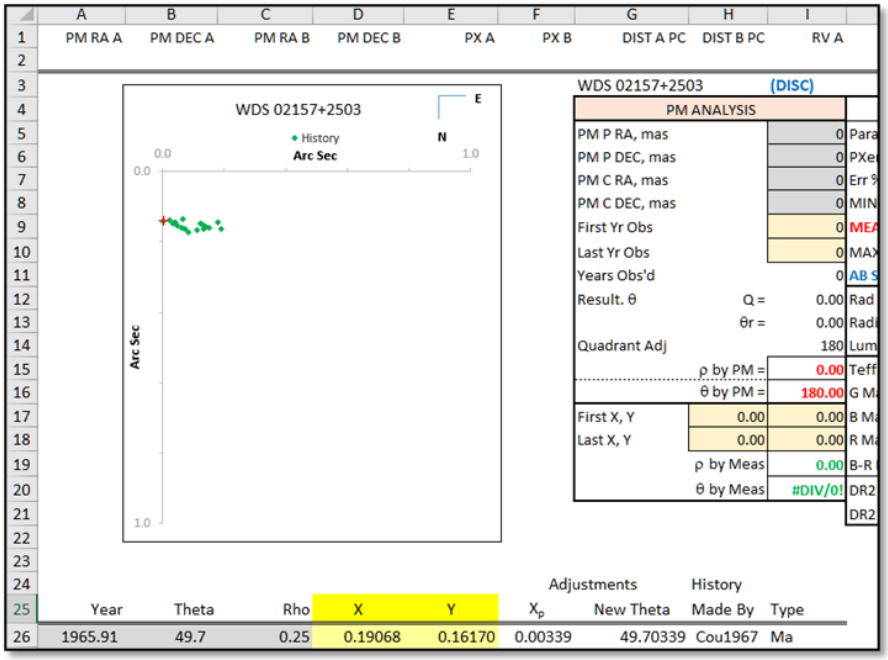

Figure 4: Unprocessed Data Plot page.

What the Data Plot Page Tells Us

First, I note that the Plot (Figure 4) is showing only a handful of the 220+ data points. What is going on?

The plot is just showing the data that fits within the parameters I programmed into Excel. We need to customize this plot. To do so, begin by clicking anywhere inside the plot frame. Small "selection" circles will appear on the border. Now click on any of the green data points. When you do, Excel draws a rectangle around the data used for the plot. You can see this as a lightly darker shading and border around the numbers in columns D and E (labeled X and Y here). Scroll down the page and see that the rectangle stops on line 42. But we have data all the way down to row 243. We need to expand the data selection. To do so, you can either drag the bottom left corner of each column's rectangle down to row 243 or you can manually type in the addresses of the cells. The easiest way is to drag the border with the mouse. If you decide to manually type in the cell address, you need to click on the green points then select the Chart Design tab and then click the Select Data button. You will get a screen that should look like Figure 5.

For now, you can clear the box for Cou1975 (by

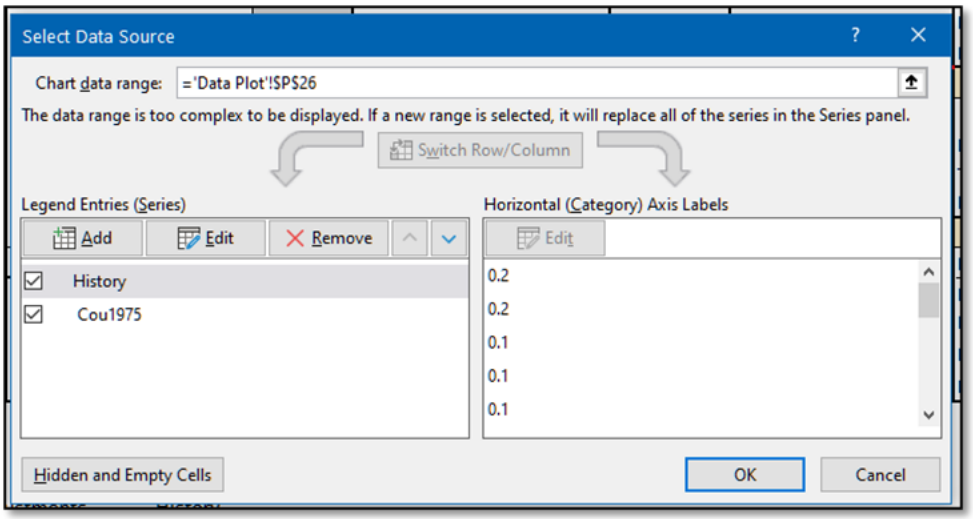

Figure 5: Editing the Data Selection.

Using Plot Tool 3.19 to Generate Graphical Representations of the Historical Measurement Data

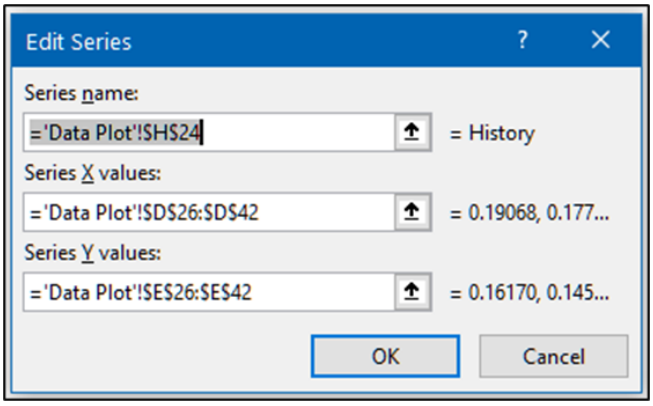

Figure 6: The Data Range edit screen.

clicking on the checkbox). This label is provided to allow the user to enter his or her own data point and have it displayed with a different data icon in a different color.

Select the History set (it is already highlighted) by clicking on it and then Ok. You will see the pop-up window shown in Figure 6.

We want to extend the data selection in columns D and E to row 243. So you should click with the mouse just to the right of $42. Then backspace twice and type "243." Do this for both the Series X Values and Series Y Values windows. Then click Ok twice. See Figure 7.

Does THAT change the plot!

We obviously are dealing with an orbit. But note how small the plot is, and we have a lot of unused space. We can (and should) expand the axis scales.

When generating a plot with the Plot Tool, I strongly suggest you make both axes the same size (in terms of arc seconds). Nothing will get a manuscript returned to you faster than two different axis scales!

To change the axis scales, note that a value of 0.5 arc seconds would easily contain the entire orbit. To change the axis scales, double-click on the horizontal axis. The axis editing dialog box appears, Figure 8.

Let's make the Minimum -0.5 and the Maximum 0.5. Let's also change the Major unit to 0.25 and the Minor unit to 0.10.

Do the same for the vertical axis.

That is much better! See Figure 9. (In fact, we might have even been able to zoom in to -0.3 and 0.3 minima and maxima and changed the major subdivision to 0.1 and minor to 0.05 and gotten an even tighter zoom.

Cardinal rule for plotting data: always be sure each axis is the same size in terms of arc seconds and linear length (centimeters). If this is not done, the plot may be skewed and lead you to a conclusion that is not warranted.

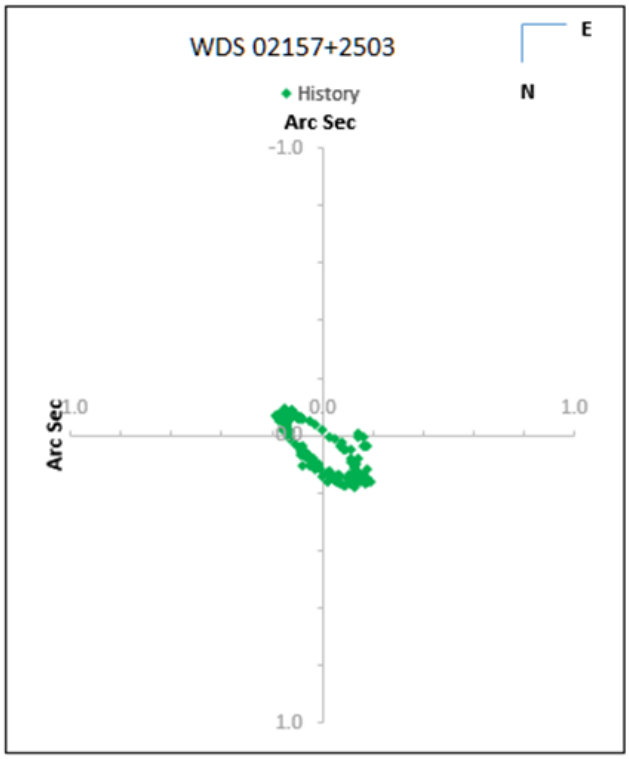

Figure 7: The Updated Data Plot.

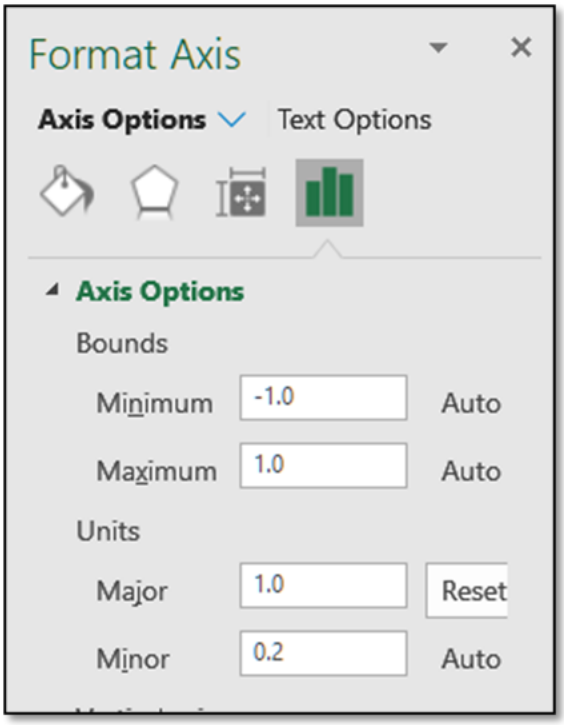

Figure 8: The Axis format dialog.

Using Plot Tool 3.19 to Generate Graphical Representations of the Historical Measurement Data

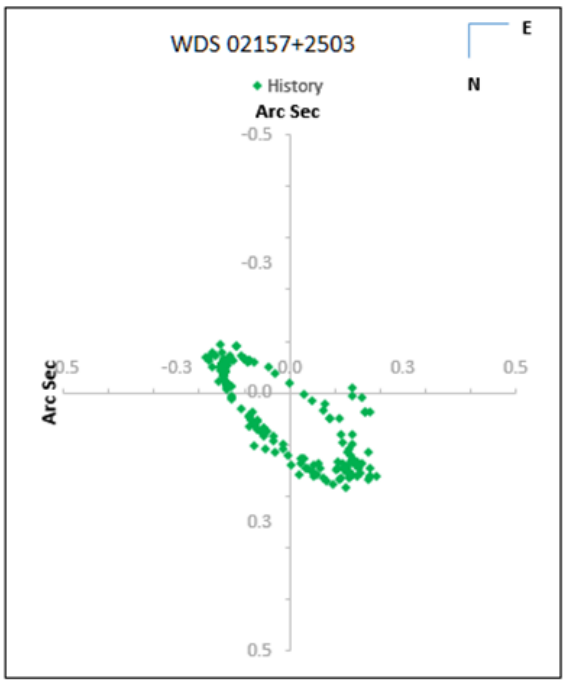

Figure 9: Resized Data Plot.

How the Plot Tool Generates the X-Y Graph

To convert the measurements for θ and ρ in the WDS into Cartesian coordinates so they can be plotted in an X-Y space, we need to apply two simple transforms to the values for θ and ρ.

To convert θ to a Cartesian point, we multiply the value for θ by this transform:

$$\text{Transform 1: } X = \rho\cos(\theta)$$

And to convert ρ to a Cartesian point, we multiply ρ by this transform:

$$\text{Transform 2: } Y = \rho\sin(\theta)$$

This is straightforward enough. However, things are not always that easy in astronomy, and this is one area where it is not easy. That is because the earth wobbles on its axis, like a spinning top on a table (a phenomenon called "precession"). The entire cycle takes around 26,000 years, but it does mean that the true north ("celestial north") is a constantly moving target. From day to day, year to year, it is not much of a change. But after a century or more, it can begin to make a serious difference in measurements.

Why? Because a measurement made, say, in 1821 was made when celestial north was a few arc minutes away from where it is today, and all readings of θ by that astronomer that night must be adjusted for our current epoch in order to get a true reading on the position angle in today's terms.

The transformation that does this adjustment is a bit complicated and is openly stated on The Plot Tool, Data Plot page, in the area bounded from cell S3 to Z13. Essentially, we must convert the star's position in RA (right ascension) and DEC (declination) into degrees of RA and DEC (no conversion needed for the DEC, of course). We also need to know the year of the original measurement and the current year so the computer will know how much to adjust the shift in the celestial pole.

That computation then feeds into the cells in columns F and G, which can be viewed by any curious user if you want to investigate the math involved.

I am indebted to William Hartkopf (retired U. S. Naval Observatory astronomer) for this algorithm.

For wide pairs, the change in θ from 1821 (or any other earlier year) to the present is hardly noticeable, but for very close pairs (pairs under 2" in separation), the change in the plots can be substantial. As Dr. Hartkopf explained to me, when an astronomer chooses to attempt to solve an orbit for a pair, they must first correct for precession because otherwise, the solution will be off by what could be a significant amount. The Plot Tool makes those changes for you automatically. The plot displayed is one that has been corrected for precession.

The Other Data Manipulations on The Plot Tool

I will explain the setup of the other data manipulation routines in the Plot Tool using a plot of ES 1083 (WDS 09013+4843). Figure 10 is the upper left portion of the Data Plot page.

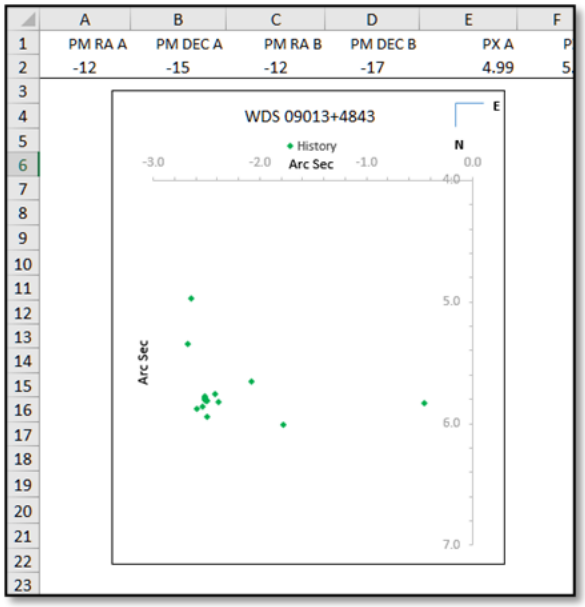

Figure 10: Plot of ES 1083.

The data seem to be somewhat haphazard and random.

To get the data handling routines to work, you will need to import data from Gaia DR2. You can either do this on-line (using such services as VizieR), or you can download the file "**`WDSGaiaDR2 Ver3B.xlsx`**" from the JDSO website. This is an extraction of the WDS from DR2 created by Dave Rowe of PlaneWave Instruments that I use almost daily. It is a large file—some 41.2 MB!

To use the Excel extraction from DR2, you need to have the Plot Tool open and on the Data Plot page with the Datarequest.txt file already read into it. Then you need to place the cursor in cell A2.

Next, jump over to the DR2 extraction (ALT+TAB works, or use the keyboard Windows button) and do a search on the star you need. You can search by either the WDS number (best) or discoverer code (tricky). The tricky part about using the discoverer code is to remember that the WDS uses a 7-place alphanumeric string for the discover code. A star like STF1783 is a no-brainer, but something like Bu47 is a bit trickier. You would need to add 3 spaces after the u in Bu to find the star. So you would need to search for Bu_ _ _47 (where the _ characters are spaces).

Once you find the star you need, move the cursor to column E. Simultaneously hold down the SHIFT key and press the RIGHT ARROW key until you highlight everything over to column AB. With all those cells highlighted (shaded light gray), issue the Copy command (I use CTRL+C) and then jump back over to the Plot Tool, Data Plot page. With the cursor in A2, paste the data (CTRL+V) into the Plot Tool.

Before you mess up and accidentally overwrite your Plot Tool file with a star, rename the Plot Tool to the star you are researching.

Figure 11 is part of the lines 1 and 2 from the Plot Tool for ES 1083, Gaia DR2 import.

Several things should be obvious from even a casual glance at this data. First, note in cells A2 through D2 that the proper motion values for these two stars are almost the same. This makes this pair what we call a "common proper motion" (CPM) pair. While this can be an important indicator that the stars may be physically interacting, it is not a sufficient condition to insure this by itself. We need other data to help us build the case.

That other data comes in several forms. Notice the data in cells E2 and F2, the parallax values. They are almost identical, suggesting the stars are at very nearly the same distance. (In this case, the difference of 0.02 milliarcseconds is not enough to worry about. These two stars are, for all practical purposes, at the same distance.) This bodes well for a physical pair!

This case also shows, however, the lower limits of parallax reliability. I find that parallaxes below 5 milliarcseconds are not to be taken as carved in stone. Granted, Gaia DR2 is the best data we have ever accumulated on the stars, but at parallaxes below 5 mas, we are straining the instruments for every bit of their accuracy. If you had a pair with parallaxes, say of 1.62 and 1.88 mas, they may or may not be at approximately the same distance. It would be best to say that the data is inconclusive.

If two stars are gravitationally bound, their radial velocities (cells I2 and J2) should not be too different. Differences greater than that suggested by the system escape velocity could mean that the stars are moving so fast that they can escape each other's gravitational pull and hence stop being a binary (or they were never a binary to begin with). (Rica, 2011)

Figure 12 is where the main data for confirming a pair's likelihood of being physical is handled in the Plot Tool.

There are six numbered zones in this part of the Plot Tool that I will now discuss in some detail.

Zone 1

Here, Plot Tool does a proper motion analysis on the pair. Note that it reads the PM factors for both RA and DEC for each star from row 2. The First Yr Obs is automatically copied from the Datatext file, but since we don't know how many measures each pair has, the Last Yr Obs cell will not contain data until you type it in. Just scroll down to the last row of measurements to get the year to enter here.

Zone 2

Plot Tool then computes how many years have elapsed between the first and last observations and then computes what the motion of the pair SHOULD have projected on the sky during that time. This is displayed in Zone 2. The numbers in red indicate the expected displacement (ρ) and the position angle of that displace-

	A	B	C	D	E	F	G	H	I	J	K	L	M	N
1	PM RA A	PM DEC A	PM RA B	PM DEC B	PX A	PX B	DIST A PC	DIST B PC	RV A	RV B	RAD A	RAD B	LUM A	LUM B
2	-12	-15	-12	-17	4.99	5.01	200.40	199.60	13.35	12.54	1.19	1.23	1.71	1.92

Figure 11: Part of a DR2 data import.

Using Plot Tool 3.19 to Generate Graphical Representations of the Historical Measurement Data

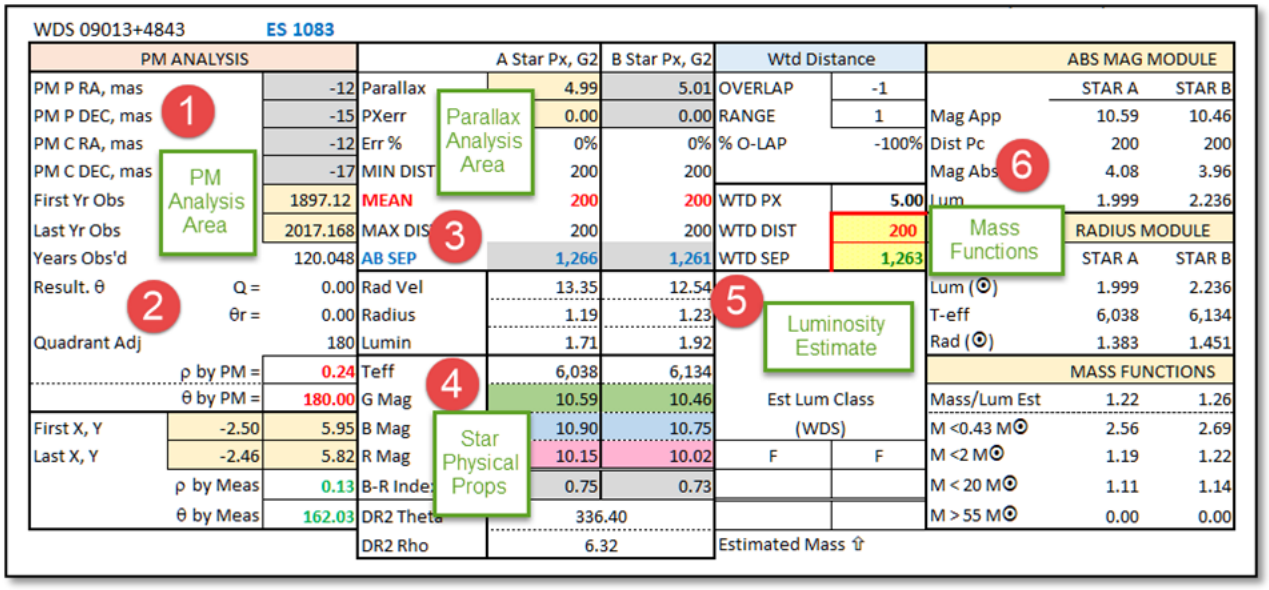

Figure 12: DR2 Analysis in the Plot Tool.

ment (θ). If the proper motion data is accurate, we should see something close to this motion and direction based on actual measurements.

That is where the next section comes in. Plot Tool reads the First X, Y from the datarequest file, but the Last X, Y data must be input manually. Just scroll down to the end of the datarequest file and enter the values for X and Y as shown in columns D and E.

Plot Tool then computes the measured θ and ρ from the measurements. If the values in green come in close to the values in red in this section, that is a good indication that the proper motion data is probably accurate and that the proper motion data can account for the motion of the system over time. This may (or may not) mean the pair is physical, but it is a good indicator that this is certainly a possibility. It is when the values in red and green differ greatly that one must suspect that the pair is not physical.

But there is a caveat. If the red and green numbers in Zone 2 are significantly different, it could be because (a) the proper motion data is invalid, or (b) either the first or last measurement is inaccurate, or both. Case (b) will apply in many cases where the first measurements were made prior to 1850, when measurement was done by filar micrometers illuminated by candles or ring micrometers and stop watches.

Zone 3

Plot Tool analyzes the parallax data in Zone 3. It reads the parallax values from row 2. The cells PXerr are where the parallax error estimate goes. When Mr. Rowe created the Gaia DR2 WDS extraction, he did not think including the error estimates was essential, but I believe it is. To get the error estimates, you will need to access the double star through a service like VizieR and call up the DR2 catalog, enter the coordinates, and select the correct star from the list of stars returned by the query. It may add 5 minutes to your analysis, but it can help confirm (or dispel) a pair being physical or not.

The MIN DIST, MEAN, and MAX DIST values are merely the minimum distance based on the parallax plus the error estimate, the parallax without error estimate, and the parallax less the error estimate.

The AB SEP numbers (in blue) are estimates of the minimum separation between the two stars. I say minimum because we have no idea yet of the orientation of the pair's orbit to earth (or if it even has an orbit), so the projected separation is merely the hypotenuse of a much more complex trig problem. Knowing that the Sixth Orbit Catalog has very few pairs where the actual separation exceeds 2,000 or so astronomical units (AU) is helpful, but not an ironclad guarantee of physicality. Mathematical modeling of double stars shows that in some cases a pair can be separated by up to 380,000 AU and more (Knapp, 2020).

To the right of the Parallax Zone (zone 3) is a section headed "Wtd Distance." This is where Plot Tool projects the distance to the pair using a weighting method. The "Wtd Px" cell computes a "median" parallax based on the relative weights of the parallaxes, with the parallax with the smaller error estimate having a higher weight than the other parallax. The formula is open to review if you want to see it. Place the cursor in cell N9

Using Plot Tool 3.19 to Generate Graphical Representations of the Historical Measurement Data

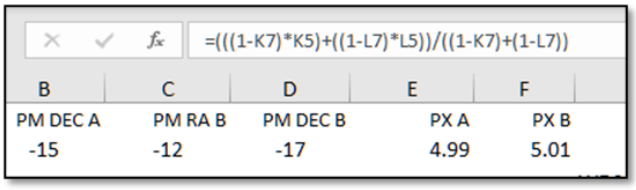

Figure 13: The Parallax Weighting Formula.

and read the formula in the formula bar at the top of Excel (Figure 13).

Once the weighted parallax is computed, Plot Tool can then determine the distance to the pair assuming that the weighted parallax is close to the actual parallax. Note that if you do not look up and enter the parallax error estimates from Gaia's DR2, the weighted parallax will be the same as the mean parallax.

I suggest that any parallax of under 5 mas (milliarcseconds) should be taken with a healthy dose of skepticism for reasons already stated.

The Overlap cell (N4) expresses how much overlap may be between the two stars when their parallaxes are different. Figure 14 is an example of overlap.

The DR2 data for the double star HJ 2687 would suggest different distances to the stars (218 and 227 parsecs respectively, making them some 9 parsecs apart—far too wide to be a gravitationally bound binary, but perhaps still being a physical pair). But the parallax error estimates suggest that the primary star could be anywhere from 188 to 261 parsecs away while the companion could be 227 to 261 parsecs. There is an obvious overlap as shown in Figure 14, but there is also a pretty large area to the left of the overlap zone where the primary star could be at a much greater distance from companion. So we cannot say with certainty that the two stars are physical, let alone binary.

The Overlap Range is the amount of overlap between the two error lines. (In Figure 14, that would be 261-227 = 34 parsecs). The "% of O-Lap" would then be 34 parsecs divided by the total distance spread of 261 parsecs less 188 parsecs (which is 73 parsecs). So the "% of O-Lap" would be 34 / 73 = 47%. This means that slightly less than half the total range of possible distances is where both stars could be close enough to be gravitationally bound.

Zone 4

Zone 4 captures the relevant physical data about the pair—radial velocities, radii, luminosities, Teff, and the G, R and B magnitudes. The B-R index is computed by Plot Tool. This section is for convenience's sake and has no direct bearing on the calculations of distance and proper motion.

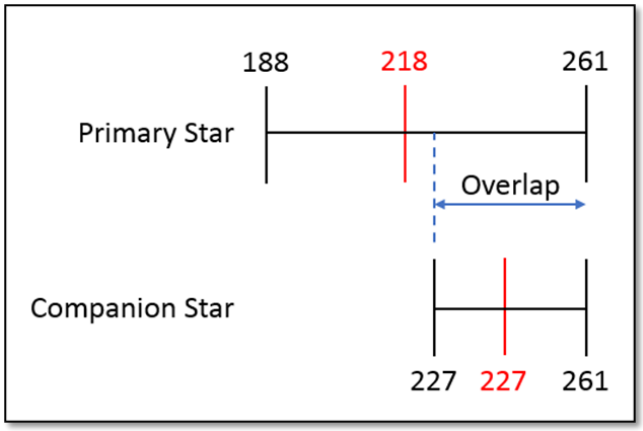

Figure 14: Graphical representation of parallax overlap (IHJ2687 as the example)

Zone 5

Zone 5 is where Plot Tool estimates the spectral class of the stars (cells M18 and N18). The letter classification is based purely on the T_{eff} value. Cells M19 and N19 are where you can type in the spectral class (including the luminosity class) from the WDS. Cells M20 and N20 are where you can enter an estimate of the masses of the two stars. This in turn is based on the outputs of Zone 6.

Zone 6

Zone 6 is where Plot Tool does some calculations of absolute magnitude and hence an indicator of the luminosity class and mass estimates based on DR2's distance estimate, T_{eff} and luminosity. If we know the apparent magnitude (how bright the star looks to us) and the distance, we can compute the absolute magnitude (how bright the star is at a standard distance of 10 parsecs). From this information, we can compute the luminosity in cells P9 and Q9. Note that the luminosity values from these calculations may or may not agree with the DR2 luminosity reported in cells K14 and L14.

The Radius Module section estimates the physical sizes of the stars based on their Teff values and luminosity. The result is an estimate of the star's radius in terms of the Sun.

The Mass Functions area estimates the stellar mass based on the mass/luminosity ratio where empirical data suggests that a star's luminosity is proportional to the star's mass to the power (1/3.5).

Figure 15 shows the estimated mass based on the

$$Mass = \left(L/n\right)^{x}$$

relationship that a star's luminosity is related to its mass along the relationship

where L is luminosity, n is a divisor based on empirical

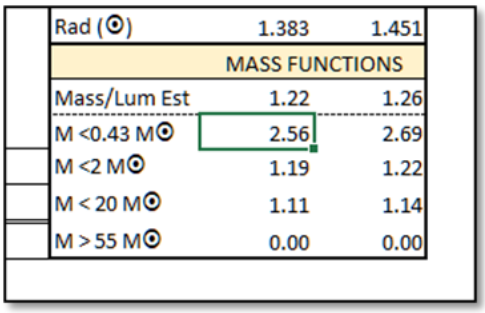

Figure 15: Mass function section.

Mass range	*n*	*x*
< 0.43 solar	0.23	1/2.3
< 2 solar	1	1/4
< 20 solar	1.4	1/3.5
Over 55 solar	32,000	1

Table 1. Values of n and x for the Mass-Luminosity relationship

studies of stars, and *x* is an exponent also derived from those empirical studies. Table 1 are the divisors and exponents.

Note that the mass derived from this process is an approximate estimate only. The only certain way to obtain stellar masses is to solve a binary orbit and know the distance to the pair. The data in the table above is derived from the pioneering work of Jakob Karl Ernst Halm and applies only to Main Sequence stars. (See this web site for a decent treatment of these factors: https://www.1728.org/masslum.htm).

Using our example of ES 1083, with predicted mass/luminosity ratios of 1.22 and 1.26, I would probably place these two stars at about 2 solar masses each. Given their slightly larger sizes and F spectral classes, we might assign them to the Main Sequence, so they would be late FV and FV classes respectively, possible F9V types.

4. A Useful Tool: Excel's Trend Lines

Once you have plotted the data for a pair, you can look at the plot to determine if you see a pattern in the data. (But be careful! The human mind is very good at creating patterns where there are none.)

Most of the time, a plot of data from the WDS will be like the one I have been using in this paper— ES 1083. The data will display a random smattering of points, not unlike the pattern of pellets from a shotgun shot at some distance from a target.

But other times, you will get plots that show tantalizing hints of a possible pattern. I am referring to two types of pattern in particular: a short arc (an arc being a segment of an ellipse, which is the projection of a 3-dimensionsal orbit onto a 2-dimensional sky) and a line (the points lie along a line of some length). Obviously, an arc suggests an orbit is involved, even if it has not yet been solved. Any short arc binary (SAB) pair should receive priority in any observing program as we need to gather more data to enable someone to someday derive an orbit.

The linear cases (LINs) are a little tougher. Sometimes, the linear pattern may be only a few arc seconds in length. Is this a true linear case (suggesting an optical pair of stars), or are we seeing a very small piece of a large nearly edge-on orbit? (Such cases could masquerade as linear examples.) But if the pathway is long (several arc seconds), and is strongly linear, it is likely (but not guaranteed) that the pair is, in fact, a linear (optical) case.

Let's examine a case of a SAB plot. In Figure 16

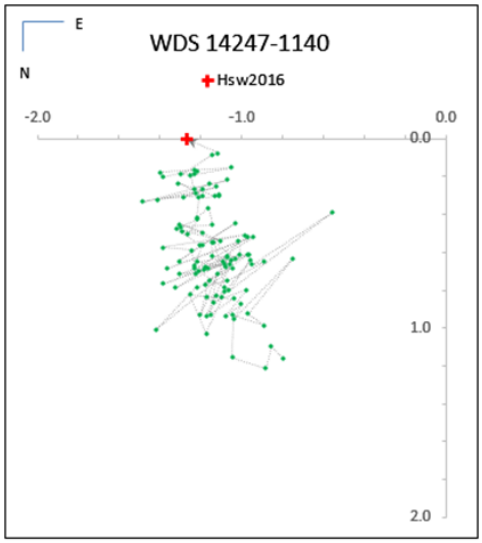

Figure 16: Plot of WDS 14247-1140.

we have the Plot Tool depiction of WDS 14247-1140 (STF1837).

I have superimposed over the data an Excel line that connects the data in chronological order. (Later you will see how this handy feature can sometimes show what looks like a LIN or SAB case to be random noise in the data.)

You can see a definite curvature to the data trend. Figure 17 is the same plot without the chronological line connecting the data. It is much harder to detect a pattern here!

And Figure 18 is the same plot with an Excel trend line (in this case, a polynomial line) and it's R^2 value.

(You can ask Excel to draw a trend line by right clicking on any data point and selecting "Add Trend-

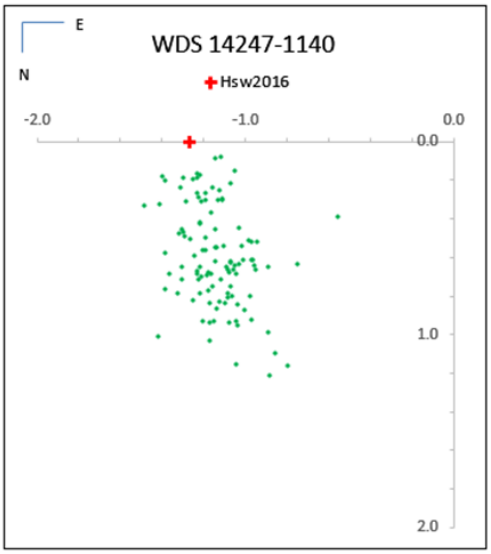

Figure 17: WDS 14247-1140 without the chronological connector.

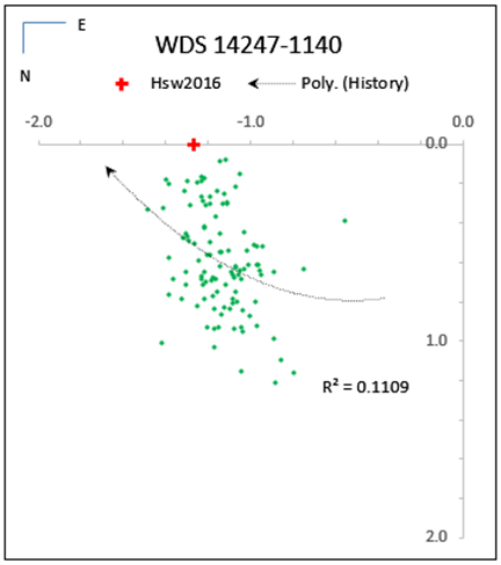

Figure 18: WDS 14247-1140 with an Excel polynomial trend line.

line" from the fly-out menu. When that option is chosen, you have control over how the trend line is displayed. I chose the polynomial trend function because orbits follow ellipses which are polynomial equations.) The R^2 value of 0.1109 is not very strong. This number represents how well the data fit the trend line. A value of 1.0000 means there is a perfect correlation between the data and the trend line. A value of 0.0000 means absolutely no correlation exists. (For comparison, a linear trend for this pair has a lower R^2 value, 0.1055.)

This case could use some weighting, and I will come back to that later in this paper.

Let's now consider a linear case (one that, surprisingly, does not yet have a solution). Figure 19 is the plot for WDS 00167+4104 (FAB 2 AB). In this case, I

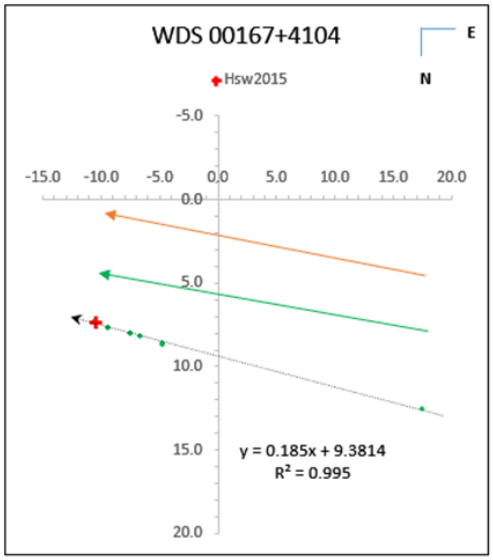

Figure 19: Plot of WDS 00157+4104.

have also included the equation of the line as well as two vector arrows, one orange and one green.

The orange vector is how the pair should have moved over the years if we are considering only the proper motion (which in this case is very large and of very different values). The green vector is the motion given my using the first and last measurements. Note how the two vectors are nearly identical in magnitude and direction. This suggests very strongly that this pair's motion can be explained by the proper motions of the stars alone and that there is no motion due to gravitationally-induced motion as in the case of a binary star. This pair is most likely optical.

[To draw the vectors, use the outputs of Plot Tool, cells I15 and I16 (for the proper motion) and cells I19 and I20 (for the measurements). Select the draw tool in Excel and choose the one-headed arrow. Draw a vector along one of the axes the same length as the values shown in either cell I15 (for proper motion) or I19 (for measurements). To get the angle of orientation, right click on the arrow and select Size and Position, then adjust the rotation to match the position angles of cells I16 or I20. Then drag the arrow to a convenient place on the plot.]

5. Weighting the Data for a Better Analysis

Excel assigns equal weight to every data point, but when analyzing measurement data, astronomers know

Using Plot Tool 3.19 to Generate Graphical Representations of the Historical Measurement Data

that some measurements are worth more than others, so they must "weight" the data. There is a simple (but cumbersome) workaround for this in Excel.

I weight data using four key factors, similar to the factors suggested by Dr. William Hartkopf [1] of the U S Naval Observatory (retired)—see http://ad.usno.navy.mil/wds/orb6/orb6ephem.html: (1) the separation of the pair compared to the Rayleigh limit of the telescope; (2) the type of measurement made; (3) the observer making the measurement; and (4) how many nights the pair was observed. I will now explain how this method works.

The Rayleigh Limit Factor

How close is the pair compared to the telescope's resolving power? The Rayleigh Limit defines a telescope's theoretical resolving power as a function of its diameter. A larger telescope can resolve smaller angles. For my weighting method, I use the following criteria:

- If the Rayleigh Limit RL is less than ρ: weight of 0.5
- If the RL is between 0.5 and 2.0 ρ: weight of 1.0
- If the RL is between 2.0 and 4.0 ρ: weight of 2
- If the RL is greater than 4.0 ρ: weight of 3

To compute the RL for a telescope, take 5.23 and divide by the objective diameter if it is in inches, or divide 0.138 by the objective if stated in meters.

The Type of Measurement

This refers to the method used by the astronomer, such as filar micrometer, photo, CCD, speckle and so on.

I took 303 known Grade 1 and Grade 2 orbits and ran residuals on every measurement made by every observer. I then analyzed the results for trends and found many. One of them was the type of method used. Certain methods routinely produced *lower* residuals (that is, better measurements) than other methods. I use five weighting levels.

Methods of weight 5 (the most accurate methods) include any satellite method (since the satellite is imaging the stars above the distortions of the atmosphere), all interferometric methods, and all speckle methods.

Weight 4.5 Methods include CCD and photographic imaging.

Weight 4 Includes adaptive optics, electronic imaging, and the Mt. Wilson interferometers.

Weight 3: Micrometers.

Weight 2: Visual interferometers, the Celestron MicroGuide (and Mead Astrometric) eyepiece, and transit circles.

Weight 1: Heliometers, occultations.

The Observer Making the Measurement

By its nature, this is very private and personal data and as such I am not comfortable sharing my findings with the general public. My analysis of the 303 orbits showed that some astronomers were consistently poor in observing quality while others were consistently high. I use a 5 point scale, with 5 getting the greatest weight. Since you don't have access to my data, you can play it safe and assign all observers a default weight of 2.5.

The Nights the Pair Was Observed

This is simply the square root of the number of nights the star was observed. Obviously, an astronomer who reports measures that are an amalgamation of four nights of work is going to have a steadier result than the one who only observes the pair one time.

Normalizing the Weights

Figure 20 is a picture of the normalization routine and weighting process I use when weighting measurements. (Note that this routine is not part of Plot Tool 3.19 but must be added if you want to do weights. I did not include it for the reason I stated earlier about distributing observer weights.)

The first column—Rho/RL—is the ratio of the value of r to the Rayleigh Limit of the telescope. Since all the values are greater than 4, I entered "3" into the Aper Gr column. The Meth Gr column is filled in based on the type of measurement. Obs Gr is a semi-objective assessment of each observer's skills. And the Sqrt N column is merely the square root of the number of nights the star was observed. The "Moment" column is the product of all the weights.

Above the Moment header are three numbers: Max, Min and Range. The Max is the largest moment in the list of measurements. The Min is the minimum moment, and Range is the difference in these two values.

				Max	135		
				Min	33.75		
				Range	101.25	20.25	
Rho/RL	Meth Gr	Obs Gr	Aper Gr	Sqrt N	Moment		Final Wt
			2.5	1	0	0	1
21.56957	5	2.5	3	1	37.5	1.851852	2
21.56957	5	2.5	3	1	37.5	1.851852	2
21.35217	5	2.5	3	1	37.5	1.851852	2
21.35217	5	2.5	3	1	37.5	1.851852	2
99.19565	4.5	2.5	3	1	33.75	1.666667	2
99.19565	4.5	2.5	3	1	33.75	1.666667	2
15.94928	4.5	5	3	2	135	6.666667	7
15.94928	4.5	5	3	2	135	6.666667	7
15.94928	4.5	5	3	2	135	6.666667	7
15.94928	4.5	5	3	2	135	6.666667	7
15.94928	4.5	5	3	2	135	6.666667	7
15.94928	4.5	5	3	2	135	6.666667	7
15.94928	4.5	5	3	2	135	6.666667	7
61.73188	5	5	3	1	75	3.703704	4

Figure 20: The weights normalization process.

The 20.25 value you see in the example (circled) is the Range divided by a number that is chosen to get the lowest Final Wt value as close to 1 as possible. In this example, Range was divided by 4 to get 20.25.

The Moments are then divided by this recomputed Range to get the numbers to the immediate right of the Moment column. For the Final Wt, I then round the adjusted moment to the nearest integer.

Example: the second measure in the list comes in at 37.5 for the moment, 1.851852 for the adjusted moment, and 2 for the Final Wt.

Once all the weights are finalized, I then go to any weight that comes in below 0.5 and delete it. For the measures that are left, I then go to the line directly below the measure and insert as many blank lines as necessary to get to the Final Wt number. (For a Final Wt of 2, I would insert one line. For a weight of 5, insert 4 blank lines.)

Next, I select the line above the blank line and copy it, then Paste it into the newly formed blank line, but be sure to use the **Paste Special, Values** option. Otherwise, the process will not work.

In this somewhat cumbersome method, Excel now properly assigns weights to each measurement and the R2 value displayed on any plots is very accurate. Of course, the line or curve will also be reshaped to some extent by this procedure.

6. The Value of a Chronological Plot in Weeding Out False Positives

Sometimes, Plot Tool generates a data plot that strongly suggests either a LIN or SAB pattern. Figure 21 is one example of a LIN case. The measurement vector (green arrow) suggests a linear pattern. But is it? Figure 22 is the same plot with the chronological plotting option displayed.

The "appearance" of linearity is due to a few measures being outliers. The first measurement (the farthest outlier) was made by John Herschel in 1829. John's error is significant, but understandable seeing how he was using an early, primitive and very difficult method to determine θ and ρ—a ring micrometer. When you look at the latest data, the points all cluster near one another in a tight pattern, something that is typical of early micrometric measurements. (The sky can distort measurements that much from night to night and observer to observer!)

Figure 23 is an even better example. There is a strong R^2 coefficient and an "obvious" linear pattern, until one looks at the data in chronological order, Figure 24.

What happened to our nice linear plot? It was never there. Instead, the data seems to be one of those

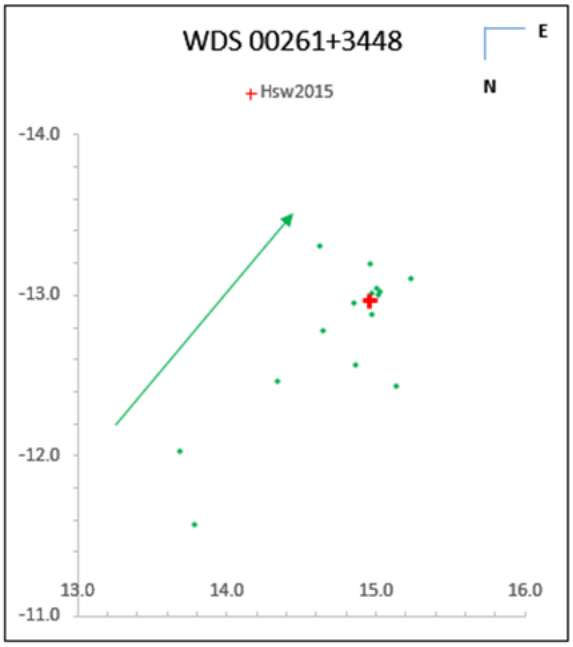

Figure 21: Plot of HJ 622.

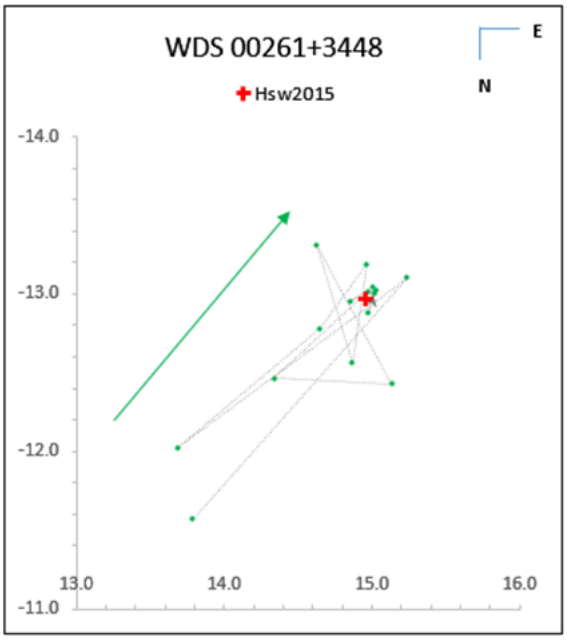

Figure 22: HJ 622 with the data plotted in chronological order.

Using Plot Tool 3.19 to Generate Graphical Representations of the Historical Measurement Data

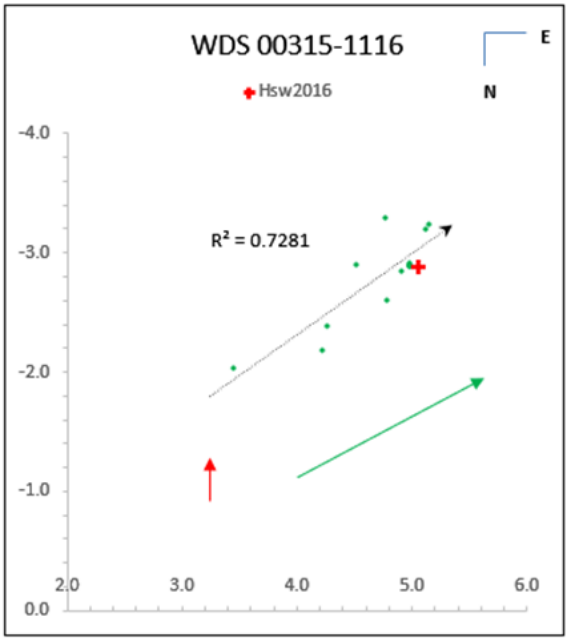

Figure 23: Possible linear case of HJ 1980.

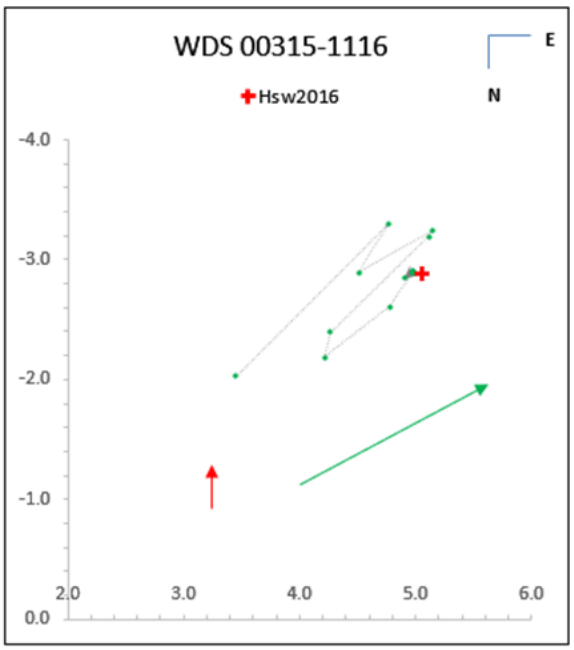

Figure 24: HJ 1980 with chronological data plot.

"random walk" illustrations shown in many statistics textbooks. If anything, there may be a very weak arc going clockwise from upper left to lower right, but that is purely subjective and not admissible in a court of scientific inquiry.

The same thing works for detecting false SAB cases. The polynomial trend line in Figure 25 produces a much better fit at $R^2 = 0.7300$ than a linear trend with an R^2 value of only 0.3317. So at first glance, we might

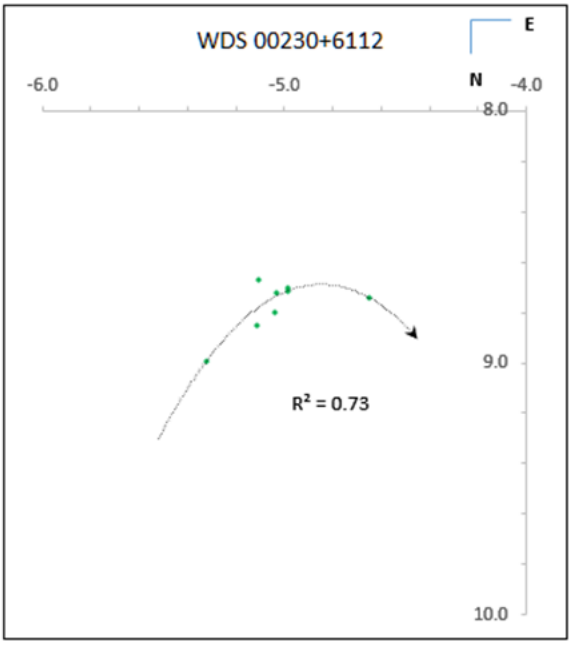

Figure 25: The SAB plot of WDS 00230+6112-- or is it?

conclude we are dealing with a SAB.

But notice how the curve does not wrap around the graph's origin point [(0,0), not shown here but off to the upper right]. All SABs should wrap around the system's origin (the location of the primary star for these plots). So that tells us right off that something is amiss with the trend data from Excel.

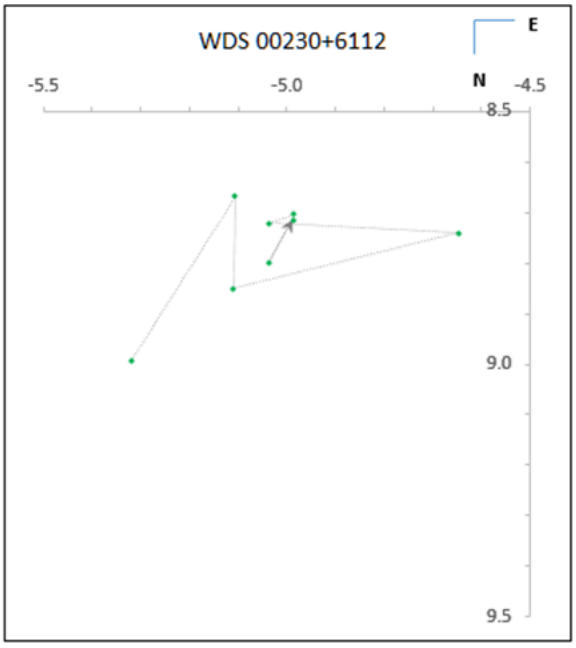

Figure 26: :The same pair with a chronological connection of the data.

In Figure 26, I have asked Excel for a chronological plot of the data and that changes things significantly. That tempting SAB is now gone. No short arc here. Just a random set of noisy observations.

Because of the power of a chronological plot, I almost always suggest that authors submitting papers to the JDSO first generate a chronological plot of the data to see if the trend they say they see is real or not. Our brains are so easily fooled by random information appearing as patterns. (Just think of the constellations of the night sky!)

8. Conclusion

If you want a copy of The Plot Tool 3.19 (for Excel, written in the Office 365 version, but should be readable by any version of Excel from 2007 on), you can download "**`Plot Tool 3.19.xlsx`**" from the JDSO website. Hopefully, use of this tool will help you see double stars in a new way and find real patterns as opposed to what merely looks like a pattern. You may also download a copy of the WDS Extraction from Gaia DR2 from the JDSO website named in Section 3, The Other Data Manipulations on The Plot Tool subhead.

9. Acknowledgements

The author would like to thank Dr. William Hartkopf of the U. S. Naval Observatory (retired) for his assistance in the precession algorithm in Plot Tool.

The author also wishes to acknowledge the valuable contribution to double star research provided by Mr. David Rowe of PlainWave Instruments for his detailed extraction of the WDS from Gaia DR2.

Finally, heartfelt appreciation goes to Dr. Brian Mason of the U. S. Naval Observatory. His tireless and cheerful response to over 8,000 datarequests generated some big "Tar balls" and led to both of us learning a thing or two about large data transfers.

10. References

Rica, F. M., 2012, "Determining the Nature of a Double Star: The Law of Conservation of Energy and the Orbital Velocity", *JDSO*, **7**, No. 4; 254-259.

Knapp, Wilfried, 2019, "The 'True' Movement of Double Stars in Space", *JDSO*, **15**, No. 3; 464-488.

The Discovery of an Equal-Mass Twin Binary System by Online Sky Survey Images

Guoyou Sun

Wenzhou Astronomical Association, China
dofur@hotmail.com

Abstract: A previously uncataloged double star (an equal-mass twin binary system) was discovered by the author while searching for planetary nebulae candidates in the online DECaLS images.

Introduction

While hunting for planetary nebulae in the online DECaLS images, I found an interesting group of three stars that give the appearance of a visual triple star system (Figure 1).

The system is composed of UCAC4 613-046272 (G= 13.9068), UCAC4 613-046274 (G=13.7953) and UCAC4 613-046273 (G= 13.9697),which I have labeled A, B, and C respectively throughout the rest of this paper.

Gaia DR2 reported the A component to have a proper motion of [3.391 -7.965] and a parallax of 5.2283 (±0.0317) milli-arcseconds (Gaia 2018b). For the B component Gaia DR2 reported a proper motion of [2.327 -7.856] and a parallax of 5.1745 (±0.0315) milli-arcseconds (Gaia 2018b). For the C component Gaia DR2 reported a proper motion of [-2.062 -2.755] and a parallax of 0.0371 (±0.0.0322) milliarcseconds (Gaia 2018b).

Gaia DR2 measurements were also used to calculate the apparent separation (Sep) and the Position angle (PA). The Gaia DR2 astrometry measurements for these stars are summarized in Table 1.

Interestingly, astrometric data from Gaia DR2 show that A-B and C are not correlated based on their parallax, but that A and B are likely related.

Using the APOP catalog (Qi+, 2015), I was able to deduce B-V color index of these stars. Using the J and K band from the 2MASS catalog (Cutri et al. 2003), I was able to deduce J-K color of these stars. Based on the absolute magnitude of the Gaia G filter (MG) , Teff and Lum (Gaia Collaboration, 2018), and their radius and mass (Stassun, Keivan G.,et al. 2019) (see Table 2), A and B should be A pair of K-type dwarf stars, and their spectral type may be K5V.

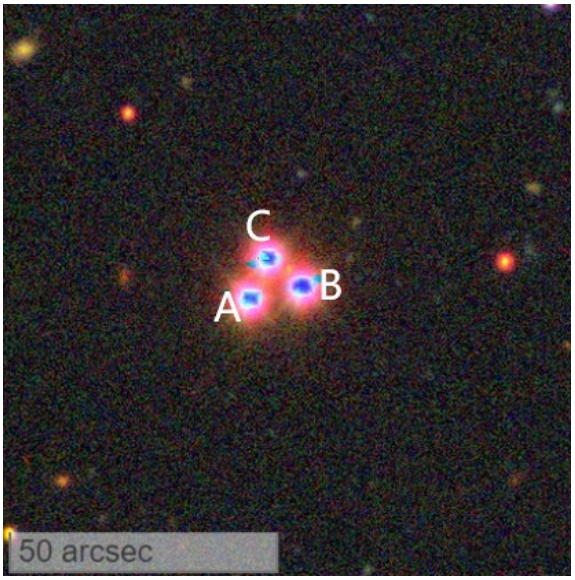

Figure 1.Discovery DECaLS DR5 image extract showing the group of three stars. Their visual appearance in this image is much like that of a triple star system.UCAC4 613-046272 (A), UCAC4 613-046274 (B) and UCAC4 613-046273 (C).

Conclusion

According to the parallax data of Gaia DR2, we exclude the correlation between A-B and C. According to Gaia parallax data, A lies at a distance of ~623ly and

Received May 10, 2020.

Star	RA+Dec	PM(RA)	PM(Dec)	Parallax	Plx_ error	Sep	PA
A	08 51 11.53 +32 35 13.58	3.391	-7.965	5.2283	±0.0317	--	--
B	08 51 10.76 +32 35 15.83	2.327	-7.856	5.1745	±0.0315	9.989"	283.019°
C	08 51 11.26 +32 35 20.96	-2.062	-2.755	0.0371	±0.0.0322	8.131"	335.185°

Table 1. Gaia DR2 Astrometry

Star	B-V	J-K	MG	Teff	Rad	Mass	Lum
A	1.51	0.788	7.5	4211.36	0.695	0.64	0.11
B	1.528	0.779	7.36	4132.63	0.708	0.65	0.13

Table 2.Photometry (APOP, 2MASS , Gaia DR2 and TESS)

B at ~630ly. If the uncertainty of measurement is taken into account, assuming B is at the same distance as A, the physical distance would be ~1900 AU. So they are likely to be physical.

Because A and B have highly similar masses (Stassun, Keivan G.,et al. 2019) and luminosity (GaiaCollaboration, 2018), A and B are likely to be an equal-mass twin binary system (Kareem El-Badry, et al. 2019).

Acknowledgements

The following tools and resources have been used for this research:

- DECaLS DR5 images
- GAIA DR2 catalog
- 2MASS Catalog
- TESS Catalog
- Washington Double Star Catalog
- CDS VizieR
- APOP catalog

References

Evans et al. 2018, “Gaia Data Release 2: Photometric content and validation”, ArXiv e-prints.

Gaia Collaboration, 2016, “The Gaia misson”, *Astronomy & Astrophysics*, **595**, A1.

Skrutskie, M.F., et al. 2006, “The Two Micron All Sky Survey (2MASS)”, *The Astronomical Journal*, **131**, 1163-1183. http://adsabs.harvard.edu abs/2006AJ....131.1163S

Qi, Zhaoxiang., et al. 2015,“Absolute Proper Motions Outside the Plane (APOP) - A Step Toward the GSC2.4”,*The Astronomical Journal*, **150**, 137, 12pp. https://ui.adsabs.harvard.edu/abs/2015AJ....150..137Q

Gaia Collaboration, 2018, “Gaia Data Release 2: Summary of the contents and survey properties”. ArXiv e-prints.

Gaia Collaboration, 2018b, “Observational Hertzsprung-Russell diagrams”, *A & A*, **616**, A10.

Lindegren, L., et al. 2018, “Gaia Data Release 2: The astrometric solution”, ArXiv e-prints.

Luri, X., et al. 2018, “Gaia Data Release 2: using Gaia parallaxes”, ArXiv e-prints.

Stassun, Keivan G., et al. 2019,“The Revised TESS Input Catalog and Candidate Target List”,*The Astronomical Journal*, **158**, 1538-388.

Kareem El-Badry, et al. 2019,“Discovery of an equal-mass “twin” binary population”, *MNRAS* 000, 1–37.

Discovery of New Members of WDS 02137-0302, and -- WDS 02137-0302 B May Not Be Physical

Guoyou Sun

Wenzhou Astronomical Association, China
dofur@hotmail.com

Abstract: The author discovered a new member of WDS 02137-0302 and judged from the parallax data of Gaia DR2 that WDS 02137-0302 B May not belong to this system.

Introduction

WDS 02137-0302 is composed of two components, A and B.

Gaia DR2 reported the A component to have a proper motion of [24.703 -23.233] and a parallax 7.9959 (±0.0497) milli-arcseconds (Gaia Collaboration, 2018). For the B component Gaia DR2 reported a proper motion of [-46.898 -51.580] and a parallax 5.3825 (±0.0549) milli-arcseconds (Gaia Collaboration, 2018).

Checking the Gaia DR2 data showed that 2MASS J02134399-0301246 is probably a member of the system. Let's call it C for the moment, Figure 1.

Gaia DR2 reported the C component to have a proper motion of [25.779 -23.950] and a parallax 8.1425 (±0.3425) milli-arcseconds (Gaia Collaboration, 2018).

Gaia DR2 measurements were also used to calculate the apparent separation (Sep) and the Position angle (PA). The Gaia DR2 astrometry measurements for these stars are summarized in Table 1.

Conclusion

According to the parallax data of Gaia DR2, we can exclude the correlation between B and A. The distance between the two is too far for them to be physical. C appears to be significantly closer. According to Gaia parallax, the distances to A and C are ~408 ly and 401 ly, respectively. If the uncertainty of measurement is taken into account, assuming C is at the same distance as A, the physical distance would be ~5050 AU. The highly similar proper motion between them, suggests that they are likely to be physical.

Received May 20, 2020.

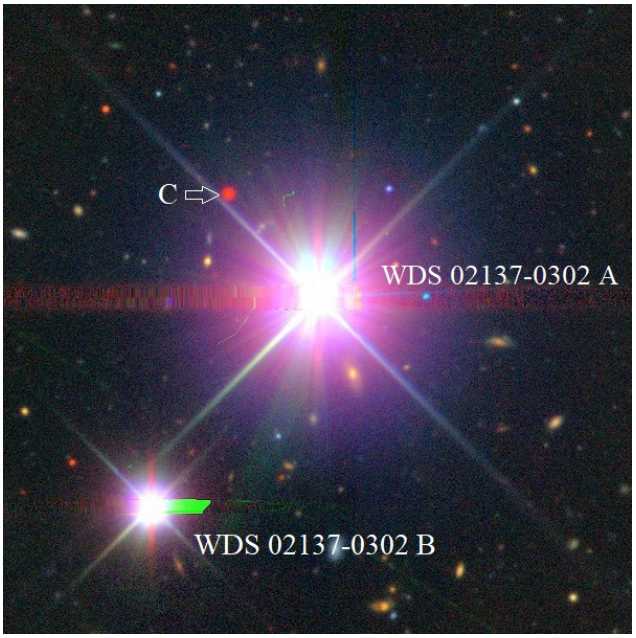

Figure 1.Discovery DECaLS DR5 image extract showing the group of three stars.

Acknowledgements

The following tools and resources have been used for this research:

- DECaLS DR5 images
- GAIA DR2 catalog
- Washington Double Star Catalog
- CDS VizieR

Star	RA+Dec	Parallax	Plx_ error	PM(RA)	PM(Dec)	Sep	PA
A	02 13 42.252 -03 01 55.66	7.9958	±0.0497	24.703	-23.233	--	--
B	02 13 45.533 -03 02 57.31	5.3825	±0.0549	-46.898	-51.580	78.842"	141.439°
C	02 13 44.017 -03 01 25.09	8.1425	±0.3425	25.778	-23.950	40.417"	40.855°

Table 1. Gaia DR2 Astrometry

References

Evans et al. 2018, "Gaia Data Release 2: Photometric content and validation", ArXiv e-prints

Gaia Collaboration, 2016, "The Gaia misson", Astronomy & Astrophysics, 595, A1.

Gaia Collaboration, 2018, "Gaia Data Release 2: Summary of the contents and survey properties". ArXiv e-prints.

Lindegren, L., et al. 2018, "Gaia Data Release 2: The astrometric solution", ArXiv e-prints.

Luri, X., et al. 2018, "Gaia Data Release 2: using Gaia parallaxes", ArXiv e-prints.

Discovery of Stellar Duplicity of TYC 1326-01111-1 During Asteroidal Occultation by (86) Semele

Jerry Bardecker
Gardnerville, Nevada USA
bardecker@frontier.com

Steve Messner
Northfield, Minnesota USA
International Occultation Timing Association (IOTA)

Abstract: An occultation of TYC 1326-01111-1 by the asteroid (86) Semele on 2019 October 17 showed this star to be a double star. Both components of the double star were occulted as seen by two observers. The separation of the two components is 0.0046 ± 0.0012 arcseconds at a position angle of 11.7 ± 6.0 degrees. The magnitude of the primary component is estimated to be 12.66(r). The magnitude of the secondary component is estimated to be 12.87(r).

Observation

On 2019 October 17 Jerry Bardecker and Steve Messner observed the asteroid (86) Semele occult the star TYC 1326 01111-1 from two locations in the USA. The observations were made with 30cm (Bardecker) and 20cm (Messner) telescopes, using video with GPS-based time insertion to record the event. Messner's two step event is shown in Figures 1. Bardecker's two step event is shown in Figure 2. The star is of magnitude 12.0 (R). The expected magnitude drop at occultation for the single star was 1.40 magnitudes. Bardecker observed a 0.54 and 0.85 magnitude drop in each of the two events (D1 and D2) – a combined magnitude drop of 1.39 which is very close to the predicted 1.40. Messner observed a 0.52 and a 0.78 magnitude drop in each of the two events (D1 and D2) – a combined magnitude drop of 1.30. All recorded occultation times and data from the observers can be found in archived IOTA records for the event. The observations were made by the observers located at the sites and with the equipment as shown in Table 1.

The star is not listed in the Fourth Interferometric Catalog, nor is it listed in the Washington Double Star catalog.

The predicted observation path is shown in Figure. 4.

Video of the occultation events at both locations was recorded using NTSC video cameras. Analysis of the recorded video and light curve analysis was made using PyMovie 2.5.1 and PyOTE 3.2.5. [1]

Individual Event Times

Times for the disappearance and reappearance of each component of the double star are shown for the two observers in Table 2. These times are corrected for camera and VTI time delays. They are also the reported times that represent the Occult4 double star plot solution shown in Figure 3.

(Text continues on page 408)

Site				Telescope				
No.	Observer	Location	State	Telescope Type	Dia (cm)	Method	Chords	Results
1	S Messner	Currie	MN	Newtonian	20	Video+GPS Time Inst	1	Two-step
2	J Bardecker	Gardnerville	NV	SCT	30	Video+GPS Time Inst	1	Two-step

Table 1—Observer(s), site locations, equipment, methods, and results

Received December 15, 2019.

Discovery of Stellar Duplicity of TYC 1326-01111-1 During Asteroidal Occultation by (86) Semele

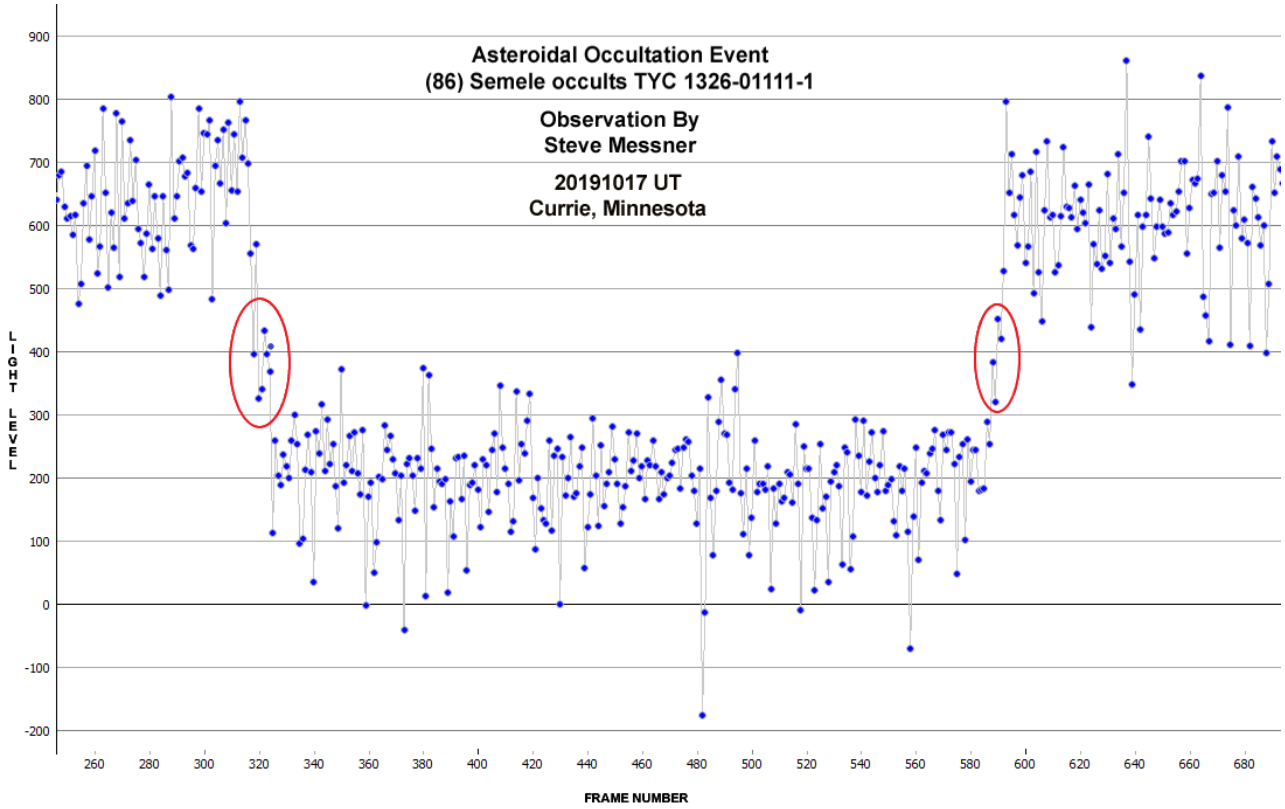

Figure 1 -- Messner event – note stepped events circled.

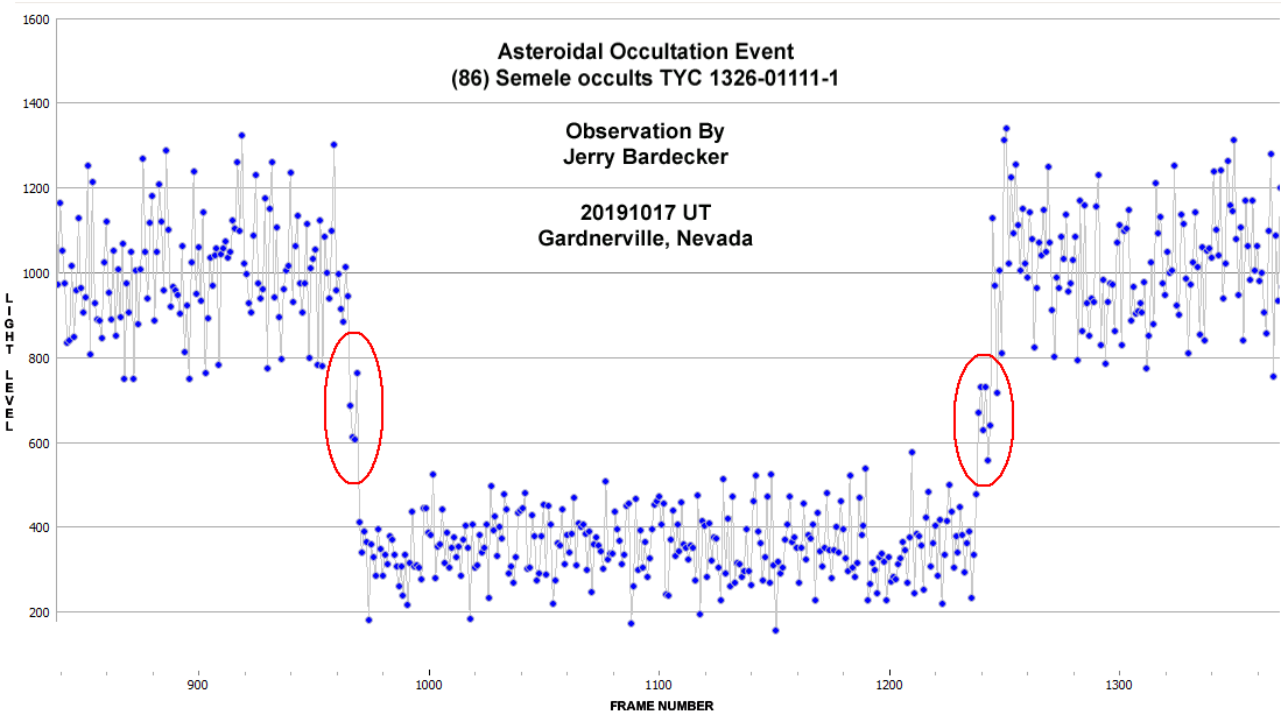

Figure 2 -- Bardecker event– note stepped events circled

Discovery of Stellar Duplicity of TYC 1326-01111-1 During Asteroidal Occultation by (86) Semele

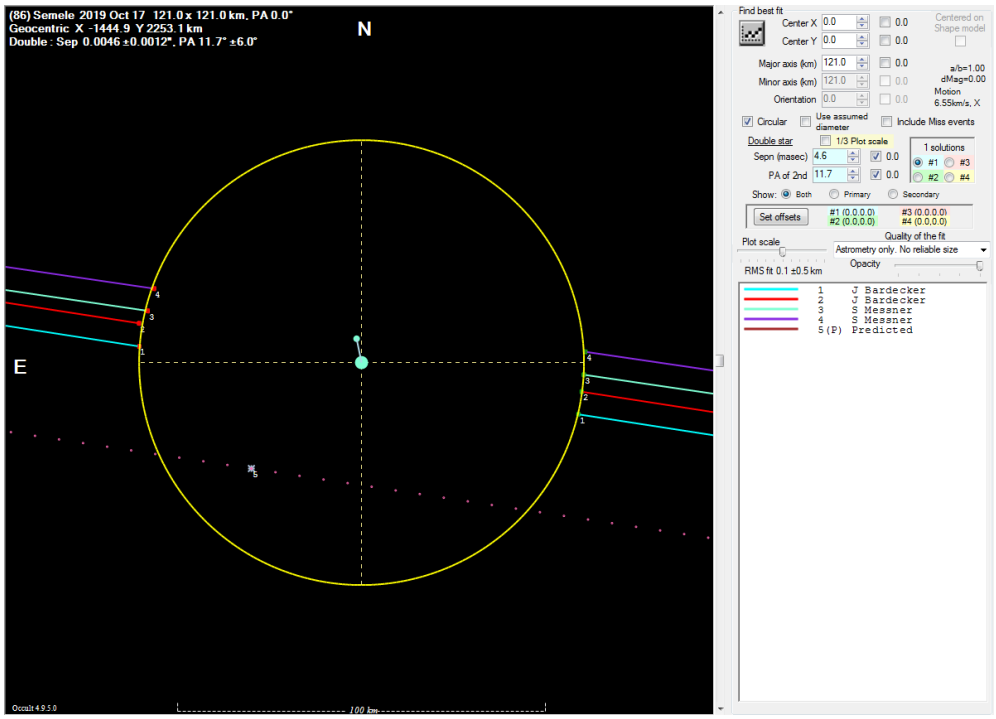

Figure 3: Occultation (86) Semele occultation of TYC 1326-0111-1 profile plot

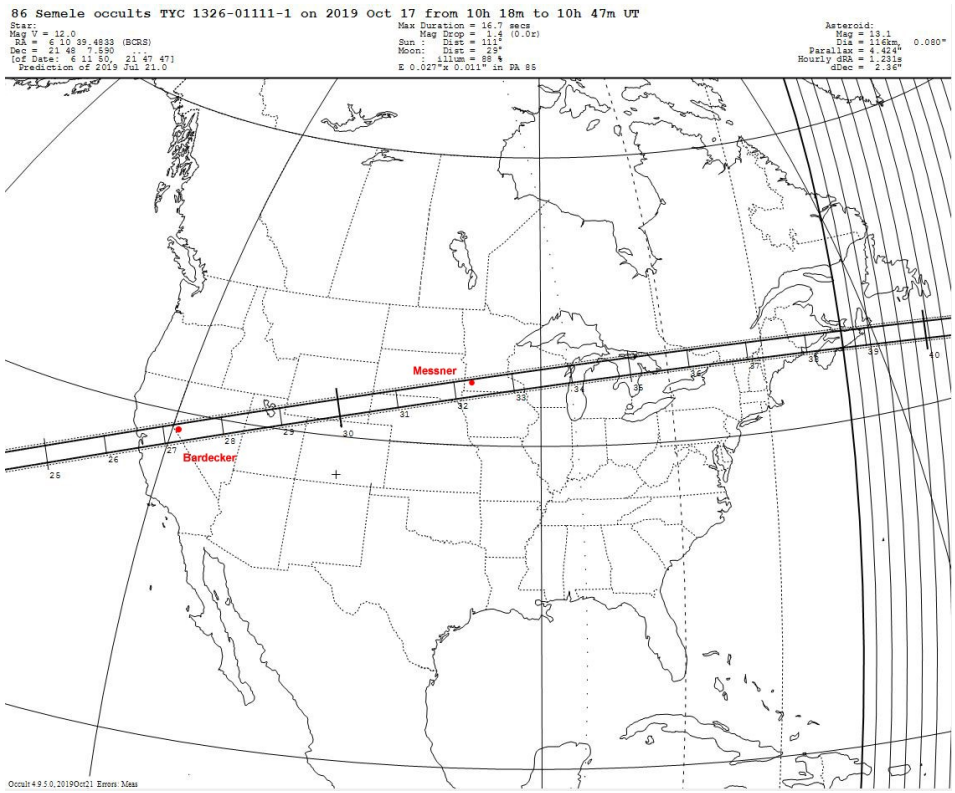

Figure 4 – Predicted Occultation Path

Discovery of Stellar Duplicity of TYC 1326-01111-1 During Asteroidal Occultation by (86) Semele

Event	Bardecker Time UT	Messner Time UT
D1	10:27:07.774	10:32:14.600
R1	10:27:25.992	10:32:32.751
D2	10:27:07.974	10:32:15.076
R2	10:27:26.326	10:32:33.018

Table 2. Event times (corrected)

Event	Bardecker Magnitude Change	Messner Magnitude Change
D1	0.54	0.52
R1	0.84	0.78
D2	0.85	0.78
R2	0.57	0.53

Table 3 – Calculated Magnitude Drops

(Continued from page 405)

Individual Event Magnitude Analysis

Each of the individual D and R events for both observers were then analysed using PyOTE 3.2.5. The estimated magnitude change for each event (D1, D2, R1, and R2) is shown in the Table 3.

Primary and Secondary Magnitude Estimates

Magnitude estimates for each component were then made using the brightness measurements derived by PyOTE 3.2.5.

Mean Photometric values were extracted from each observers light curves for the D2 and R1 events (the stepped events). These values, along with the baseline and event bottom values from the PyOTE analysis were used to calculate the primary and secondary star magnitudes. The Magnitude Calculator routine in Occult4 (Method 3 – Magnitudes from light curve values) was used for this analysis.

Light levels for the Messner observation:
* Light levels at D of 602 => 404 => 198
* Light levels at R of 198 => 394 => 602

Calculated star magnitudes for the Messner observation:
* Assuming a combined magnitude of 12.00
Magnitudes for sequence A-B-B-A: Mag A = 12.75, Mag B = 12.76
Magnitudes for sequence B-A-A-B: Mag A = 12.76, Mag B = 12.75

Light levels for the Bardecker observation:
* Light levels at D of 929 => 668 => 272
* Light levels at R of 272 => 660 => 929

Calculated star magnitudes for the Bardecker observation:
* Assuming a combined magnitude of 12.00
Magnitudes for sequence A-B-B-A: Mag A = 12.99, Mag B = 12.56
Magnitudes for sequence B-A-A-B: Mag A = 12.56, Mag B = 12.99

Although the calculated magnitudes of the primary (P) and secondary (S) components are somewhat similar, there is sufficient difference to establish a probable event sequence. Based on these values, a SPPS (or BAAB) event sequence is the most likely for this set of observations. Note: In this context: B=the secondary (dimmer) star and A=the primary (brighter) star.

A profile plot of the observational chords and calculated position angle and separation are represented in Figure 3.

Based on the data presented in this report, the double star characteristics are:

Star	TYC 560-1111-1 UCAC4 560-025472 3UC 224-053300 NOMAD 1118-0119007 PPMX 061039.4+214807 spectral type not known to authors
Coord (J2000)	RA 06h10m39.5s DEC +21°48'07.519"
Mag A	12.56-12.76
Mag B	12.75-12.99
Separation	0.0046 (± 0.0012 arcseconds)
Position Angle	11.7 (± 6.0 degrees)

Acknowledgements

The authors would like to acknowledge and thank Tony George, for his invaluable assistance in the analysis of these events. Without his knowledge and encouragement this presentation would not have been possible.

References

[1] PyMovie and PyOTE – Bob Anderson. PyMovie: http://occultations.org/observing/software/pymovie/PyOTE : http://occultations.org/observing/software/ote/

[2] Occult v4.1.0. Occultation prediction software by David Herald. http://www.lunar-occultations.com/iota/occult4.htm

Journal of Double Star Observations

September 1, 2020
Volume 16, Number 4

The Journal of Double Star Observations (ISSN 2572-4436) is an electronic journal published quarterly. Copies can be freely downloaded from http://www.jdso.org.

Questions, comments, or submissions may be directed to rclark@southalabama.edu or to rmollise@bellsouth.net

The *Journal of Double Star Observations* (*JDSO*) publishes articles on any and all aspects of astronomy involving double and binary stars. The *JDSO* is especially interested in observations made by amateur astronomers. Submitted articles announcing measurements, discoveries, or conclusions about double or binary stars may undergo a peer review. This means that a paper submitted by an amateur astronomer will be reviewed by other amateur astronomers doing similar work.

Submitted manuscripts must be original, unpublished material and written in English. They should contain an abstract and a short description or biography (2 or 3 sentences) of the author(s). For more information about format of submitted articles, please see our web site at http://www.jdso.org

Submissions should be made electronically via e-mail to rclark@southalabama.edu or to rmolise@bellsouth.net. Articles should be attached to the email in Microsoft Word, Word Perfect, Open Office, or text format. All images should be in jpg or fits format.